

# Gold-Silver Mining Districts, Alteration Zones, and Paleolandforms in the Miocene Bodie Hills Volcanic Field, California and Nevada



Scientific Investigations Report 2015–5012

**Cover.** Photograph showing ore bins at head of aerial tramway from the Sarita Mine to the Masonic mill, Masonic Mining District.

# **Gold-Silver Mining Districts, Alteration Zones, and Paleolandforms in the Miocene Bodie Hills Volcanic Field, California and Nevada**

By Peter G. Vikre, David A. John, Edward A. du Bray, and Robert J. Fleck

Scientific Investigations Report 2015–5012

**U.S. Department of the Interior**  
**U.S. Geological Survey**

**U.S. Department of the Interior**  
SALLY JEWELL, Secretary

**U.S. Geological Survey**  
Suzette M. Kimball, Acting Director

U.S. Geological Survey, Reston, Virginia: 2015

For more information on the USGS—the Federal source for science about the Earth, its natural and living resources, natural hazards, and the environment—visit <http://www.usgs.gov/> or call 1–888–ASK–USGS.

For an overview of USGS information products, including maps, imagery, and publications, visit <http://www.usgs.gov/pubprod/>.

Any use of trade, firm, or product names is for descriptive purposes only and does not imply endorsement by the U.S. Government.

Although this information product, for the most part, is in the public domain, it also may contain copyrighted materials as noted in the text. Permission to reproduce copyrighted items must be secured from the copyright owner.

Suggested citation:

Vikre, P.G., John, D.A., du Bray, E.A., and Fleck, R.J., 2015, Gold-silver mining districts, alteration zones, and paleolandforms in the Miocene Bodie Hills volcanic field, California and Nevada: U.S. Geological Survey Scientific Investigations Report 2015–5012, 160 p., <http://dx.doi.org/10.3133/sir20155012>.

ISSN 2328-0328 (online)

## Contents

Abstract.....	1
Introduction.....	3
Bodie Hills Volcanic Field .....	11
Methods.....	12
Masonic Mining District .....	13
Location .....	13
History and Production .....	13
Stratigraphy .....	13
Structure.....	17
Forms of Gold-Silver-Copper Deposits.....	17
Breccias and Vein Deposits in High-Angle, Subplanar Fault Zones .....	17
Mineral and Rock Compositions of Breccias and Vein Deposits .....	18
Clastic and Hydrothermal Sedimentary Deposits .....	22
Interpretation of Clastic and Hydrothermal Sedimentary Deposits .....	22
Mineral and Rock Compositions of Clastic and Hydrothermal Sedimentary Deposits .....	23
Other Minerals and Forms of Mineralization .....	25
Wall-Rock Alteration .....	25
Sulfur Isotope Compositions and Equilibrium Temperatures .....	27
Aster Imagery.....	28
Short Wave Infrared (SWIR) Spectra.....	28
Host Rock and Alteration Mineral Ages .....	28
Red Wash-East Walker River Alteration Zone .....	28
Location .....	28
Definition .....	28
History and Production .....	30
Stratigraphy .....	30
Structure.....	30
Hydrothermal Alteration .....	30
Minor Elements in Rocks.....	31
Sulfur Isotope Composition.....	31
ASTER Imagery .....	31
SWIR Spectra .....	31
Hydrothermal Mineral Ages.....	31
East Brawley Peak Alteration Zone .....	33
Location .....	33
Definition .....	33
History and Production .....	33
Stratigraphy .....	33
Structure.....	33

Hydrothermal Alteration .....	35
Minor Elements in Rocks .....	35
ASTER Imagery .....	35
SWIR Spectra .....	35
Fluid Inclusion Microthermometry and Composition .....	35
Hydrothermal Mineral Ages .....	36
Sawtooth Ridge Alteration Zone .....	36
Location .....	36
Definition .....	36
History and Production .....	36
Stratigraphy .....	36
Structure.....	36
Hydrothermal Alteration .....	36
Sulfur Isotope Composition.....	38
ASTER Imagery .....	38
SWIR Spectra .....	38
Hydrothermal Mineral Age.....	38
Aurora Canyon Alteration Zone.....	38
Location .....	38
Definition .....	38
History and Production .....	38
Stratigraphy .....	38
Structure.....	40
Hydrothermal Alteration .....	40
Minor Elements in Rocks .....	40
ASTER Imagery .....	40
SWIR Spectra .....	40
Hydrothermal Mineral Age.....	40
Potato Peak Alteration Zone .....	41
Location .....	41
Definition .....	41
History and Production .....	41
Stratigraphy .....	41
Structure.....	41
Hydrothermal Alteration .....	41
Minor Elements in Rocks .....	41
Sulfur Isotope Compositions .....	43
ASTER Imagery .....	43
SWIR Spectra .....	43
Hydrothermal Mineral Age.....	43
Aurora Mining District.....	43
Location .....	43
History and Production .....	43
Stratigraphy .....	46
Structure.....	46

Forms of Gold-Silver Mineralization .....	47
Veins and Vein Zones .....	47
Ore Bodies.....	48
Juniata-Prospectus Vein Minerals .....	49
Mineral Compositions in Silver Hill and Middle Hill Veins .....	50
Minor Elements in Rocks .....	50
Fluid Inclusion Microthermometry and Compositions.....	50
Sulfur Isotope Compositions of Vein Minerals.....	53
Wall-Rock Alteration .....	54
ASTER Imagery .....	54
SWIR Spectra .....	54
Hydrothermal Mineral Ages.....	54
Four Corners Alteration Zone.....	54
Location .....	54
Definition .....	54
History and Production .....	56
Stratigraphy .....	56
Structure.....	56
Hydrothermal Alteration .....	56
ASTER Imagery .....	56
SWIR Spectra .....	56
Hydrothermal Mineral Ages.....	56
Paramount-Bald Peak Alteration Zone .....	56
Location .....	56
Definition .....	56
History and Production .....	60
Stratigraphy .....	60
Structure.....	60
Hydrothermal Alteration .....	64
Paramount Mine Area.....	64
Minor Elements in Rocks .....	64
Atastra Creek Area.....	65
Bald Peak Area.....	65
Sulfur Isotope Compositions.....	69
ASTER Imagery .....	69
SWIR Spectra .....	69
Hydrothermal Mineral Ages.....	69
Cinnabar Canyon-US 395 Alteration Zone .....	70
Location .....	70
Definition .....	70
History and Production .....	70
Stratigraphy .....	70
Structure.....	70
Forms of Mercury and Sulfur Mineralization .....	71

Hydrothermal Alteration .....	71
Minor Elements in Rocks .....	75
Sulfur Isotope Compositions .....	76
ASTER Imagery .....	76
SWIR Spectra .....	76
XRD Mineralogy .....	76
Hydrothermal Mineral Ages .....	76
Bodie Mining District.....	77
Location .....	77
History and Production .....	77
Stratigraphy .....	80
Structure.....	81
Forms of Silver-Gold Deposits .....	81
Incline Series Veins .....	84
Burgess Series Veins .....	88
Silver Hill Series Veins .....	90
Veins On and Near Queen Bee Hill .....	91
Wall-Rock Alteration .....	91
Absolute and Relative Vein and Sinter Ages.....	95
Minor Elements in Veins and Wall Rocks .....	95
Fluid Inclusion Microthermometry.....	97
Oxygen and Hydrogen Isotope Compositions of Vein Minerals and Fluid Inclusion Water .....	97
Sulfur Isotope Compositions of Vein Minerals.....	97
ASTER Imagery .....	98
SWIR Spectra; XRD Analyses.....	98
Spring Peak Sinter .....	98
Location .....	98
Definition .....	98
History and Production .....	98
Stratigraphy .....	98
Structure.....	100
Hydrothermal Alteration .....	100
Hydrothermal Mineral Ages.....	100
Evolution of Landforms During Assembly and Alteration of the Miocene Bodie Hills Volcanic Field.....	100
Aldrich Station Flora and Fossils in the Bodie Hills .....	100
Eureka Valley Tuff in the Bodie Hills .....	106
Landforms in Mining Districts and Alteration Zones .....	106
Synthesis [Masonic Mining District] .....	107
Synthesis [Aurora Mining District] .....	109
Synthesis [Bodie Mining District] .....	110
Summary.....	114
Acknowledgments .....	114
References Cited.....	115
Appendixes .....	121



## Figures

1. Map showing locations of mining districts and alteration zones in the Bodie Hills, California and Nevada .....	4
2. Geologic map of the southwestern part of the Masonic Mining District, Mono County, California, and Lyon and Mineral Counties, Nevada.....	14
3. Geologic map of the northeastern part of the Masonic Mining District, Mono County, California, and Mineral County, Nevada .....	15
4. Images of volcanoclastic deposits in the Red Wash-East Walker River alteration zone and Masonic Mining District.....	16
5. Images of mineralized fault breccias and veins in the Masonic Mining District.....	19
6. Secondary electron images of fault breccia, Masonic Mining District .....	20
7. Secondary electron images of fault breccia, Masonic Mining District .....	21
8. Secondary electron image of quartz+alunite+sulfide vein in granodiorite, Masonic Mining District .....	22
9. Image of a dump sample from the Masonic Mining District, Sarita Mine .....	23
10. Images of dump samples from the Masonic Mining District, Sarita Mine .....	24
11. Images of dump samples from the Masonic Mining District, Sarita Mine .....	25
12. Secondary electron images of minerals in very fine-grained brown quartz beds from the Sarita Mine open cut, Masonic Mining District .....	26
13. Image of a dump sample from the Masonic Mining District, Sarita Mine .....	27
14. Geologic map of the Red Wash-East Walker River alteration zone, Lyon and Mineral Counties, Nevada, and Mono County, California.....	29
15. Advanced Spaceborne Thermal Emission and Reflection Radiometer imagery of the Red Wash-East Walker River alteration zone.....	32
16. Geologic map of the East Brawley Peak alteration zone, Mineral County, Nevada, and Mono County, California.....	34
17. Geologic map of the Sawtooth Ridge alteration zone, Mineral County, Nevada, and image of a remnant bowl-shaped thermal vent.....	37
18. Geologic map of the Aurora Canyon alteration zone, Mono County, California, and image showing a concentrically exfoliated rhyolite dome .....	39
19. Geologic map of the Potato Peak alteration zone, Mono County, California, and image showing landslides developed on altered volcanoclastic strata .....	42
20. Geologic map of the Aurora Mining District, Mineral County, Nevada .....	44
21. Image of a sample from the Aurora Mining District .....	49
22. Secondary electron images of an archival vein specimen from the Crocket Mine on Last Chance Hill, Aurora Mining District.....	51
23. Secondary electron images of an archival vein specimen from the Antelope Mine, Silver Hill, Aurora Mining District .....	52
24. Secondary electron images of an archival vein specimen from the Antelope Mine, Silver Hill, Aurora Mining District .....	53
25. Geologic map of the Four Corners alteration zone, Mono County, California .....	55
26. Images of hydrothermal features, Four Corners alteration zone.....	57
27. Geologic map of the Paramount-Bald Peak alteration zone, Mono County, California, and Mineral County, Nevada, showing sinters, sinter groups, and prospects .....	58
28. Geologic map of the Paramount Hg Mine area, Mono County, California, and image showing unoriented, multisized blocks of terrace sinter .....	61

29.	Images of Paramount-Bald Peak alteration zone .....	62
30.	Images of hydrothermal features in the Paramount-Bald Peak alteration zone .....	63
31.	Image showing oriented consecutive sections, graphs showing relative element concentrations, and bulk sample element concentrations of sinter from a dismembered terrace at the western base of Paramount Mine hill, Paramount-Bald Peak alteration zone.....	66
32.	Image showing oriented consecutive sections, graphs showing relative element concentrations, and bulk sample element concentrations of a chalcedonic quartz vein exposed at the upper adit of the Paramount Mine, Paramount-Bald Peak alteration zone.....	67
33.	Image showing oriented consecutive sections, graphs showing relative element concentrations, and bulk sample concentrations of sinter from sinter terrace on Atastra Creek, Paramount-Bald Peak alteration zone .....	68
34.	Geologic map and schematic stratigraphic section of the Cinnabar Canyon-US 395 alteration zone, Mono County, California.....	72
35.	Images showing volcanoclastic deposits from the Cinnabar Canyon-US 395 alteration zone.....	74
36.	Cross section through the Cinnabar Canyon elemental sulfur resource, Cinnabar Canyon-US 395 alteration zone, Mono County, California .....	75
37.	Geologic map of the Bodie Mining District, Mono County, California .....	78
38.	Geologic cross sections of the Bodie Mining District.....	79
39.	Images of veins in the Bodie Mining District.....	82
40.	Secondary and backscatter electron images of samples representative of Incline series veins on Bodie Bluff, and of vein samples from the Noonday Mine near Silver Hill, Bodie Mining District.....	87
41.	Secondary electron images of samples representative of Burgess series veins on Standard Hill, Bodie Mining District.....	89
42.	Secondary electron images of samples representative of Silver Hill series veins on and near Oro Mine dump, Silver Hill, Bodie Mining District.....	91
43.	Secondary electron images of samples representative of Silver Hill series veins on and near Addenda Mine, Silver Hill, Bodie Mining District .....	92
44.	Secondary electron images of samples representative of Silver Hill series veins on and near Red Cloud mine dump, Silver Hill, Bodie Mining District.....	93
45.	Secondary electron images of samples representative of Silver Hill series veins on and near Red Cloud, Contention, and Maybelle Mine dumps, Silver Hill, Bodie Mining District.....	94
46.	Image showing oriented consecutive sections, graphs showing relative element concentrations, and bulk sample element concentrations of sinter from Bodie Bluff summit, Bodie Mining District .....	96
47.	Graph of Ag, As, Sr concentrations versus Au, Sb, Rb concentrations in sinter from the dismembered sinter terrace, sinter fragments in volcanoclastic deposits, and Incline series veins, Bodie Mining District, Bodie Bluff summit.....	97
48.	Geologic map of the Spring Peak sinter, Mineral County, Nevada, and image showing nearly intact sinter beds from the northern margin of the terrace .....	99
49.	Image of sample, and graphs showing relative element concentrations and bulk sample element concentrations of Spring Peak sinter from the Hg prospect in the sinter terrace, Spring Peak alteration zone .....	101
50.	Image showing sample, and graphs showing relative element concentrations and bulk sample element concentrations of Spring Peak sinter from the Hg prospect in the sinter terrace, Spring Peak alteration zone.....	102

51. Image showing oriented consecutive sections, and graphs showing relative element concentrations and bulk sample element concentrations of sinter from the northern edge of the Spring Peak sinter terrace.....	103
52. Maps showing assembly of the Miocene Bodie Hills volcanic field, California and Nevada, from 15 to 8 Ma based on volcanic stratigraphy, mineral deposits, alteration zones, and geochronology.....	104

## Tables

1. $^{40}\text{Ar}/^{39}\text{Ar}$ dates (Ma) of igneous and hydrothermal minerals in mining districts and alteration zones of the Bodie Hills, determined by incremental heating and laser fusion.....	5
2. Sulfur isotope compositions of sulfide and sulfate minerals and sulfur from mining districts and alteration zones, and calculated sulfur isotope equilibrium temperatures .....	9
3. Reporting limits for element concentrations in tables 1-1 through 1-12 .....	11
4. Characteristics of Incline, Burgess, and Silver Hill series veins in the Bodie Mining District.....	83
5. Gold and silver production and precious metal grades for mines and veins in the Bodie Mining District from 1875 to 1942, and relative value of gold and silver in bullion from 1878 to 1881 .....	85
6. Vein attitudes and widths derived from surface mapping and published descriptions .....	86
1-1. Minor element concentrations in rock samples from the Masonic Mining District .....	122
1-2. Minor element concentrations in rock samples from the Red Wash-East Walker River alteration zone .....	125
1-3. Minor element concentrations in rock samples from the East Brawley Peak alteration zone.....	128
1-4. Minor element concentrations in rock samples from the Sawtooth Ridge alteration zone.....	129
1-5. Minor element concentrations in rock samples from the Aurora Canyon alteration zone.....	131
1-6. Minor element concentrations in rock samples from the Potato Peak alteration zone.....	132
1-7. Minor element concentrations in rock samples from the Aurora Mining District.....	133
1-8. Minor element concentrations in rock samples from the Four Corners alteration zone.....	135
1-9. Minor element concentrations in rock samples from the Paramount-Bald Peak alteration zone.....	137
1-10. Minor element concentrations in rock samples from the Cinnabar Canyon-US 395 alteration zone.....	145
1-11. Minor element concentrations in rock samples from the Bodie Mining District.....	149
1-12. Minor element concentrations in rock samples of Spring Peak sinter .....	159

## Conversion Factors

### Inch/Pound to International System of Units

Multiply	By	To obtain
Length		
inch (in.)	2.54	centimeter (cm)
foot (ft)	0.3048	meter (m)
mile (mi)	1.609	kilometer (km)
Area		
square mile (mi <sup>2</sup> )	2.590	square kilometer (km <sup>2</sup> )
Mass		
ounce, troy (oz)	31.10	gram (g)
ton, short (2,000 lb)	0.9072	tonne, metric

### International System of Units to Inch/Pound

Multiply	By	To obtain
Length		
centimeter (cm)	0.3937	inch (in.)
millimeter (mm)	0.03937	inch (in.)
micron ( $\mu\text{m}$ )	0.00003937	inch (in.)
meter (m)	3.281	foot (ft)
kilometer (km)	0.6214	mile (mi)
Area		
square kilometer (km <sup>2</sup> )	0.3861	square mile (mi <sup>2</sup> )
Mass		
tonne, metric (Mt)	1.1023	ton, short (2000 lb)

## Acronyms and Abbreviations Used

<b>AA</b>	cold-vapor and hydride generation atomic absorption
<b>ASTER</b>	Advanced Spaceborne Thermal Emission and Reflection Radiometer
<b>FA-ICPMS</b>	fire assay-inductively coupled plasma-mass spectrometry
<b>ICP-AES-MS</b>	inductively coupled plasma-atomic emission spectrometry-mass spectrometry
<b>LA ICP-MS</b>	laser ablation inductively coupled plasma-mass spectrometry
<b>Ma</b>	million years before present
<b>Moz</b>	million ounces
<b>SEM</b>	scanning electron microscopy
<b>SWIR</b>	short wave infrared radiation
<b>USGS</b>	U.S. Geological Survey
<b>XRD</b>	x-ray diffraction

## Chemical Symbols Used

<b>Ag</b>	silver	<b>Mo</b>	molybdenum
<b>Al</b>	aluminum	<b>Na</b>	sodium
<b>As</b>	arsenic	<b>Nb</b>	niobium
<b>Au</b>	gold	<b>Ni</b>	nickel
<b>Ba</b>	barium	<b>O</b>	oxygen
<b>Be</b>	beryllium	<b>P</b>	phosphorus
<b>Bi</b>	bismuth	<b>Pb</b>	lead
<b>C</b>	carbon	<b>Rb</b>	rubidium
<b>Ca</b>	calcium	<b>S</b>	sulfur
<b>Cd</b>	cadmium	<b>Sb</b>	antimony
<b>Ce</b>	cerium	<b>Sc</b>	scandium
<b>Co</b>	cobalt	<b>Se</b>	selenium
<b>Cr</b>	chromium	<b>Sn</b>	tin
<b>Cs</b>	cesium	<b>Sr</b>	strontium
<b>Cu</b>	copper	<b>Te</b>	tellurium
<b>Fe</b>	iron	<b>Th</b>	thorium
<b>Ga</b>	gallium	<b>Ti</b>	titanium
<b>Hg</b>	mercury	<b>Tl</b>	thallium
<b>In</b>	indium	<b>U</b>	uranium
<b>K</b>	potassium	<b>V</b>	vanadium
<b>La</b>	lanthanum	<b>W</b>	tungsten
<b>Li</b>	lithium	<b>Y</b>	yttrium
<b>Mg</b>	magnesium	<b>Zn</b>	zinc
<b>Mn</b>	manganese		

# Gold-Silver Mining Districts, Alteration Zones, and Paleolandforms in the Miocene Bodie Hills Volcanic Field, California and Nevada

By Peter G. Vikre, David A. John, Edward A. du Bray, and Robert J. Fleck

## Abstract

The middle-late Miocene Bodie Hills volcanic field, Mono County, California, and Mineral and Lyon Counties, Nevada, contains three precious metal mining districts, with combined production of ~3.4 million ounces (Moz) gold (Au) and ~28 Moz silver (Ag), and nine variably sized alteration zones. Minor amounts of mercury (Hg) have been produced from three alteration zones; a significant sulfur resource has been identified in one alteration zone. The ~40 by ~30 kilometer (km) volcanic field is made up of coalescing, 15–6 Ma, subduction-related, trachyandesite stratovolcanoes, trachydacite and rhyolite lava domes, and related volcanoclastic deposits that cover an irregular erosional surface of Paleozoic and Mesozoic metavolcanic and metasedimentary rocks and Mesozoic granitic rocks of the Sierra Nevada batholith. Hydrothermal systems that formed precious metal deposits and most alteration zones were intermittently active during and soon after the development of trachyandesite stratovolcanoes and rhyolite flow-domes at 13.4–11 Ma, and following eruption of trachyandesite to rhyolite flows, domes, and associated volcanoclastic deposits at ~9–8 Ma.

In the Masonic Mining District, Au (0.056 Moz), Ag (0.04 Moz), and small amounts of copper (Cu) were produced from 0.075 million metric tons (Mt) of ore mostly during the period 1906–20. Deposits formed at ~13.4–13.3 Ma and 13.0 Ma, and comprise two styles of mineralization: (1) high-angle, fault breccia deposits in Mesozoic granitic rocks and 15–14 Ma trachyandesite flows; and (2) stratiform volcanoclastic and chemical sedimentary deposits in 15–14 Ma trachyandesite. Both types of deposits consist of quartz, enargite (and lesser luzonite), pyrite, small inclusions (tens of micrometers in size) and intergrowths of numerous Cu-As-Sb-Fe-Bi-Au-Ag-S-Se-Te minerals including Au-rich electrum, alunite, kaolinite and dickite, pyrophyllite, and sericite. Fault breccia deposits are enclosed by meters-wide selvages comprised of quartz, alunite, pyrite, kaolinite and dickite, pyrophyllite, sericite, and montmorillonite.

In the Aurora Mining District, an estimated 1.91 Moz of Au and 21 Moz of Ag were recovered from ~3.9 Mt of vein ore, mostly during several periods of mining: 1860–64, 1906–18, and 1988–98. The ~10.5 Ma vein system, in 13.1–12.6 Ma trachyandesite of Aurora, is comprised of numerous north- to northeast-striking en echelon segments, which have a cumulative strike length of ~7.5 km. Veins are composed of fine-grained, layered to granular quartz, sulfide minerals, electrum, sericite, potassium feldspar (K-feldspar), and paragenetically late calcite. Quartz layers locally include finely dispersed pyrite, electrum, acanthite, naumannite, sphalerite, galena, polybasite, tetrahedrite, an Ag-Au-S mineral (~Ag<sub>4</sub>AuS<sub>3</sub>), and clumps of these minerals (millimeters to centimeters in size). Trachyandesite wall rocks proximal to veins, vein zone septa, and internal breccia fragments have been altered to sericite, K-feldspar, and pyrite. Distal, pervasively altered trachyandesite contains variable proportions of chlorite, albite, calcite, and montmorillonite, and lesser fine-grained quartz, sericite, pyrite (and iron oxides after pyrite), and epidote.

In the Bodie Mining District, 1.46 Moz of Au and 7.3 Moz of Ag were produced from ~1.5 Mt of vein ore, mostly during the period 1877–1913. Deposits comprise at least three types of N±30°-striking veins that formed from ~8.9 to 8.1 Ma in ~9 Ma dacite of Silver Hill domes and flows. Incline series veins, the most productive vein type, consist of numerous layers (millimeters thick) of quartz±adularia with electrum and Ag-S-Se minerals dispersed on some layers. Burgess series veins are composed of relatively coarse-grained and less distinctly layered quartz±adularia, and contain as much as 5 volume percent electrum, Ag-S-Se minerals, pyrite, sphalerite, and galena. These vein types are enclosed by <1-meter-wide selvages of dacite altered to variable amounts of K-feldspar, quartz, sericite, and pyrite. Silver Hill series veins consist mostly of fault breccia cemented by quartz, adularia, sericite, calcite, and as much as 10 volume percent metallic minerals, predominantly sphalerite, galena, tetrahedrite, and chalcopyrite, and lesser pyrite, acanthite, electrum, bornite, hessite, and sylvanite. They are enclosed

## 2 Gold-Silver Mining Districts, Alteration Zones, and Paleolandforms in the Miocene Bodie Hills Volcanic Field

by selvages of dacite (meters wide) altered to quartz, pyrite, and sericite. Heterolithic volcanoclastic deposits fill a graben on Bodie Bluff, contain clasts of sinter at the highest exposed elevation (Bodie Bluff), and record the youngest volcanic and hydrothermal events in the district.

The areally extensive (>30 square kilometers [km<sup>2</sup>]) 13.3 Ma Red Wash-East Walker River alteration zone, which formed simultaneously with the oldest Au-Ag-Cu deposits in the Masonic Mining District, and the large (~30 km<sup>2</sup>) ~8.8–8.2 Ma Cinnabar Canyon-US 395 alteration zone, which contains a significant S<sup>o</sup> (native sulfur) resource (16.1 Mt @ 17.9 percent S) and a small Hg deposit, formed in sequences of permeable volcanoclastic rocks and subordinate 15–8.9 Ma trachyandesite flows. The zones consist of resistant quartz±alunite±pyrite-dominant hydrothermal mineral assemblages enclosed by strata variably altered to kaolinite, pyrite, sericite, pyrophyllite, and montmorillonite. The large (~30 km<sup>2</sup>) Paramount-Bald Peak alteration zone mostly formed in a permeable sequence of rhyolite tuff, volcanoclastic strata, and lesser rhyolite (sedimentary rocks and tuff of Paramount) that accumulated in a northeast-trending basin at ~10.3–9.3 Ma. These strata have been variably leached and altered to silica minerals, montmorillonite, and lesser kaolinite, dickite, and pyrite, and include groups of intact and dismembered sinter terraces, one of which is associated with the intermittently mined (1878–1968) Hg vein deposit at the Paramount Mine. Smaller alteration zones, including the ~12 Ma East Brawley Peak (~7.7 km<sup>2</sup>), 11.1 Ma Sawtooth Ridge (~2 km<sup>2</sup>), 10.9 Ma Aurora Canyon (~8.1 km<sup>2</sup>), and 10.8 Ma Potato Peak (~1.3 km<sup>2</sup>), formed in ~15–11.2 Ma trachyandesite, rhyolite, and volcanoclastic strata. Hydrothermal mineral assemblages in these zones are similar to those of the Red Wash-East Walker River and Cinnabar Canyon-US 395 alteration zones. Small quantities of Hg (tens of flasks) were produced from the Cinnabar Canyon-US 395, Paramount-Bald Peak, and Potato Peak alteration zones, but no production is recorded from the other zones. The undated (~14–10 Ma) Four Corners alteration zone (<0.02 km<sup>2</sup>) consists of brecciated trachyandesite of Masonic that has been cemented by quartz and pyrite (and iron oxides after pyrite) and contains local clastic and chemical sedimentary deposits. The partially dismembered and undated sinter terrace at Spring Peak (0.02 km<sup>2</sup>) lies on Cretaceous granitic and metamorphic rocks, and on altered volcanoclastic deposits. Slope detritus of these strata, adjacent to the terrace, include clasts of layered veins.

Based on volcanic stratigraphy, geochronology, remnant paleosurfaces, and paleopotentiometric surfaces in mining districts and alteration zones, present landforms in the Bodie Hills volcanic field reflect incremental construction of stratovolcanoes and large- to small-volume flow-domes, magmatic inflation, and fault displacements. In the northwestern part of the field, the extensive (~350 km<sup>2</sup>) 15–14 Ma Masonic volcanic center, consisting of trachyandesite flows, domes, and volcanoclastic deposits, was erupted on Mesozoic granitic and metamorphic rocks, and intruded by 13.5–13.4 Ma and 12.9 Ma porphyritic trachyandesite. These intrusions closely

correspond in age to the Au-Ag-Cu deposits in the Masonic district (13.4–13.3 Ma and 13 Ma) and to the areally extensive Red Wash-East Walker River alteration zone (13.3 Ma). Paleorelief among domes of the younger intrusions, domes of older trachyandesite, and prominences of Mesozoic rocks, was meters to tens of meters (tens to hundreds of feet).

In the eastern part of the volcanic field, the 13.1–12.6 Ma Aurora volcanic center was dominated by a prominent ridge of trachyandesite (~130 km<sup>2</sup>) flanked by lower-elevation flow-domes of trachyandesite and rhyolite. These large- and small-volume volcanoes were emplaced on Mesozoic rocks. Parts of the volcanic center were altered at ~12 Ma (East Brawley Peak alteration zone), 11 Ma (Sawtooth Ridge alteration zone), and 10.5 Ma during formation of Au-Ag veins of the Aurora district. Paleorelief within the volcanic center was hundreds of meters (hundreds to >1,000 feet [ft]<sup>1</sup>) above ancestral Fletcher Valley to the north that was an established basin by 11 Ma.

From ~11–9.5 Ma, pre-Tertiary rocks in the central and southwestern parts of the field were mostly covered by large- to small-volume flows and domes of trachyandesite, rhyolite, and trachydacite. These flow-domes and older volcanic uplands shed detritus into the ~10.3–9.3 Ma Paramount basin, which was nearly simultaneously altered by hydrothermal systems that produced groups of sinter terraces and subjacent, locally Hg-mineralized veins (Paramount-Bald Peak alteration zone; Paramount Hg Mine). At 9.5–9.3 Ma, externally sourced Eureka Valley Tuff partly filled the drainages and depressions that had been incised into volcanic uplands in the western half of the volcanic field. The distribution of Eureka Valley Tuff remnants shows that paleorelief among volcanic and pre-Tertiary landforms was tens to hundreds of meters (hundreds of feet).

From ~10 to 8 Ma, large-volume stratovolcanoes and flow-dome fields, including trachydacite of Potato Peak, dacite of Silver Hill, trachyandesite and volcanoclastic deposits of Mount Biedeman, and trachyandesite of Willow Springs, were erupted in the southern part of the volcanic field. The volcanoclastic flow sequence exposed between Cinnabar Canyon and US 395 was pervasively altered and locally mineralized with Hg and S (Cinnabar Canyon-US 395 alteration zone), nearly simultaneously with the formation of multiple Au-Ag vein deposits in dacite flow-domes of the Bodie district at 8.9–8.1 Ma.

The present elevation of Potato Peak (10,237 ft) is ~1,100 ft higher than the highest elevation of Eureka Valley Tuff (9,150 ft) on Potato Peak, ~4,600 ft higher than the lowest elevation of Eureka Valley Tuff (5,600 ft) along the East Walker River, and ~4,200 ft higher than Fletcher Valley. Assuming a common Eureka Valley Tuff paleoelevation at 9.3 Ma, these present elevation differences, and few significant faults in the southern part of the field, indicate that most present relief in the volcanic field reflects construction of 10–8 Ma large-volume volcanic centers, and related magmatic inflation. Relatively small increments of relief (tens to hundreds of

<sup>1</sup>Elevations are reported in feet for the purpose of comparing paleoelevations to present elevations, which are reported in feet on topographic maps..



meters) have been added to northwestern and eastern parts of the field by displacement along east-west, and north- to northeast-trending normal faults in the Masonic and Aurora districts, and in the Paramount basin. Pliocene volcanic rocks of the Aurora volcanic field, which initially erupted at ~3.9 Ma, do not appear to be significantly offset by faults, implying that most fault displacement occurred between 9.3 and 3.9 Ma. Between 8 and 3.9 Ma, only a few small-volume, ~6–5 Ma rhyolite and dacite flow-domes were erupted.

The higher of two paleoelevation ranges estimated for the 11 Ma Aldrich Station flora, located ~22.5 km north of the Aurora district, is more consistent with post-Eureka Valley Tuff relief added to the volcanic field (4,200–4,600 ft). Based on the flora, paleoelevations in the 15–10 Ma Masonic and Aurora volcanic centers varied from ~4,300 to ~6,900 ft. Following eruption of large-volume stratovolcanoes and flow-dome fields in the southern part of the volcanic field at 10–8 Ma, maximum paleoelevations exceeded 8,500 ft. If fossils in ~11 Ma Fletcher basin sediments are stratigraphically equivalent to Aldrich Station flora, then paleorelief may have been ~10,000 ft.

## Introduction

Three precious metal mining districts and nine areas of extensive hydrothermally altered rocks, or alteration zones, occur in the Bodie Hills, an upland of Tertiary-Quaternary volcanic and Mesozoic granitic and metamorphic rocks that straddles the California-Nevada state boundary between Mono Lake and the East Walker River (fig. 1). Cumulative production from the mining districts, Bodie, Aurora, and Masonic, is 3.4 million ounces (Moz) of gold (Au) and 28 Moz of silver (Ag). Small amounts of Hg were produced from the Potato Peak, Paramount-Bald Peak, and Cinnabar Canyon-US 395 alteration zones; a native sulfur (S<sup>0</sup>) resource in the Cinnabar Canyon-US 395 alteration zone has been identified by drilling. There are no known mineral resources in the other six alteration zones, Red Wash-East Walker River, East Brawley Peak, Sawtooth Ridge, Aurora Canyon, Four Corners, and Spring Peak. The mining districts and alteration zones formed between 13.4 and 8.1 Ma in predominantly ~15–9 Ma volcanic rocks of the Bodie Hills volcanic field. Ages of hydrothermal minerals in the districts and zones are the same as, or somewhat younger than, the ages of volcanic host rocks (table 1).

Mining districts and alteration zones have been characterized briefly and integrated with the interpreted evolution of the Bodie Hills volcanic field by John and others (2012). Descriptions and genetic models of several mineral deposit types and alteration zones are included in Vikre and Henry (2011). This report provides an expanded characterization of the mining districts and alteration zones, including <sup>40</sup>Ar/<sup>39</sup>Ar ages of igneous and hydrothermal minerals (table 1), minor element concentrations in mineralized and altered rocks, and modal,

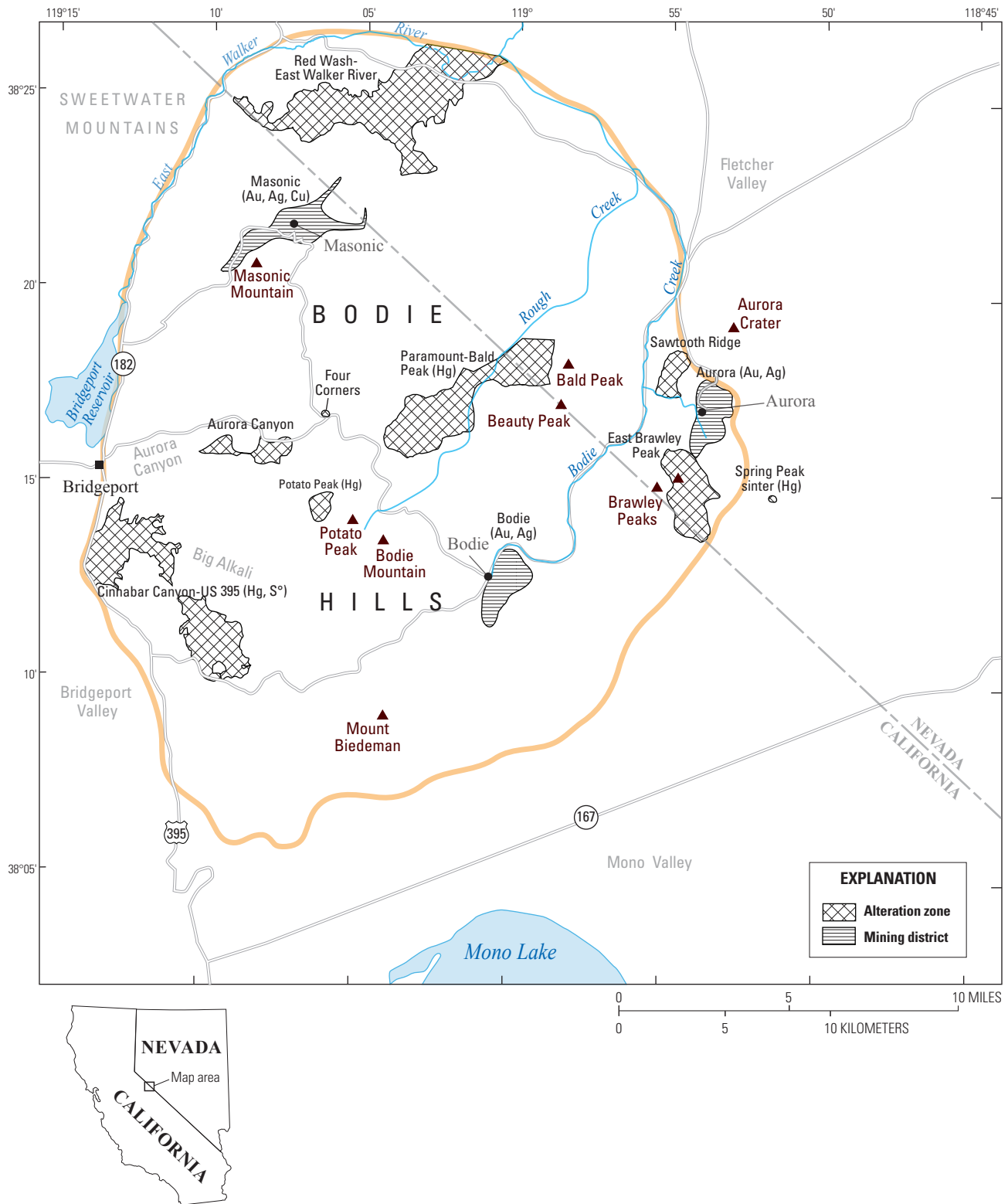
chemical and sulfur isotope compositions of hydrothermal mineral assemblages (tables 2, 3, 1-1 through 1-12). Paleo-hydrology, determined from attributes of mineral deposits and alteration zones, is also integrated with volcanic stratigraphy and mineral ages to reconstruct landform evolution during assembly and alteration of the volcanic field.

Descriptions of the Miocene mining districts and alteration zones are organized from the oldest (Masonic) to youngest (Spring Peak), as determined by <sup>40</sup>Ar/<sup>39</sup>Ar ages of igneous and hydrothermal minerals and by stratigraphic constraints. Characteristics systematically described include definition of the district or alteration zone, history and production, stratigraphy, petrography, structure, forms of deposits, hydrothermal alteration, minor elements, reflectance spectra, and hydrothermal mineral ages. Fluid inclusion micro-thermometry and sulfur isotope compositions are also summarized for several districts and alteration zones. Small mines and prospects in pre-Tertiary rocks at the south end of Masonic Mountain, near Rancheria Gulch, and in the Aurora district (fig. 1) contain minor amounts of tungsten (W), copper (Cu) oxide, and Cu sulfide minerals that probably formed during the Mesozoic. Minor amounts of placer Au were recovered from Bodie Creek, and from drainages on the southwest margin of the Bodie Hills (Kleinhampl and others, 1975). These pre-Tertiary and placer mineral occurrences are not described.

Volcanic (Le Bas and others, 1986) and plutonic (Streckeisen, 1976) rock unit names used herein are in accord with the International Union of Geological Sciences (IUGS) nomenclature system. The composition of each rock unit is the average composition computed from analyses in du Bray and others (2013), but the full range of compositional variation within each unit is also specified. Average abundances and grain sizes of phenocrysts in volcanic rocks are based on microscopic observations. Modal compositions of Mesozoic plutons are based on analyses of stained slabs.

The Masonic, Aurora, and Bodie Mining Districts were established, named, and renamed in the mid-1800s, in part during confirmation of the boundary between California and Nevada. In this report, the three districts are given informal dimensions that encompass all productive mines and most prospects. The nine alteration zones, named after local geographic features, are defined on the basis of significant volumes of mostly Miocene volcanic rocks in which (1) primary minerals have been partially or entirely replaced by hydrothermal minerals; and (2) fabric has been modified substantially by hydrothermal mineral replacement, brecciation, and veining, and by hydrothermal leaching. The largest alteration zones, Red Wash-East Walker River, Paramount-Bald Peak, and Cinnabar Canyon-US 395, record strong disequilibrium between hydrothermal fluids and permeable volcanoclastic rocks, resulting in (1) extensive volumes of discolored, fine-grained, pyritic, and low-density rocks that are susceptible to weathering; and (2) stratiform masses of densely silicified rocks that comprise resistant hills, ridges, spines, and mesa-like landforms. Visual contrasts between

4 Gold-Silver Mining Districts, Alteration Zones, and Paleolandforms in the Miocene Bodie Hills Volcanic Field



**Figure 1.** Map showing locations of mining districts (line pattern) and alteration zones (crosshatch pattern) in the Bodie Hills, California and Nevada; commodity produced or resource shown in parentheses. Base from Fleck and others (2015).

**Table 1.**  $^{40}\text{Ar}/^{39}\text{Ar}$  dates (Ma) of igneous and hydrothermal minerals in mining districts and alteration zones (AZ) of the Bodie Hills, determined by incremental heating and laser fusion. Some K-Ar and  $^{40}\text{Ar}/^{39}\text{Ar}$  dates (see footnotes) are from Kleinhampl and others (1975), Morton and others (1977), Breit (2000), and Larry Snee (written commun.); most  $^{40}\text{Ar}/^{39}\text{Ar}$  dates of igneous minerals are from John and others (2012). Dates are based on Fish Canyon Tuff sanidine=28.02 Ma. Coordinates are NAD27.

[—, no data; qtz, quartz; Kspar, potassium feldspar; K, potassium; py, pyrite; chlor, chlorite]

Sample number	Latitude (decimal degrees)	Longitude (decimal degrees)	Lithology and (or) location	Mineral	Age (Ma) and error (1 $\sigma$ )	Sample index number on figures
<b>Masonic Mining District</b>						
Trachyandesite of Masonic (Tma, Tmai)						
10-BA-9	38.3528	-119.0207	Porphyritic plug in trachyandesite of Masonic	Plagioclase	14.998 $\pm$ 0.019	—
098-12B	38.38762	-119.18139	Lava flow in trachyandesite of Masonic	Plagioclase	14.715 $\pm$ 0.025	—
09-BA-7	38.33786	-119.08727	Lava flow in trachyandesite of Masonic	Plagioclase	14.674 $\pm$ 0.025	—
098-12D	38.4	-119.1194	Lava flow in trachyandesite of Masonic	Plagioclase	14.590 $\pm$ 0.02	4 (fig. 14)
10-BA-13	38.3515	-119.1042	Porphyritic dome in trachyandesite of Masonic	Plagioclase	14.410 $\pm$ 0.016	—
088-23F	38.31068	-119.117	Lava flow in trachyandesite of Masonic	Plagioclase	14.193 $\pm$ 0.038	—
MAS10-76	38.38169	-119.11534	Hornblende andesite dome in trachyandesite of Masonic	Hornblende	14.190 $\pm$ 0.021	7 (fig. 14)
10-BA-15	38.3413	-119.1157	Lava flow in trachyandesite of Masonic	Plagioclase	14.140 $\pm$ 0.017	—
08-BA-62	38.32005908	-119.0494277	Lava flow in trachyandesite of Masonic	Plagioclase	14.130 $\pm$ 0.031	—
10-BA-69	38.3054	-119.1365	Lava flow in trachyandesite of Masonic	Plagioclase	14.107 $\pm$ 0.014	—
098-12F	38.37542	-119.11418	Lava flow in trachyandesite of Masonic	Hornblende	14.094 $\pm$ 0.017	11 (fig. 3)
088-22B	38.37937	-119.07802	Lava flow in trachyandesite of Masonic	Plagioclase	14.067 $\pm$ 0.08	12 (fig. 3)
Trachyandesite of Masonic Gulch (Tamg)						
MAS10-75	38.39169	-119.11549	Porphyritic trachyandesite dome in trachyandesite of Masonic	Plagioclase	13.497 $\pm$ 0.023	13 (fig. 14)
MAS10-72	38.40189	-119.13718	Porphyritic trachyandesite dome in trachyandesite of Masonic	Plagioclase	13.485 $\pm$ 0.017	14 (fig. 14)
MAS10-73	38.39643	-119.1347	Porphyritic trachyandesite dome in trachyandesite of Masonic	Plagioclase	13.467 $\pm$ 0.016	15 (fig. 14)
098-12E	38.39143	-119.12397	Porphyritic trachyandesite dome in trachyandesite of Masonic	Plagioclase	13.441 $\pm$ 0.026	16 (fig. 14)
Andesite of Lakeview Spring (Tals)						
07-BA-38	38.36049	-119.14502	Andesite of Lakeview Spring dome	Plagioclase	12.930 $\pm$ 0.03	17 (fig. 2)
Hydrothermal minerals						
MAS12-10 (#2)	38.33762	-119.15973	Success Mine area	Alunite	13.638 $\pm$ 0.077	—
MAS12-10 (#1)	38.33762	-119.15973	Success Mine area	Alunite	13.398 $\pm$ 0.081	—
MAS07-1A	38.34991667	-119.1483167	Chemung Mine; volcanoclastic rocks	Alunite	13.390 $\pm$ 0.07	20 (fig. 2)
MAS09-1A	38.35847	-119.13824	Red Rock Mine area; volcanoclastic-flow sequence	Alunite	13.370 $\pm$ 0.11	21 (fig. 2)
MAS09-1	38.35783	-119.13268	Red Rock Mine area; volcanoclastic-flow sequence	Alunite	13.320 $\pm$ 0.14	22 (fig. 2)
MAS07-3	38.35968	-119.12682	Sarita mine; hydrothermal and clastic sedimentary strata	Alunite	13.260 $\pm$ 0.05	23 (fig. 2)
07-BA-40	38.36546	-119.11607	Pittsburg-Liberty Mine; granodiorite	Alunite	13.020 $\pm$ 0.05	24 (fig. 2)
088-22A	38.36731	-119.10727	Maybell Mine; granodiorite	Alunite	13.018 $\pm$ 0.061	25 (fig. 3)
MAS11-2B	38.36064	-119.08681	Perrini Mine, trachyandesite, upper dump	Alunite	12.960 $\pm$ 0.020	26 (fig. 3)
MAS11-1	38.36041	-119.08369	Perrini Mine, trachyandesite, lower dump	Alunite	12.956 $\pm$ 0.014	27 (fig. 3)
Basin-fill of Fletcher Valley						
08SB032	38.34561	-118.95589	Unwelded tuff, Fletcher Valley sediments	Plagioclase	11.075 $\pm$ 0.041	—
10-BA-62	38.36327	-119.00635	Tephra, Fletcher Valley sediments	Plagioclase	10.582 $\pm$ 0.023	—
				Biotite	10.464 $\pm$ 0.042	—
<b>Red Wash-East Walker River AZ</b>						
Hydrothermal minerals						
RW08-1	38.41123	-119.12414	Quartz-alunite matrix breccia	Alunite	13.340 $\pm$ 0.035	28 (fig. 14)
MAS10-55	38.41419	-119.10259	Quartz-alunite matrix breccia	Alunite	13.270 $\pm$ 0.02	29 (fig. 14)
<b>East Brawley Peak AZ</b>						
Hydrothermal minerals						
89EB002	—	—	Altered andesite, East Brawley Peak	Alunite	<sup>1,2</sup> 13.7 $\pm$ 0.5	—
FA66	38.2375	-118.9008	Silicified andesite, south slope East Brawley Peak	Alunite	<sup>1,2</sup> 12.34 $\pm$ 0.04	—
AUR10-3	38.23752	-118.89919	Silicified andesite, south slope East Brawley Peak	Alunite	11.954 $\pm$ 0.016	—

## 6 Gold-Silver Mining Districts, Alteration Zones, and Paleolandforms in the Miocene Bodie Hills Volcanic Field

**Table 1.**  $^{40}\text{Ar}/^{39}\text{Ar}$  dates (Ma) of igneous and hydrothermal minerals in mining districts and alteration zones (AZ) of the Bodie Hills, determined by incremental heating and laser fusion. Some K-Ar and  $^{40}\text{Ar}/^{39}\text{Ar}$  dates (see footnotes) are from Kleinhampl and others (1975), Morton and others (1977), Breit (2000), and Larry Snee (written commun.); most  $^{40}\text{Ar}/^{39}\text{Ar}$  dates of igneous minerals are from John and others (2012). Dates are based on Fish Canyon Tuff sanidine=28.02 Ma. Coordinates are NAD27.—Continued

[—, no data; qtz, quartz; Kspar, potassium feldspar; K, potassium; py, pyrite; chlor, chlorite]

Sample number	Latitude (decimal degrees)	Longitude (decimal degrees)	Lithology and (or) location	Mineral	Age (Ma) and error (1 $\sigma$ )	Sample index number on figures
<b>Sawtooth Ridge AZ</b>						
Volcanic rocks						
077-9C	38.27661	-118.93036	Porphyritic lava flow in rhyolite of Del Monte Canyon	Plagioclase	11.258 $\pm$ 0.14	—
077-9D	38.27661	-118.93036	Porphyritic lava flow in rhyolite of Del Monte Canyon	Plagioclase	11.197 $\pm$ 0.03	—
077-9C	38.27661	-118.93036	Porphyritic lava flow in rhyolite of Del Monte Canyon	Sanidine	11.187 $\pm$ 0.02	—
077-9D	38.28562	-118.92803	Porphyritic lava flow in rhyolite of Del Monte Canyon	Sanidine	11.136 $\pm$ 0.02	—
10-BA-21	38.30315	-118.8974	Glassy lava flow in rhyolite of Aurora Creek	Sanidine	11.181 $\pm$ 0.022	—
10-BA-20	38.31679	-118.91129	Glassy pyroxene rhyolite, rhyolite of Aurora Creek	Plagioclase	11.177 $\pm$ 0.013	—
Hydrothermal mineral						
SAW11-9	38.29036	-118.91657	Brecciated rhyolite of Aurora Creek	Alunite	11.105 $\pm$ 0.018	—
<b>Aurora Canyon AZ</b>						
Hydrothermal mineral						
PP09-10A1	38.25309	-119.13844	Silicified breccia matrix	Alunite	10.870 $\pm$ 0.07	—
Volcanic rocks						
098-13D	38.27655	-119.16062	Porphyritic plug in trachyandesite of Clark Canyon	Plagioclase	11.341 $\pm$ 0.017	—
09-BA-43	38.26358	-119.16825	Porphyritic lava flow in trachyandesite of Clark Canyon	Plagioclase	11.268 $\pm$ 0.11	—
088-21A	38.27363	-119.13962	Flow dome in trachyandesite of Aurora Canyon	Plagioclase	10.358 $\pm$ 0.025	—
098-13B	38.26802	-119.13218	Porphyritic intrusion in rhyolite of Bodie Hills	Sanidine	9.813 $\pm$ 0.027	—
088-24B	38.25504	-119.14115	Porphyritic lava flow in trachyandesite of Willow Springs	Plagioclase	8.575 $\pm$ 0.22	—
088-24A	38.25278	-119.13951	Porphyritic dome in rhyolite of Big Alkali	Plagioclase	6.201 $\pm$ 0.026	—
098-13A	38.25754	-119.12788	Porphyritic dome in rhyolite of Big Alkali	Plagioclase	6.173 $\pm$ 0.028	—
09-BA-42	38.27001	-119.14887	Porphyritic dome in rhyolite of Big Alkali	Biotite	5.455 $\pm$ 0.026	—
<b>Potato Peak AZ</b>						
Hydrothermal mineral						
08-BA-46	38.2443	-119.10385	Matrix of silicified breccia	Alunite	10.830 $\pm$ 0.06	—
Rhyolite of Bodie Hills						
08-BA-50	38.24816	-119.09663	Rhyolite	Sanidine	9.757 $\pm$ 0.013	—
Trachydacite of Potato Peak						
088-24D	38.22678	-119.10376	Porphyritic lava flow	Plagioclase	9.090 $\pm$ 0.04	—
108-12B	38.23830	-119.00784	Porphyritic biotite-hornblende dacite	Biotite	9.032 $\pm$ 0.022	—
098-13C	38.25072	-119.09223	Biotite rhyolite/dacite	Plagioclase	8.998 $\pm$ 0.021	—
088-24C	38.24786	-119.11208	Porphyritic lava flow	Plagioclase	8.996 $\pm$ 0.025	—
08-BA-68	38.1932	-119.0684	Porphyritic trachyandesite flow	Plagioclase	8.99 $\pm$ 0.02	—
098-10C	38.24919	-119.09203	Biotite-hornblende dacite	Plagioclase	8.982 $\pm$ 0.023	—
108-12A	38.24252	-119.04825	Porphyritic biotite-hornblende dacite	Plagioclase	8.963 $\pm$ 0.016	—
08-BA-61	38.2077	-119.1017	Block and ash flow	Plagioclase	8.93 $\pm$ 0.7	—
088-24E	38.21809	-119.10188	Biotite-hornblende dacite	Plagioclase	8.925 $\pm$ 0.03	—
088-21E	38.23457	-119.08582	Porphyritic lava flow	Plagioclase	8.860 $\pm$ 0.05	—
088-21B	38.2642	-119.0750	Porphyritic trachyandesite flow	Plagioclase	8.84 $\pm$ 0.13	—
088-21D	38.2433	-119.09209	Porphyritic lava flow	Plagioclase	8.810 $\pm$ 0.07	—
10-BA-46	38.1738	-119.1151	Porphyritic trachyandesite flow	Plagioclase	8.779 $\pm$ 0.013	—
10-BA-66	38.17250	-119.10125	Porphyritic lava flow	Plagioclase	8.749 $\pm$ 0.019	—

**Table 1.**  $^{40}\text{Ar}/^{39}\text{Ar}$  dates (Ma) of igneous and hydrothermal minerals in mining districts and alteration zones (AZ) of the Bodie Hills, determined by incremental heating and laser fusion. Some K-Ar and  $^{40}\text{Ar}/^{39}\text{Ar}$  dates (see footnotes) are from Kleinhampl and others (1975), Morton and others (1977), Breit (2000), and Larry Snee (written commun.); most  $^{40}\text{Ar}/^{39}\text{Ar}$  dates of igneous minerals are from John and others (2012). Dates are based on Fish Canyon Tuff sanidine=28.02 Ma. Coordinates are NAD27.—Continued

[—, no data; qtz, quartz; Kspar, potassium feldspar; K, potassium; py, pyrite; chlor, chlorite]

Sample number	Latitude (decimal degrees)	Longitude (decimal degrees)	Lithology and (or) location	Mineral	Age (Ma) and error (1 $\sigma$ )	Sample index number on figures
<b>Aurora Mining District</b>						
Volcanic rocks						
00-BA-16	38.2708	-118.8908	Porphyritic lava flow in trachyandesite of Aurora	Hornblende	<sup>3</sup> 13.130 $\pm$ 0.44	—
00-BA-26	38.2542	-118.8841	Porphyritic lava flow in trachyandesite of Aurora	Hornblende	<sup>3</sup> 13.130 $\pm$ 0.08	—
108-10A	38.27293	-118.91272	Fine-grained pyroxene trachyandesite of Aurora	Plagioclase	12.58 $\pm$ 0.024	—
108-10C	38.2805	-118.9062	Porphyritic lava flow in trachyandesite of West Brawley Peak	Plagioclase	11.514 $\pm$ 0.019	—
10-BA-21	38.30315	-118.8974	Porphyritic lava flow in rhyolite of Aurora Creek	Sanidine	11.181 $\pm$ 0.022	—
10-BA-27	38.275	-118.9045	Porphyritic intrusion(?) in rhyolite of East Brawley Peak	Sanidine	11.178 $\pm$ 0.016	—
10-BA-20	38.3168	-118.9113	Sparsely porphyritic lava flow in rhyolite of Aurora Creek	Plagioclase	11.177 $\pm$ 0.013	—
Hydrothermal minerals						
ESM	—	—	Altered andesite wall rock, Esmeralda vein	Illite	<sup>1,2</sup> 12.2 $\pm$ 0.3	—
CH8Z1	38.28361	-118.86889	Andesite altered to qtz-Kspar-K-mica-py-chlor; Juniata vein	Whole rock	<sup>2,4</sup> 10.9 $\pm$ 0.3	—
AU-1/58/DD61	38.266	-118.9	Esmeralda vein	K-feldspar	<sup>2,3</sup> 10.47 $\pm$ 0.1	—
AU-2/59/DD61	38.28437	-118.8934	Last Chance Hill, Del Monte shaft dump	K-feldspar	<sup>2,3</sup> 10.35 $\pm$ 0.05	—
FA1	38.2931	-118.8914	Prospectus vein	Adularia	<sup>1,2</sup> 10.04 $\pm$ 0.03	—
37	—	—	Quartz-adularia vein	Adularia	<sup>2,5</sup> 10.6 $\pm$ 0.2	—
<b>Four Corners AZ</b>						
Trachyandesite of Aurora Canyon						
088-23A	38.27852	-119.10021	Porphyritic flow dome	Biotite	10.580 $\pm$ 0.03	—
088-23B	38.27831	-119.09908	Porphyritic flow dome	Biotite	10.540 $\pm$ 0.05	—
088-23D	38.28113	-119.10206	Porphyritic flow dome	Biotite	10.460 $\pm$ 0.032	—
088-25A	38.27322	-119.09077	Porphyritic flow dome	Plagioclase	10.430 $\pm$ 0.03	—
088-23B	38.27831	-119.09908	Porphyritic flow dome	Plagioclase	10.310 $\pm$ 0.02	—
088-23A	38.27852	-119.10021	Porphyritic flow dome	Plagioclase	10.270 $\pm$ 0.11	—
088-23D	38.28113	-119.10206	Porphyritic flow dome	Plagioclase	10.270 $\pm$ 0.05	—
<b>Paramount-Bald Peak AZ</b>						
Volcanic rocks						
09-BA-35	38.2905	-119.0464	Porphyritic dacite plug	Biotite	11.269 $\pm$ 0.034	—
077-8B	38.2833	-119.0562	Porphyritic dacite plug	Sanidine	11.160 $\pm$ 0.03	—
077-8C	38.27145	-119.07783	Flow dome in trachyandesite of Aurora Canyon	Biotite	10.467 $\pm$ 0.04	—
077-8C	38.27145	-119.07783	Flow dome in trachyandesite of Aurora Canyon	Sanidine	10.447 $\pm$ 0.01	—
077-8C	38.27145	-119.07783	Flow dome in trachyandesite of Aurora Canyon	Plagioclase	10.426 $\pm$ 0.03	—
08-BA-65	38.3107146	-118.978084	Glassy lava flow in rhyolite of Bald Peak	Sanidine	9.686 $\pm$ 0.01	—
09-BA-49	38.26389	-119.04748	Trachydacite ignimbrite in Eureka Valley Tuff	Biotite	9.267 $\pm$ 0.019	—
<b>Cinnabar Canyon-US 395 AZ</b>						
Trachyandesite of Mount Biedeman						
108-9A	38.1654	-119.0982	Biotite hornblende andesite lava	Plagioclase	9.947 $\pm$ 0.019	—
108-12F	38.1634	-119.0992	Glassy porphyritic andesite lava	Plagioclase	9.939 $\pm$ 0.024	—
10-BA-61	38.1401	-119.0155	Glassy block and ash flow	Plagioclase	9.676 $\pm$ 0.061	—
6-215-1	38.1344	-119.0825	Hornblende andesite lava	Plagioclase	<sup>3</sup> 9.24 $\pm$ 0.008	—
098-11E	38.1110	-119.1584	Hornblende andesite lava	Plagioclase	9.019 $\pm$ 0.028	—
09-BA-22	38.1430	-119.1797	Pyroxene andesite flow	Plagioclase	8.996 $\pm$ 0.10	—
09SB015A	38.1231	-119.1484	Porphyritic trachyandesite lava	Plagioclase	8.895 $\pm$ 0.06	—

## 8 Gold-Silver Mining Districts, Alteration Zones, and Paleolandforms in the Miocene Bodie Hills Volcanic Field

**Table 1.**  $^{40}\text{Ar}/^{39}\text{Ar}$  dates (Ma) of igneous and hydrothermal minerals in mining districts and alteration zones (AZ) of the Bodie Hills, determined by incremental heating and laser fusion. Some K-Ar and  $^{40}\text{Ar}/^{39}\text{Ar}$  dates (see footnotes) are from Kleinhampl and others (1975), Morton and others (1977), Breit (2000), and Larry Snee (written commun.); most  $^{40}\text{Ar}/^{39}\text{Ar}$  dates of igneous minerals are from John and others (2012). Dates are based on Fish Canyon Tuff sanidine=28.02 Ma. Coordinates are NAD27.—Continued

[—, no data; qtz, quartz; Kspar, potassium feldspar; K, potassium; py, pyrite; chlor, chlorite]

Sample number	Latitude (decimal degrees)	Longitude (decimal degrees)	Lithology and (or) location	Mineral	Age (Ma) and error (1 $\sigma$ )	Sample index number on figures
<b>Hydrothermal minerals</b>						
CC09-9D1	38.19869	-119.1705	Matrix of silicified breccia in altered dacite(?)	Alunite	8.820 $\pm$ 0.29	—
CC09-9D2	38.19869	-119.1705	Veins cutting silicified breccia	Alunite	8.680 $\pm$ 0.02	—
39509-3K	38.20793	-119.22751	Partially leached clasts in volcanoclastic deposits	Alunite	8.169 $\pm$ 0.013	—
<b>Trachyandesite of Willow Springs</b>						
088-24B	38.25504	-119.14115	Porphyritic hornblende-pyroxene trachyandesite	Plagioclase	8.575 $\pm$ 0.022	—
08-BA-51	38.17449	-119.15441	Dacite flow breccia	Plagioclase	8.305 $\pm$ 0.017	—
088-24F	38.20176	-119.08978	Olivine-pyroxene trachyandesite	Plagioclase	8.154 $\pm$ 0.02	—
077-7B	38.19178	-119.1524	Lava flow	Biotite	8.124 $\pm$ 0.03	—
077-7B	38.19178	-119.1524	Lava flow	Plagioclase	8.094 $\pm$ 0.03	—
077-7B	38.19178	-119.1524	Lava flow	Hornblende	8.073 $\pm$ 0.02	—
077-7A	38.19178	-119.1524	Lava flow	Plagioclase	8.053 $\pm$ 0.02	—
077-7A	38.1786	-119.19476	Lava flow	Biotite	8.002 $\pm$ 0.04	—
<b>Dacite of Hot Springs Canyon</b>						
39509-10	38.21532	-119.22755	Lava flow	Plagioclase	8.070 $\pm$ 0.017	—
<b>Bodie Mining District</b>						
<b>Dacite of Silver Hill</b>						
108-12E	38.20763	-118.96489	Porphyritic biotite-hornblende dacite	Plagioclase	9.140 $\pm$ 0.020	1
09-BA-26	38.2036	-119.00021	Block and ash flow in dacite of Silver Hill	Biotite	9.132 $\pm$ 0.02	2 (fig. 37)
108-12C	38.18925	-118.98343	Porphyritic clinopyroxene-biotite dacite	Plagioclase	9.088 $\pm$ 0.014	3
077-6F	38.18809	-119.00854	Dome in dacite of Silver Hill	Plagioclase	9.088 $\pm$ 0.03	4 (fig. 37)
08-BA-66	38.1863	-119.0568	Block and ash flow	Plagioclase	9.07 $\pm$ 0.024	5
108-12D	38.17315	-118.97800	Porphyritic oxyhornblende-biotite dacite	Plagioclase	9.017 $\pm$ 0.014	6
077-7F	38.20252	-119.0263	Late intrusion in dacite of Silver Hill	Plagioclase	8.925 $\pm$ 0.03	7 (fig. 37)
<b>Silver Hill series veins</b>						
09-BA-28I	38.2015	-119.0036	Red Cloud Mine dump	Adularia	8.852 $\pm$ 0.013	8 (fig. 37)
BOD09-3	38.20146	-119.0048	Red Cloud Mine dump	Adularia	8.628 $\pm$ 0.014	9 (fig. 37)
BOD09-5	38.2043	-119.0066	Oro Mine dump	Adularia	8.473 $\pm$ 0.007	10 (fig. 37)
AU-18/65/DD61	38.201	-119.004	Red Cloud Mine dump	Adularia	<sup>2,3</sup> 8.46 $\pm$ 0.02	11 (fig. 37)
<b>Burgess series veins</b>						
BOD11-3B	38.21257	-119.00402	Layered vein; Upper Hobart Tunnel dump	Adularia	8.542 $\pm$ 0.025	12 (fig. 37)
11-BA-22	38.21257	-119.00402	Bodie Mine dump	Adularia	8.498 $\pm$ 0.005	13 (fig. 37)
BOD11-4E	38.21257	-119.00402	Bodie Mine dump	Adularia	8.426 $\pm$ 0.003	14 (fig. 37)
AU-16/63/DD61	38.215	-119.004	Roseklip open-cut, southeast slope Standard Hill	Adularia	<sup>2,3</sup> 8.38 $\pm$ 0.02	15 (fig. 37)
<b>Incline series veins</b>						
077-6A	38.2149	-119.0037	Upper southeast slope Standard Hill	Adularia	8.290 $\pm$ 0.02	16 (fig. 37)
AU-17/64/DD61	38.215	-118.997	Tioga Mine dump	Adularia	<sup>2,3</sup> 8.28 $\pm$ 0.04	17 (fig. 37)
11-BA-7G	38.2042	-119.00649	Oro Mine dump	Adularia	8.217 $\pm$ 0.012	18 (fig. 37)
11-BA-21	38.2037	-119.00919	Nooday Mine dump	Adularia	8.124 $\pm$ 0.006	19 (fig. 37)
<b>Uncorrelated veins</b>						
12-BA-17	38.21961	-119.00083	Euhedrons in lenticular vug in narrow vein; dump, top of Bodie Bluff	Adularia	8.358 $\pm$ 0.029	20 (fig. 37)
BOD11-3A	38.21961	-119.00354	Euhedrons in lenticular vug in narrow vein; Upper Hobart Tunnel dump	Adularia	8.194 $\pm$ 0.005	21 (fig. 37)

<sup>1</sup>Breit (2000); age standard not provided; location coordinates for some samples not provided.

<sup>2</sup>Age standard not provided and age may have been calculated using Taylor Creek rhyolite age=27.84 Ma.

<sup>3</sup>Analysis by L. Snee.

<sup>4</sup>Morton and others, 1977.

<sup>5</sup>Kleinhampl and others, 1975.

**Table 2.** Sulfur isotope compositions (‰) of sulfide and sulfate minerals and sulfur (S°) from mining districts and alteration zones, and calculated sulfur (S) isotope equilibrium temperatures.

[Some analyses are from Vikre (2000) and Vikre and Henry (2011); others were provided by Simon Poulson (University of Nevada Reno, Reno, Nev.). Sulfur isotope equilibrium temperatures (T °C SO<sub>4</sub>-py) were calculated from fractionation equations in Field and Fifarek (1985). AZ, alteration zone; en, enargite; py, pyrite; ISV, Incline series vein; BSV, Burgess series vein; FV, Fortuna vein; SHSV, Silver Hill series vein; —, no data]

Sample number	Mineral	Location	$\delta^{34}\text{S}$ sulfide minerals	$\delta^{34}\text{S}$ S°	$\delta^{34}\text{S}$ alunite; barite	T °C SO <sub>4</sub> -py
<b>Masonic Mining District</b>						
Sarita Mine						
MAS07-3	Enargite	Mill loading bin reject	-10.4	—	—	<sup>1</sup> 192; en=py
MAS07-3A	Alunite	Mill loading bin reject	—	—	18.1	—
Red Rock Mine						
MAS09-1	Alunite	Mine dump, hillside	—	—	13.4	—
MAS09-1	Pyrite	Mine dump, hillside	-11.0	—	—	231
MAS09-1	Enargite	Mine dump, hillside	-10.5; -10.2	—	—	<sup>1</sup> 238; 228; en=py
MAS09-1	Alunite	Mine dump, hillside	—	—	14.5	—
MAS09-3a	Enargite	Mine dump	-12.2	—	—	—
Chemung Mine						
MAS07-1A	Alunite	Cut	—	—	15.4	—
MD82-2A	Sulfur	Mill dump	—	-16.8	—	—
MD82-2A	Sulfur	Mill dump	—	-16.5	—	—
MD82-2A	Sulfur	Mill dump	—	-16.9	—	—
MD88-1s	Pyrite	Mill dump	-9.4	—	—	—
MD88-4s	Luzonite	Mill dump	-11.8	—	—	—
MD88-1Bs	Barite	Mill dump	—	—	13.6	—
MD88-3As	Alunite	Mill dump	—	—	7.1	—
Pittsburg-Liberty Mine						
MAS10-62	Pyrite	Dump on Masonic Gulch	-10.6	—	—	218
MAS10-62	Alunite	Dump on Masonic Gulch	—	—	15.1	—
Perini Mine						
MAS11-2B	Pyrite	Upper dump on Red Wash	-9.4	—	—	188
MAS11-2B	Alunite	Upper dump on Red Wash	—	—	19.6	—
MAS11-3B	Enargite	Upper dump on Red Wash	-12.2	—	—	<sup>1</sup> 167; en=py
Maybell-Alton Jack Mine						
MAS08-21	Pyrite	Middle dump	-10.0	—	—	—
MAS08-22	Pyrite	Lower dump	-8.0	—	—	—
Aspen Grove Mine						
MAS08-23	Pyrite	Prospect dump	-7.9	—	—	198
MAS08-23	Enargite	Prospect dump	0.2	—	—	<sup>1</sup> 283; en=py
MAS08-23	Alunite	Prospect dump	—	—	19.9	—
<b>Red Wash-East Walker River AZ</b>						
RW08-1	Alunite	Western end of AZ	—	—	20.60	—
<b>Sawtooth Ridge AZ</b>						
SAW11-9	Alunite	Del Monte Creek	—	—	-3.2	—
<b>Potato Peak AZ</b>						
POTPK08-1	Cinnabar	Alta Plana Mine open cut	-10.30	—	—	—
POTPK08-1	Cinnabar	Alta Plana Mine open cut	-9.80	—	—	—
POTPK08-1	Barite	Alta Plana Mine open cut	—	—	11.60	—
08-BA-46	Alunite	Alta Plana Mine open cut	—	—	16.30	—

## 10 Gold-Silver Mining Districts, Alteration Zones, and Paleolandforms in the Miocene Bodie Hills Volcanic Field

**Table 2.** Sulfur isotope compositions (‰) of sulfide and sulfate minerals and sulfur (S°) from mining districts and alteration zones, and calculated sulfur (S) isotope equilibrium temperatures.—Continued

[Some analyses are from Vikre (2000) and Vikre and Henry (2011); others were provided by Simon Poulson (University of Nevada Reno, Reno, Nev.). Sulfur isotope equilibrium temperatures (T °C SO<sub>4</sub>-py) were calculated from fractionation equations in Field and Fifearek (1985). AZ, alteration zone; en, enargite; py, pyrite; ISV, Incline series vein; BSV, Burgess series vein; FV, Fortuna vein; SHSV, Silver Hill series vein; —, no data]

Sample number	Mineral	Location	δ <sup>34</sup> S sulfide minerals	δ <sup>34</sup> S S°	δ <sup>34</sup> S alunite; barite	T °C SO <sub>4</sub> -py
<b>Aurora District</b>						
K011	Sulfides	Antelope Mine <sup>2</sup>	8.3	—	—	—
K229	Sulfides	Antelope Mine <sup>2</sup>	-8.7	—	—	—
K147	Sulfides	Amador Mine <sup>2</sup>	10.6	—	—	—
K155	Sulfides	Amador Mine <sup>2</sup>	10.9	—	—	—
K208	Sulfides	Martinez Tunnel <sup>2</sup>	-8.5	—	—	—
K2079	Sulfides	Wide West Mine	-7	—	—	—
AUR12-1A	Pyrite	New Esmeralda Mine cut	-6.3	—	—	—
AUR12-2A	Sulfides	Esmeralda vein, S end	-5.4; -2.4	—	—	—
<b>Paramount-Bald Peak AZ</b>						
PM08-1A	Cinnabar	Paramount Mine upper adit	-4.70	—	—	—
PM08-1B	Cinnabar	Paramount Mine upper adit	-5.30	—	—	—
<b>Cinnabar Canyon-US 395 AZ</b>						
CC08-1	Cinnabar	Calmono Mine dump	-0.1	—	—	—
CC08-1	Cinnabar	Calmono Mine dump	-0.7	—	—	—
08-BA-54A	Alunite	drainage W of Cinnabar Canyon	—	—	2.5	—
CAMO91-1As	Sulfur	DDH core <sup>3</sup>	—	-4.6	—	—
CAMO91-1Bs	Sulfur	DDH core <sup>3</sup>	—	-5.2	—	—
CCD7	Sulfur	DDH core; surface discards	—	-4.7	—	—
CCD7	Sulfur	DDH core; surface discards	—	-4.7	—	—
CCD8B	Sulfur	DDH core; surface discards	—	—	—	—
CCD8B	Pyrite 1	DDH core; surface discards	-8.0	—	—	—
CCD16	Pyrite 2	DDH core; surface discards	-9.8	—	—	—
CCD16	Barite	DDH core; surface discards	—	—	1.1	—
<b>Bodie Mining District</b>						
BOD11-11A	Pyrite	Bodie Mine dump; ISV	1.4	—	—	—
OD 7604	Sulfides	Standard Mine, 528 level; FV <sup>4</sup>	0.6	—	—	—
CSMMM-1793	Sulfides	Jupiter Mine; BSV? <sup>5</sup>	-2.4	—	—	—
CSMMM-7045	Sulfides	Mono Mine; BSV <sup>5</sup>	-4.7	—	—	—
CSMMM-7638	Sulfides	Belvedere Mine; BSV <sup>5</sup>	0.3	—	—	—
BOD09-7	Acanthite	Lent Mine dump; BSV?	-1.8	—	—	—
BOD11-1	Galena	Oro Mine dump; SHSV	-1.5	—	—	—
BOD11-1F	Chalcopyrite	Oro Mine dump; SHSV	-0.1	—	—	—
CSMMM-5304	Sulfides	Oro Mine, 520 level; SHSV <sup>5</sup>	-0.9	—	—	—
BOD11-2A	Tetrahedrite	Contention Mine dump; SHSV	0.5	—	—	—
BOD11-5	Tetrahedrite	Red Cloud Mine dump; SHSV	-3.4	—	—	—
BOD11-22B	Chalcopyrite	S slope Bodie Bluff; SHSV	0.1	—	—	—
CSMMM-2009	Sulfides	Addenda Mine, 500 level; SHSV <sup>5</sup>	-0.0	—	—	—
CSMMM-7568	Tetrahedrite	West Noonday Mine; SHSV <sup>5</sup>	0.6	—	—	—

<sup>1</sup>Temperature calculated based on pyrite-alunite fractionation.

<sup>2</sup>Keck collection, University of Nevada Reno (Reno, Nev.).

<sup>3</sup>Sample provided by M. Ward.

<sup>4</sup>Mackay-Stanford collection, University of Nevada Reno (Reno, Nev.).

<sup>5</sup>California State Mining and Mineral Museum collection (Mariposa, Calif.).



**Table 3.** Reporting limits (concentration range) for element concentrations in tables A-1 through A-12.

[Concentrations were determined by fire assay-inductively coupled plasma-mass spectrometry (Au, Pd, Pt), cold-vapor and hydride generation atomic absorption (Hg), hydride generation atomic absorption (Se), automated sulfur analyzer (S), and inductively coupled-atomic emission spectrometry-mass spectrometry (all other elements); ppm, part per million; ppb, part per billion]

Element	Concentration range	
Aluminum, Al	0.01%	15%
Antimony, Sb	0.05 ppm	1%
Arsenic, As	1 ppm	1%
Barium, Ba	5 ppm	1%
Beryllium, Be	0.1 ppm	100 ppm
Bismuth, Bi	0.04 ppm	1%
Cadmium, Cd	0.1 ppm	1%
Calcium, Ca	0.01%	40%
Cerium, Ce	0.05 ppm	0.10%
Cesium, Cs	0.05 ppm	0.10%
Chromium, Cr	1 ppm	1%
Cobalt, Co	0.1 ppm	1%
Copper, Cu	0.5 ppm	1%
Gallium, Ga	0.05 ppm	500 ppm
Gold	1 ppb	10 ppm
Indium, In	0.02 ppm	0.05%
Iron, Fe	0.01%	50%
Lanthanum, La	0.5 ppm	0.10%
Lead, Pb	0.5 ppm	5%
Lithium, Li	1 ppm	5%
Magnesium, Mg	0.01%	15%
Manganese, Mn	5 ppm	5%
Mercury, Hg	0.02 ppm	not provided
Molybdenum, Mo	0.05 ppm	1%
Nickel, Ni	0.5 ppm	1%
Niobium, Nb	0.1 ppm	0.1%
Palladium, Pd	1 ppb	10 ppm
Phosphorous, P	50 ppm	1%
Platinum, Pt	0.5 ppb	10 ppm
Potassium, K	0.01%	15%
Rubidium, Rb	0.2 ppm	1%
Scandium, Sc	0.1 ppm	0.10%
Selenium, Se	0.2 ppm	4 ppm
Silver, Ag	1 ppm	1%
Sodium, Na	0.01%	15%
Strontium, Sr	0.5 ppm	1%
Sulfur, S	0.01%	5%
Sulfur, S	0.05%	35%
Tellurium, Te	0.1 ppm	0.05%
Thallium, Tl	0.1 ppm	1%
Thorium, Th	0.2 ppm	1%
Tin, Sn	0.1 ppm	0.10%
Titanium, Ti	0.01%	15%
Tungsten, W	0.1 ppm	1%
Uranium, U	0.1 ppm	1%
Vanadium, V	1 ppm	1%
Yttrium, Y	0.1 ppm	1%
Zinc, Zn	1 ppm	5%

gray, green, and purplish, unaltered to propylitically altered andesite, dacite, and rhyolite, and the beige to red-brown coloration of pervasively altered rocks have been used to approximate the areal extent of alteration zones. The margins of alteration zones are marked by a transition outward from pervasive discoloration and primary mineral hydrolysis to alteration mineral assemblages that are confined to fracture selvages and phenocrysts. However, because of map scale, margin irregularities, and transitional contacts, small volumes of less-altered rocks are included within alteration zones, and small volumes of pervasively altered rocks are excluded.

Descriptions of mining districts and alteration zones in the Bodie Hills provide information on characteristics that may be useful to exploration programs and mineral resource assessments. In addition, the evolution of landforms presented in this report is pertinent to the tectonic history of the Sierra Nevada and western Great Basin.

## Bodie Hills Volcanic Field

The Bodie Hills comprise a >700 square kilometers (km<sup>2</sup>), 15–6 Ma volcanic field north of Mono Lake, California. The field consists of coalescing stratovolcanoes and lava domes that were assembled onto an irregular pre-Tertiary surface composed of Paleozoic and Mesozoic metavolcanic and metasedimentary rock, and Cretaceous granitic rocks of the Sierra Nevada batholith ~8 kilometers (km) to the west (Eaton and others, 1978; John and others, 2012). The field includes ~25 major eruptive units that comprise four trachyandesite stratovolcanoes emplaced along the margins of the field, and numerous, more centrally located, silicic trachyandesite to rhyolite flow-dome complexes. The ~40 by ~30 km field is in the southern segment of the ancestral Cascades magmatic arc, a subduction-related alignment of predominantly andesitic eruptive rocks that parallels the western margin of North America from southern Nevada to British Columbia. Compositions of most Bodie Hills volcanic rocks closely resemble those of subduction magmas worldwide, with SiO<sub>2</sub> varying from 50 to 77 weight percent, and high K, Ba/Nb, Ba/Ta, and La/Nb (see table 3 for a complete list of elemental abbreviations). Most of the rocks are porphyritic, commonly containing 15–35 volume percent phenocrysts of plagioclase, pyroxene, hornblende, and biotite. Geophysical data imply that the volcanic rocks were derived from shallow (<2 km deep), subjacent magma reservoirs that solidified to low-density plutons (John and others, 2012). The field is within the Walker Lane, a major northwest-trending zone of right-lateral structural accommodation between the Pacific and North American plates (Stewart, 1988, 1992). It is northwest of and marginal to the Mina deflection, a complex, northeast-trending structural zone of faults that offset Walker Lane faults north of the Bodie Hills to the east (Stewart, 1988; Hardyman and Oldow, 1991; Oldow, 1992; Oldow, 2003; Wesnousky, 2005; Faulds and Henry, 2008). Present elevations of volcanic rocks in the field are between ~6,500 feet (ft) (~1,970 meters [m]), the elevation of Bridgeport Valley, and 10,240 ft (~3,110 m), the elevation of Potato Peak.

Trachyandesite stratovolcanoes and trachydacite to rhyolite dome complexes in the Bodie Hills are as much as 16 km in diameter. Most formed during two periods of eruptive activity: trachyandesite stratovolcanoes at 14.7–12.9 Ma, and trachyandesite-dacite complexes at 9.2–8.0 Ma (John and others, 2012). Smaller rhyolite domes and flow-domes were emplaced from ~6.2 to 5.5 Ma (John and others, 2012). The Miocene volcanic rocks are interbedded with, and overlain by, conglomerate and sandstone of Fletcher and Bridgeport Valleys (Gilbert and Reynolds, 1973). Following a 2 m.y. (million year) hiatus in volcanism, postsubduction rocks of the ~3.9–0.1 Ma, bimodal (trachybasalt to rhyolite), high-K Aurora volcanic field erupted unconformably onto rocks of the Bodie Hills volcanic field (Gilbert and others, 1968; Al-Rawi, 1969; Chesterman and Gray, 1975; Kleinhampl and others, 1975; Lange and others, 1993).

The scarcity of dikes in the volcanic field indicates a low horizontal component of stress in the middle and late Miocene. However, veins and faults in the three mining districts mark a change in strain vectors during evolution of the field from transtension, characteristic of Walker Lane tectonism, to extension at ~10 Ma when subduction ceased at the latitude of the Bodie Hills (Atwater and Stock, 1998). Compared to other volcanic fields in the southern segment of the Cascades arc, the prevalence of stratovolcanoes and domes of intermediate to silicic composition and absence of mafic rocks in the Bodie Hills may signify that a relatively thick crust lies beneath the volcanic field. Mafic, mantle-derived magma differentiated within this crust to form predominantly silicic eruptives with uniformly porphyritic texture (John and others, 2012). Plagioclase, pyroxene, hornblende, and biotite phenocrysts are present in most of the volcanic rocks. Olivine phenocrysts occur in some andesites; sanidine and quartz phenocrysts are present in most rhyolites. The groundmass of most rocks contains variable microphenocryst assemblages, chiefly plagioclase, but also Fe-Ti oxide minerals, clinopyroxene, and less commonly, hornblende and (or) biotite. Common accessory minerals are apatite and zircon.

## Methods

Descriptions of mining districts and alteration zones are based on mapping and geophysical surveys, on published and unpublished reports and maps, and on samples collected and borrowed from archival repositories for mineral identification and textural analysis by petrography, X-ray diffraction (XRD), scanning electron microscopy (SEM), and short wave infrared spectrometry (SWIR). Other samples were collected for radioisotopic dating, and for determination of sulfur isotope compositions and minor element concentrations. Remotely sensed spectra, Advanced Spaceborne Thermal Emission and Reflection Radiometer (ASTER) data, were analyzed to determine the large-scale distribution and characteristics of hydrothermal mineral assemblages throughout the Bodie Hills.

Archival samples were borrowed from the Keck Museum at the University of Nevada Reno (Reno, Nevada), and from

the California State Mining and Mineral Museum (Mariposa, California). Instrumental analyses (XRD, SEM, geochronology, isotope compositions, and element concentrations) were performed in laboratories at the U.S. Geological Survey (Menlo Park, California; Denver, Colorado), University of Nevada Reno (Reno, Nevada), and SGS Mineral Services (Toronto, Canada). SWIR analyses of hand samples used a portable infrared mineral analyzer (PIMA).

Some K-Ar and  $^{40}\text{Ar}/^{39}\text{Ar}$  ages used in this investigation are from Kleinhampl and others (1975), Morton and others (1977), Breit (2000), John and others (2012), and Larry Snee (unpublished analyses). Additional  $^{40}\text{Ar}/^{39}\text{Ar}$  ages (Ma) of igneous and hydrothermal minerals were determined by the incremental heating (multi-step) and laser fusion (single-step) methods (table 1). Following neutron irradiation of a single split of a sample, radiogenic  $^{40}\text{Ar}$  and potassium-derived  $^{39}\text{Ar}$  from neutron activation were simultaneously measured (for example, Dalrymple and Lanphere, 1974; McDougall and Harrison, 1999). Heating to release Ar was provided by laser, induction furnace, or resistance furnace. A series of incremental heating steps that comprises more than 50 percent of the total argon release, and in which each step gives an age within two standard deviations of the mean, defines a “plateau” age (Fleck and others, 1977). Laser fusion and furnace experiments that release all Ar from the sample in a single heating step provide “laser-fusion” or “total-gas” ages. Ages calculated by mathematically recombining the Ar released in all steps of incremental-heating experiments are referred to as “integrated” ages. Uncertainties for all Ar ages are reported at 1 standard error of the weighted mean (Renne and others, 2009).

Some sulfur isotope compositions ( $\delta^{34}\text{S}$ ) of sulfide minerals, sulfate minerals, and native sulfur ( $\text{S}^0$ ) used in this investigation are from Vikre (2000) and Vikre and Henry (2011; table 2). Additional  $\delta^{34}\text{S}$  values were determined by Simon Poulson (University of Nevada Reno) using a Eurovector model 3028 elemental analyzer interfaced to a Micromass IsoPrime stable isotope ratio mass spectrometer, and following the methods of Giesemann and others (1994) and Grassineau and others (2001). The  $\delta^{34}\text{S}$  values are reported in units of per mil, part per thousand (‰) versus VCDT (Vienna Canyon Diablo troilite), and have an uncertainty of  $\pm 0.2$  ‰. Sulfur isotope equilibrium temperatures were calculated from fractionation equations in Field and Fifarek (1985).

Geochemical analyses were obtained under a U.S. Geological Survey contract with SGS Mineral Services. Element concentrations were determined using several multi-element analytic methods with variable reporting limits (given as concentration ranges in table 3). Analytic methods included fire assay (FA)-inductively coupled plasma mass spectrometry (ICPMS) for Au, Pd, Pt, cold-vapor atomic absorption (AA) for Hg, hydride generation AA for Se, and inductively coupled plasma-atomic emission spectrometry-mass spectrometry (ICP-AES-MS) for all other elements except sulfur. Sulfur concentrations were determined using an automated sulfur analyzer. These methods were selected to include elements of economic interest (Au, Ag, Hg, As, Sb, Te, Se, Sn, Cu, Pb, Zn, and S).

Atomic proportions of minerals and some mineral identities shown on SEM images were determined using integrated software. Atomic proportions of elements were normalized to one. Atomic proportions of sulfide, selenide, and telluride minerals were calculated to positive integers of S, Se, or Te atoms, with the number of S, Se, or Te atoms corresponding to atoms per formula unit of the petrographically identified mineral. For minerals in which petrographic characteristics and atomic proportions do not correspond to documented minerals, atomic proportions were iteratively calculated relative to positive integers of S atoms to produce positive integers, or integers plus fractions, of other major atoms (for example, Cu, Ag). Comparison of atomic proportions of analyzed chalcopyrite to stoichiometric chalcopyrite, and replicate analyses, suggest an accuracy of  $\pm 0.2$  atoms.

## Masonic Mining District

### Location

Secs. 14, 15, 16, 17, 20, 21, 22, 23, 29, 30, T. 6 N., R. 26 E., Mono County, California, Lyon County, Nevada (fig. 1)

### History and Production

Gold was discovered in the Masonic Mining District in the 1860s by placer miners from Monoville (abandoned; originally located on Virginia Creek near Conway Summit), who named the district after the Freemasonry fraternal organization. In the latter half of the 19th century, mining activity in the Bodie Hills was focused on high-grade Au-Ag veins at Aurora and Bodie, and little development took place at Masonic until 1900–1902 when the Jump-Up-Joe and Pittsburg-Liberty Mines were located. Three towns were established: Upper, Middle, and Lower Masonic had a combined population that reached  $\sim 1,000$ . Gold and lesser Ag and Cu production occurred mainly during the period 1906–20 (McLaughlin, 1915; Eakle, and others, 1917; Eakle and McLaughlin, 1919; Sampson, 1940). Production was sporadic because mining small, irregular deposits was often unprofitable, and because Au recovery by different milling operations was, at best, marginally successful. Episodic but short-lived mining revivals with small and mostly unrecorded production took place from the 1920s to 1960s (Sampson, 1940; Jenkins, 1951; Wedertz, 1969; Mono County Historical Society 2004 Newsletter).

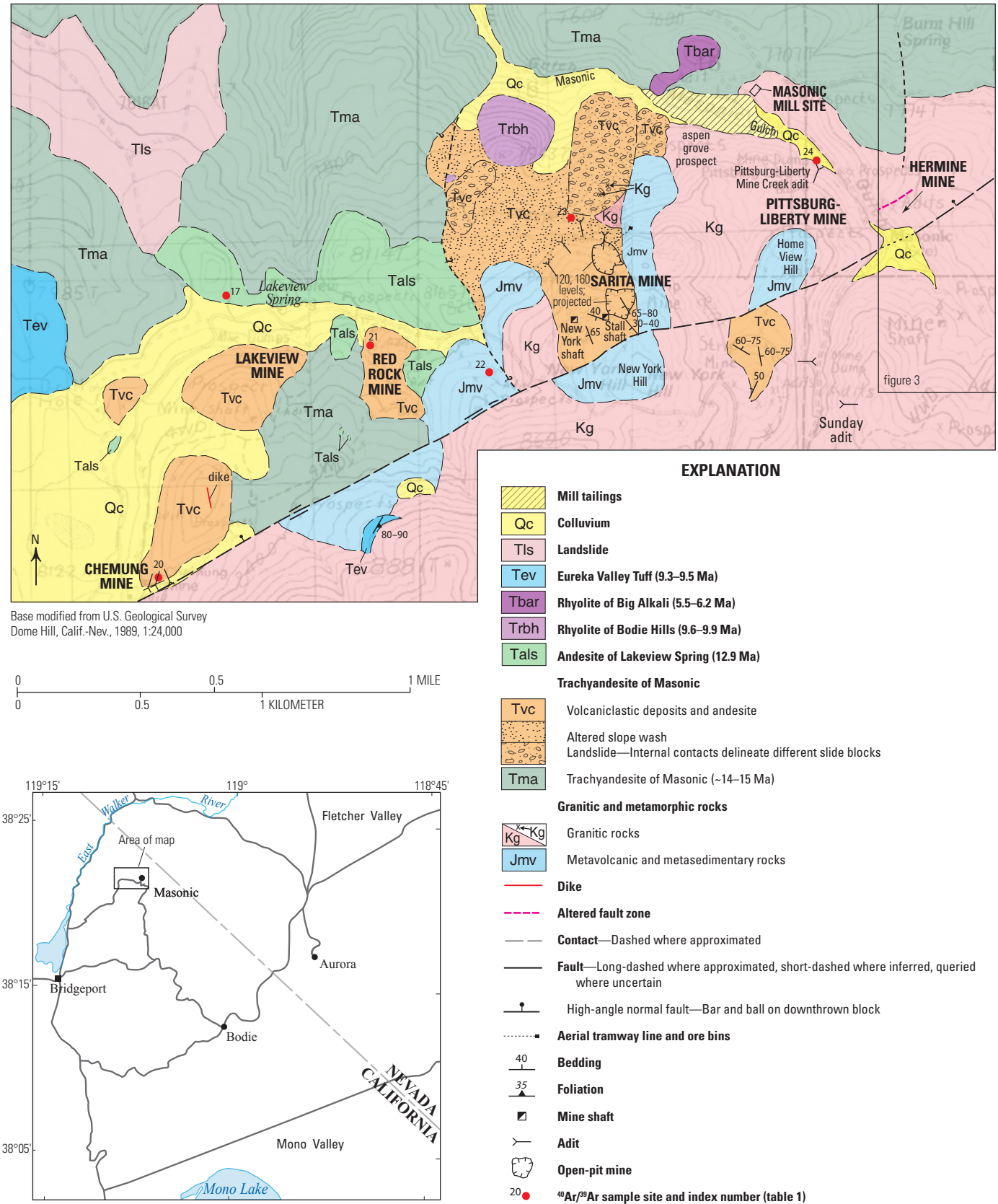
Production totals are incompletely known because of the numerous small and episodic mining operations that spanned five or more decades. Total district production from 1902 through 1959 is estimated at 55,800 ounces (oz) of Au, and 39,000 oz of Ag from  $\sim 75,000$  tons (t) of ore; minor amounts of Cu were also recovered (Long and others, 1998). The first ore shipment in 1907 (to the Selby, California, smelter), from the Pittsburg-Liberty Mine, consisted of 17 t valued at \$1,040 per ton, or about 50 troy ounces per ton (opt) Au if all

value was gold (at  $\sim \$20/\text{oz}$ ). Pittsburg-Liberty production is estimated at \$600,000 to \$700,000 ( $\sim 30,000$  to 35,000 oz of Au, if all value was Au; Eakle and McLaughlin, 1919). Sarita Mine production was \$425,000 ( $\sim 20,000$  oz of Au, if all value was Au), and Chemung Mine production was 3,700 oz of Au (R.T. Wilson and W.A. Rehrig, written commun., 1987). Ore grades at the Sarita and Lakeview Mines were reportedly 0.2–2 opt Au (Eakle and McLaughlin, 1919). An unpublished assay plan ( $\sim 1930$ s) of Sarita underground levels shows similar Au grades. An unpublished (1935) map of the Perrini Mine underground workings includes eight samples containing trace–0.18 opt Au, and 0.6–30.02 opt Ag over widths of 2–6.7 ft (R.T. Wilson and W.A. Rehrig, written commun., 1987). Drilling programs by several mining companies in the 1980s identified a resource of  $\sim 180,000$  tons at 0.15 opt Au at the Sarita Mine (R.T. Wilson and W.A. Rehrig, written commun., 1987). It appears that some of this resource was mined from an open cut on the northwest side of New York Hill since the 1980s, although processing facilities for this excavation are not evident.

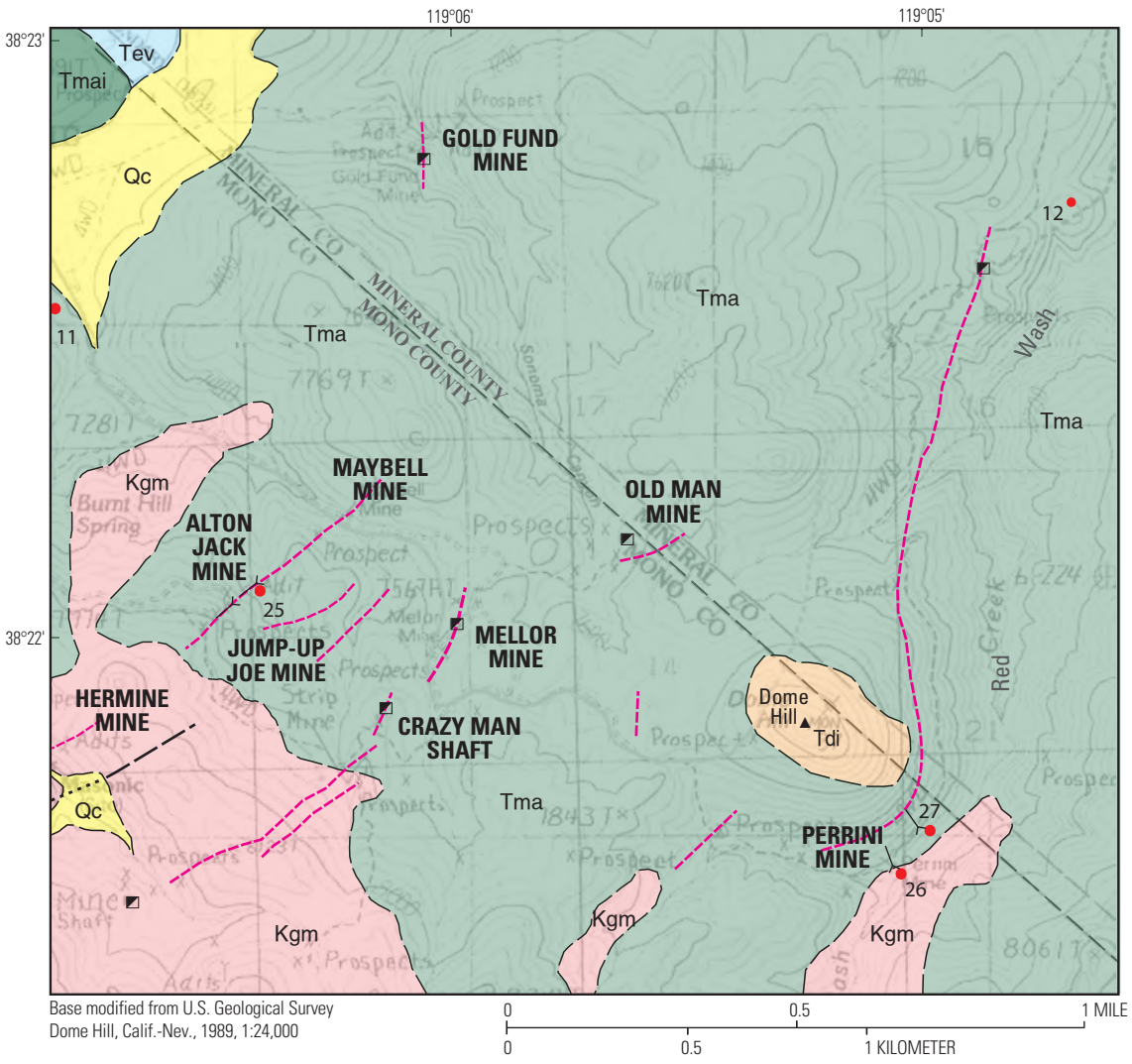
### Stratigraphy

Published geologic maps and lithologic descriptions of the Masonic Mining District include those in Eakle and McLaughlin (1919), Johnson (1951), Vikre and Henry (2011), and John and others (2012). The oldest rocks in the district are Jurassic(?) metavolcanic rocks (Jmv) that are extensively exposed at lower elevations on Masonic Mountain (9,195 ft). These pre-Tertiary rocks, thought to represent metasomatized rhyolite (Johnson, 1951), form pendants in Mesozoic granitic rocks (Kg; fig. 2). Mesozoic granitic rocks consist of pale-gray to pinkish-gray, hypidiomorphic granular, equigranular to porphyritic granodiorite and minor monzogranite that comprise Masonic Mountain; a smaller mass of granodiorite is exposed about 6 km to the east (John and others, 2012). The medium-grained, 95.2 Ma granodiorite (Robinson and Kistler, 1986) contains prominent, euhedral, perthitic, pink potassium feldspar megacrysts 2–5 centimeters (cm) long, and about 3 volume percent red-brown biotite (Johnson, 1951; John and others, 2012; du Bray and others, 2013). The granitic rocks form a plutonic mass covered in most places by trachyandesite of Masonic.

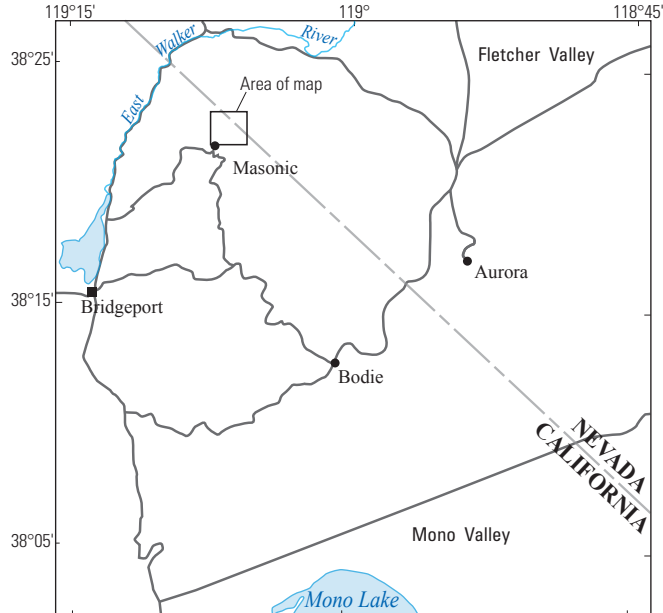
The trachyandesite of Masonic is pale- to medium-dark-gray, gray-green, and purplish, and variably porphyritic, and includes basaltic trachyandesite, trachydacite, basaltic andesite, and andesite. It comprises interbedded lava flows and mostly small-volume plugs and domes of trachyandesite that were erupted from 15 to 14 Ma (Tma, table 1), and includes associated volcanoclastic deposits (Tvc; figs. 2, 3, 4). Trachyandesite flows and volcanoclastic deposits aggregate tens to hundreds of meters in thickness. Combined, the lava flows, intrusions, and volcanoclastic deposits that make up the trachyandesite of Masonic define the nearly circular Masonic stratovolcano in the northwestern part of the Bodie Hills volcanic field (John and others, 2012).



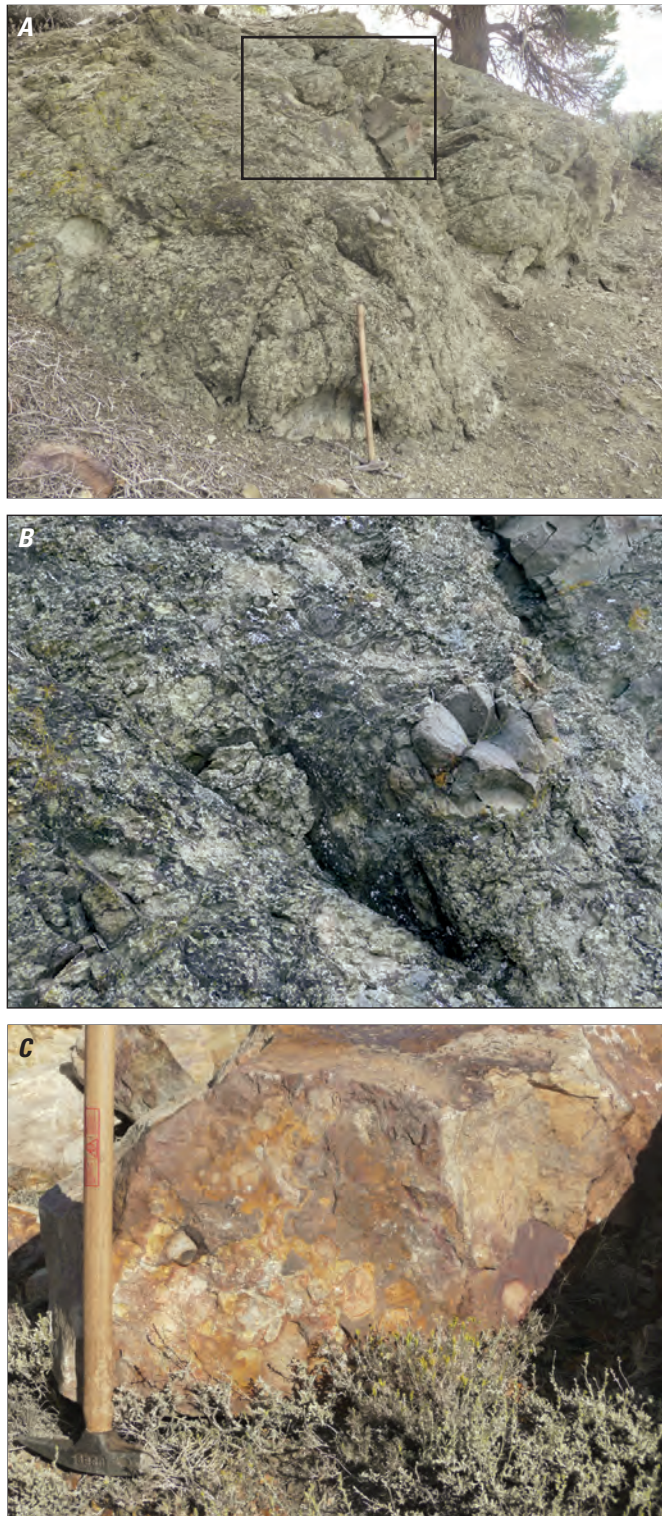
**Figure 2.** Geologic map of the southwestern part of the Masonic Mining District, Mono County, California, and Lyon and Mineral Counties, Nevada. Aerial tramway ore bins (also shown on report cover) are ~120 m northeast of the Sarita Mine adit that accesses the 120 and 160 levels.



- EXPLANATION**
- Qc Colluvium
  - Tev Eureka Valley Tuff (9.3–9.5 Ma)
  - Tdi Trachydacite intrusion
  - Trachyandesite of Masonic**
  - Tmai Trachyandesite intrusions of Masonic (14.2 Ma)
  - Tma Trachyandesite of Masonic (~14–15 Ma)
  - Granitic rocks**
  - Kgm Granodiorite of Masonic Mountain (Cretaceous)
  - Contact—Dashed where approximated
  - Fault—Dashed where approximated, dotted where concealed
  - Altered fault zone
  - ▣ Mine shaft
  - └─ Adit
  - <sup>40</sup>Ar/<sup>39</sup>Ar sample site and index number (table 1)



**Figure 3.** Geologic map of the northeastern part of the Masonic Mining District, Mono County, California, and Mineral County, Nevada.



**Figure 4.** Images of volcaniclastic deposits in the Red Wash-East Walker River alteration zone and Masonic Mining District. *A*, Propylitically altered debris flow in trachyandesite of Masonic, hill 6696 (elevation), and Red Wash-East Walker River alteration zone. Hammer for scale. *B*, Closeup view of black rectangle shown in *A*. *C*, Volcaniclastic deposits replaced by quartz, alunite, kaolinite, and pyrite (weathered to iron oxides), Sarita Mine. Hammer for scale.

Trachyandesite flows and intrusions contain 2–53 volume percent phenocrysts of plagioclase, clinopyroxene, hornblende, and trace amounts of biotite and olivine in a variably devitrified groundmass or, less commonly, in a felty intergrowth of plagioclase, opaque oxides, and clinopyroxene. Euhedral, acicular hornblende phenocrysts (2–5 millimeters [mm]) are a distinctive constituent in many places. Volcaniclastic deposits include laharic debris flows and lesser block and ash-flow deposits. These strata are massively to distinctly bedded, generally poorly sorted, clast- to matrix-supported, mass wasting deposits with a clay- and ash-rich matrix (fig. 4). Clasts are 1 cm to several meters in diameter, angular to subangular, and principally consist of volcanic rock fragments similar to the associated trachyandesite lavas and intrusions.

Between the Masonic Mining District and the Red Wash-East Walker River alteration zone (fig. 1) some trachyandesite flows were erupted from small plugs marked by low-relief spires, generally meters in dimension, with steep foliations and joints. Conical to rounded hills in the northern and northeastern parts of the district comprise a group of larger trachyandesite and trachydacite domes that are the same age as trachyandesite flows (15.0, 14.4, and 14.2 Ma porphyritic and hornblende andesite plug and domes; Tmai, fig. 3; table 1), or younger than trachyandesite flows (13.5–13.4 Ma trachyandesite of Masonic Gulch; Tamg, table 1; undated trachydacite intrusion of Dome Hill; Tdi, fig. 3). Trachyandesite of Masonic also has been intruded by 12.9 Ma andesite of Lakeview Spring (Tals, fig. 2; table 1; John and others, 2012) that forms small-volume domes north of Masonic Mountain. The medium-pale-gray, moderately porphyritic andesite contains about 16 volume percent phenocrysts of plagioclase, hornblende, clinopyroxene, and trace amounts of olivine set in a moderately devitrified groundmass. Plagioclase phenocrysts are characteristically larger than those in most rocks in the Bodie Hills volcanic field.

Trachyandesite of Masonic west, northwest, and north of Masonic Mountain is overlain by 9.5–9.3 Ma Eureka Valley Tuff (Eureka Valley Tuff; Tev, figs. 2, 3; Pluhar and others, 2009; John and others, 2012), and by Miocene and younger sedimentary deposits, including Fletcher Valley basin-filling fanglomerate, talus (Qfg and Qt, respectively), landslide deposits northwest of Lakeview Spring (Tls, fig. 2), perched terrace gravels, and perched fluviolacustrine sediments (Tg and Ts, respectively). The Eureka Valley Tuff is a grayish-black, moderately porphyritic trachydacite ash-flow tuff. It contains about 13 volume percent phenocrysts of plagioclase, biotite, clinopyroxene, and trace amounts of hornblende set in a grayish-black to iron-stained, reddish-brown, glassy groundmass. Clasts are composed of the same phenocrysts and matrix. In the Bodie Hills, where tuff is moderately to densely welded, most exposures appear to fill paleochannels. Abundance of biotite suggests that most Eureka Valley Tuff exposures in the Bodie Hills correlate with the lower, Tollhouse Flat Member, but upper member deposits also could be present.

Basin-fill of Fletcher Valley consists of fanglomerate and braided stream deposits (Tfg, at least 200 m thick) that contain well-rounded volcanic pebbles and, in places, interbedded felsic tephra. The braided stream deposits are moderately well-sorted, clast-supported sandstone and siltstone that contain 0.1–2 mm subangular detrital clasts composed of plagioclase and lesser quartz. Mafic silicate minerals (clinopyroxene>olive-green hornblende>biotite) comprise about 1 volume percent of detrital grains. These deposits also contain lithologically diverse volcanic rock fragments. Interbedded tephra deposits have dates of 11.7 Ma (Gilbert and Reynolds, 1973), 11.07 Ma (John and others, 2012), and 10.6–10.5 Ma (table 1). Landslide deposits northwest of Lakeview Spring (Tls) consist predominantly of altered volcanoclastic-flow sequence detritus derived from the northwest side of Masonic Mountain, and also include clasts of Eureka Valley Tuff, Mesozoic granitic rocks, metamorphic rocks, and andesite of Lakeview Spring. The unconsolidated, perched terrace gravels (Tg) vary from thin veneers to massive deposits of poorly sorted, silt- to boulder-size clasts in a sandy to silty matrix. Clasts include cobbles of Mesozoic granitic rocks, petrified wood, Eureka Valley Tuff, and diverse volcanic rocks. The semiconsolidated, gray- to dark-gray, perched fluviolacustrine sediments (Ts) are predominantly relatively well-sorted and distinctly bedded, coarse sand, sand, and silt.

In the Masonic Mining District and in the Red Wash-East Walker River alteration zone, large volumes of interstratified volcanoclastic deposits and trachyandesite lava flows were pervasively altered to hydrothermal mineral assemblages that include quartz, alunite, kaolinite, pyrophyllite, and pyrite (mostly weathered to iron oxides). Adjacent to and gradational with these quartz-alunite-altered volcanoclastic-flow sequences, are large volumes of less-altered, gray-green and purple lava and debris flows (figs. 2, 3) in which phenocrysts are partly to entirely replaced by chlorite, montmorillonite, iron oxide minerals, sericite (fine-grained white mica containing K), and calcite (propylitic alteration). Thin veneers (tens of meters thick) of quartz-alunite-altered sequence strata that overlie pre-Tertiary rocks on the west and north sides of Masonic Mountain (Tvc, figs. 2, 3) contain the Au-Ag-Cu deposits at the Sarita, Lakeview, and Chemung Mines. Thicker quartz-alunite-altered sequences are exposed between Sonoma Canyon and Red Wash, south of the East Walker River.

The quartz-alunite-altered volcanoclastic-flow sequences have been designated separate stratigraphic units by others (for example, Red Wash volcanics and Masonic Gulch volcanics, Johnson, 1951). Based on igneous and hydrothermal mineral ages, chemistry, petrography, and stratigraphy (John and others, 2012), the altered sequences reflect contrasting primary permeability among largely conformable volcanoclastic deposits and lava flows rather than separate lithologic units. More permeable volcanoclastic deposits and interstratified volcanoclastic-flow sequences have been intensely altered and discolored, whereas thicker sequences of homogenous flows have largely retained primary mineralogy and darker

coloration. The volcanoclastic-flow sequences are cogenetic eruptives with limited lateral continuity (common on the flanks of stratovolcanoes) and their designation as separate map units is not warranted.

## Structure

North and west of Masonic Mountain, trachyandesite of Masonic has been displaced along west-east and northeast-striking, high-angle normal faults (fig. 2). Down-to-the-north displacement along these faults, estimated at tens of meters, enabled preservation of relatively thick sections of the volcanoclastic-flow sequence along the East Walker River, and preservation of perched gravel terraces and fluviolacustrine sediments between the Masonic Mining District and East Walker River. Faults bounding granitic rocks on the west side of Masonic Mountain (Johnson, 1951; Stanford Geological Survey, 1961; John and others, 2012) are subparallel to mineralized structures and are inferred to have been active both during and after hydrothermal events in the district.

Mineralized structures in the Masonic Mining District are attributed to stress accommodation within the Walker Lane transtensional structural zone of strike-slip displacement, extension, and rotated tectonic blocks. Attitudes of these structures and kinematic indicators are consistent with maximum horizontal extension and compression oriented N60°W and N30°E, respectively (John and others, 2012).

## Forms of Gold-Silver-Copper Deposits

Two forms of Au-Ag-Cu deposits occur in the Masonic Mining District (1) breccia and vein deposits in high-angle, subplanar fault zones, and (2) clastic and hydrothermal sedimentary deposits.

### Breccias and Vein Deposits in High-Angle, Subplanar Fault Zones

Faults that contain mineralized breccias and veins are part of a north- to northeast-trending, curvilinear series of en echelon faults that extend for ~6.5 km along the west and north sides of Masonic Mountain, and north of Masonic Mountain along Red Wash (figs. 2, 3). Individual fault segments are vertical to near-vertical, tens to several hundreds of meters long, and strike N15°W–N60°E. Most mineralized faults occur in granodiorite, metavolcanic rocks, and trachyandesite of Masonic north of Masonic Mountain, although the Chemung and Red Rock Mine workings follow high-angle fault zones partly in a volcanoclastic-flow sequence (fig. 2). District production was mostly derived from near-vertical, N15–20°W-striking faults in granodiorite and metavolcanic rocks in the Pittsburgh-Liberty Mine. Other small mines north of the Pittsburgh-Liberty, including Hermine, Maybell, Mellor, and Perrini (fig. 3), were excavated in similar north- to

northeast-striking, high-angle faults in granodiorite and trachyandesite of Masonic, but produced little or no ore. None of these mines are deeper than ~60 m (~200 ft). Stopes exposed at several mines indicate that mineable fault segments were as much as 2 m wide (fig. 5).

Based on textures of mineral assemblages, alunite dates, and sulfur isotope compositions, the sulfide, telluride, sulfate and silicate minerals, and electrum, described below and imaged by scanning electron microscopy (SEM), are largely if not entirely hypogene. Some complex Cu-As-Sb-Fe-Bi-Pb-Ba-Al-Te-S-O phases may have been produced during weathering of sulfide minerals, or may represent submicron intergrowths of sulfide and oxide minerals. Iron oxide minerals that marginally replace pyrite are interpreted to have formed during weathering, and mineral assemblages in fault breccia and veins that formed during weathering are not further characterized.

Mineralized fault breccias consist of angular to sub-rounded clasts (millimeters to centimeters in size) of trachyandesite and pre-Tertiary rocks that have been variably replaced by quartz, alunite, pyrite (commonly weathered to iron oxide minerals), and lesser kaolinite, dickite, pyrophyllite, and diaspore. Some clasts consist of fine-grained to chalcedonic, gray to white quartz±pyrite (partly to entirely weathered to iron oxides) in which little to no primary texture is evident (fig. 5). Fault breccias are locally multigenerational. Clasts that have been completely replaced by fine-grained white-gray quartz are juxtaposed with voids that represent leached clasts, and with clasts of porphyritic volcanic rocks in which phenocrysts have been leached. Breccia clasts in faults at the Perrini and Chemung Mines are replaced by quartz+pyrite(iron oxides)±alunite, but many retain porphyritic texture.

Similar to altered clasts, breccia matrices consist predominantly of quartz, alunite, pyrite (iron oxides), and kaolinite, but locally include small amounts of pyrite, enargite, numerous other metallic minerals, and barite. Enargite in some samples is intergrown with quartz, pyrite, and alunite in centimeter-sized aggregates (fig. 5). Breccia matrices of dump samples from the Chemung Mine contain discrete crystals and intergrowths of pyrite, chalcopyrite, electrum, enargite, sphalerite, naumannite, and pyrrhotite; some enargite is encrusted on breccia clasts. The source of these samples is uncertain because the Chemung mill also processed ore from the Success, Sarita, and Lakeview Mines; sulfur ( $S^{\circ}$ ) in some samples links them to the Success Mine (Vikre, 2000).

Well-defined planar veins having sharp wall-rock contacts are relatively uncommon in the district. Veins cutting breccias in fault zones were mined with enclosing breccia at the Pittsburgh-Liberty Mine, and, to a lesser extent, at the Red Rock and Lakeview Mines. The relationship between breccias and veins is evident in dump samples from the lower Pittsburgh-Liberty Mine in Masonic Gulch that mostly consist of granodiorite that was altered to quartz+alunite+pyrite, brecciated, and cemented by dense fine-grained quartz+pyrite. Mineralized granodiorite breccia is cut by planar veins (millimeters to centimeters in size) composed of fine-grained,

vuggy quartz, pyrite, and lesser enargite (fig. 5). Veins in the volcanoclastic-flow sequence at the Red Rock and Lakeview Mines are centimeters wide, and consist of fine- to medium-grained, locally banded quartz, and lesser alunite, pyrite, and enargite.

## Mineral and Rock Compositions of Breccias and Vein Deposits

Samples of mineralized fault breccia from upper Pittsburgh-Liberty Mine dumps (fig. 2) consist of completely silicified clasts that have been cemented by dense to porous (leached) matrices of fine-grained, gray to white quartz and aggregates of pyrite, enargite, famatinite, alunite, and lesser barite (millimeters to centimeters in size; fig. 5). Enargite and famatinite contain a large variety of <10  $\mu\text{m}$  mineral inclusions of predominantly gold, silver, and copper minerals, based on semiquantitative SEM analyses. Gold minerals include Au-rich electrum ( $\text{Au}_{>0.8}\text{Ag}_{<0.2}$  with minor Cu), an Au-Cu-Ag alloy ( $\sim\text{Au}_{7.1}\text{Cu}_2\text{Ag}_{0.9}$ ), an Au-Ag-S mineral ( $\sim\text{Au}_2\text{Ag}_{1.7}\text{S}_2$ ), a Cu-Ag-Au-Se-S mineral with variable Cu/Ag/Au, and an Au-Ag-Se mineral. Silver minerals are naumannite ( $\sim\text{Ag}_2\text{Se}$  with minor Cu and Fe), and an Au-Ag-Cu-Se mineral ( $\sim\text{Ag}_{4.5}\text{Au}_{1.3}\text{Cu}_{1.2}\text{Se}_3$ ). Copper minerals include  $\sim\text{Cu}_6\text{Bi}_{1.7}\text{S}_5$ ;  $\text{Cu}_3\text{Bi}_2\text{S}_5$  with minor Se;  $\text{Cu}_{4.3}\text{As}_{1.2}\text{Sb}_{0.1}\text{S}_5$ ;  $\text{Cu}_{1.5}\text{S}$  with minor Sb;  $\text{Cu}_{2.3}\text{S}$  with minor Se;  $\text{Cu}_5\text{Ag}_{0.5}\text{Fe}_{0.4}\text{Se}_3\text{S}_{1.3}$  (possibly atthascaite);  $\text{Cu}_3\text{As}_2$  with minor Sb, Au, Fe, S; and a Cu-Se mineral (figs. 6, 7). Atomic proportions of some Cu-S inclusions correspond to those of digenite. Textures of Cu-As-O minerals intergrown with enargite and famatinite appear to be hypogene.

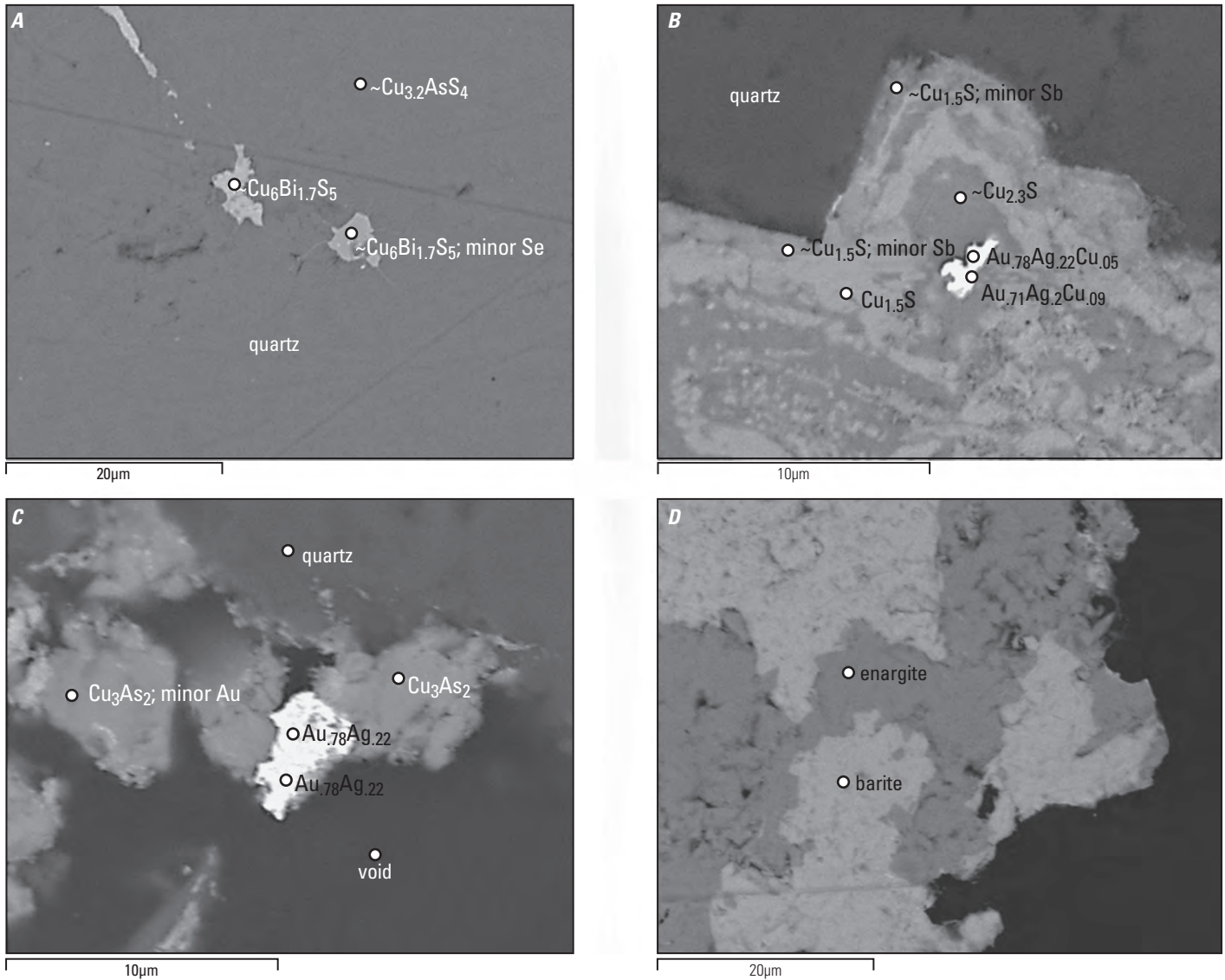
A sample from the lower Pittsburgh-Liberty adit dump in Masonic Gulch (figs. 2; 5) consists of Mesozoic granodiorite that has been altered to quartz and alunite, and cut by millimeter to ~1 cm veins of quartz, pyrite, enargite (As/Sb weight percent ~1.2–11; minor Te), famatinite (As/Sb weight percent ~0.3–0.8), and lesser goldfieldite ( $\text{Cu}_{12}(\text{Te},\text{Sb},\text{As})_4\text{S}_{13}$ ). Numerous minerals with variable Cu-Sb-As-Zn-Te-S, and variable Cu-Bi-S-Se, occur as intergrowths with, and inclusions in, pyrite, famatinite, and goldfieldite (fig. 8). Atomic proportions of many intergrown and inclusion phases in Pittsburgh-Liberty Mine samples may represent submicron-sized intergrowths of several minerals (based on backscattered electron images), or undocumented minerals. Dump samples from Lakeview and Red Rock Mines consist of quartz, alunite, “goldfieldite” (with minor Zn), naumanite (with minor Te and S), argentite, and an Ag-Te-Se-S mineral.

Bulk samples of the imaged sections contain 27.6 and 53.9 parts per million (ppm) Au, 136 and 395 ppm Ag, 92.1 and 149 ppm Pb, 26.9 and 461 ppm Sn, >10 ppm Hg, >500 ppm Te, and >1,000 ppm As, Ba, Bi, Cu, and Sb (table 1-1; Se was not determined). Other bulk samples from the Success, Chemung, and Pittsburgh-Liberty Mine dumps contain concentrations of minor elements that are broadly similar to, or lower than, concentrations in mineralized fault breccia from upper Pittsburgh-Liberty dumps.

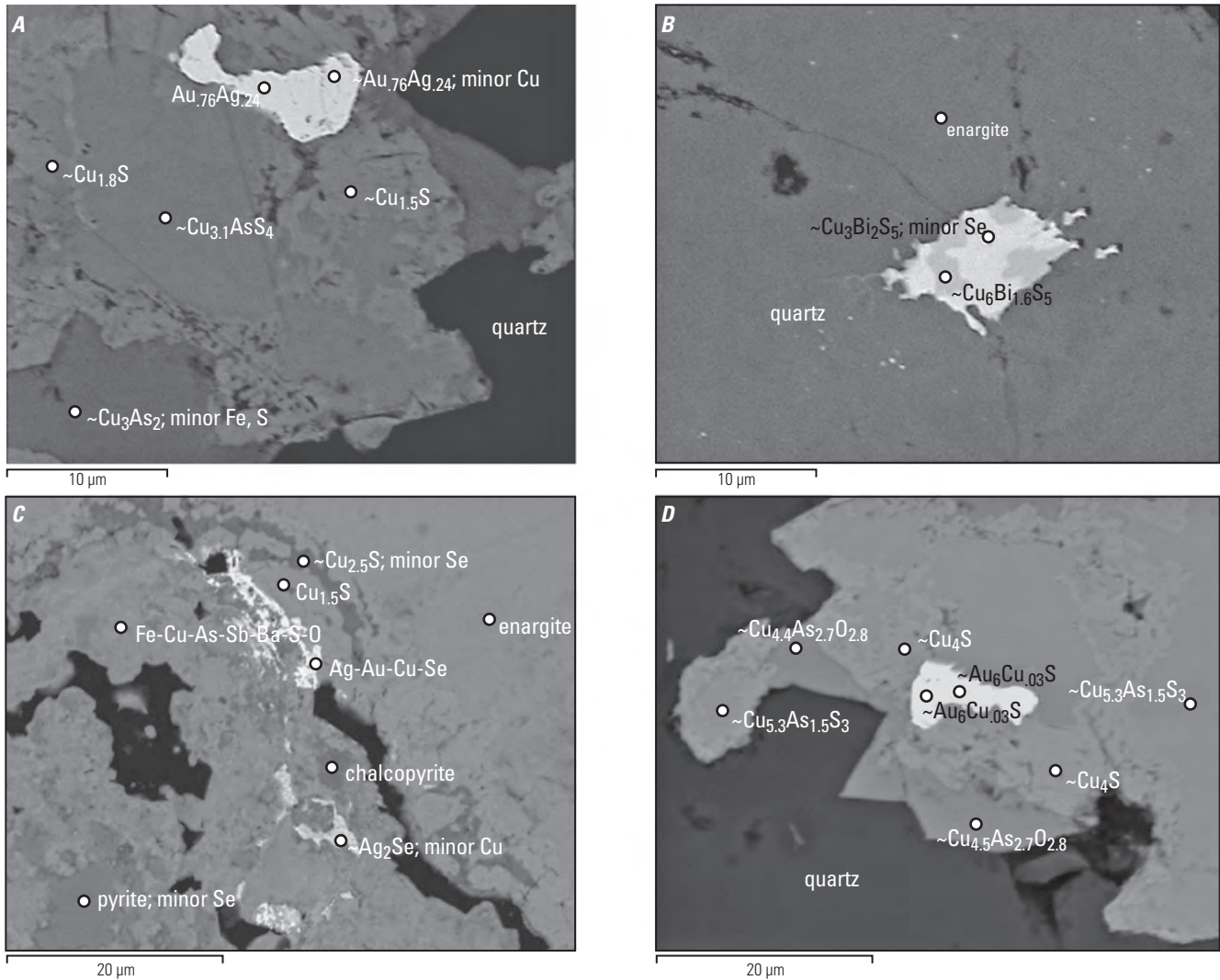




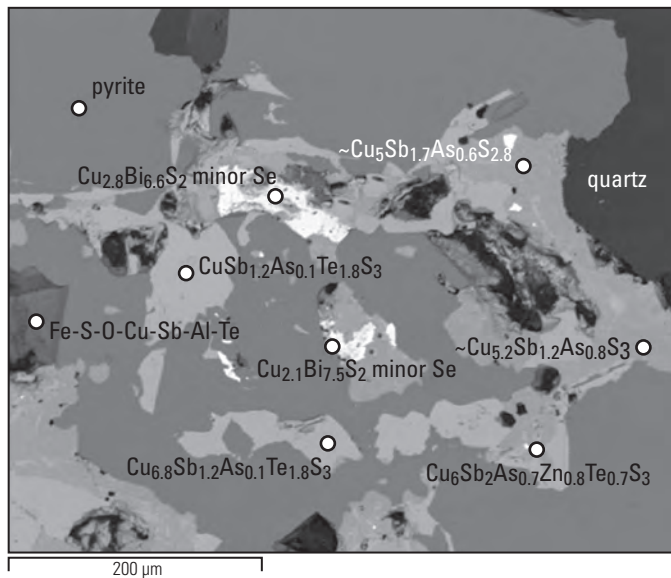
**Figure 5.** Images of mineralized fault breccias and veins in the Masonic Mining District. *A, B*, ~N-S-trending fault breccias cemented by quartz, alunite, and pyrite; *A*, Maybell-Alton Jack Mine upper adit (elevation ~7,750 ft) and *B*, Mellor Mine shaft (elevation ~7,600 ft; fig. 2). *C*, Fault breccia replaced by fine-grained quartz, alunite, pyrite, enargite, gold, and numerous other Cu-As-Sb-Bi-Fe-Te-Se-S minerals, unnamed mine dump, upper Pittsburg-Liberty Mine workings, 0.5 km (1,650 ft) east of New York Hill (sample MAS09-3b, elevation ~8,350 ft; fig. 2). *D*, Quartz+pyrite+alunite+enargite veins cutting granodiorite (left sample, Pittsburg-Liberty Mine, creek adit dump, elevation ~7,500 ft) and trachyandesite (right sample, Red Rock Mine dump, elevation ~8,080 ft; fig. 2).



**Figure 6.** Secondary electron images of fault breccia shown in figure 5C, Masonic Mining District (sample MAS09-3b, elevation ~8,350 ft). Mineral identifications and approximate atomic proportions in this figure and in figures 7, 8, and 9 were determined petrographically and by scanning electron microscopy algorithms. Imaged phases include quartz, barite, enargite, a Cu-Bi-S mineral ( $\sim\text{Cu}_6\text{Bi}_{1.7}\text{S}_5$ ), a Cu-As mineral ( $\sim\text{Cu}_3\text{As}_2$ ), Au-rich electrum with minor Cu, and Cu-S minerals ( $\sim\text{Cu}_{1.5}\text{S}$ ;  $\sim\text{Cu}_{2.3}\text{S}$ ).



**Figure 7.** Secondary electron images of fault breccia shown in figure 5C, Masonic Mining District (sample MAS09-3b, elevation ~8,350 ft). Imaged phases include quartz, enargite, a Cu-As mineral ( $\sim\text{Cu}_3\text{As}_2$ ), Au-rich electrum with minor Cu, chalcopyrite, naumannite, Cu-S minerals ( $\sim\text{Cu}_{1.5}\text{S}$ ;  $\sim\text{Cu}_{1.8}\text{S}$ ;  $\sim\text{Cu}_{2.5}\text{S}$ ;  $\text{Cu}_4\text{S}$ ), Cu-Bi-S minerals ( $\sim\text{Cu}_6\text{Bi}_{1.6}\text{S}_5$ ;  $\text{Cu}_3\text{Bi}_2\text{S}_5$ ), Cu-As-S minerals ( $\sim\text{Cu}_{5.3}\text{As}_{1.5}\text{S}_3$ ;  $\sim\text{Cu}_{3.1}\text{AsS}_4$ ), and an Au-S mineral ( $\sim\text{Au}_{8.6}\text{S}_{1.4}$ ). Some multielement analytical sites may represent submicrometer intergrowths of several minerals (see B, Ag-Au-Cu-Se, for example), or partially oxidized Cu-As-S minerals (see D,  $\sim\text{Cu}_{4.4}\text{As}_{2.7}\text{O}_{2.8}$ , for example).



**Figure 8.** Secondary electron image of quartz+alunite+sulfide vein in granodiorite shown in figure 5D, left sample, Masonic Mining District (Pittsburg-Liberty Mine, creek adit dump, sample MD83-2, site 2A, elevation ~7,500 ft). Imaged phases include quartz, pyrite, Cu-Bi-S minerals, Cu-Sb-As-S minerals, and Cu-Sb-As-Te-Zn-S minerals.

If gold-bearing inclusions in enargite (described previously) are representative of Au occurrences in the district, then the absence of placer deposits and historically difficult gold recovery can be attributed to a predominance of micron-sized Au minerals. However, visible Au has been reported at several mines (Success, Chemung, Maybell, and Jump-Up Joe Mines; Eakle and others, 1917; Johnson, 1951; R.H. Kern, written commun., 1977; F.M. Smith, written commun., 1984). Gold at the Chemung Mine is described as “fine particles in milky quartz”, and “very fine particles in chalcedonic bands” in vugs (R.H. Kern, written commun., 1977). Gold at the Maybell Mine is described as “+1 mm pieces” in fine-grained quartz (F.M. Smith, written commun., 1984). Such relatively coarse Au apparently was not sufficiently abundant to form placer deposits.

## Clastic and Hydrothermal Sedimentary Deposits

Distinctive, mineralized clastic and hydrothermal bedding sets occur within the volcanoclastic-flow sequence at the Sarita and Lakeview Mines (fig. 2). Open-cut and underground workings of these mines do not clearly follow structures and thus attest to lateral dispersion of precious metals within parts of the sequence. Mineralized bedding sets are best exposed at the Sarita Mine on New York Hill and in mine workings on the adjacent hill ~0.5 km (~1,650 ft) to the east, where the volcanoclastic-flow sequence unconformably overlies granodiorite and pendants of pre-Tertiary metavolcanic rocks (fig. 2). At the Sarita Mine, volcanoclastic-flow strata are as much as ~90 m (300 ft) thick, strike N30–70°W, and dip 30–80°SW. On

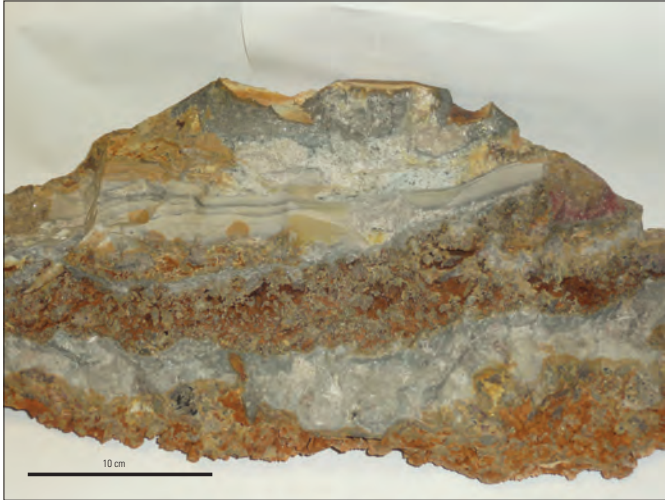
the hill to the east, these strata are tens of meters thick, have variable northwest-northeast strikes, and dip 50°NW to 75°NE.

At the Sarita Mine, Au, Ag, and Cu were recovered from ore initially mined underground in the early 1900s and between 1951 and 1989, from an open cut on the northwest slope of New York Hill (the cut postdates the mine photograph in Jenkins (1951) and predates an unpublished mining company map dated 1989). The underground workings, open cut, and Au resource are in a zone of silicified, relatively well-sorted volcanoclastic strata that contains bedding sets of very fine-grained, quartz-rich chemical sedimentary strata that trend north-northeast. Similar mineralized strata were mined from a small open cut and underground workings on the hill to the east. At the Sarita Mine, the 120 (haulage) and 160 levels on an unpublished (~late 1930s) map outline roughly circular areas, about 145 m in diameter, of rib assays that vary mostly between 0.1 and 1 opt Au (converted from dollar values at \$35/oz). Based on descriptions in Eakle and others (1917) and Eakle and McLaughlin (1919), these levels apparently represent two of five juxtaposed, stratiform ore bodies. The ore bodies were as much as 10 m thick, indistinctly bounded, and within ~48 m of the surface. Ore reportedly consisted of dense to porous chalcedony and brecciated “chert” with seams of yellow-brown clay (Eakle and others, 1917; Eakle and McLaughlin, 1919; Jenkins, 1951). The Sarita open cut may coincide with one of the upper ore bodies, as two shafts and numerous small stopes occur south and west of the cut at the same or higher elevations (fig. 2).

## Interpretation of Clastic and Hydrothermal Sedimentary Deposits

Based on examination of dump samples and limited mine exposures, mineralized strata at lower elevations, including the 120 haulage level, are predominantly coarse, unsorted volcanoclastic deposits that are variably silicified and leached. Leached to partially leached breccia clasts, ≤5 cm in dimension, are represented by voids and by skeletal aggregates of fine-grained quartz, alunite, and kaolinite that largely reflect original clastic texture. Some voids are encrusted with millimeter-sized alunite euhedral crystals and mixtures of alunite and kaolinite. Matrix of the volcanoclastic deposits consists of dense, fine-grained quartz with variable amounts of pyrite and alunite. Small amounts of enargite occur with iron oxides in fractures and in leached clast sites.

Mineralized strata at higher elevations, including the open cut, comprise two distinct bedding sets (a) sequences of alternating, relatively poorly to well-sorted volcanoclastic beds and thinly laminated brown and white beds (≤1 mm thick) of very fine-grained anhedral quartz with minor pyrite, hematite, enargite, and other minerals (fig. 9); and (b) sequences of thinly laminated brown and white beds of very fine-grained quartz±Fe-Cu-S-O minerals that conformably and unconformably overlie coarser, relatively unsorted volcanoclastic beds (fig. 10). A conformable layer of relatively coarse-grained enargite+iron oxide and millimeter-sized, euhedral quartz



**Figure 9.** Image of a dump sample from the Masonic Mining District, Sarita Mine (elevation ~8,400 ft). Semiconformable set of beds that includes silicified and leached, coarse volcanoclastic detritus, variably sorted gravel and sand beds, and very fine-grained white quartz beds. Subsequence a (described in text).

crystals commonly occur between quartz bed sequences (such as sequence [a], described previously) and voids (leached clast sites). Enargite+iron oxide+fine-grained quartz also form millimeter-wide veins that cut thinly laminated, brown quartz beds and feather into layers of enargite+iron oxide-vuggy quartz. Sedimentary structures in thinly laminated, brown and white quartz beds include channel scour and fill, crossbedding, soft-sediment folds and slumps with sag micro-faults, and bed draping on clasts. Supersaturation textures in these beds are reflected by very fine-grained quartz and sulfide minerals, and by intergrowths of pyrite+hematite in hopper-like cubic euhedral crystals.

Based on sedimentary textures, structures, and stratigraphy, and on grain sizes and mineral modes, thinly laminated quartz beds in both bedding sets are interpreted to have precipitated from aqueous fluid (1) intermittently with volcanoclastic detritus; (2) conformably and unconformably on hummocky surfaces of unsorted and sorted volcanoclastic deposits; and (3) in depressions and spaces among blocks of silicified and leached, coarse volcanoclastic deposits. Paragenetically, the coarse volcanoclastic deposits were silicified following deposition of sorted volcanoclastic beds (such as sequence [a], described previously), and subsequently partially leached. These silicified and partially leached volcanoclastic strata were then eroded and slumped, creating channels in, and voids between, silicified and leached blocks that were filled with brown and white quartz beds (such as sequence [b], described previously), and with fine and coarse volcanoclastic detritus. The presence of angular leached dropstones in thinly laminated white and brown beds of sequence b (fig. 11) supports these paragenetic interpretations. Given the fairly steep present attitudes of these strata in the vicinity of New York Hill (described previously), slumping was most likely caused

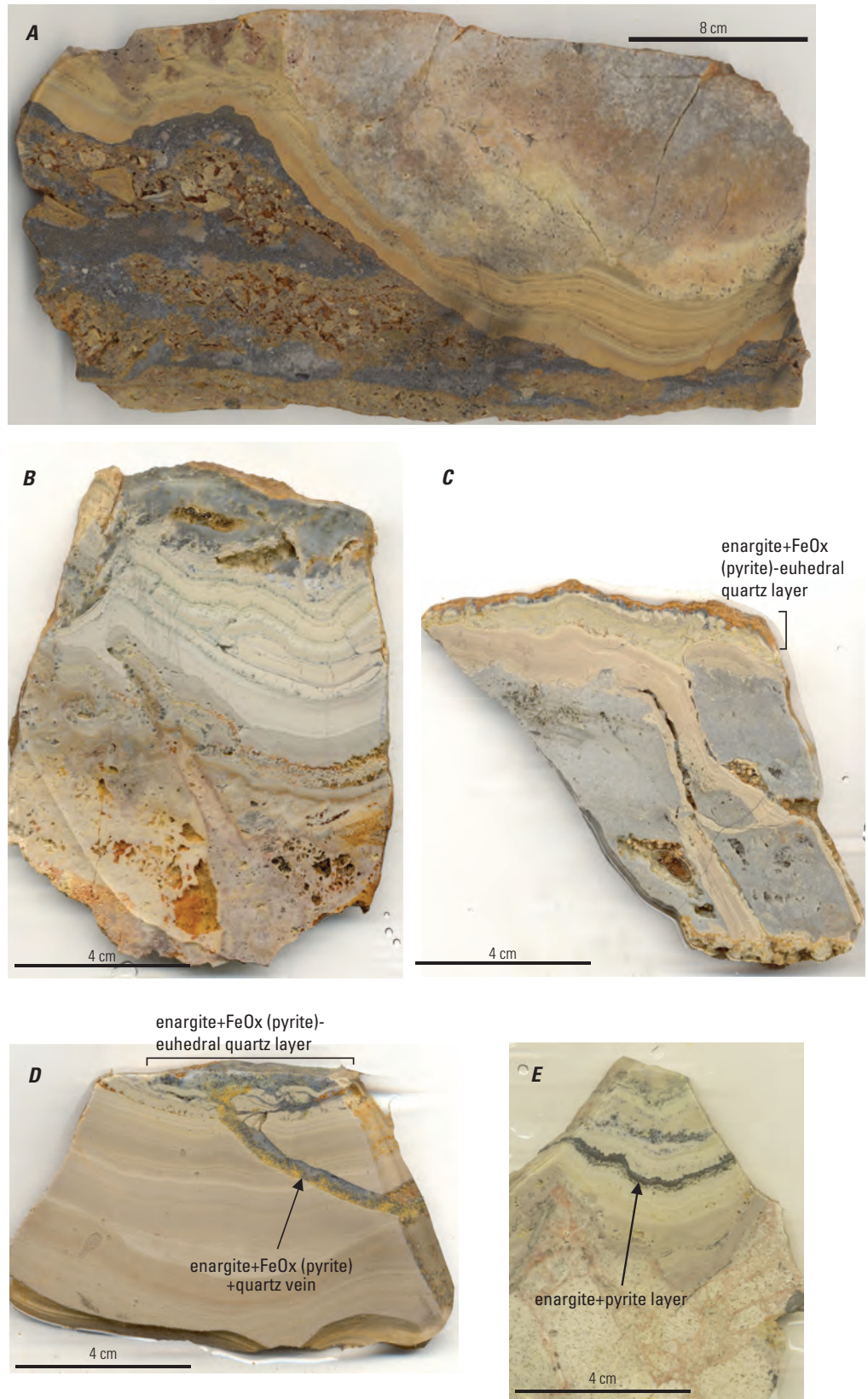
by uplift or tilting associated with faulting, and (or) with slope failure enhanced by deflation related to hydrothermal leaching of volcanoclastic strata. Vein and vug-filling quartz, enargite, and iron oxide that cut and conformably overlie, respectively, brown quartz beds constitute the youngest hydrothermal event that affected sequence b strata. Hydrous fluids that altered, leached, and mineralized the volcanoclastic deposits and chemical beds may have circulated in north-northwest to northeast-striking faults that contain the slightly younger mineralized breccias and veins. However, district-scale faults directly associated with Au-Ag-Cu deposits at the Sarita Mine and east of New York Hill are not evident at present levels of exposure.

Based on textures of mineral assemblages, alunite dates, and sulfur isotope compositions, the sulfide, telluride, sulfate and silicate minerals, and electrum in fault breccias and veins, and in sedimentary deposits, are hypogene. Some iron oxide minerals that occur with pyrite and enargite may also be hypogene. Iron oxide minerals that marginally replace pyrite, occur in fractures, and encrust void margins, are interpreted to have formed during weathering. These supergene iron oxide minerals and other minerals in sedimentary deposits that formed during weathering are not further characterized.

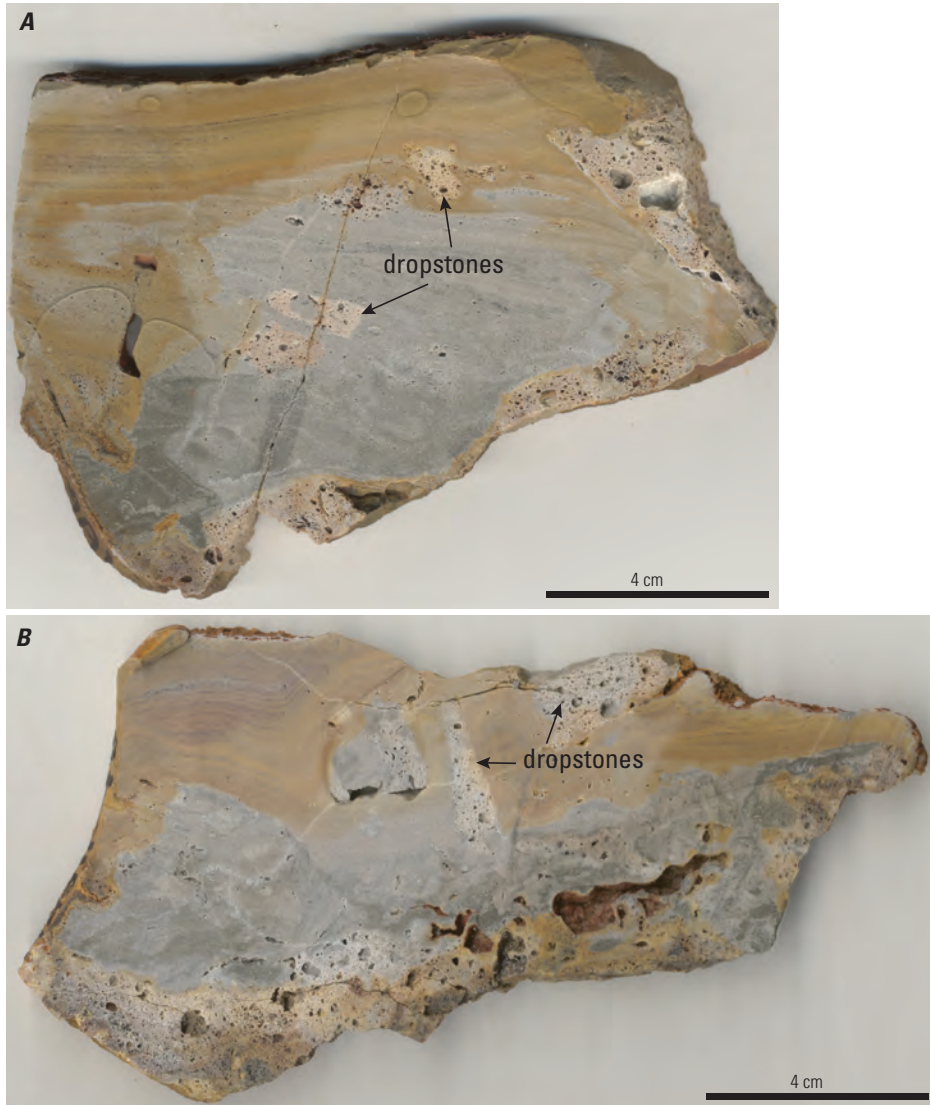
## Mineral and Rock Compositions of Clastic and Hydrothermal Sedimentary Deposits

Thinly laminated, brown and white beds of very fine-grained quartz at the Sarita Mine contain small amounts of very fine-grained pyrite, iron oxide, and enargite, in places intergrown with goldfieldite, a Cu-Sn-S mineral (with minor Se and Sb), a Bi-Se-Mo-S mineral (with minor Cu), and numerous Cu-Bi-As-Te-Sb-Pb-S-O minerals (fig. 12). Other quartz beds include complexly zoned pyrite(?) crystals that are pseudomorphically replaced by cores and concentric to partially annular zones of multielement phases. These euhedral crystals consist of (1) cores of iron oxide phases  $\pm$ quartz with 1–9.8 weight percent Si, S, Cu, and Sb, and with 1–3 weight percent Cu, As, Sb, Si, and S, and quartz with 1–3 weight percent Al, Fe, and S; (2) medial zones of Fe-Cu-Sb-As-Si-S-Ca-O, local Ba, W, Ag, Bi, and quartz; and (3) margins of iron oxides or multiphase margins with 1–9.8 weight percent Si, S, Cu, and Sb; one multiphase margin consists of iron oxides with <1–7 weight percent Cu, Sb, Si, and S, and Cu-Fe-Sb-As-Si-Ca-O. Some pyrite remains in medial zones, along with minor barite, and in <1  $\mu$ m inclusions in iron oxides with minor Cu and Se. These zoned euhedral crystals appear to be remnants of pyrite and Cu-As-Sb minerals, and other Se and Ag minerals that have been re-equilibrated in iron oxide and quartz-dominant zones. However, it is unclear if these zoned pseudomorphs were produced by hypogene or supergene processes, although the presence of sulfide minerals in the dense, finely laminated quartz beds suggests limited weathering.

Samples (collected from 2007 to 2012) of clastic and chemical (hydrothermal) sedimentary strata with enargite from Sarita Mine exposures and dumps contain elevated



**Figure 10.** Images of dump samples from the Masonic Mining District, Sarita Mine (elevation ~8,400 ft). *A*, Silicified and leached, sorted gravel and sand-sized clastic beds unconformably overlain by channel-filling sets of very fine-grained, brown quartz beds, and an unleached, coarse volcaniclastic deposit. Dark-gray beds contain pyrite. *B*, Very fine-grained white and brown quartz beds filling depressions in silicified and leached volcaniclastic deposits. *C*, Very fine-grained brown quartz beds filling fractures in silicified and brecciated trachyandesite, and overlain by a conformable vuggy layer of enargite+iron oxide(pyrite)+euhedral quartz. *D*, Very fine-grained brown quartz beds cut by a coarser-grained, quartz-enargite-iron oxide(pyrite) vein that is contiguous with a conformable layer of enargite+iron oxide (pyrite)-euhedral quartz. *E*, A bed of enargite+pyrite (~2 mm thick) within a set of very fine-grained, white quartz beds that fills a channel in brecciated trachyandesite. Subsequence b (described in text).



**Figure 11.** Images of dump samples from the Masonic Mining District, Sarita Mine (elevation ~8,400 ft). Silicified and leached volcaniclastic deposits overlain by very fine-grained white and brown quartz beds with dropstones of leached trachyandesite. Subsequence b (described in text).

concentrations of Au (9.2–82.3 ppm), Ag (15–238 ppm), Bi (~57–3,110 ppm), Cu (~73–1,310 ppm), Pb (~98–216 ppm), Hg (~2–86 ppm), Se (~6–198 ppm), and ~100–860 ppm As, Ba, Sb, and Te. Other samples (collected in 1988) contain higher Hg (16–43 ppm), Ag (<300 ppm), and Sb (<4,600 ppm), in addition to elevated concentrations of As (174–3,107 ppm), and Te (<3,220 ppm; table 1-1). The elevated element concentrations in these bulk samples reflect the presence of numerous Cu-Bi-As-Te-Sb-Pb-Sn-Se-S-O minerals and also indicate the presence of additional Au- and Ag-bearing phases.

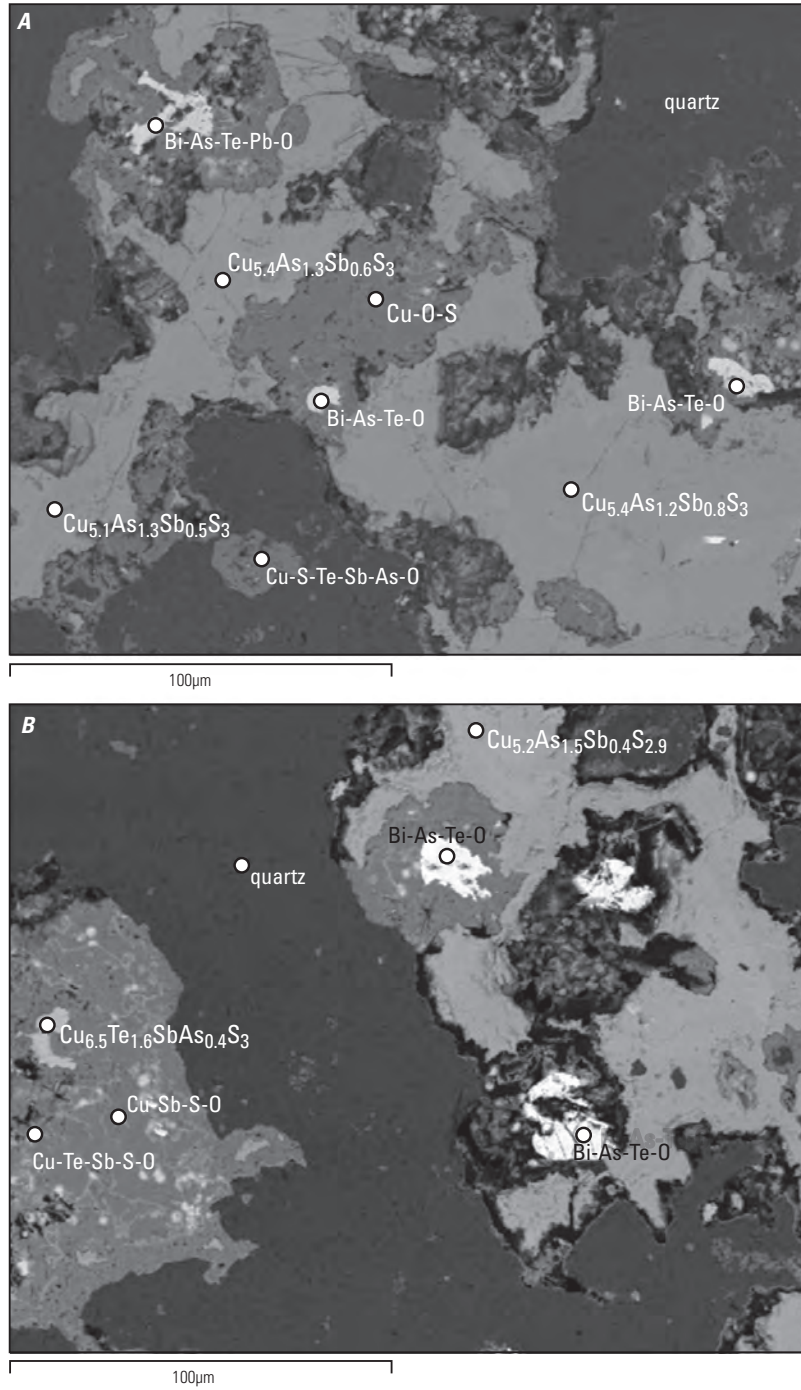
### Other Minerals and Forms of Mineralization

Other minerals reported in the Masonic Mining District include tellurides, bismuthinite, argentite, bornite, and cinnabar (for example, Johnson, 1951). Although telluride minerals and bismuthinite were not identified in the samples examined, high concentrations of Te and Bi in bulk samples

(table 1-1) imply the presence of telluride minerals and possibly bismuthinite in addition to the Te and Bi minerals imaged (figs. 6, 7, 8, 9). Other forms of mineralization in the district include (1) a 0.6–1.2-m-wide quartz vein in granodiorite at the Sunday Mine that contains sparse 3–4 mm crystals of galena and pyrite; and (2) discontinuous, <30-cm-wide quartz veins with minor pyrite and chalcopyrite in pre-Tertiary metavolcanic rocks southeast of the Success Mine near McMillan Spring. Other quartz veins occur in the granodiorite of Masonic Mountain. However, all of these veins differ in form, mineralogy, and structural control from the mineralized fault breccias and veins described previously.

### Wall-Rock Alteration

Mineralized faults are bordered by dense to porous selvages of brecciated trachyandesite and granodiorite, or by trachyandesite flows that are extensively replaced by quartz, alunite, iron oxides (weathered pyrite), and lesser dickite,



**Figure 12.** Secondary electron images of minerals in very fine-grained brown quartz beds from the Sarita Mine open cut, Masonic Mining District (fig. 2). *A* and *B* correspond to sample MAS07-3A (elevation ~8,300 ft). Imaged phases include quartz, a Cu-As-Sb-S mineral ( $\sim\text{Cu}_{5.2}\text{As}_{1.3}\text{Sb}_{0.6}\text{S}_{2.9}$ ), a Cu-Te-Sb-As-S mineral ( $\sim\text{Cu}_{5.2}\text{Te}_{1.3}\text{Sb}_{0.8}\text{As}_{0.3}\text{S}_{2.4}$ ), and several Cu-Bi-As-Te-Pb-S-O minerals or mineral intergrowths.



pyrophyllite, and diaspore. Wide fault zones (for example, Maybell-Alton Jack Mine structures; fig. 3) are represented by resistant ridges as much as 15 m wide and 5 m high (fig. 5) in which primary rock textures in breccia clasts and flows are partly to entirely obscured. Narrower, meters-wide selvages of trachyandesite adjacent to other stoped fault breccias (for example, Mellor and Perrini Mines), largely retain primary igneous texture; phenocrysts and matrices in these selvages are replaced by pink to white mixtures of fine-grained alunite, kaolinite, pyrite, iron oxides after pyrite, and other clay minerals. With increasing distance from faults, illite and montmorillonite become the dominant replacement minerals. Wall-rock hydrothermal mineral associations are mainly the same as, and contiguous with, hydrothermal minerals in adjacent fault breccias that were stoped. Stoped fault breccias are distinguished by greater abundances of quartz, sulfide minerals, and precious metals.

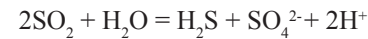
Hydrothermal alteration associated with mineralized clastic and chemical sedimentary deposits is coextensive with those strata, as described previously. Lateral permeability of volcanoclastic deposits within the volcanoclastic-flow sequence on the west and northwest sides of Masonic Mountain enabled pervasive hydrothermal alteration; the quartz-alunite-pyrite-kaolinite alteration mineral association is fairly homogenous throughout these rocks. The presence of silicified and leached volcanoclastic deposits, clastic and chemical quartz beds, and Au-Ag-Cu-Fe sulfide minerals distinguish mineralized strata in the vicinity of New York Hill. Lateral boundaries of mineralized strata appear to be gradational, whereas vertical boundaries are largely stratigraphic, based on the absence of significant mineralization in underlying pre-Tertiary rocks. Volcanoclastic deposits and brecciated trachyandesite on Sarita Mine dumps, and lateral to mineralized strata at lower elevations, have been extensively replaced by quartz, alunite, and kaolinite, and cut by millimeter-wide veins composed of fine-grained quartz and alunite (fig. 13). On New York Hill, metavolcanic rocks in workings near the Sarita open cut have been altered to clay minerals, and granitic and metavolcanic rocks exposed on the hill to the east are extensively silicified and cut by planar and stockwork quartz veins. Density and competency contrasts between altered volcanoclastic-flow strata and subjacent pre-Tertiary rocks, and slopes oversteepened by fault displacement, caused masses of altered rocks tens of meters in dimension to slide down the north side of New York Hill (fig. 2).

## Sulfur Isotope Compositions and Equilibrium Temperatures

Most sulfur isotope values ( $\delta^{34}\text{S}$ ) for enargite, pyrite, and luzonite vary from  $-7.9$  to  $-12.2$  ‰, and values for alunite vary from  $13.4$  to  $19.9$  ‰ (table 2). No clear compositional differences exist between the two forms of mineralization

(breccia and vein deposits in fault zones; clastic and hydrothermal sedimentary deposits). One higher  $\delta^{34}\text{S}_{\text{enargite}}$  value ( $0.2$  ‰), and one lower  $\delta^{34}\text{S}_{\text{alunite}}$  value ( $7.1$  ‰; table 2) presumably reflect sample impurity because both minerals occur in sulfide-sulfate mixtures.

The relatively low  $\delta^{34}\text{S}$  sulfide and relatively high  $\delta^{34}\text{S}$  sulfate values of most samples are consistent with disproportionation of magmatic  $\text{SO}_2$  into  $\text{H}_2\text{S}$  and  $\text{SO}_4^{2-}$  (Rye, 2005) during the formation of both deposit types. Disproportionation occurs when  $\text{SO}_2$  derived from magma degassing condenses in overlying groundwater at temperatures  $<400$  °C:



Groundwater acidified by this reaction decomposes silicate rocks to hydrothermal mineral assemblages dominated by quartz, alunite, and pyrite.  $\text{K}^+$ ,  $\text{Fe}^{2+}$ , and  $\text{Al}^{3+}$ , solubilized during silicate mineral decomposition, react with aqueous  $\text{SO}_4^{2-}$  and  $\text{H}_2\text{S}$  to form alunite and pyrite with markedly different sulfur isotope values.

Calculated sulfur isotope equilibrium temperatures ( $\delta^{34}\text{S}_{\text{sulfide}} - \delta^{34}\text{S}_{\text{sulfate}}$ ) of coexisting pyrite, enargite, and alunite in samples from the Red Rock and Sarita Mine dumps are  $228$ ,  $231$ , and  $238$  °C, and  $192$  °C (all calculations are based on pyrite-alunite fractionation; table 2; Vikre and Henry, 2011). Calculated sulfur isotope equilibrium temperatures of coexisting pyrite and alunite from the lower dump of the Pittsburgh-Liberty Mine, from a small mine dump in Masonic Gulch (“aspen grove” mine), and from the lower Perrini Mine dump, are  $218$ ,  $198$ , and  $188$  °C, respectively (table 2).



**Figure 13.** Image of a dump sample from the Masonic Mining District, Sarita Mine (elevation ~8,200 ft). Trachyandesite of Masonic that has been altered to quartz, alunite, kaolinite, and pyrite, brecciated, and cemented by veins of fine-grained quartz and alunite.

## Aster Imagery

ASTER imagery of the Masonic Mining District (Rockwell, 2010) shows a fairly uniform cluster of pixels that corresponds to kaolinite, montmorillonite, illite, and locally, quartz on Masonic Mountain, and on granitic rocks and trachyandesite of Masonic to the northeast to Masonic Gulch. Several clusters of pixels that correspond to alunite and kaolinite are coincident with the Sarita Mine and altered slide blocks on the north slope of New York Hill, and on the hill ~0.5 km east of New York Hill. Smaller and more diffuse groups of alunite±kaolinite pixels are coincident with the Red Rock Mine, the Pittsburg-Liberty Mine, the north slope of Masonic Gulch above (lower) Masonic town site, and the Lakeview Mine. Four relatively dense clusters of alunite pixels are coincident with the landslides north of the Lakeview Mine (Tls, fig. 2).

## Short Wave Infrared (SWIR) Spectra

SWIR spectra of hydrothermally altered and mineralized hand samples correspond to the same minerals identified by field and petrographic examination. Trachyandesite of Masonic on the Success, Chemung, Maybell-Alton Jack, and Perrini Mine dumps contains alunite, kaolinite, dickite and lesser pyrophyllite and illite. Granodiorite and meta-volcanic rocks on New York Hill, and on Sarita and Pittsburg-Liberty Mine dumps, contain alunite, kaolinite, dickite, and lesser pyrophyllite.

## Host Rock and Alteration Mineral Ages

The granodiorite that encloses mineralized faults is ~98 Ma (Robinson and Kistler, 1986). Based on  $^{40}\text{Ar}/^{39}\text{Ar}$  ages of plagioclase and hornblende in unaltered flows and domes, trachyandesite of Masonic is ~15–14 Ma (table 1). The volcanoclastic-flow sequence that hosts Au-Ag-Cu mineralization in the central and southern parts of the district has not been directly dated; however, stratigraphic relations indicate that the age of the volcanoclastic-flow sequence is probably close to the youngest ages determined for trachyandesite of Masonic (~14 Ma), and could be as young as 13.3 Ma, the age of alunite in clastic and chemical sedimentary deposits at the Sarita Mine. Locally altered porphyritic trachyandesite domes in the northern part of the district are ~13.5–13.4 Ma (table 1). Unaltered andesite of Lakeview Spring in the southwestern part of the district is ~12.9 Ma (fig. 2; table 1).

The  $^{40}\text{Ar}/^{39}\text{Ar}$  dates of hydrothermal alunite mostly consist of two groups. Alunite in the volcanoclastic-flow sequence in the southwestern part of the district (Sarita, Red Rock, and Chemung Mines) is ~13.4–13.3 Ma; one alunite date near the Success Mine is 13.6 Ma (table 1). With the exception of the 13.6 alunite date, the older alunite dates are

similar to the dates of alunite in the Red Wash-East Walker River alteration zone (table 1); they are slightly younger than the ages of porphyritic trachyandesite domes (trachyandesite of Masonic Gulch) north of the district. Alunite in fault breccias in granodiorite and trachyandesite in the northern part of the district is ~13 Ma (Pittsburgh-Liberty, Maybell-Alton Jack, and Perrini Mines; table 1), and is indistinguishable from the age of andesite of Lakeview Spring when analytical error is considered.

## Red Wash-East Walker River Alteration Zone

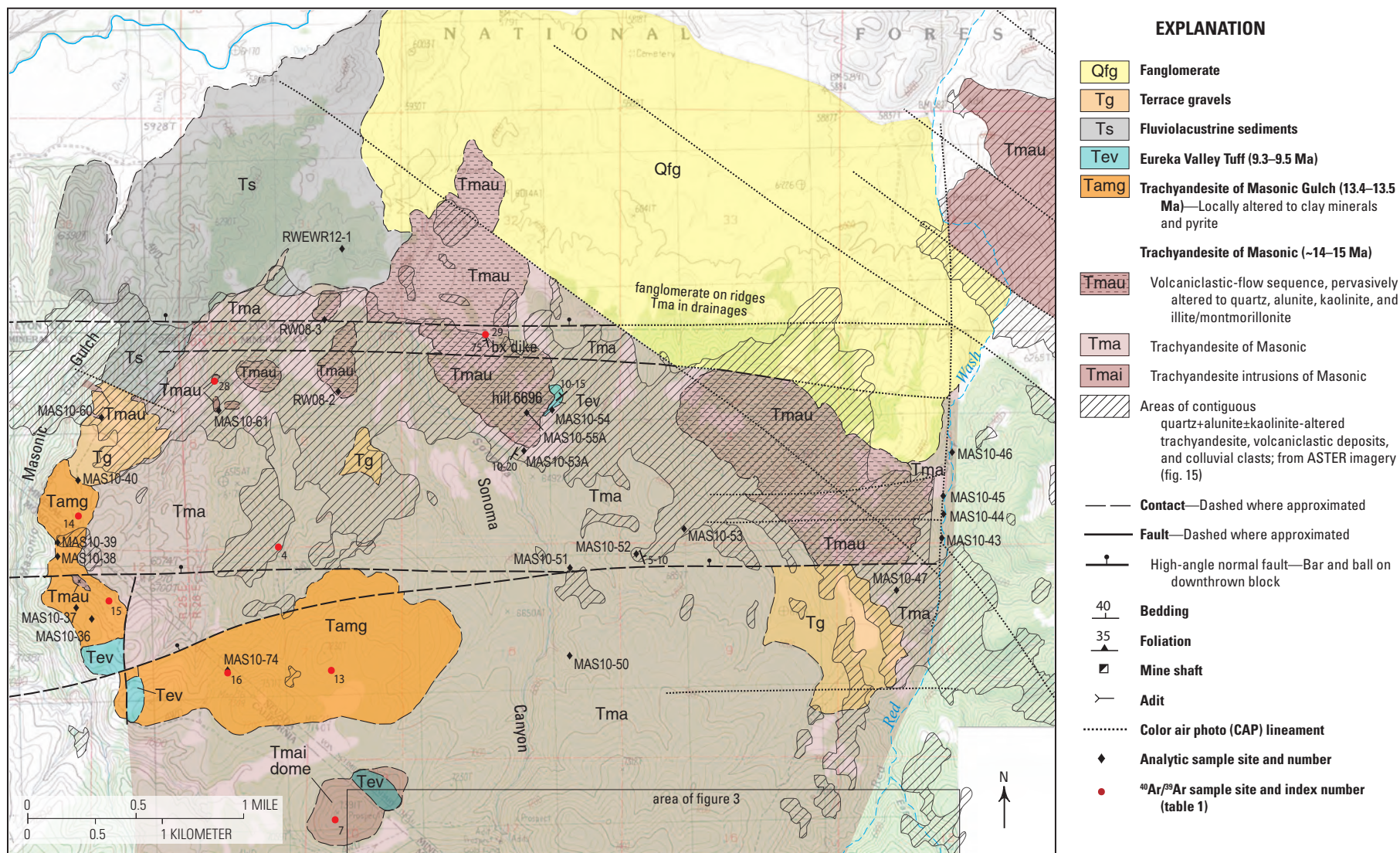
### Location

Secs. 2, 31, 32, Tps. 6 and 7 N., R. 26 E. (incompletely surveyed); secs. 31, 32, 33, 34, 35, 36, T. 7 N., R. 26 E., Lyon County, Nevada (fig. 1)

### Definition

The Red Wash-East Walker River alteration zone (RW-EWR AZ; fig. 14) is the western part of a larger, approximately west-east-trending alteration zone between the East Walker River and Fletcher Valley. The western part of the zone described here is bordered on the west and northeast by the East Walker River, and occurs entirely in volcanoclastic strata and lavas of trachyandesite of Masonic. In the vicinity of Red Wash, the alteration zone bifurcates with (1) an east-northeast-trending branch that extends across meanders of the East Walker River into Fletcher Valley, and (2) a more diffuse branch that extends south along Red Wash and southeast of Red Wash for ~2 km. To the north, the zone is covered by Tertiary and Quaternary sediments and colluvium (in part, Tfg, Ts, and Tg; fig. 14; John and others, 2012). The minimum dimensions of the western part of the zone are ~12 km west-east and <1–6 km north-south (~22 km<sup>2</sup>; figs. 1, 14). The entire zone from the East Walker River to Fletcher Valley covers at least 30 km<sup>2</sup>.

The approximately west-east-oriented, central part of the zone consists of volcanoclastic strata and lesser trachyandesite lavas that have been pervasively altered to quartz, alunite, and other minerals described below. Numerous small areas of quartz-alunite-kaolinite-altered rocks occur within 1 km south and north of the central part of the zone. Because of mapping scale and alteration zone definition, some of these outliers are not shown on figure 14. Between contiguous quartz-alunite-kaolinite-altered rocks of the zone and the Masonic Mining District (south of the area of fig. 14), extensive volumes of trachyandesite of Masonic have been partially altered to chlorite, sericite, clay minerals, calcite, and pyrite, which have mostly weathered to iron oxide minerals.



**Figure 14.** Geologic map of the Red Wash-East Walker River alteration zone, Lyon and Mineral Counties, Nevada, and Mono County, California.

## History and Production

Despite its relatively large size, no production is recorded for the RW-EWR AZ. Approximately 15 scattered and small prospect pits and trenches have been excavated, mostly in and adjacent to resistant exposures of volcaniclastic rocks and flows of trachyandesite of Masonic that are replaced by quartz, alunite, kaolinite, pyrite (iron oxide), and minor pyrophyllite. The workings presumably sought precious metals or Hg. Drill roads and drill cuttings, probably from exploration for precious metals ~1980–2000, are evident in secs. 5, 6, T. 7 N., R. 26 E. between Masonic Gulch and Sonoma Canyon, and in secs. 34, 35, T. 7 N., R. 26 E. southeast of the confluence of Red Wash and the East Walker River. Exploration leases for alunite, uranium, and clay minerals were filed in the 1970s over parts of the alteration zone (Gilbert, 1976).

## Stratigraphy

The RW-EWR AZ is in volcaniclastic strata and trachyandesite flows of trachyandesite of Masonic (fig. 14). Volcaniclastic strata are predominantly debris flows that are as much as ~60 m thick, and are nearly completely replaced by hydrothermal minerals. Less altered (propylitized) debris flows in one exposure consist of greenish-gray, rounded, and poorly sorted blocks of trachyandesite (<0.7 m in dimension) in a fine-grained matrix of comminuted andesite (fig. 4). Bedding, reflected approximately by outcrop orientation, strikes N30°E and dips 10–20°NW. Beneath and south of the volcaniclastic deposits are green to greenish-gray trachyandesite flows that have been variably altered to chlorite, mica-clay minerals, calcite, and pyrite (iron oxides).

Adjacent north-south and west-east alignments of porphyritic trachyandesite domes (trachyandesite of Masonic Gulch) occur ~1–1.5 km south of the central part of the alteration zone at the northern margin of the Masonic Mining District (fig. 14). The domes rise tens of meters above adjacent flows of trachyandesite of Masonic that have been variably altered to chlorite, mica-clay minerals, calcite, and pyrite (iron oxides). East of Masonic Gulch, the domes are partly overlain by Eureka Valley Tuff (Tev) and perched terrace gravels (Tg). Based on four <sup>40</sup>Ar/<sup>39</sup>Ar ages of plagioclase, the domes are 13.5–13.4 Ma, ~0.5 m.y. younger than the trachyandesite of Masonic lavas that they intrude (table 1). The porphyritic domes consist of 12–20 volume percent plagioclase crystals (1–4 mm), 3–5 volume percent subhedral and euhedral hornblende and clinopyroxene (0.5–3.5 mm), and <1 volume percent subhedral biotite (0.5–1.2 mm) in a pale-tan to olive-green matrix composed of partly devitrified glass, submillimeter-sized plagioclase, hornblende, biotite, pyroxene, and small amounts of apatite. Parts of the domes are altered to mica-clay minerals and pyrite (iron oxides).

Semiconsolidated gray- to dark-gray, fluviolacustrine sediments cover the north side of the alteration zone between Sonoma Canyon and East Walker River (Ts, fig. 14). These

relatively well-sorted and distinctly bedded, coarse sands, sands, and silts are distinguished from other basin-fill and colluvial deposits by color, sorting, bedding, and sparse, rounded heterolithic clasts that are mostly <10 cm in dimension. Gray sediments west of Masonic Gulch are overlain by thin (meters thick) gravel deposits consisting of rounded heterolithic cobbles and lesser boulders that partially cover several of the low, flat-topped ridges of trachyandesite south of the zone (Tg, fig. 14). Slopes of most north-south drainages that flank these ridges are partially covered with cobbles, which represent remnants of more extensive colluvial terraces that accumulated south of a more contiguous west-east landform of silicified volcaniclastic deposits. The gray sediments and dissected gravel terraces, together with west-east and northeast-trending normal faults between the Masonic Mining District and the alteration zone, suggest (1) uplift of Masonic Mountain and the district relative to the alteration zone since 11 Ma, the approximate age of the oldest basin-fill of Fletcher Valley (table 1); and (2) deposition during at least two hydrologic regimes based on differing clast size and sorting within the sedimentary deposits.

## Structure

Structures that may have channeled hydrothermal fluids into permeable volcaniclastic strata and trachyandesite to form the RW-EWR AZ are evident at contrasting scales. Veins and crosscutting breccias, described below, are common within the alteration zone, but most can be traced for only a few meters to a few tens of meters and are not aligned. On the scale of the entire zone, linear and slightly curvilinear structures are conspicuous on color air photos and, to a lesser extent, on ASTER imagery (Rockwell, 2010). Within the alteration zone these lineaments trend predominantly west-east and northwest-southeast (figs. 14, 15). Because of their linearity, these structures most likely represent postalteration faults, but little to no stratigraphic displacement can be demonstrated. A north-south lineament along Red Wash may displace the zone east of Red Wash to the north, although evidence of stratigraphic offset also is minimal (John and others, 2012). Furthermore, silicified carapaces of volcaniclastic strata, which cap most uplands in the RW-EWR AZ, are not significantly displaced vertically, nor do they appear to be displaced laterally. The lateral dimensions of the zone are probably controlled by a series of en echelon west-east faults with minor vertical and lateral displacement, and by local breccias, which were likely conduits for hydrothermal fluids.

## Hydrothermal Alteration

Topographic definition of the RW-EWR AZ is reflected by the west-east series of flat-topped to rounded landforms with resistant, silicified carapaces that are flanked by recessive-weathering slopes of clay-mica-pyrite-altered volcaniclastic strata and trachyandesite flows. The farthest

western part of the alteration zone consists of low, en echelon ridges and small spires, mostly meters in dimension, of silicified volcanoclastic strata and trachyandesite that commonly are brecciated and cemented by quartz and alunite. These resistant ridges and spires in part occur in clay-mica-pyrite-altered trachyandesite and locally protrude through overlying Tertiary-Quaternary sedimentary deposits. Outcrops of the silicified strata vary in color from gray to mottled, intense red-brown and beige, depending on iron oxide abundance, and have hackly to dense, smooth surfaces. In contrast, clay-mica-pyrite-altered volcanoclastic strata and trachyandesite are beige to reddish-brown with rough surfaces, although most exposures have largely degraded into fine talus.

Silicified volcanoclastic strata and trachyandesite flows consist of very fine-grained aggregates of quartz and alunite, and lesser pyrophyllite, dickite, and kaolinite (figs. 14, 15). Alunite and clay minerals also occur in breccia matrices, and in irregular and discontinuous, millimeter-thick veins, usually with quartz. At least three sets of crosscutting breccias and veins are evident. The youngest breccia matrices are locally vuggy, with vugs encrusted by submillimeter-sized, euhedral quartz, and rarely by euhedral alunite. The interpreted age of alteration, ~13.3 Ma (table 1), is based on the ages of relatively coarse-grained matrix alunite (samples RW08-1 and MAS10-55, fig. 14) of the youngest breccias. Older veins and breccia matrices consist of fine-grained to microcrystalline aggregates of quartz±alunite. Breccia clasts are gray to beige, and consist of very fine-grained aggregates of quartz±alunite±pyrite. Some relict trachyandesite clasts comprise very fine-grained gray quartz with casts of leached phenocrysts. On recessively weathered slopes adjacent to carapaces, breccia clasts and matrices consist of quartz+clay-mica minerals±pyrite.

## Minor Elements in Rocks

Although the exploration workings are in or near the most intensively altered rocks, they have exposed no obvious evidence of element concentrations. Most minor element analyses of 26 rock samples indicate zero to somewhat elevated concentrations of metals and other elements (table 1-2). Samples of intensely altered rocks contain variably elevated concentrations of Hg (1–5.2 ppm), As (205; 477 ppm), Bi (1–7 ppm), Co (~6; 30 ppm), Cu (148; 189 ppm), Mo (21–168 ppm), Pb (66–258 ppm), and Te (~1–7 ppm). Elevated concentrations of Ba, W, Se, Sr, Cr, Mn, and Ni occur in individual samples. Samples with sulfur abundances >1 volume percent and >1,000 ppm Ba contain alunite, pyrite, and barite.

## Sulfur Isotope Composition

The sulfur isotope value ( $\delta^{34}\text{S}$ ) of matrix alunite in a dated sample (RW08-1) of brecciated and silicified volcanoclastic strata is 20.6 ‰ (table 2). This  $\delta^{34}\text{S}$  value is consistent with disproportionation of magmatic  $\text{SO}_2$  (Rye, 2005) as the fundamental process responsible for pervasive quartz-alunite-pyrite (iron oxides) alteration of the volcanoclastic strata and trachyandesite flows.

## ASTER Imagery

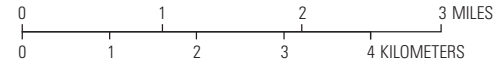
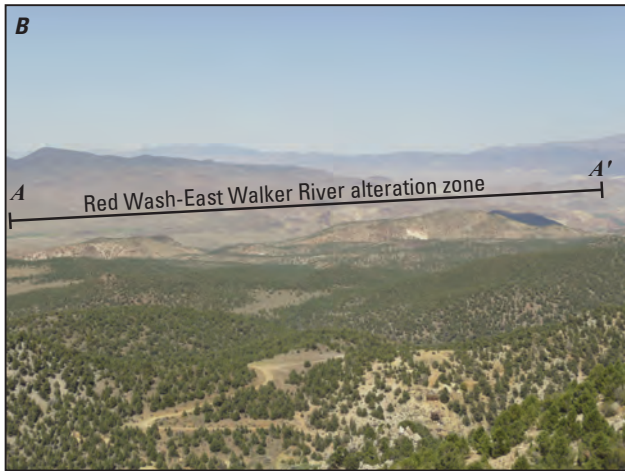
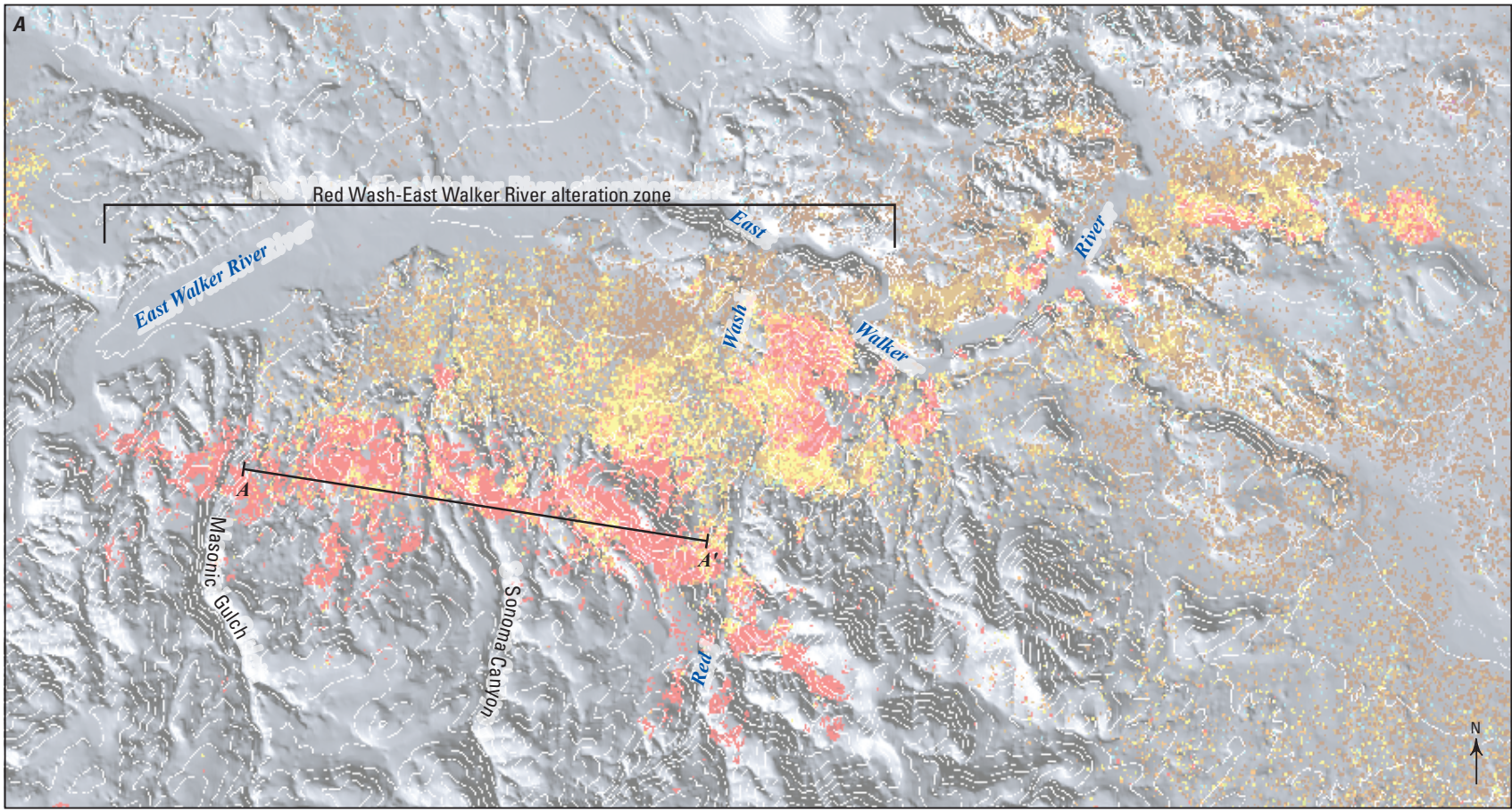
ASTER spectra of the RW-EWR AZ (fig. 15; Rockwell, 2010) show that an extensive quartz-alunite±pyrophyllite association spatially coincides with erosionally resistant, stratiform carapaces of volcanoclastic strata that form the west-east alignment of landforms. Pixels interpreted as representing kaolinite and montmorillonite are within and north of the main area of quartz-alunite-pyrophyllite-altered rocks. Many of these pixels are coincident with Tertiary-Quaternary sedimentary deposits that contain altered clasts, but exposures of clay-altered trachyandesite beneath sedimentary deposits in drainages, and in Red Wash, indicate that, for the most part, the pixels represent bedrock. East of Red Wash, kaolinite-montmorillonite-altered rocks overlap and extend south of the area of quartz-alunite-pyrophyllite-altered rocks. These alteration patterns continue east-northeast into Fletcher Valley.

## SWIR Spectra

SWIR analyses of representative samples from the RW-EWR AZ confirm the presence of alunite, pyrophyllite, dickite, kaolinite, and montmorillonite in and adjacent to the resistant stratiform carapaces of altered volcanoclastic strata.

## Hydrothermal Mineral Ages

Within the RW-EWR AZ, alunite in the matrices of silicified breccias near Masonic Gulch, and near Sonoma Canyon, has  $^{40}\text{Ar}/^{39}\text{Ar}$  dates of  $13.34 \pm 0.035$  Ma and  $13.27 \pm 0.02$  Ma, respectively (fig. 14; table 1). These alunite dates are analytically indistinguishable from the dates of alunite at the Sarita, Red Rock, and Chemung Mines in the Masonic Mining District ~5 km south of the RW-EWR AZ. They are slightly younger than the ages of porphyritic domes of trachyandesite of Masonic Gulch (13.5–13.4 Ma; table 1) in the northern part of the Masonic Mining District, ~1–1.5 km south of the central part of the alteration zone (fig. 3).



**EXPLANATION**

- | Clay-bearing assemblages   | Sulfate-bearing assemblages                               |
|--|---|
| Kaolinite <sup>1</sup>   | Possible prophyllite (± alunite) <sup>2</sup>             |
| Kaolinite ± sericite   | Alunite (± prophyllite) <sup>2</sup>                      |
| Kaolinite ± sericite <sup>1</sup> (high-albedo surfaces with minor and (or) impure kaolinite, often supergene) | Natroalunite, or alunite and minor kaolinite <sup>2</sup> |
| Montmorillonite/smectite, or low-abundance sericite  | Alunite and kaolinite <sup>2</sup>                        |
|  | Jarosite ± gypsum, or ferric iron and hydrous quartz      |
|  | Gypsum ± clays  |

<sup>1</sup>Kaolinite-bearing assemblages may be misidentified in areas with sparse, dry vegetation ± sericite or montmorillonite

<sup>2</sup>These assemblages may represent areal mixtures of clay/mica and dry vegetation, or areas of sensor instability related to low or high surface albedo

## East Brawley Peak Alteration Zone

### Location

Secs. 24, 25, 36, T. 5 N., R. 27 E.; secs. 30, 31, T. 5 N., R. 28 E., Mineral County, Nevada; secs. 4, 5, T. 4 N., R. 28 E., Mono County, California (fig. 1)

### Definition

The East Brawley Peak alteration zone (EBP AZ; fig. 16) is southwest of the adjacent Aurora Mining District, and lies mostly north of the California-Nevada border. It has a north-south dimension of ~4.5 km, an average west-east dimension of ~1.7 km (~7.7 km<sup>2</sup>), and is approximately centered on East Brawley Peak. The alteration zone is underlain predominantly by trachyandesite of Aurora, bordered to the west by trachyandesite of West Brawley Peak, and bordered to the north by rhyolite of Del Monte Canyon and rhyolite of East Brawley Peak (fig. 16). To the northeast and south, quartz-alunite-pyrite-dominant mineral assemblages of the EBP AZ grade into propylitically altered trachyandesite of Aurora. To the east, the EBP AZ adjoins a west-east-aligned zone of variably altered Tertiary and pre-Tertiary rocks that includes the Spring Peak sinter (fig. 16). Temporal relationships of the Spring Peak sinter, the EBP AZ, and the Aurora Mining District, have not been determined by geochronology.

### History and Production

No production is recorded from the EBP AZ. A drilling access road to the top of East Brawley Peak was constructed in the 1980s(?), and at least one hole was drilled from a site ~0.2 km north of the summit. Several shallow bulldozer excavations near the summit may predate the drill access road and site.

### Stratigraphy

Most of East Brawley Peak is mantled by slope wash consisting of strongly silicified rocks exposed on and near the

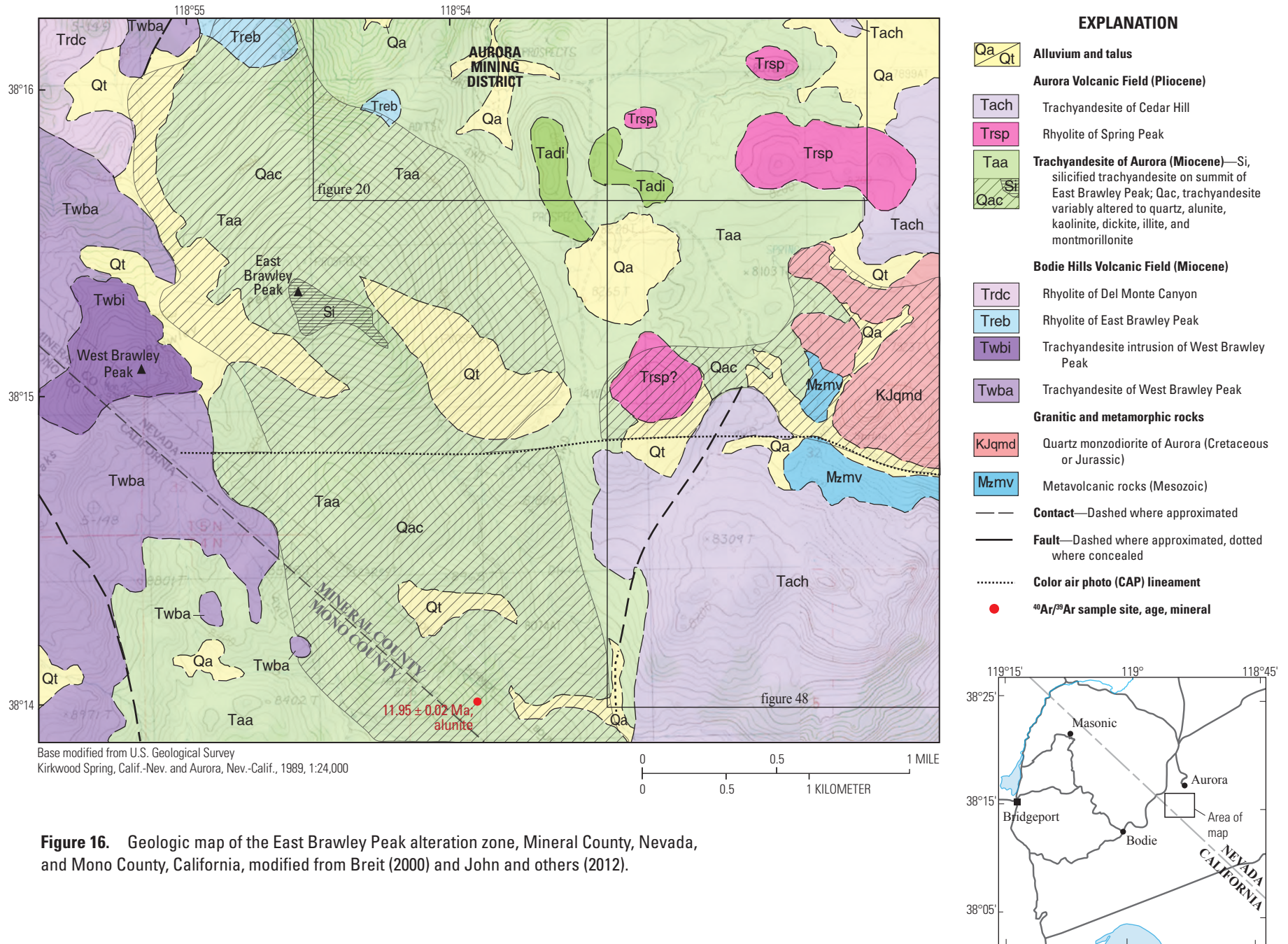
summit, and on the hill ~1 km south of the summit. Based on relict textures in silicified and subjacent altered rocks, and on exposures in the Aurora Mining District, the EBP AZ is underlain entirely by trachyandesite of Aurora. The trachyandesite of Aurora forms a series of moderate-volume lava flows and associated laharic debris flows and volcanoclastic deposits similar to those included in the trachyandesite of Masonic. The abundance of debris flows interbedded with compositionally equivalent lava flows, both intruded by numerous small, intermediate-composition intrusions, suggests that these rocks comprise a stratovolcano centered near the Aurora Mining District. Trachyandesite of Aurora is a medium- to pale-gray, moderately porphyritic trachyandesite, and includes andesite and trachydacite. It contains about 3–42 volume percent phenocrysts, trachytically layered in some places, of plagioclase, distinctive 1–5 mm hornblende euhedra, and trace amounts of clinopyroxene and biotite set in a moderately devitrified groundmass.

K-Ar ages of trachyandesite of Aurora range from 15.8 to 13.8 Ma (Silberman and McKee, 1972; Kleinhampl and others, 1975). More precise <sup>40</sup>Ar/<sup>39</sup>Ar dates of hornblende and plagioclase are 13.13–12.58 Ma (table 1). Based on <sup>40</sup>Ar/<sup>39</sup>Ar dates of plagioclase, unaltered trachyandesite of West Brawley Peak, which overlies altered rocks of the EBP AZ, is 11.51–11.32 Ma (table 1; John and others, 2012).

### Structure

Breit (2000) attributed structural control of the EBP AZ to a N75°W-striking “left-stepping dilational jog in a N45°W-striking strike-slip fault near the summit of East Brawley Peak.” This fault pair is defined by the distribution of silicified trachyandesite, N75°W-striking quartz veins, and high temperature, saline fluid inclusions in quartz fragments in veins atop East Brawley Peak that may have been transported upward from a deep source. On a regional scale, the north-south Esmeralda vein, which trends into the EBP AZ, other N40–70°E-trending veins in the Aurora Mining District, and the structures atop East Brawley Peak, may be related to right lateral faults produced by N40–45°W-oriented shear (Sylvester, 1988; Breit, 2000). However, northwest-trending structures with significant oblique displacement have not been recognized elsewhere in the Bodie Hills.

**Figure 15. (Facing page)** A, Advanced Spaceborne Thermal Emission and Reflection Radiometer (ASTER) imagery of the Red Wash-East Walker River alteration zone (after Rockwell, 2010). B, Image showing view to the northeast of the alteration zone.



**Figure 16.** Geologic map of the East Brawley Peak alteration zone, Mineral County, Nevada, and Mono County, California, modified from Breit (2000) and John and others (2012).



A west-east lineament that is conspicuous on color aerial photography (CAP lineament; fig. 16) trends through the EBP AZ and is coincident with the southern border of the west-east zone of altered rocks that includes the Spring Peak sinter (fig. 16). Although stratigraphic displacement of Miocene and Pliocene volcanic rocks along this lineament has not been recognized, Pliocene trachyandesite of Cedar Hill straddles the lineament. This relationship suggests that, if the lineament is a fault, then displacement along it is pre-Pliocene. High-angle displacement along this lineament may have contributed to relief and the relatively large amount of erosion of the Aurora Mining District.

## Hydrothermal Alteration

According to Breit (2000), hydrothermal alteration minerals within the EBP AZ are vertically zoned. Quartz-alunite-kaolinite-pyrite-altered trachyandesite and vuggy silica (presumably hydrothermal and residual quartz) are dominant between 8,050 and 8,800 ft elevation, and pervasively silicified and brecciated trachyandesite is dominant from 8,800 to 9,400 ft elevation (summit of East Brawley Peak). Laterally adjacent to quartz-alunite-kaolinite-altered trachyandesite on East Brawley Peak, are zones of “intermediate argillic alteration” (Breit, 2000) and propylitically altered trachyandesite.

Alteration mineral assemblages within the EBP AZ appear to grade to the north into propylitically altered trachyandesite of Aurora in the Aurora Mining District, but the transition occurs on slopes mantled by silicified trachyandesite shed from the summit of East Brawley Peak. Hydrothermal mineral ages indicate that the Aurora veins are younger than the EBP AZ. Detailed mapping, geochronology, and paragenetic examinations required to determine the relationship of the EBP AZ to veins of the Aurora Mining District, and to the Spring Peak alteration zone, have not been completed.

## Minor Elements in Rocks

Breit (2000) reported elevated Ti (>1 weight percent) and Zr in samples of pervasively silicified trachyandesite, and somewhat elevated concentrations of Au, Ag, As, Sb, Hg, Cu, Pb, Bi, Mo, Se, Te, and Ba in a small percentage of samples categorized as argillized, argillized and iron-stained, propylitized, silicified, silicified and iron-stained, and vein rock. This geochemical characterization was derived from three sets of samples collected during 1967–68, 1988, and 1992 that were analyzed by different methods.

## ASTER Imagery

ASTER imagery (Rockwell, 2010) of the EBP AZ shows clusters of pixels on East Brawley Peak and on the hill to the south that represent quartz-alunite±pyrophyllite and lesser kaolinite. The clusters are spatially coincident with silicified trachyandesite of Aurora that contains variable amounts of alunite. Scattered pixels that represent sericite are distributed near the south and southeast margins of the zone. On the north-northeast side of the alteration zone, quartz-alunite±pyrophyllite-altered trachyandesite and kaolinite-altered trachyandesite terminate rather abruptly against relatively dense pixelation that represents sericite-altered trachyandesite of Aurora in the Aurora Mining District.

## SWIR Spectra

SWIR spectral analyses of rock samples within the EBP AZ show that recessively weathered greenish, altered trachyandesite of Aurora in the saddle on the summit of East Brawley Peak contains montmorillonite. Veins and breccia matrix in silicified trachyandesite north of the summit consist of dickite; adjacent trachyandesite wall rocks contain dickite and kaolinite. Trachyandesite of Aurora and rhyolite of East Brawley Peak (?), north and south of the summit, contain alunite, dickite, kaolinite, montmorillonite, illite, and illite/montmorillonite.

## Fluid Inclusion Microthermometry and Composition

Breit (2000) described narrow cryptocrystalline quartz veins near the summit of East Brawley Peak that contain quartz fragments with four populations of fluid inclusions, and silicate melt inclusions. One type of inclusion containing halite and other daughter minerals homogenized to liquid at  $T \geq 470$  °C; another type contains liquid  $\text{CO}_2$ . According to Breit (2000) high homogenization temperatures and the presence of silicate melt inclusions suggest that these quartz fragments are magmatic in origin and were transported upward from an unexposed intrusion.

## Hydrothermal Mineral Ages

Breit (2000) reported K-Ar and  $^{40}\text{Ar}/^{39}\text{Ar}$  dates of  $13.7\pm 0.5$  Ma and  $12.34\pm 0.04$  Ma, respectively, for alunite from East Brawley Peak. The  $^{40}\text{Ar}/^{39}\text{Ar}$  date of  $11.954\pm 0.016$  Ma (sample AUR10-3, table 1) was obtained for alunite on the south slope of East Brawley Peak (approximately the same location as the samples dated by Breit). This latter alunite occurs as millimeter-sized crystals that encrust fractures and irregular pockets in silicified and leached trachyandesite of Aurora. The alunite dates are older than  $^{40}\text{Ar}/^{39}\text{Ar}$  dates of K-feldspar in veins in the Aurora Mining District, which range in age from 10.5 to 10.0 Ma (table 1).

## Sawtooth Ridge Alteration Zone

### Location

Secs. 12, 13, T. 5 N., R. 27 E., Mineral County, Nevada (fig. 1)

### Definition

The Sawtooth Ridge alteration zone (SR AZ; fig. 17) is mostly in rhyolite of Aurora Creek ( $11.18\pm 0.01$  Ma, table 1; John and others, 2012) that has been altered to quartz and opaline silica, alunite, and clay minerals. The SR AZ covers  $\sim 2$  km<sup>2</sup> immediately north of Aurora Creek and adjoins the Aurora Mining District to the south and east. It is distinguished from alteration of rhyolite of Aurora Creek in the northern part of the Aurora Mining District by alteration mineral associations, by age ( $11.105\pm 0.018$  Ma, table 1), and by the presence of Aurora district veins ( $\sim 10$ – $10.5$  Ma, table 1) in rhyolite of Aurora Creek east of the Aurora cemeteries, but not in altered rocks of the zone to the west.

### History and Production

No production is recorded from the SR AZ. A prospect near the north edge of the zone was excavated in brecciated rhyolite with dense iron oxide matrix. Roads in the southern part of the zone, west of the Aurora cemeteries, apparently provided access to drill sites, but most have been partly reclaimed and no drill cuttings were identified. A small open cut and shaft in rhyolite of Aurora Creek east of the SR AZ expose narrow quartz veins that most likely represent a northern extension of Aurora district veins.

## Stratigraphy

The rhyolite of Aurora Creek consists of coalescing domes and proximal flows of flow-banded rhyolite and subordinate lithic-rich tuff that are gray where unaltered and beige to white where altered (fig. 17). The rhyolite is overlain to the west and northeast by trachyandesite of Del Monte (11 Ma), to the southwest by nearly coeval rhyolite of Del Monte Canyon (11.2 Ma; John and others, 2012), and to the north and northeast by late Pleistocene trachyandesite of Aurora Crater (north and northeast of the area of fig. 16). Rhyolite of Aurora Creek overlies trachyandesite of Aurora ( $\sim 13.1$ – $12.6$  Ma; table 1), which is extensively exposed immediately south of the SR AZ in the Aurora Mining District. Trachyandesite of West Brawley Peak ( $\sim 11.5$  Ma, table 1) crops out in the north part of the alteration zone and is locally clay-altered.

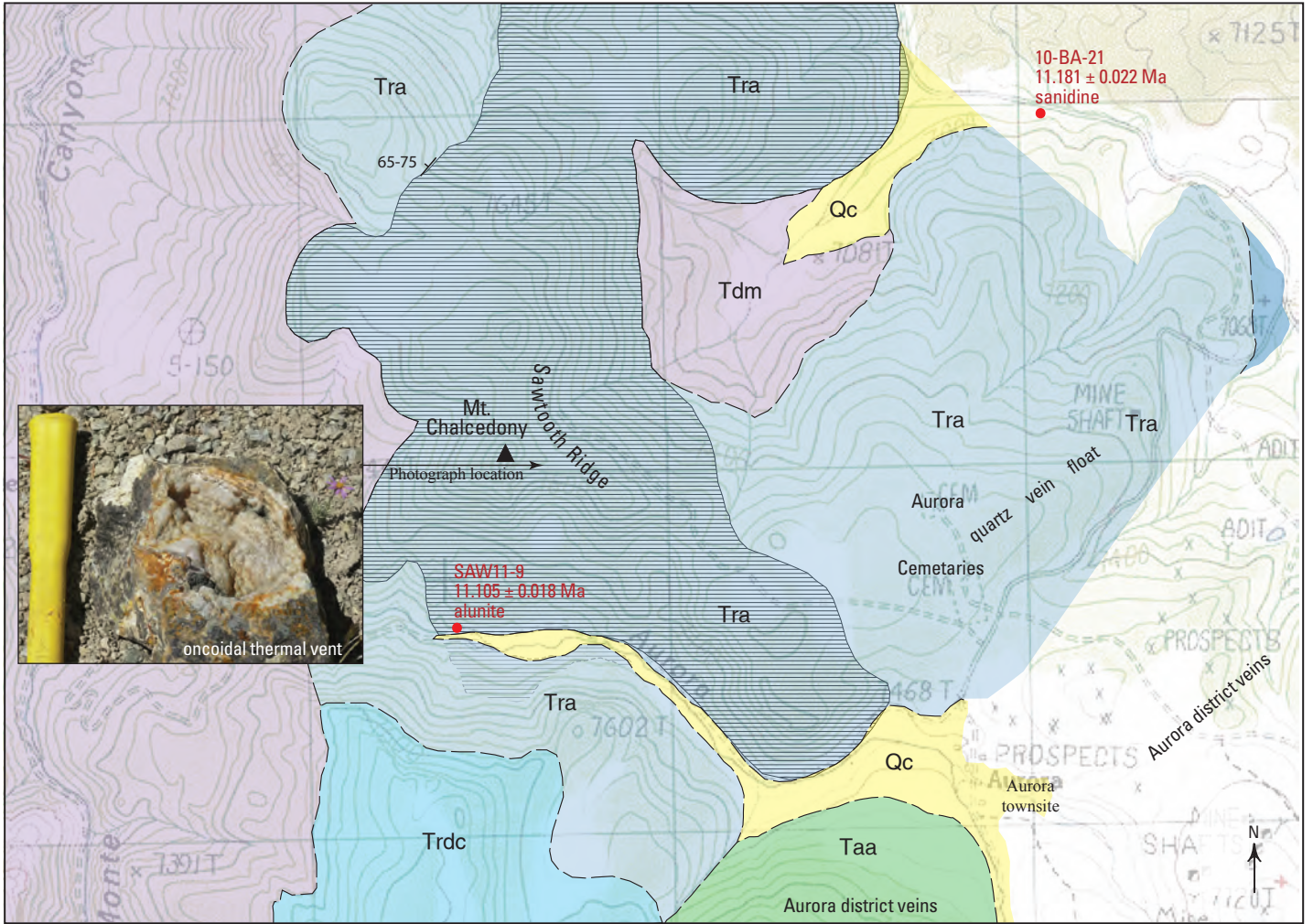
### Structure

No faults transect rhyolite of Aurora Creek within the area of figure 17, nor can any be demonstrably projected into the SR AZ from available geologic maps (John and others, 2012).

## Hydrothermal Alteration

Alteration of rhyolite of Aurora Creek within the SR AZ is most pervasive in an area bounded by Aurora Creek to the south and extending about 2.5 km north of Aurora Creek (fig. 17). In this area, rhyolite is variably altered to quartz and opal, and lesser amounts of alunite, kaolinite, montmorillonite, and illite. Sparse feldspar and biotite phenocrysts commonly are replaced by sericite and clay minerals. The most intensely altered rocks are flow breccias or breccias related to dome emplacement on the ridge top north of Aurora Creek (fig. 17). The high point on that ridge was known as “Mt. Chalcedony” during the main period of production in the Aurora Mining District (Wasson, 1878). On Sawtooth Ridge between Mt. Chalcedony and the Aurora cemeteries, thermal vents are represented by small, bowl-shaped depressions of layered chalcedonic quartz and oncoids, or quartz spheres that were turbulently agglomerated (Lynne, 2012; fig. 17). Abundant alunite occurs in chalcedonic quartz stockwork veins and in matrices of brecciated rhyolite  $\sim 135$  m below the oncoidal thermal vents.

Float blocks of layered quartz veins that strongly resemble Aurora district veins are sporadically distributed in and east of the Aurora cemeteries. Narrow quartz veins (millimeters to centimeters thick) are exposed in a small open cut in rhyolite of Aurora near the eastern margin of figure 17 (sample AUR11-19). Montmorillonite in light-colored tuff exposed along haul roads to the Esmeralda mill northeast of the cut (fig. 17, sample AUR11-18) may also be related to vein mineralization in the Aurora Mining District.

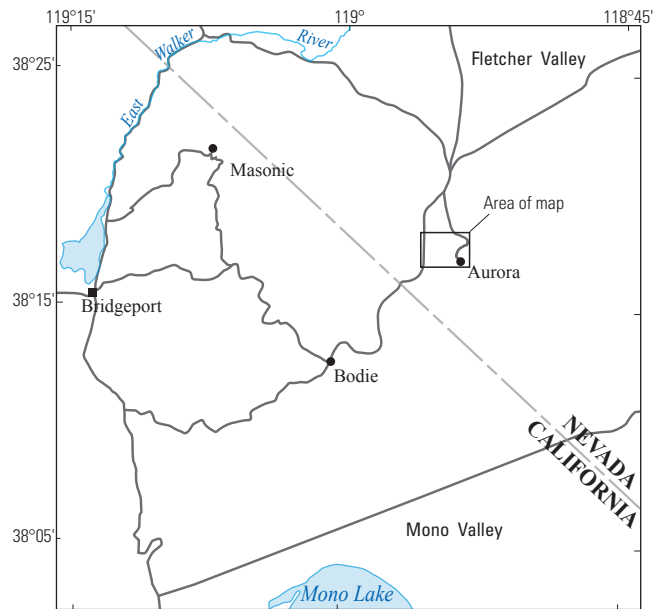


Base modified from U.S. Geological Survey  
Aurora, Nev.-Calif., 1989, 1:24,000

0 0.5 1 MILE  
0 0.5 1 KILOMETER

**EXPLANATION**

- Qc** Colluvium
- Tdm** Trachyandesite of Del Monte
- Trdc** Rhyolite of Del Monte Canyon
- Tra** Rhyolite of Aurora Creek
- Tuff
- Silica-alunite-kaolinite alteration
- Taa** Trachyandesite of Aurora
- Contact**—Dashed where approximated
- 65-75** Bedding
- <sup>40</sup>Ar/<sup>39</sup>Ar sample site**—Number, age, mineral



**Figure 17.** A, Geologic map of the Sawtooth Ridge alteration zone, Mineral County, Nevada. B, Image of a remnant bowl-shaped thermal vent consisting of layered chalcedonic quartz and turbulently agglomerated, spherical quartz oncoids.

Most samples of altered rhyolite in the SR AZ do not contain elevated concentrations of minor elements; however, several samples of rhyolite and iron oxide-matrix breccia contain variably elevated concentrations of Ag, As, Hg, Mo, Rb, Sb, Sr, and Te (table 1-4).

## Sulfur Isotope Composition

Alunite in veined and brecciated rhyolite below oncoidal thermal vents that was collected for  $^{40}\text{Ar}/^{39}\text{Ar}$  dating has a  $\delta^{34}\text{S}$  value of  $-3.2\text{‰}$  (table 2), and is not associated with sulfide minerals. This isotope composition and the absence of sulfide minerals indicate that SR AZ alunite formed by near-surface oxidation of  $\text{H}_2\text{S}$  (steam-heated environment of Rye, 2005).

## ASTER Imagery

ASTER imagery (Rockwell, 2010) shows that the SR AZ is coincident with a central area of relatively dense pixels that correspond to alunite±kaolinite and lesser quartz, surrounded by a more diffusely altered area of illite-altered rocks.

## SWIR Spectra

SWIR spectra of hand samples of rhyolite of Aurora Creek from the SR AZ correspond to opal, alunite, kaolinite, dickite, and montmorillonite.

## Hydrothermal Mineral Age

Alunite (±chalcedonic quartz) matrix that cements angular clasts of brecciated rhyolite of Aurora Creek (fig. 17, sample SAW11-9) has a  $^{40}\text{Ar}/^{39}\text{Ar}$  date of  $11.105\pm 0.018$  Ma (table 1).

## Aurora Canyon Alteration Zone

### Location

Secs. 17, 18, 19, 20, 21, 30, 31, T. 5 N., R. 26 E. (unsurveyed); sec. 24, T. 5 N., R. 25 E. (unsurveyed), Mono County, California (fig. 1)

### Definition

The Aurora Canyon alteration zone (AC AZ; fig. 18) is a contiguous volume of predominantly trachyandesite of Masonic that has been extensively altered to quartz±alunite, pyrite (iron oxides), mica, and clay minerals. The AC AZ occurs in and south of Aurora Canyon, has west-east and north-south dimensions of 4.5 and 2.3 km, respectively, and covers  $\sim 8.1$  km<sup>2</sup>. The AC AZ is overlain by younger volcanic

rocks to the south (trachydacite of Potato Peak and trachyandesite of Willow Springs), and may be coextensive with the Potato Peak alteration zone  $\sim 2$  km to the southeast. Alteration intensity within the AC AZ decreases to the west and east into unaltered trachyandesite of Clark Canyon; small internal areas of unaltered trachyandesite are mostly represented by float.

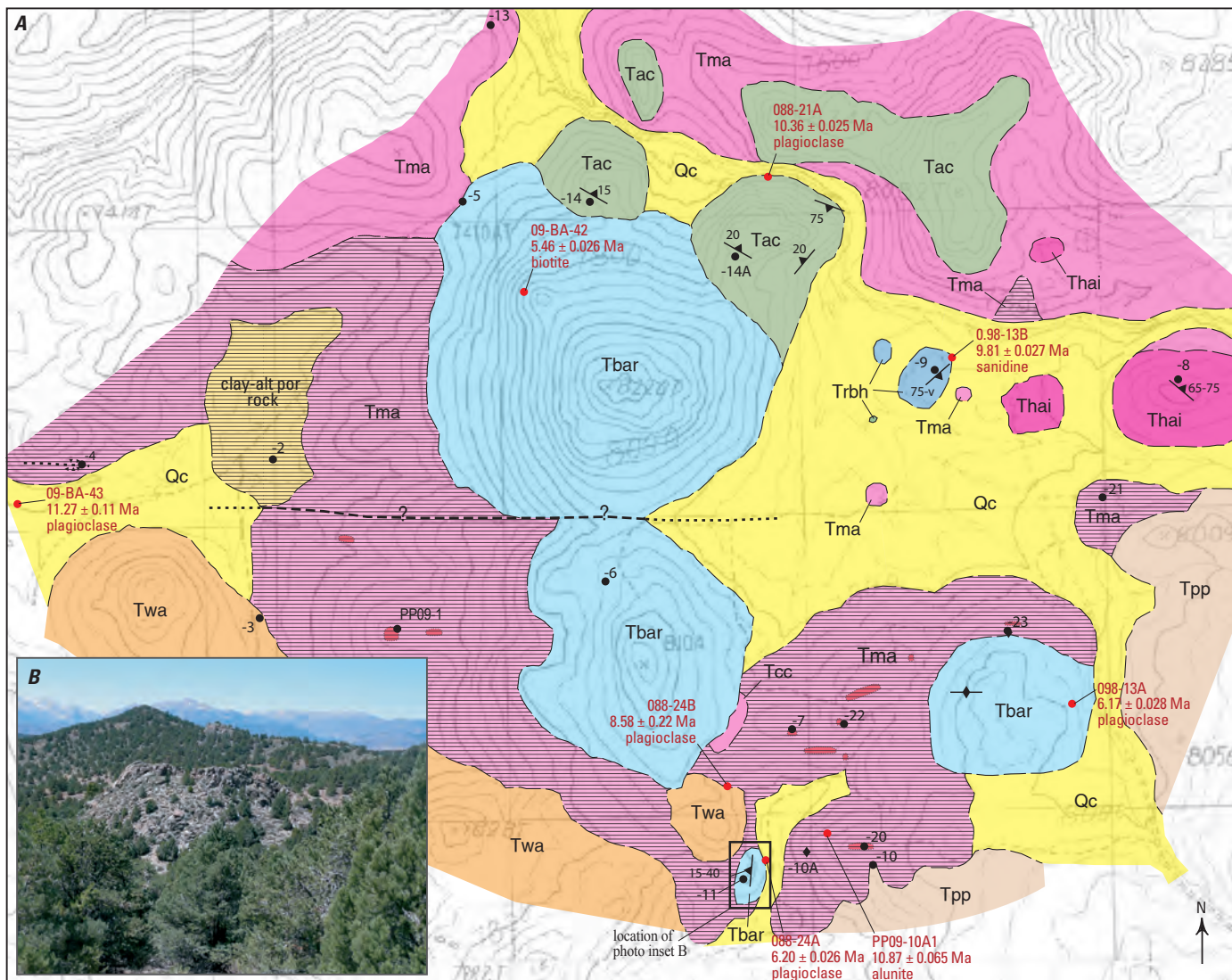
## History and Production

No production is recorded from the AC AZ, consistent with the small scale of surface disturbance, scattered prospect pits, trenches, and drill roads. Roads in the eastern part of the alteration zone probably provided drill site access, although no drill cuttings were identified. Ages of these workings and roads are unknown, but the absence of reclamation suggests that they predate land use regulations of the Federal Land Policy Management Act (FLPMA) of 1976.

## Stratigraphy

Trachyandesite of Masonic flows and debris flows ( $\sim 15$ – $14$  Ma) were erupted and extensively altered prior to emplacement of younger volcanic rocks that intrude and enclose the AC AZ (fig. 18). Younger, unaltered rocks include trachyandesite of Aurora Canyon (10.6–10.3 Ma; John and others, 2012), rhyolite of Bodie Hills (9.9–9.7 Ma) near the center of the AC AZ, trachydacite of Potato Peak (9.1–8.8 Ma) to the southeast, and trachyandesite of Willow Springs (8.6–8.0 Ma) to the southwest. Unaltered trachyandesite of Clark Canyon (11.3 Ma; John and others, 2012) is exposed west of the alteration zone. Trachyandesite of Willow Springs that unconformably overlies altered trachyandesite flows comprise domelike landforms that partly filled depressions between resistant hills and ridges of altered trachyandesite. Three prominent domes of rhyolite of Big Alkali (6.2–5.5 Ma) have intruded the alteration zone; the internal structure of these domes is depicted by a small concentrically foliated “half” dome in NW $\frac{1}{4}$ /NW $\frac{1}{4}$  sec. 31, T. 5 N., R. 26 E. (fig. 18). The youngest deposits in the AC AZ consist of colluvium that accumulated in recessively weathered areas of clay-altered trachyandesite, and in active drainages.

The trachyandesite of Clark Canyon forms a series of small-volume plugs, arrayed along an east-northeast trend in Aurora Canyon, and includes a small-volume lava flow about 1.5 km south of Aurora Canyon. The trachyandesite of Aurora Canyon forms a discontinuous series of small-volume lava domes; coarse block and ash flow deposits and (or) carapace breccias are preserved along the margins of some domes. The trachydacite of Potato Peak forms an elliptical eruptive center of moderate volume consisting of coalesced lava flows and exogenous flow domes. The trachyandesite of Willow Springs forms a north-northwest elongate set of moderate-volume, coalesced, lava domes and flows. These four units contain 6–38 volume percent phenocrysts of plagioclase, clinopyroxene, hornblende, and biotite that are locally trachytically



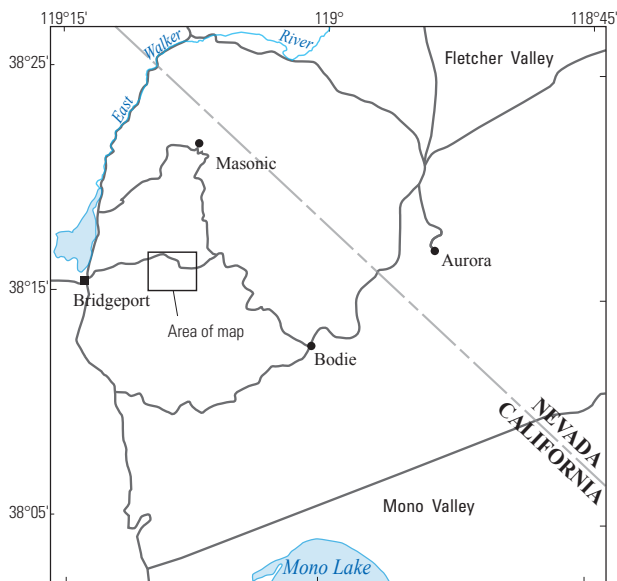
Base modified from U.S. Geological Survey  
Bridgport, Calif., and Dome Hill, Calif.-Nev., 1989, 1:24,000

0 0.5 MILE  
0 0.5 KILOMETER

**EXPLANATION**

- Qc Colluvium
- Tbar Rhyolite of Big Alkali
- Twa Trachydacite of Willow Springs
- Tpp Trachydacite of Potato Peak
- Trbh Rhyolite of Bodie Hills
- Tac Trachydacite of Aurora Canyon
- Thai Hornblende andesite intrusion
- Tma Trachyandesite of Masonic—  
Line-patterned where hydrothermally altered; dense red color shows quartz-alunite ledge

- Contact
- Fault—Dashed where approximated, dotted where concealed
- 35  Foliation
- ◆ Vertical foliation
- Sample locality
- <sup>40</sup>Ar/<sup>39</sup>Ar sample site—Number, age, mineral
- ∴ Breccia



**Figure 18.** A, Geologic map of the Aurora Canyon alteration zone, Mono County, California. B, Image showing a concentrically exfoliated rhyolite dome (unit Tbar, rhyolite of Big Alkali) near the southern map boundary.

aligned. Trachyandesite of Willow Springs contains rare olivine phenocrysts, and plagioclase phenocrysts in this unit are characteristically larger than those in most rocks of the Bodie Hills volcanic field.

Rhyolite of Bodie Hills forms a series of small-volume lava domes, many with carapace and (or) basal flow breccias. It contains 1–23 percent phenocrysts of plagioclase, quartz, sanidine, biotite, hornblende, and rarely clinopyroxene in locally glassy and flow-banded matrix. The rhyolite of Big Alkali forms a prominent north-trending array of low-volume domes. It contains 6–42 volume percent phenocrysts of plagioclase, hornblende, and biotite, and trace amounts of quartz and sanidine. Small exposures of hornblende andesite along the Aurora Canyon road in the eastern part of the AC AZ contain prominent hornblende phenocrysts.

## Structure

No faults have been identified in the AC AZ, and the distribution of alteration mineral associations and lithology does not require significant fault displacement. However, a west-east ( $\pm 10^\circ$ ) structural trend is implied by the distribution of altered trachyandesite, by alignment of resistant exposures of quartz-altered trachyandesite, and by west-east and east-northeast-trending linear ridges of silicified breccia (fig. 18). On a larger scale, rhyolite of Big Alkali domes in the AC AZ are roughly collinear with a north-south alignment of other rhyolite of Big Alkali domes to the south and north (John and others, 2012). Although the rhyolite domes are  $\sim 4$ – $5$  m.y. younger than the AC AZ, their alignment may reflect an older structure that controlled alteration within the zone. The AC AZ is the same age as the Potato Peak alteration zone, but is  $\sim 1,000$  ft ( $\sim 300$  m) lower in elevation, and the two alteration zones may be displaced by an unrecognized fault. Alternatively, the Potato Peak alteration zone has been elevated relative to the Aurora Canyon alteration zone by magmatic inflation during construction of the Potato Peak stratovolcano.

## Hydrothermal Alteration

Within the AC AZ, nearly all trachyandesite of Masonic has been altered to assemblages dominated by quartz $\pm$ alunite, clays, and mica. Quartz-altered trachyandesite consists of gray to light-brown, very fine-grained to microcrystalline quartz in which some relict feldspar phenocrysts are discernible. Most quartz-altered trachyandesite has been brecciated and locally veined. Breccia matrices and veins, mostly  $< 5$  mm in width, consist of very fine-grained to microcrystalline quartz, and quartz+alunite $\pm$ pyrite (iron oxides). Quartz-alunite-pyrite-altered trachyandesite and silicified breccia are erosionally resistant, capping hills and forming linear ridges as much as 5 meters high and meters to tens of meters long. These resistant ledges are flanked by recessively weathered zones of trachyandesite (tens of meters wide) altered to alunite,

clay-mica minerals, pyrite (mostly weathered to iron oxides), and lesser chlorite. Kaolinite, where present, is proximal to quartz-alunite-pyrite-altered trachyandesite, whereas clay minerals distal to quartz-altered trachyandesite are dominated by illite and montmorillonite. An altered porphyritic rock that rests on altered trachyandesite in a small basin (SW4/SW4 S30, T5N, R26E) is characterized by polygonally desiccated soil, indicative of expandable clays, recessive weathering, sparse ground flora and little outcrop.

## Minor Elements in Rocks

Eight samples of quartz-alunite-pyrite(iron oxides)- and clay-pyrite(iron oxides)-altered trachyandesite of Masonic, and silicified breccia, contain very low concentrations of Au (most  $< 5$  parts per billion [ppb]) and Ag ( $< 1$  ppm; table 1-5). Several samples contain elevated concentrations of Hg ( $\sim 2$ – $21$  ppm), As (81–480 ppm), Bi ( $\sim 1$ – $5$  ppm), Te ( $\sim 2$ – $4$  ppm), and Sb (tens of ppm). As much as several percent sulfur, and Ba concentrations  $> 1,000$  ppm, reflect the presence of alunite, pyrite, and probably barite, although no barite was observed.

## ASTER Imagery

ASTER imagery of the AC AZ (Rockwell, 2010) shows alunite $\pm$ pyrophyllite and lesser alunite+kaolinite, and kaolinite-dominant pixels coincident with altered trachyandesite of Masonic. Kaolinite, alunite+kaolinite, and kaolinite/montmorillonite pixels are coincident with altered porphyritic rock in SW $\frac{1}{4}$ SW $\frac{1}{4}$  sec. 30, T. 5 N., R. 26 E. Although these rocks are pervasively altered, pixels that represent alteration mineral assemblages are discontinuously distributed in small clusters because of tree (pinion pine) cover, unaltered float of younger volcanic rocks, and imagery resolution.

## SWIR Spectra

Hand samples of quartz-alunite-clay-altered trachyandesite and silicified breccia have SWIR wavelength absorption bands characteristic of alunite, dickite, jarosite, and possibly montmorillonite, which support ASTER imagery interpretations and field observations. A sample of the altered porphyritic rock contains montmorillonite.

## Hydrothermal Mineral Age

Alunite in the matrix of silicified breccia near the exfoliated half dome (fig. 18) has a  $^{40}\text{Ar}/^{39}\text{Ar}$  date of  $10.87 \pm 0.065$  Ma (table 1). This alunite date is analytically indistinguishable from the date of alunite at the Alta Plana Mine in the Potato Peak alteration zone ( $10.83 \pm 0.06$  Ma, table 1)  $\sim 1$  km to the southeast.

## Potato Peak Alteration Zone

### Location

Secs. 33, 34, T. 5 N., R. 26 E.; secs. 3, 4, T. 4 N., R. 26 E. (unsurveyed), Mono County, California (fig. 1)

### Definition

The Potato Peak alteration zone (PP AZ; fig. 19) on the northwest slope of Potato Peak consists of a contiguous volume of volcanoclastic rocks, thought to be trachyandesite of Masonic (John and others, 2012), that is extensively altered to quartz, and assemblages comprised of quartz, alunite, mica-clay minerals, and pyrite (iron oxides). The roughly circular area of altered strata covers ~1.3 km<sup>2</sup> and is entirely enclosed by younger volcanic rocks (trachydacite of Potato Peak; rhyolite of Bodie Hills), and by colluvium. Some altered strata beneath slope wash have been exposed by landslides. The PP AZ extends under cover to the north, east, and northwest where it may be contiguous with the Aurora Canyon alteration zone.

### History and Production

Mercury from the Alta Plana Mine, an open cut in the central part of the alteration zone, was recovered ~1942 (Holmes, 1965) in a retorting mill (dismantled) at the mouth of Aurora Canyon. Mill feed included cinnabar in brecciated and silicified volcanoclastic rocks. The dimensions of mine workings and volume of mill calcines suggest that production was probably no more than tens of flasks of Hg. Trenches and small excavations tens to hundreds of meters northeast of the Alta Plana Mine in clay-altered and silicified volcanoclastic rocks contain no obvious metallic minerals other than pyrite.

### Stratigraphy

Volcanoclastic rocks in the alteration zone consist of debris flows derived from volcanic uplands associated with trachyandesite of Masonic that predate the trachydacite of Potato Peak and the present Potato Peak landform (fig. 19). Because of pervasive alteration, the volcanoclastic rocks are mottled gray, beige, and white, and are only exposed in mine workings and landslide scarps. These strata consist of as much as 70 volume percent angular, subangular, and subrounded clasts of aphanitic and faintly porphyritic volcanic rocks (millimeters to centimeters in size) that have been replaced by forms of hydrothermal silica, clay minerals, pyrite (iron oxides), and lesser alunite. Matrices are composed of variable proportions of the same hydrothermal minerals. No unaltered exposures were observed, and bedding and foliation are not evident.

Altered and partly leached rocks, exposed in landslide scarps and toes ~0.5 km southeast and south of the Alta Plana Mine, include several textural varieties of porphyritic rocks.

These pre-alteration porphyritic rocks are either interstratified flows or intrusions within volcanoclastic strata, all of which may be trachyandesite of Masonic.

### Structure

Exposure of the PP AZ through younger rocks is a consequence of erosional resistance of silicified landforms (below), and slope failure caused by unstable mica-clay-altered substrates. A fault northeast of the Alta Plana Mine is marked by a linear ridge of silicified breccia, but displacement could not be determined and is probably small. The PP AZ is coeval with the Aurora Canyon alteration zone but is 1,000 or more feet higher in elevation; the two alteration zones may have been displaced by an unrecognized fault on the west side of the PP AZ or by magmatic inflation during assembly of the large Potato Peak flow-dome complex (fig. 19).

### Hydrothermal Alteration

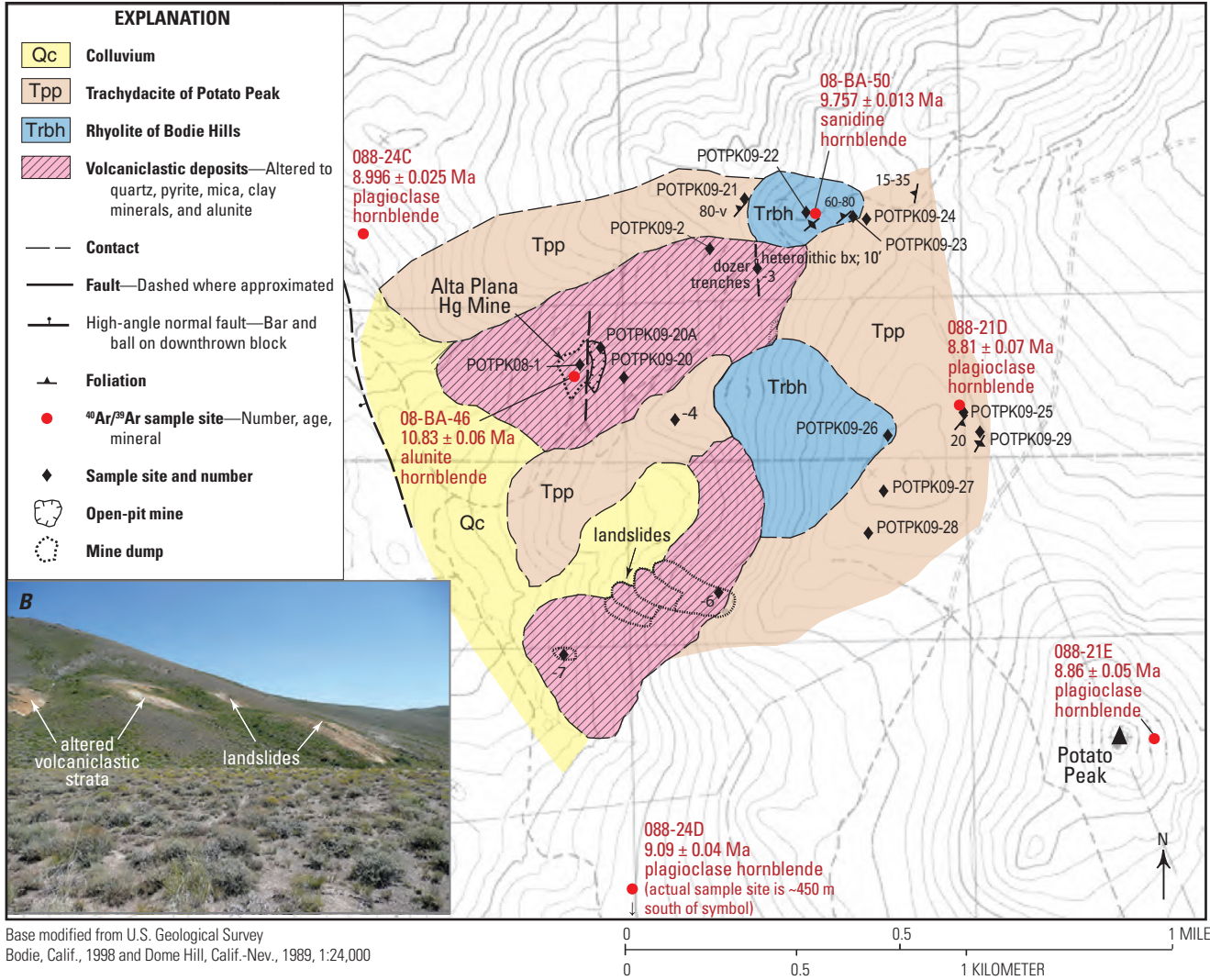
The Alta Plana Hg Mine is in a resistant knob, a few tens of meters in dimension, composed of light-gray to beige, fine-grained to microcrystalline, slightly vuggy quartz that replaced volcanoclastic strata. Near-vertical joint sets, one of which strikes ~N70°W, give parts of the knob a columnar aspect. Silicified volcanoclastic deposits on the west and northwest sides of the knob exposed by mining have been brecciated and cemented by at least three matrices that consist of (1) dense, gray, fine-grained to microcrystalline quartz and lesser opaline silica; (2) soft, white to beige kaolinite and alunite; and (3) fine-grained quartz, cinnabar, barite, jarosite, and voids. Cinnabar also occurs in millimeter-thick veins and on irregular fractures in densely silicified volcanoclastic strata.

A north-south-oriented, resistant ridge composed of silicified, multigenerational, pyritic breccia ~0.5 km northeast of the Alta Plana Mine has been explored by shallow cuts and trenches. Mottled gray-brown volcanoclastic rocks exposed in workings near this ridge consist of subangular to angular clasts (millimeters to centimeters in size) of fine-grained to microcrystalline quartz and variable amounts of white clay minerals. The altered clasts are enclosed by white to gray matrices of fine-grained to microcrystalline clay minerals and quartz, and up to 20 volume percent voids lined with submillimeter quartz crystals. Some gray, fine-grained quartz clasts are pocked with small voids where phenocrysts have been leached.

### Minor Elements in Rocks

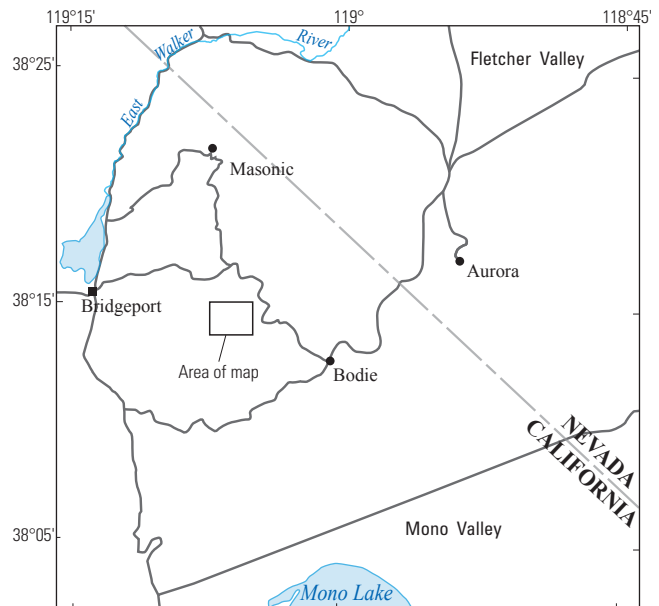
Samples of breccia with quartz-cinnabar matrix from the Alta Plana Mine (table 1-6) contain 1.9–17 weight percent Hg, and 64–900 ppb Au. These samples and four others from the alteration zone contain elevated concentrations of Hg (several parts per million to percents), As (tens to hundreds of parts per million), Bi (~1–19 ppm), Te (~1–3 ppm), Sb (as much as tens of parts per million), and sulfur (as much as several percent), presumably residing in cinnabar, pyrite, and lesser barite and alunite.

A



Base modified from U.S. Geological Survey  
Bodie, Calif., 1998 and Dome Hill, Calif.-Nev., 1989, 1:24,000

**Figure 19.** A, Geologic map of the Potato Peak alteration zone, Mono County, California. B, Image showing landslides developed on altered volcaniclastic strata.





## Sulfur Isotope Compositions

The S isotope compositions ( $\delta^{34}\text{S}$ ) of matrix cinnabar in a sample of brecciated and silicified volcanoclastic rocks in the Alta Plana Mine are  $-10.3$  and  $-9.8$  ‰ (table 2). Alunite and barite in matrices of breccia samples from the mine have  $\delta^{34}\text{S}$  values of  $16.3$  and  $11.6$  ‰, respectively. The low  $\delta^{34}\text{S}$  sulfide and high  $\delta^{34}\text{S}$  sulfate values are consistent with disproportionation of magmatic  $\text{SO}_2$  (Rye, 2005) during formation of the alteration zone. Sulfur isotope equilibrium temperatures were not calculated because cinnabar, alunite, and barite do not coexist in the samples examined.

## ASTER Imagery

ASTER imagery (Rockwell, 2010) of the PP AZ shows small clusters of pixels that correspond to quartz and alunite±kaolinite centered on the Alta Plana Mine and on the ridge of silicified breccia to the northeast.

## SWIR Spectra

Based on SWIR analyses of hand samples, breccia from the Alta Plana Mine consists of quartz, probable opal, jarosite, kaolinite, alunite, and topaz. Mica-clay minerals in altered volcanoclastic rocks in mine workings near the ridge of silicified breccia northeast of the Alta Plana Mine are dickite and probable halloysite, based on SWIR and XRD analyses. Alteration minerals in porphyritic rocks exposed in landslide scarps southeast and south of the Alta Plana Mine include illite and dickite.

## Hydrothermal Mineral Age

Alunite in the matrix of silicified breccia from the Alta Plana Hg Mine has a  $^{40}\text{Ar}/^{39}\text{Ar}$  date of  $10.83 \pm 0.06$  Ma (table 1), which is analytically indistinguishable from the date of alunite in the Aurora Canyon alteration zone ( $10.87 \pm 0.07$  Ma) ~2 km to the northwest.

## Aurora Mining District

### Location

Secs. 9, 10, 17, 18, 19, 20, 30, T. 5 N., R. 28 E., Mineral County, Nevada (fig. 1)

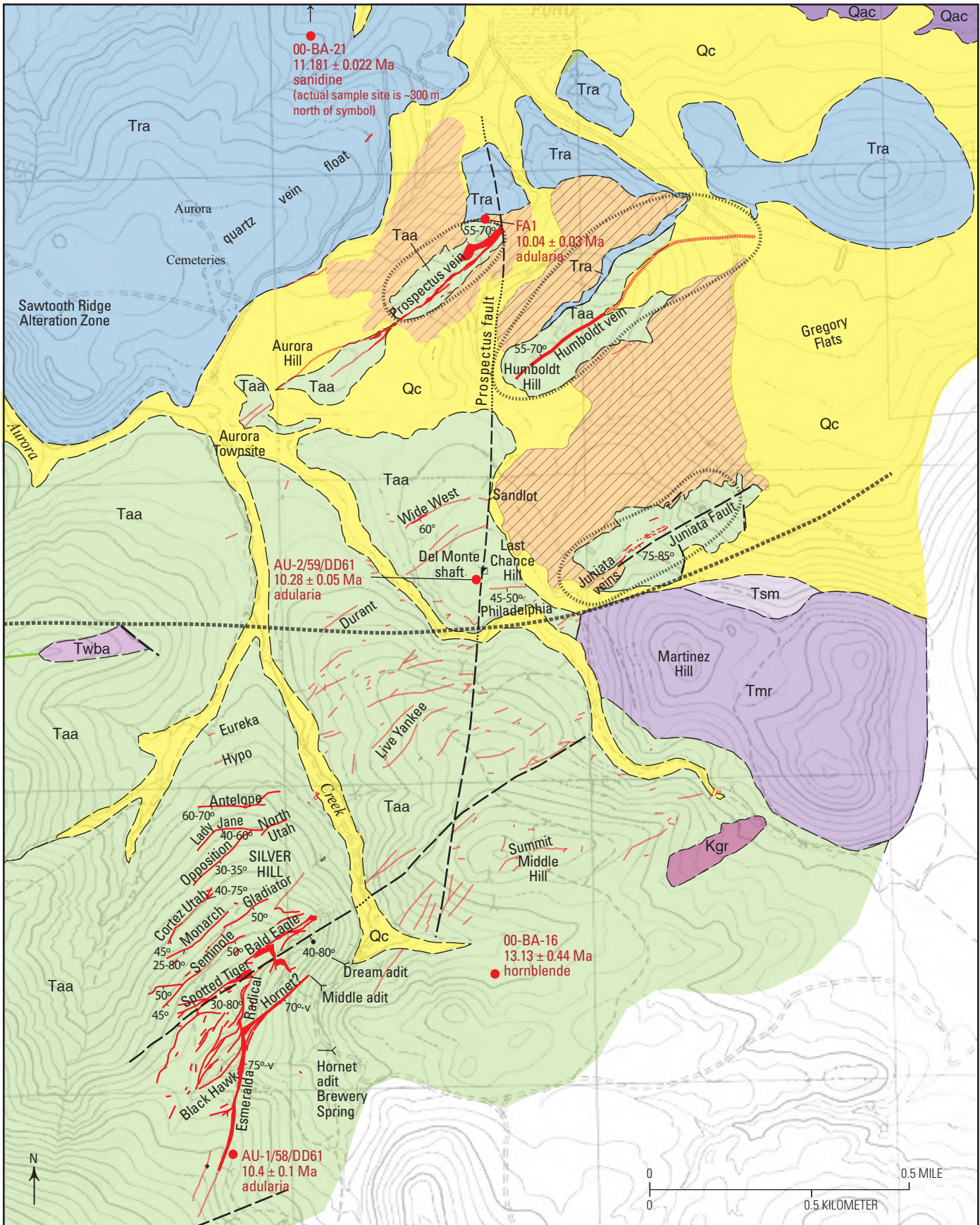
### History and Production

Gold-silver veins were discovered in 1860 in an area of the Bodie Hills initially called the Esmeralda Mining District and thought to be in Mono County, California. The

Esmeralda Mining District was soon thereafter renamed the Aurora Mining District, and in 1864 was found by a state boundary survey to be in Nevada Territory (originally Esmeralda County, now Mineral County, Nevada). The towns of Esmeralda and Aurora were established in the early 1860s. Most underground mining occurred between 1860 and 1864 (Stretch, 1867; Wasson, 1878; Clarke, 1882; Hill, 1915), when the population of the district exceeded 6,000. After 1864, production declined precipitously, and by 1865 mining stocks were worth less than “Confederate script” (Wasson, 1878). By 1880, production had decreased to 907 oz Au and 4,834 oz Ag recovered from 250 t of ore (King and others, 1885). During the early 20th Century (~1906–18), estimated production of 0.6 Mt @ 0.15 opt Au equivalent (Lawrence, 1987; Couch and Carpenter, 1943; Stone, 1982) was derived from cyanidation of tailings and from small amounts of ore recovered from dumps and old workings (Vanderburg, 1937). In the late 1940s, ~10,000 t of ore containing >1 opt Au (Stone, 1982; Tingley, 1990) were produced from underground mining of the Juniata vein system (fig. 20). Production since the 1980s has been derived from open-cut and underground mining of the Humboldt-Hilton, Prospectus, Juniata, and Ann vein systems on Martinez and Humboldt Hills, and in the New Esmeralda area, ~4.2 km northeast of the Prospectus vein (Gilbert, 1976; Osborne, 1985; Shaddrick, 1989; Tingley, 1990; Knudsen and Prens, 2002). From ~1988 to 1998 these vein systems yielded an estimated 0.3–0.4 Moz Au and 0.5–0.8 Moz Ag from 3 to 4 Mt of ore that graded ~0.1 opt Au (Knudsen and Prens, 2002; Nevada Bureau of Mines and Geology, 2009). Production during this period was derived from separate mining operations and may have been counted twice or more in total district production. Measured and indicated resources include a bulk-mineable resource of ~31 Mt @ 0.031 opt Au, and an underground resource of 0.19 Mt @ 0.5 opt Au (Nevada Bureau of Mines and Geology, 2009). Perlite deposits on Aurora and Bodie Creeks, and on a tributary of Bodie Creek, north and northwest of the district have been episodically mined at small scales (Archbold, 1966).


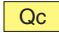
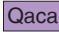
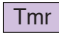
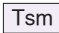
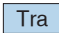
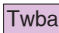
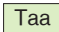



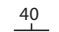


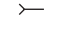




Total district production reported by Long and others (1998) for the period 1860–1995 is 1.817 Moz Au, 20.605 Moz Ag, and 3.86 Mt of ore. Total production through 1998 was estimated by Knudsen and Prens (2002) at 1.91 Moz Au. These production totals are largely based on dollar values of bullion and estimated Au/Ag from the most productive period (1860–64), when an estimated 1.5 Moz Au was recovered (Wasson, 1878; Angel, 1881; Ferguson, 1929; Vanderburg, 1937; Couch and Carpenter, 1943).

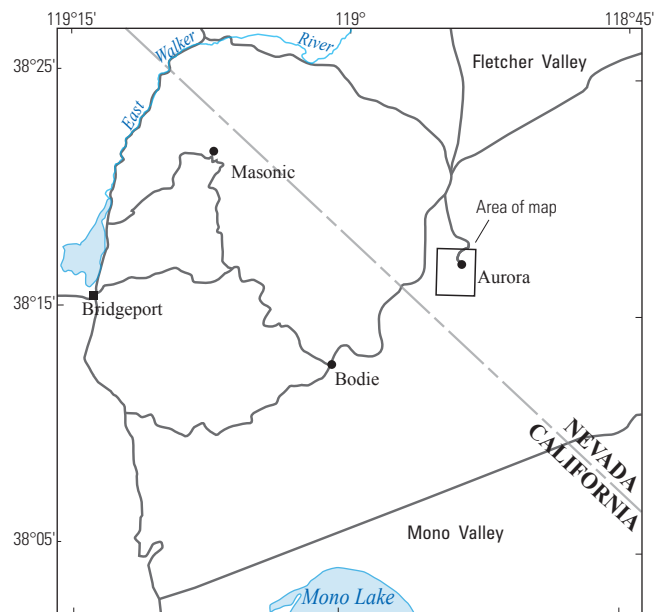
Accurate weight records do not exist for most early production. Production through 1869, estimated at \$2.4–29.5M (Wasson, 1878; Ross, 1961), was in part reconstructed from recollections of shipping agents and newspaper accounts, as most shipping and assay records were lost or destroyed. Early Aurora production may include initial production from the Bodie Mining District that was milled at Aurora (Blake, 1869; Angel, 1881; Wasson, 1878; Vanderburg, 1937). Furthermore, Au/Ag used to convert value to weight varied considerably



Base modified from U.S. Geological Survey  
Aurora, Nev.-Calif., 1989, 1:24,000

**EXPLANATION**

-  Mine dumps and disturbed ground
-  **Qc** Colluvium and volcaniclastic deposits (Quaternary–Pliocene)
-  **Qaca** Trachyandesite of Aurora Crater (Pleistocene)
-  **Tmr** Rhyolite of Martinez Hill (Pliocene)
-  **Tsm** Sedimentary rocks of Martinez Hill (Pliocene and Miocene)
-  **Tra** Rhyolite of Aurora Creek (Miocene)
-  **Twba** Trachyandesite of West Brawley Peak (Miocene)
-  **Taa** Trachyandesite of Aurora (Miocene)
- Granitic rocks**
-  **Kgr** Cretaceous granite
-  **Contact**—Dashed where approximated
-  **Fault**—Dashed where approximated, dotted where concealed
-  **40** **Bedding**
-  **40** **Foliation**
-  **Mine shaft**
-  **Adit**
-  **Quartz vein zones**—Numbers indicate dip
-  **Color air photo (CAP) lineament**
-  **Open-pit mine**
-  **<sup>40</sup>Ar/<sup>39</sup>Ar sample site**—Number, age, mineral



**Figure 20. (Facing page)** Geologic map of the Aurora Mining District, Mineral County, Nevada. Geology and vein locations and names modified from Hill (1915), Lawrence (1987), Osborne (1985), Shaddrick (1989), Knudsen and Prens (2002), and John and others (2012).

by reference (Hill, 1915; Ferguson, 1929) and mine (Osborne, 1985). From “detailed records” Knudsen and Prens (2002) estimated a grade of >2 opt Au for the first 1.5 Moz, implying  $\leq 3$  Mt of ore. This tonnage would have been derived from underground vein mining mostly during the 1860s. Based on dimensions of veins, stopes, dumps, and tailings, estimated ore tonnage and recovered Au seem unrealistically high, unless a large volume of early tailings was eroded and (or) Au grades were tens to hundreds of ounces per ton. Wasson (1878) stated that during the first few years “many thousands of tons were milled that produced several thousand dollars per ton.” However, specimens of such multiounce ore apparently were not archived.

## Stratigraphy

Mesozoic granitic and metavolcanic rocks and Tertiary trachyandesite and rhyolite are exposed in the eastern and southeastern parts of the district (Hill, 1915; John and others, 2012; fig. 20). Trachyandesite of Aurora (~13.1–12.6 Ma; table 1), which encloses nearly all veins, unconformably overlies Mesozoic quartz monzodiorite of Aurora and metavolcanic rocks. It is exposed in a roughly elliptical area, ~10 km north-south by ~5 km west-east, which is largely defined by younger volcanic rocks. Trachyandesite of Aurora may be as much as 400 m thick if exposures between the top of East Brawley Peak and granite on the east slope of Middle Hill are unfaulted. Trachyandesite flows and volcanoclastic strata on Middle, Silver, and Martinez Hills have been intruded by porphyritic rocks, including rhyolite and latite dikes and plugs (Lawrence, 1987; Osborne, 1985; Knudsen and Prens, 2002; John and others, 2012). Altered trachyandesite of Aurora on and south of East Brawley Peak, adjacent to the southwest edge of the district, comprises the East Brawley Peak alteration zone.

Rhyolite of Aurora Creek (11.2 Ma; table 1), rhyolite of Del Monte Canyon (~11.2 Ma; John and others, 2012), trachyandesite of Del Monte (11 Ma), and trachyandesite of West Brawley Peak (~11.5–11.3 Ma; John and others, 2012) unconformably overlie trachyandesite of Aurora to the north, northwest, and west. Rhyolite of Aurora Creek forms a group of small-volume lava domes and includes minor cogenetic pyroclastic flow deposits, especially in the lower reaches of Bodie Creek. It contains 1–9 volume percent phenocrysts of plagioclase and rare quartz, sanidine, hornblende, clinopyroxene, and biotite in a glassy groundmass. Altered flow-domes of rhyolite of Aurora Creek north of Aurora Creek and northwest of the Aurora town site comprise the Sawtooth Ridge alteration zone (fig. 20). Veins in rhyolite of Aurora Creek in and northeast of the Aurora cemeteries, represented largely by float, closely resemble veins in trachyandesite of Aurora.

Rhyolite of Del Monte Canyon forms a set of low-volume lava domes and associated pyroclastic deposits that are well-bedded, lithic rich, and underlie the lava flows. It contains 6–26 volume percent phenocrysts of plagioclase, quartz, hornblende, biotite, and sanidine in glassy (perlitic in places) to moderately devitrified groundmass. The trachyandesite of Del Monte, which includes basaltic trachyandesite and trachydacite, forms a discontinuous, north-trending series of exposures that consist of lava flows and associated, heterogeneous, laharic debris flow and volcanoclastic deposits. It contains 0–50 volume percent phenocrysts of plagioclase, biotite, clinopyroxene, and hornblende in a weakly devitrified groundmass. The trachyandesite of West Brawley Peak forms a series of lava flows erupted from the moderate-volume composite volcano centered on West Brawley Peak. It contains ~10–35 volume percent phenocrysts of plagioclase, hornblende, biotite, clinopyroxene, and trace amounts of olivine in a moderately devitrified groundmass. Plagioclase phenocrysts in trachyandesite of West Brawley Peak are characteristically larger (commonly >1 cm) than those in most rocks of the Bodie Hills volcanic field.

Pliocene-Pleistocene rocks of the Aurora volcanic field (John and others, 2012) overlie the trachyandesite of Aurora and other premineralization rocks north, east, and south of the district. These rocks include the rhyolite of Martinez Hill, sedimentary rocks of Martinez Hill, trachydacite of Aurora Peak, trachyandesite of Aurora Crater, and various other trachyandesite and trachydacite lava flows of the Aurora volcanic field. These eruptive rocks vary in age from 3.4 to 0.1 Ma (Gilbert and others, 1968; Silberman and McKee, 1972; Lange and others, 1993; Lange and Carmichael, 1996). Based on drill hole intercepts near Fletcher Junction, ~4 km north of the Aurora Mining District, trachyandesite of Aurora Crater covers ~150 m of unaltered colluvial deposits that overlie at least 455 m of altered mafic tuffs and lacustrine deposits (Nevada Exploration Inc., 2013). These strata comprise basin-fill of Fletcher Valley (Tfv of John and others, 2015), and alteration of the mafic tuffs and lacustrine deposits is interpreted to have coincided with formation of Aurora veins.

## Structure

Predominant faults in the district contain quartz veins that number in the hundreds if all the short and unaligned vein segments are counted (Brady’s map of Aurora and Esmeralda, 1862; fig. 20). Fault sets (and veins in them) presumably reflect stress accommodation within the Walker Lane transtensional structural zone of strike-slip displacement and extension. Vein attitudes and kinematic indicators in the Aurora Mining District are consistent with maximum horizontal extension oriented N60°W and maximum horizontal compression oriented N30°E, similar to those of mineralized structures in the Masonic Mining District (John and others, 2012).

Most veins strike N45–70°E and dip 20–75°SE, reflecting fault orientations in which the veins formed. Episodic displacement along northeast-striking faults created dilatancies in which vein minerals precipitated, as evidenced by distinct opposing layers of vein minerals, by numerous narrow cross-cutting veins in wall rocks, and to a lesser extent, by several generations of internal wall-rock fragments in wide veins.

Several short vein segments, the prominent Esmeralda vein, and the Prospectus Fault, strike north-south to N10°E, and dip at high angles or are vertical. These veins and the Prospectus Fault define a second significant structural trend in the district. Post-vein, right-lateral movement of at least 545 m on the Prospectus Fault has been invoked to explain offset of veins and rhyolite of Aurora Creek in the eastern part of the district from veins and rhyolite in the western part (fig. 20; Hill, 1915; Green, 1964; Osborne, 1985, 1991). Other pre-(?) and post-vein faults (not shown of fig. 20) include a N10–30°W-trending set on Middle Hill, N70°W faults that are most prominent on East Brawley Peak (Silberman and others, 1995; Lawrence, 1987; Breit, 2000), and a west-east set that has dismembered and laterally displaced northeast-striking veins for as much as 15 m (Knudsen and Prens, 2002). Post-vein faults offset alteration zones and volcanoclastic deposits in the vicinity of the Juniata vein system (fig. 20; Osborne, 1985).

Thin seams of gouge, mostly in hanging walls of veins, and fluvial gravels interpreted as sag deposits (Knudsen and Prens, 2002), also attest to post-vein strike-slip movement. Clasts of 2.5 Ma Martinez rhyolite in the sag deposits, coupled with the absence of clasts of trachyandesite of Aurora Crater (~0.25 Ma; Silberman and McKee, 1972), constrain sag deposit ages and at least some postmineralization fault displacement to <2.5 Ma. A west-east lineament that is conspicuous on color aerial photography (CAP lineament, fig. 20) separates veins on Last Chance Hill and Humboldt from Martinez Hill and veins on Middle Hill and Silver Hill. This lineament may mark a fault that displaced some veins and volcanic strata down-to-the-north.

Veins apparently extend northeast of the district under colluvium and trachyandesite of Aurora Crater to the New Esmeralda area where veins similar to those in the Aurora Mining District were mined underground in the 1860s and by open cut in the 1990s. The presence of veins beneath Aurora Crater north of the district has been proposed based on float and geochemical anomalies in the tributary of Bodie Creek that drains the district to the north. Other evidence of covered veins includes altered and geochemically anomalous strata intersected in drill holes (Nevada Exploration Inc., 2013). Float of chalcedonic and layered quartz veins, and a mined vein in rhyolite of Aurora Creek ~0.5 km northeast of Aurora cemeteries, may be coeval with veins in trachyandesite of Aurora; the rhyolite may contain or cover other veins. Poorly exposed veins also have been intersected by drill holes southeast of the Juniata Mine (Osborne, 1985), and additional veins may be covered by rhyolite of Martinez Hill.

## Forms of Gold-Silver Mineralization

### Veins and Vein Zones

All precious metal production in the Aurora Mining District has been derived from veins mined underground prior to ~1950, and mined by open pit in the 1980s, 1990s, and early 2000s. Between 1860 (when the district was discovered) and 1862, more than 300 veins were located and named on Silver, Middle, Last Chance, Humboldt, and Martinez Hills (Brady's map of Aurora and Esmeralda, 1862). Ore was produced from ~30 veins. Other veins are exposed in the New Esmeralda area ~4.2 km northeast of the Prospectus vein. Although partially covered by younger strata, the Aurora district vein system apparently extends northeast from Silver Hill to at least the New Esmeralda area, a distance of ~7.5 km.

Many of the early claim locations covered segments and branches of veins that, based on structural and textural characteristics, can be grouped into vein zones (fig. 20). Vein zones on Silver Hill consist of meters-thick tabular segments of layered quartz veins and subparallel, centimeters-thick layered quartz veins that occur commonly in the footwall of thicker vein segments. Thick vein segments are contiguous along strike for tens to hundreds of meters, although thicknesses and dips vary considerably over short strike distances. Extremities of vein zones are marked by thin anastomosed veins that merge with fractures. With the exception of the Esmeralda vein zone, which strikes N10°E and dips 75°E-vertical, vein zones on Silver Hill predominantly strike N40°E and dip 50±20°SE. One of the largest vein zones, the Spotted Tiger-Bald Eagle, is ~0.6 km long, dips 30–80°SE, and is as much as ~9 m thick (fig. 20).

Thick veins consist of tens to >100 laterally symmetrical layers of fine-grained and chalcedonic quartz. Central and internal layers commonly enclose small (centimeter dimensions) voids lined with millimeter-sized or smaller quartz crystals; other layers consist of opposed centimeter-sized euhedral quartz crystals. Adularia is sparingly present in some quartz layers, but most has been replaced by quartz or sericite. Calcite is uncommon in layers, although calcite pseudomorphs and perimorphs are present in most veins. They form unoriented "blades" of fine-grained quartz, and tabular voids enclosed by fine-grained quartz crystals, respectively ("lattice-type" bladed quartz after calcite; Etoh and others, 2002); both forms occur in centimeter-wide layers that are as much as 50 volume percent void. Ore in vein zones reportedly occurred as discontinuous layers (submillimeters to centimeters thick) and clots (millimeters to centimeters wide) of fine-grained sulfide minerals, electrum, and sericite that alternate with quartz layers and constituted as much as several volume percent of the vein.

The Prospectus, Humboldt, Juniata, and New Esmeralda vein systems, and some veins on Last Chance Hill, were inaccessible during the period of this investigation because of active milling operations (ore transported from the Midas district, Humboldt County, Nevada). The N50–60°E-trending

Prospectus-Humboldt vein system is exposed for ~1,850 m, and consists of veins that vary in width from <30 cm to 9.1 m and dip 55–70°NW (Osborne, 1985). The Juniata vein system consists of three subparallel veins that strike N60–85°E, dip 75–85°SE, and are as much as 15 m thick. Descriptions and images of these vein systems in Osborne (1985) demonstrate a similarity to Silver Hill vein zones. The New Esmeralda vein system is exposed in an open pit in secs. 9, 10, T. 5 N., R. 28 E. The vein system in the pit consists of six layered veins that are 1–1.5 m wide, and numerous narrower veins between and adjacent to wider veins. Wide veins strike ~N30°E and dip ~75°NW. Based on attitudes of chalcedonic sediments that filled a void internal to quartz layers, original vein dips were 50–70° (fig. 21).

Present vein dips may be ~5–25° steeper than vein dips during deposition. If present vein declinations have been reversed by fault displacement, then the dip change approaches vertical. However, no stratigraphic evidence for significant tilting exists, and present and original vein attitudes apparently differ by no more than a few degrees.

A second type of vein zone consists of numerous closely spaced, subparallel quartz veins, quartz-matrix breccias, and internal trachyandesite septa that collectively define a tabular geometry. These vein zones are tens to hundreds of meters long and meters to tens of meters wide; most dip steeply southeast (for example, Wide West and other veins on Last Chance Hill and Middle Hill; fig. 20). Within these vein zones, individual veins are centimeters to tens of centimeters wide and consist of fine-grained to chalcedonic quartz in which layering is less pronounced or absent. Tabular quartz-matrix breccias, also centimeters to tens of centimeters wide, consist of centimeter-sized fragments of trachyandesite in matrices of fine-grained to chalcedonic quartz, lesser K-feldspar, sericite, and calcite, and rare sulfide minerals, mostly pyrite. Calcite is typically coarse-grained (millimeter-sized crystals) and usually occurs in central parts of veins and matrices, suggesting a late paragenetic position. Fluorite, mostly in cubic crystals, is locally found in veins near the Del Monte shaft (fig. 20) on surfaces of fine-grained drusy quartz, and encrusted by similar quartz; it is also paragenetically late. Trachyandesite between closely spaced veins, and trachyandesite fragments in breccias, are densely silicified or replaced by quartz-sericite-pyrite assemblages. Internal trachyandesite septa in wide vein zones are altered to propylitic assemblages.

A third type of vein zone is represented solely by the N10°E-striking, near-vertical Esmeralda-Radical vein zone on Silver Hill (fig. 20), which was the district discovery site in 1860. The Esmeralda-Radical vein zone is as much as 18 m wide (Hill, 1915) and is the widest in the district, and among the longest at 0.8 km. It consists of a resistant tabular mass that includes several generations of quartz breccia and stockwork (arbitrarily distinguished by relative matrix and clast proportions) that include trachyandesite clasts, much

like the Comstock Lode (Vikre, 1989). Breccia matrices and stockwork veins are composed of quartz, lesser K-feldspar, sericite, and calcite, and uncommon sulfide minerals (mostly pyrite). Euhedral quartz crystals in vugs and veins vary in size from submillimeters to centimeters. Most calcite is internal to quartz in matrices, implying a late paragenetic position. Trachyandesite clasts are largely replaced by fine-grained to chalcedonic quartz, K-feldspar, and pyrite; some K-feldspar has been altered to sericite.

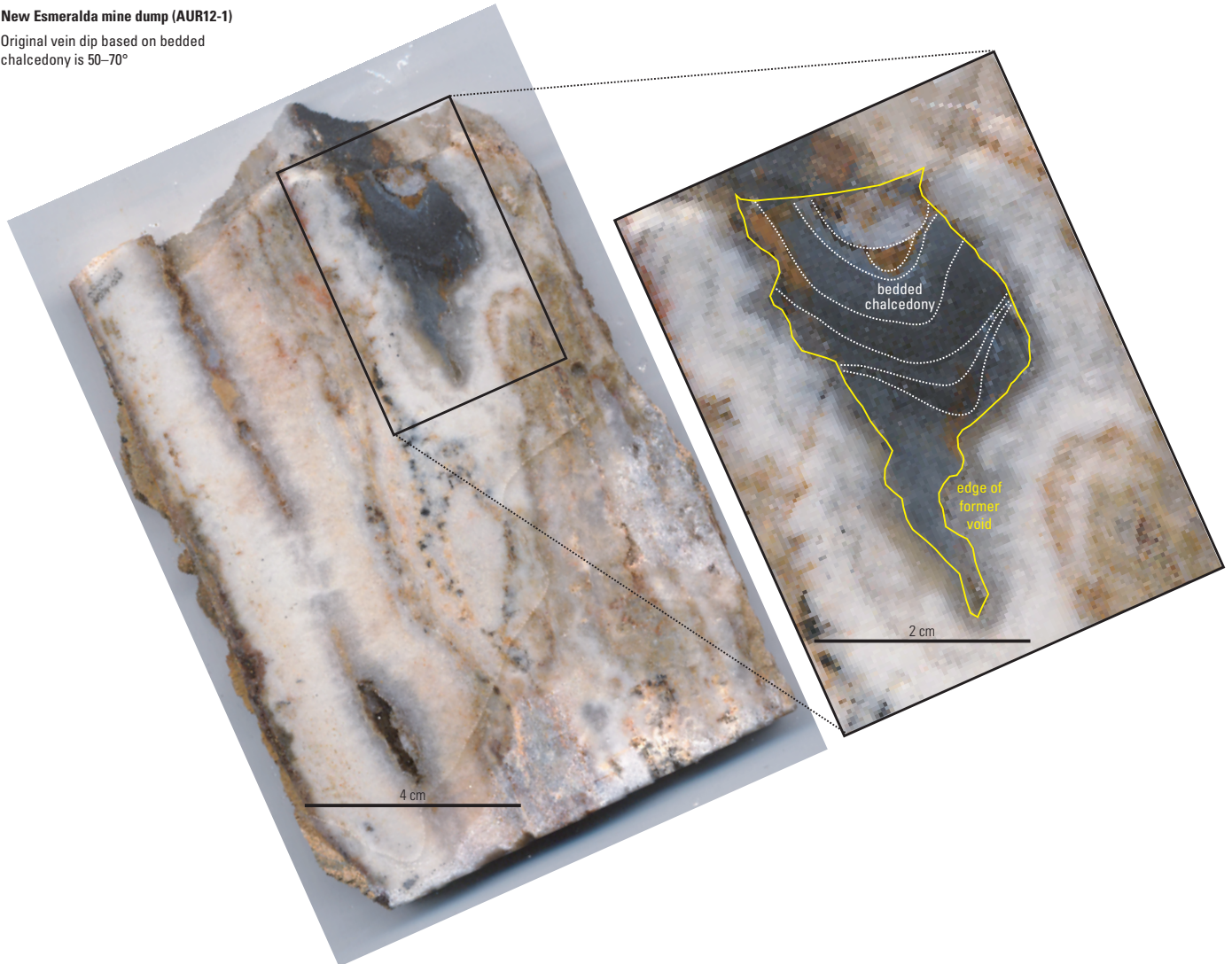
## Ore Bodies

Mines in the Aurora Mining District are largely inaccessible, mineralized samples on dumps are sparse, and documented archival ore specimens are few and small (most are centimeter in size). Descriptions of 19th century mining, stopes, and ore occurrences, mostly from early literature and unpublished reports (Clarke, 1882; Hill, 1915; Payne, 1965; Lawrence, 1987; Shaddrick, 1989; Rhoden, 1992), are uneven in detail, and ore bodies can only be described generally. Ore produced from 1860 to 1864 apparently contained several or more ounces per ton gold. As described by Hill (1915), ore occurred in rich “streaks,” as much as 15 cm wide, that consisted of quartz, adularia, tetrahedrite, pyrite, chalcocopyrite, Au (presumably electrum), and a Au-Ag-Se phase. The value of Au in early mined ores exceeded that of Ag, where reported, by 2–5 times (Burchard, 1884), implying Au/Ag of ~0.13–0.31 (gold=\$20.68/oz; silver=\$1.29/oz).

Ore within vein zones on Silver Hill raked down dip at high angles. It usually was positioned along or internal to hangingwalls or footwalls, and seldom comprised entire vein widths. Clarke (1882) described the high-grade ores (called “rich chambers”), which were mined out by 1864, as occurring in wider parts of otherwise barren veins. Five such chambers were mined from a 1,500 ft-long section of the Utah-Cortez vein on Silver Hill. One chamber that extended from the surface to –150 ft, was 50–75 ft long, 20–25 ft wide, and contained 20,000 t @ ~5 opt Au. Unmineralized parts of the vein were 3 ft wide. Ore in Antelope vein on Silver Hill averaged ~7–15 opt Au equivalent (Lawrence, 1987). On Last Chance Hill, five high-grade ore shoots in the Wide West vein were 60–120 ft below the surface, 16–60 ft wide, and 100–200 ft long (Lawrence, 1987). Some veins were mined to depths of 500 ft, but most stopping terminated tens to several hundreds of feet below the surface. At 800 ft in the Del Monte and Juniata shafts, heavy water flows prevented deeper excavation (Burchard, 1884). Veins have been intercepted in drill holes at depths exceeding 300 m, although on Silver Hill, veins transitioned downward from contiguous veins (meters wide) at the surface to narrower, low-grade to barren, zones of stockwork veins and silicification (Lawrence, 1987; Rhoden, 1992).

**New Esmeralda mine dump (AUR12-1)**

Original vein dip based on bedded chalcidony is 50–70°



**Figure 21.** Image of a sample from the Aurora Mining District. Layered vein from New Esmeralda Mine dump with a restored 65° dip based on bedded chalcidonic sediments that filled an internal void (enlarged inset on left). Relative to ~75° dips of wide veins exposed in the high wall, vein declinations may have changed since deposition (~10.5 Ma) by 5° to as much as 80° if declinations are reversed.

## Juniata-Prospectus Vein Minerals

Detailed published descriptions of vein mineral assemblages, textures, and paragenetic relationships are limited to veins in the northeastern part of the district (Osborne, 1985). The Juniata and Prospectus vein systems consist of variable proportions of quartz, adularia, pyrite, chlorite, electrum, acanthite, naumannite, bromargyrite, and barite that comprise three partially cospatial depositional stages: early barren, ore stage, and post-ore stage barren. In Juniata veins, stage 1 mineralization is mainly situated along vein

margins. It consists of trachyandesite fragments with as much as 30 volume percent pyrite that are cemented by crustiform quartz and lesser calcite that is replaced by quartz±adularia. At higher elevations, most stage 1 quartz has colloform or botryoidal textures. Stage 2, the ore stage, consists of greenish-tinted quartz+adularia that has textural and grain size similarities to stage 1. In stage 2, electrum, with variable Au/Ag, acanthite, naumannite, and pyrite are closely associated. Stage 3 is characterized by crustiform vuggy quartz and replacement of calcite by quartz. Throughout the Juniata vein, Au/Ag decreases with depth.

## Mineral Compositions in Silver Hill and Middle Hill Veins

Based on petrographic and semiquantitative SEM and XRD analyses, metallic minerals in archival specimens and dump samples from the Antelope, Wide West, Martinez, Crocket (figs. 22, 23, 24), and Amador Mines include pyrite, acanthite (with minor amounts of Se, Cu, and Sb), naumannite, sphalerite (with minor Cd and no detectable Fe or Mn), galena, polybasite ( $\sim\text{Ag}_{15}\text{Cu}_{26}\text{Sb}_{15}\text{As}_{0.7}\text{Se}_{0.7}\text{S}_{11}$ ), tetrahedrite ( $\sim(\text{Cu}_7\text{Ag}_3\text{Zn}_2)_{12}\text{Sb}_{4.2}\text{S}_{13}$ ), chalcopyrite, arsenopyrite, and a Ag-Au-S mineral ( $\sim\text{Ag}_4\text{AuS}_3$ ). SEM analyses also suggest the presence of submicrometer intergrowths of Ag-Au-Sb-S-Se minerals, because atomic proportions of many metallic phases do not match those of documented minerals. Two compositional groups of electrum,  $\sim\text{Ag}_{0.5\pm 0.1}\text{Au}_{0.5\pm 0.1}$  and  $\sim\text{Ag}_{0.2\pm 0.1}\text{Au}_{0.8\pm 0.1}$ , may be present within a single petrographic section; variable electrum compositions may, in part, reflect the absence of buffering by an Ag phase. Based on textures of mineral assemblages and on the absence of copper and iron oxide minerals, most imaged minerals are interpreted to be hypogene. Some Ag-As-Au-S phases that enclose other sulfide minerals may be all or part supergene.

In addition to the imaged minerals, pearcite, proustite, covellite, and barite have been reported (Vanderburg, 1937; Osborne, 1985; Knudsen and Prens, 2002). Breit (2000) reported Te concentrations of as much as 20 ppm in vein samples analyzed by bulk methods, but no Te minerals were identified during this investigation.

## Minor Elements in Rocks

Samples of veins and altered wall rock (mostly trachyandesite of Aurora), collected and analyzed in 1967–68 by the U.S. Geological Survey (Breit, 2000), contain elevated concentrations of Au, Ag, As, Sb, Hg, F, Mo, Te, Cu, Pb, Zn, and W, with the highest values in vein samples. The distribution of W abundances in altered trachyandesite and vein samples was interpreted by Breit (2000) as evidence that Silver Hill was the hottest and deepest part of the Aurora district vein system. Other geochemical zonation, including decreasing Ag/Au and As/Sb, and, to an extent, decreasing Te, Mo, W, and Sn concentrations northeast from Silver Hill, was attributed by Breit (2000) to a hydraulic (topographic) gradient, to regional zoning of coeval alteration on East Brawley Peak and Aurora veins, or to separate hydrothermal cells within the Aurora vein system. Minor element concentrations in 14 samples of trachyandesite wall rocks of the Juniata and Prospectus vein systems include local, elevated concentrations of Mo, Ag, As, F, and Hg (Osborne, 1985). Elevated minor element concentrations in 13 vein samples from mine dumps throughout the district (table 1-7) include Au (0.51–84.8 ppm),

Ag (6–1,370 ppm), Hg (0.43–1.18 ppm), As (257–4,290 ppm), Bi (~4–37 ppm), Cu (131–1,090 ppm), Mo (~53–1,310 ppm), Sb (~21–275 ppm), Se (~1–203 ppm), and Te (~4–16 ppm). One or two samples contain elevated concentrations of Co, Mn, Bi, Pb, Tl, and (or) Zn.

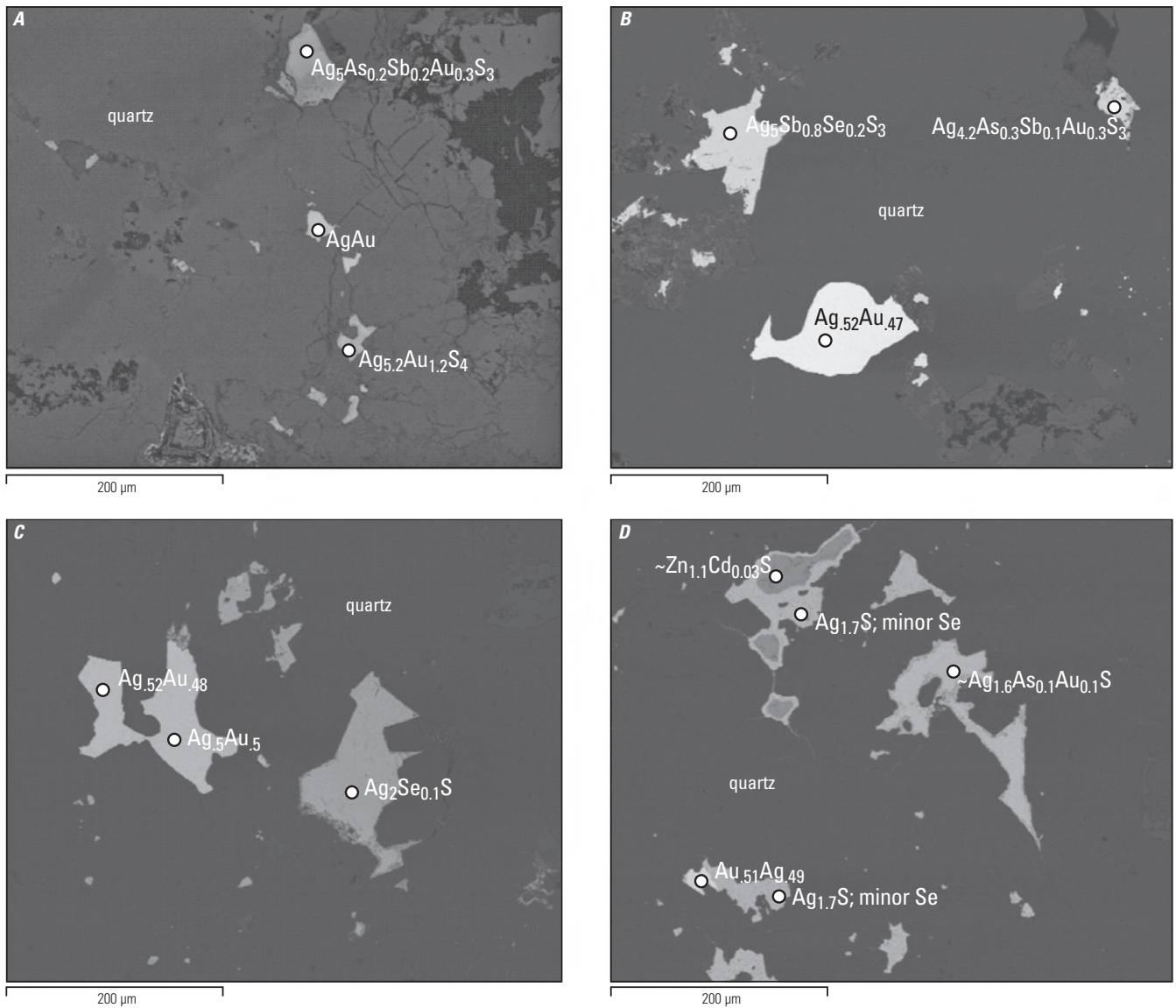
## Fluid Inclusion Microthermometry and Compositions

Fluid inclusion microthermometric data have been obtained from samples of the Juniata, Wide West, Humboldt, and other veins (Nash, 1972; Osborne, 1985; Knudsen and Prens, 2002), and one fluid stable isotope composition is reported (O'Neil and Silberman, 1974). However, most analyzed samples are not precisely located or paragenetically well constrained. The following microthermometry summary is derived largely from Knudsen and Prens (2002), supplemented by deductions regarding spatial relationships among veins.

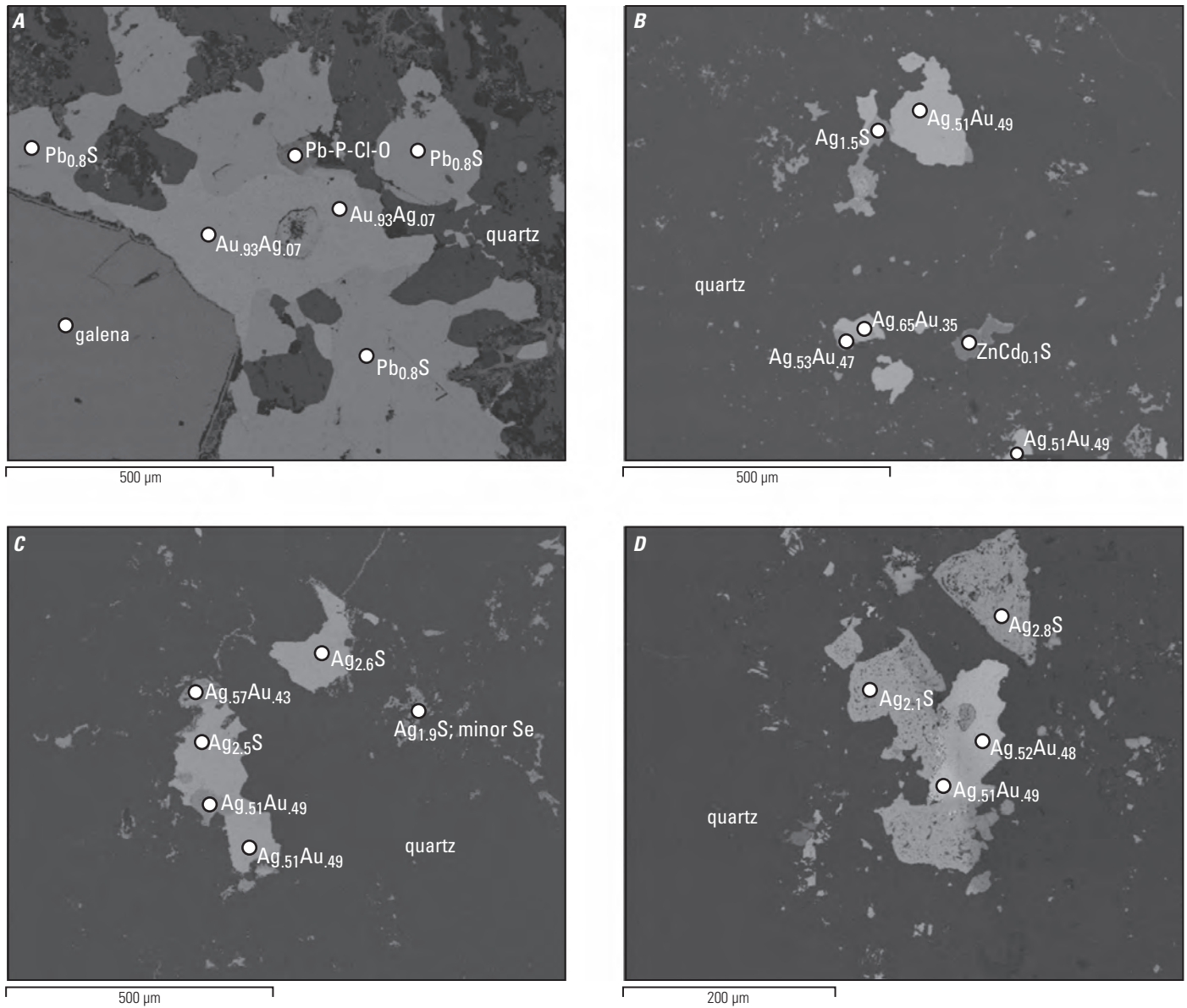
Fluid temperature ranges implied by inclusion homogenization in samples of vein quartz in the main part of the district (Silver, Middle, Last Chance, Aurora, and Humboldt Hills) are <180, 190–240, and >250 °C; most fluid salinities are less than a few weight percent NaCl equivalent. These temperature ranges correspond to different veins and to different layers and stages within veins. The episodic presence of K-feldspar in quartz samples with 190–240 °C fluids, and sericite alteration of wall-rock feldspars, suggests that fluid pH was controlled by the K-feldspar-muscovite stability boundary at near-neutral pH. Inclusion populations inferred to represent boiling at <180 °C occur in some clear quartz crystals, and apparently represent late-stage fluids. Inclusions with homogenization temperatures >250 °C have salinities of 3–6 weight percent NaCl equivalent; some contain a daughter mineral that may be dawsonite. Lower inclusion homogenization temperatures (<200 °C) in New Esmeralda area veins broadly correlate with relatively abundant chalcedonic quartz, implying shallower depths of formation. Temperature-elevation relationships of fluid inclusion populations show no clear district-wide trends, and in Juniata Mine samples they imply a “reversed” thermal gradient because populations with higher temperatures occur in vein samples collected near the present surface.

Fluid inclusions in quartz, most closely associated paragenetically with ore minerals in the Wide West vein and in veins on Silver Hill, homogenize at 230–236 °C, have salinities of 1–3 weight percent NaCl equivalent, and boiled intermittently, requiring minimum quartz depositional depths of 260 m (Haas, 1971) below the potentiometric surface. Relative to the present elevation of the Wide West vein (~7,600 ft), a paleopotentiometric surface (paleowater table) was at ~8,460 ft. Relative to present elevations of stoped veins on Silver Hill, ~7,800 ft at the Antelope vein to 8,400 ft at the

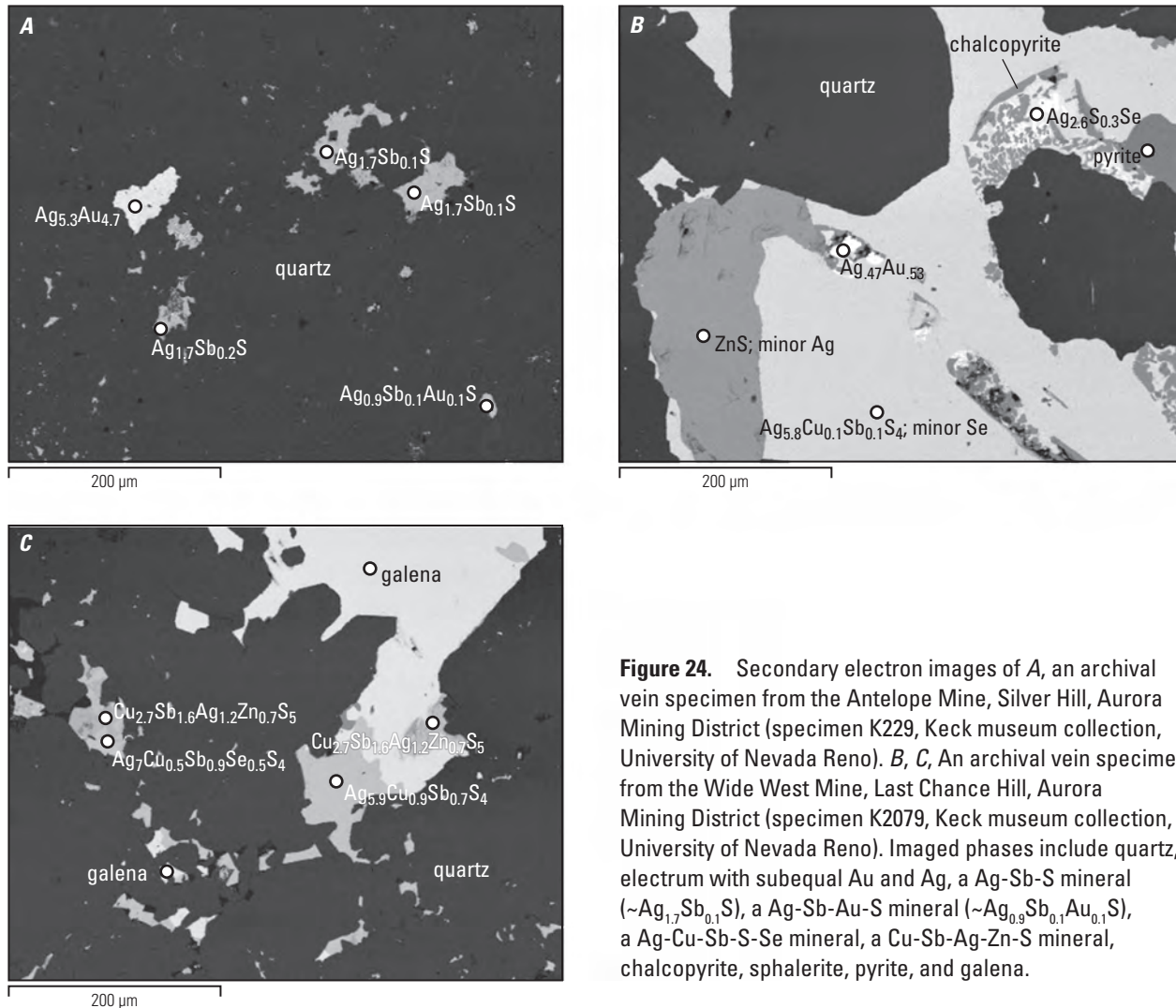




**Figure 22.** Secondary electron images of an archival vein specimen from the Crocket Mine on Last Chance Hill, Aurora Mining District. *A*, *B*, *C*, and *D* correspond to specimen K2085 (Keck museum collection, University of Nevada Reno). Mineral identifications and approximate atomic proportions for these images, and for images in figures 23 and 24, were determined petrographically and by scanning electron microscopy algorithms. Imaged phases include quartz, electrum with subequal Au and Ag, a Ag-As-Sb-Au-S mineral or intergrowth of minerals, Ag-Au-S ( $\sim\text{Ag}_{5.2}\text{Au}_{1.2}\text{S}_4$ ), Ag-Sb-S-Se ( $\sim\text{Ag}_5\text{Sb}_{0.8}\text{S}_3\text{Se}_{0.2}$ ), acanthite with minor Se, and sphalerite with minor Cd.



**Figure 23.** Secondary electron images of *A*, an archival vein specimen from the Antelope Mine, Silver Hill, Aurora Mining District (specimen K011, Keck museum collection, University of Nevada Reno). *B*, *C*, *D*, An archival vein specimen from the Martinez Mine, Martinez Hill, Aurora Mining District (specimen K208, Keck museum collection, University of Nevada Reno). Imaged phases include quartz, galena, electrum with variable Au and Ag, acanthite with minor Se, and sphalerite with minor Cd.



**Figure 24.** Secondary electron images of *A*, an archival vein specimen from the Antelope Mine, Silver Hill, Aurora Mining District (specimen K229, Keck museum collection, University of Nevada Reno). *B*, *C*, An archival vein specimen from the Wide West Mine, Last Chance Hill, Aurora Mining District (specimen K2079, Keck museum collection, University of Nevada Reno). Imaged phases include quartz, electrum with subequal Au and Ag, a Ag-Sb-S mineral ( $\sim\text{Ag}_{1.7}\text{Sb}_{0.1}\text{S}$ ), a Ag-Sb-Au-S mineral ( $\sim\text{Ag}_{0.9}\text{Sb}_{0.1}\text{Au}_{0.1}\text{S}$ ), a Ag-Cu-Sb-S-Se mineral, a Cu-Sb-Ag-Zn-S mineral, chalcopyrite, sphalerite, pyrite, and galena.

southern extremity of the Esmeralda vein (fig. 20), paleopotentiometric surfaces were at 8,660–9,260 ft. Although there is no identified Esmeralda vein microthermometry to further constrain paleoelevations, a paleopotentiometric surface at 9,260 ft is near the present elevation of East Brawley Peak ( $\sim 9,400$  ft),  $\sim 1.3$  km southwest of the Esmeralda vein. The summit of East Brawley Peak consists of densely silicified and clay-altered trachyandesite of Aurora. However, East Brawley Peak alteration zone assemblages include  $\sim 12$  Ma alunite, and Aurora district veins formed at 10.5–10 Ma (table 1), precluding a close temporal link between the alteration zone and veins.

The stable isotope composition of fluid in an unattributed vein sample, determined by bulk analysis, is within the range of present meteoric waters in the Great Basin ( $\delta\text{D} = -124$  ‰; calculated  $\delta^{18}\text{O}_{250^\circ\text{C}} = -12$  ‰; O'Neil and Silberman, 1974).

## Sulfur Isotope Compositions of Vein Minerals

The  $\delta^{34}\text{S}$  values of sulfide minerals in Aurora district veins vary from  $-8.7$  to  $10.9$  ‰ (table 2). This relatively large range may, in part, reflect sample quality in that most analyzed samples contain small proportions of sulfide minerals and large proportions of vein quartz. High  $\delta^{34}\text{S}$  values ( $10.9$ ,  $10.6$ , and  $8.3$  ‰) may indicate unrecognized sulfate minerals in the analyzed samples. Low  $\delta^{34}\text{S}$  values ( $-8.7$ ,  $-8.5$ ,  $-8.3$ ,  $-7.0$ , and  $-6.3$  ‰) are similar, in part, to those of sulfide minerals in the Masonic Mining District (table 2), which are consistent with  $\text{SO}_2$  disproportionation. Therefore, Aurora vein sulfide minerals may record sulfide-sulfate isotope fractionation, or several sulfur sources. Detailed paragenetic, geochronologic, and microthermometric investigations are needed to resolve temporal relationships among the numerous hydrothermal mineral assemblages in the vicinity of Aurora (East Brawley Peak, Spring Peak, and Sawtooth Ridge alteration zones).

## Wall-Rock Alteration

Several styles of hydrothermal alteration have modified volcanic rocks that enclose Aurora district veins. The trachyandesite of Aurora, the host rock for nearly all veins, has been altered throughout the district by partial to complete replacement of plagioclase, hornblende, clinopyroxene, and biotite phenocrysts, and matrix minerals, to variable proportions of chlorite, albite, calcite, montmorillonite, and lesser fine-grained quartz, sericite, and pyrite (iron oxides). Although few continuous exposures exist, these gray-green to greenish propylitized rocks apparently extend to contacts with younger rocks. The critical relationship between propylitized trachyandesite that encloses the Esmeralda vein and quartz-alunite-clay-mica-altered trachyandesite of Aurora of the East Brawley Peak alteration zone is masked by float, and crosscutting relationships that might distinguish the two alteration assemblages have not been observed. The distribution of epidote, which occurs in thin veins ( $\leq 1$  mm) in trachyandesite on mine dumps along Aurora Creek east of the Esmeralda vein (for example, Dream adit), may reflect older, high temperature fluids that formed the East Brawley Peak alteration zone. Elevated fluid temperatures in altered rocks on East Brawley Peak, and minor element zonation in the Aurora Mining District (Breit, 2000) also support alteration of trachyandesite of Aurora in the southwestern part of the district prior to vein deposition.

Gray-lavender trachyandesite adjacent and internal to Aurora district veins is variably replaced by quartz and K-feldspar, which partially obscure primary porphyritic texture. Light-gray to beige trachyandesite, adjacent to and in vein zones, reflects alteration of K-feldspar to sericite, illite, quartz, pyrite, and montmorillonite, and replacement of trachyandesite phenocrysts and matrices by these minerals. In densely veined trachyandesite, quartz replacement is more pronounced between and adjacent to veins. Quartz-K-feldspar-sericite-illite-pyrite-montmorillonite alteration grades distally from veins into propylitized trachyandesite, although pyrite is most abundant in vein selvages and in internal fragments of trachyandesite. Vein K-feldspar and sericite occur in aggregates, seams, and pockets (millimeters to centimeters in size) in quartz.

## ASTER Imagery

ASTER imagery (Rockwell, 2010) of the Aurora Mining District shows diffuse and small clusters of pixels that extend from Silver Hill to Gregory Flat (fig. 20); these pixels correspond to illite and lesser quartz. Densely clustered pixels coincident with the Prospectus, Humboldt, and Juniata open pits, dumps, and tailings correspond to quartz and montmorillonite±kaolinite.

## SWIR Spectra

SWIR analyses of hand samples of propylitized trachyandesite from the Del Monte shaft, and from other mine dumps on Last Chance Hill and Silver Hill, show weak spectra characteristic of illite and montmorillonite, and less-prevalent chlorite and epidote. Brecciated and veined rhyolite of Aurora Creek in the small open cut  $\sim 0.6$  km northeast of the Aurora cemeteries contains kaolinite and montmorillonite.

## Hydrothermal Mineral Ages

The  $^{40}\text{Ar}/^{39}\text{Ar}$  dates of adularia from the Esmeralda vein, and in a vein sample from the Del Monte shaft dump are  $10.47 \pm 0.1$  Ma and  $10.35 \pm 0.05$  Ma, respectively (fig. 20; table 1). Breit (2000) reported a  $^{40}\text{Ar}/^{39}\text{Ar}$  date of  $10.04 \pm 0.03$  Ma for adularia in the Prospectus vein. Kleinhamp and others (1975) reported a K-Ar date of  $10.6 \pm 0.2$  Ma for adularia in an unnamed quartz-adularia vein. Morton and others (1977) reported a K-Ar date of  $10.9 \pm 0.3$  Ma for trachyandesite altered to quartz, K-feldspar, sericite, pyrite, and chlorite in or near the Juniata vein. Breit (2000) reported a  $^{40}\text{Ar}/^{39}\text{Ar}$  date of  $12.2 \pm 0.3$  Ma for illite in altered wall rocks adjacent to the Esmeralda vein.

Most hydrothermal mineral dates are  $\sim 2$ – $3$  m.y. younger than the age range of trachyandesite of Aurora ( $\sim 13.1$ – $12.6$  Ma; table 1), the host rock for nearly all veins, and  $\sim 1.5$ – $2$  m.y. younger than alunite in trachyandesite of Aurora on East Brawley Peak ( $\sim 12$  Ma; table 1) adjacent to Silver Hill. No known magmatism in the Aurora Mining District is coeval with vein and most hydrothermal mineral dates, whereas in the Masonic and Bodie Mining Districts, igneous rocks are coeval with, or  $\sim 0.5$  m.y. older than, hydrothermal mineral dates (table 1). However, most feldspar and biotite dates of Rhyolite of Bodie Creek and Trachyandesite of Del Monte,  $\sim 4$ – $5$  km southwest and north, respectively, of the Aurora townsite (fig. 20), are  $\sim 10$ – $11$  Ma (Fleck and others, 2015), indicating the presence of magmas near the Aurora Mining District during vein deposition.

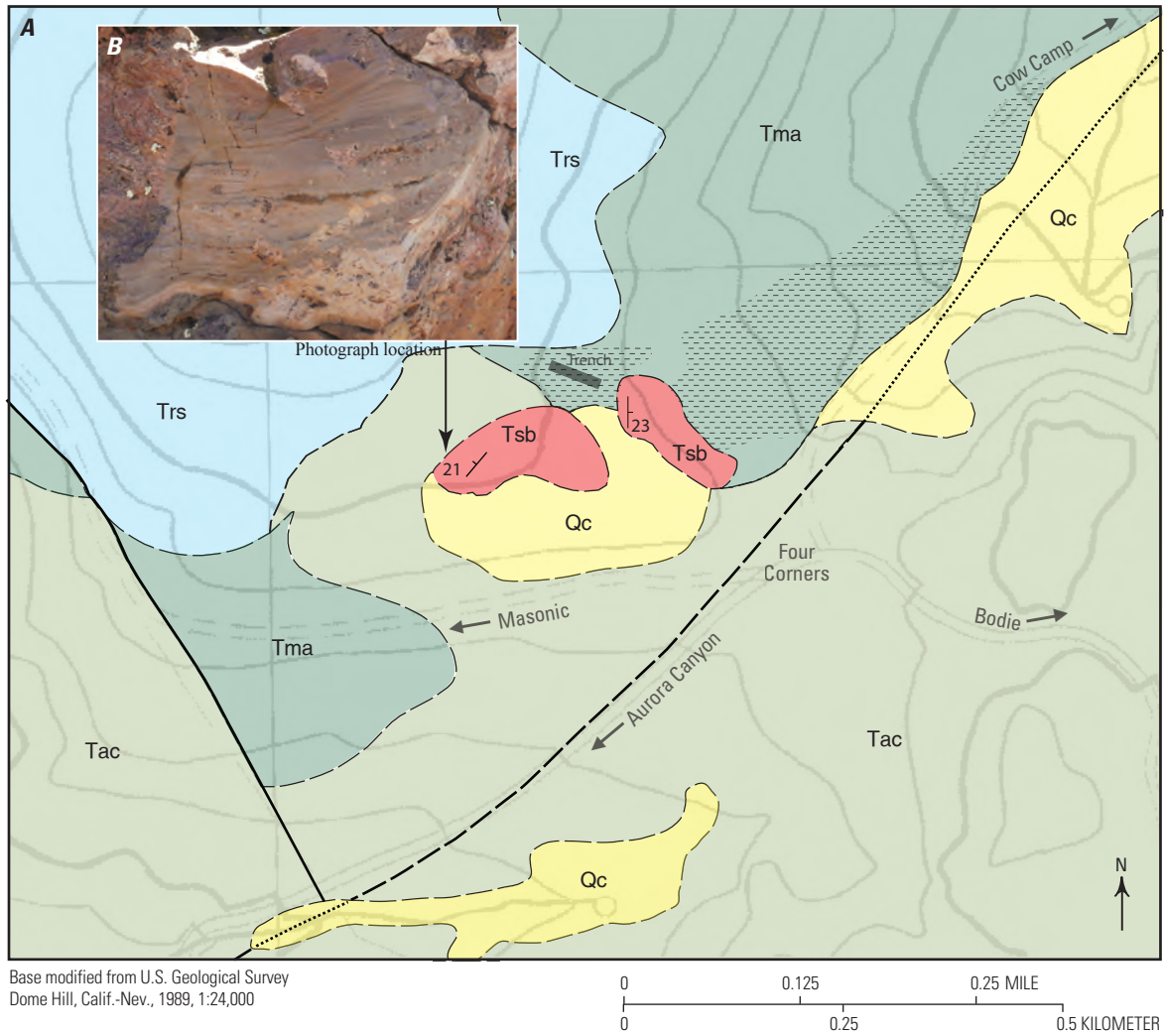
## Four Corners Alteration Zone

### Location

Sec. 15, T. 5 N., R. 26 E., Mono County, California (fig. 1)

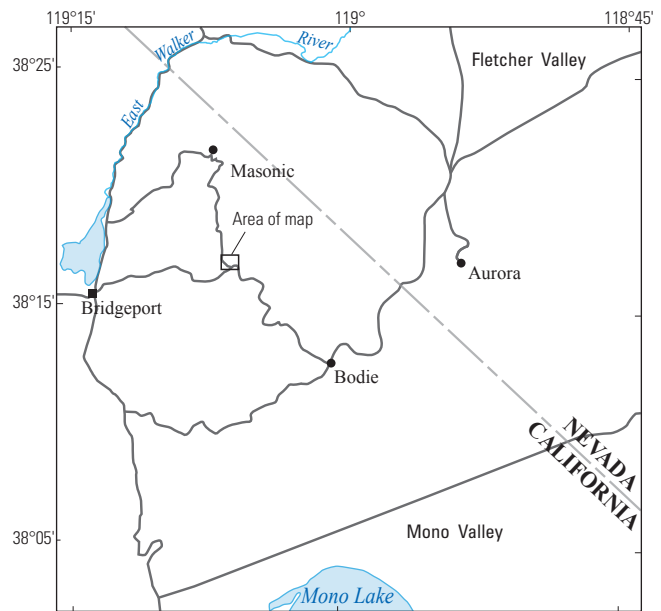
### Definition

The Four Corners alteration zone (FC AZ) is defined by low outcrops of silicified, volcanic-hydrothermal breccia that cover  $< 0.02$  km<sup>2</sup> immediately northwest of the intersection of roads to Masonic, Aurora Canyon, Cow Camp, and Bodie (Four Corners; fig. 25).



**EXPLANATION**

- Qc** Colluvium
- Tac** Trachyandesite of Aurora Canyon
- Trs** Rhyolite of Rock Springs Canyon
- Tsb** Silicified breccia
- Tma** Trachyandesite of Masonic
- Paleosol**
- Contact**—Dashed where approximated
- Fault**—Dashed where approximated
- 40 **Bedding**



**Figure 25.** A, Geologic map of the Four Corners alteration zone, Mono County, California. B, Image showing figure 26C and location.

## History and Production

No production is recorded from the FC AZ. A short bulldozer cut in argillized trachyandesite of Masonic, about 50 m north of the silicified breccia outcrops, is the only surface disturbance indicative of mechanized mineral exploration. Extensive production of tools and implements by Native Americans is evident from the scatter of locally derived obsidian flakes.

## Stratigraphy

Two low outcrops of silicified breccia lying on a paleosol in a window of the trachyandesite of Masonic are exposed between domes of rhyolite of Rock Springs Canyon to the north and trachyandesite of Aurora Canyon to the south (fig. 25). The rhyolite of Rock Springs Canyon forms two prominent, small-volume, aphyric lava domes that include flow lobes entirely composed of grayish-black obsidian. It contains trace to 3 volume percent phenocrysts of plagioclase, sanidine, hornblende, and biotite in a weakly devitrified, locally glassy groundmass.

The two outcrops of silicified breccia are crudely bedded and form an outward-dipping semicircle that is tentatively interpreted as eruption breccias and overlying hydrothermal sediments. These features partly outline a hydrothermal eruption crater that was centered about 200 m west of the road intersection (figs. 25, 26). A prominent zone of dark-red clay underlies the breccias and overlies the trachyandesite of Masonic on the north and east sides of the breccias and extends approximately 700 m northeast along Cow Camp road. The clay zone is interpreted as a paleosol developed on the trachyandesite of Masonic, although parts of the clay zone near the breccia outcrops may have a hydrothermal origin and formed at the same time as the breccias. The breccias contain a variety of shallow hydrothermal features including finely bedded and crossbedded siliceous sediments filling small open spaces (cavern fill) and silicified hematitic muds and dripstones (fig. 26).

## Structure

The silicified outcrops are crudely bedded with north to northeast strikes and shallow ( $\sim 20^\circ$ ) northwest to east dips (fig. 25). A proposed northeast-trending fault southeast of the breccia outcrops has no apparent temporal relationship to the alteration zone.

## Hydrothermal Alteration

Breccia clasts and matrix consist of quartz, hematite, jarosite, kaolinite, and montmorillonite. Ten samples of silicified breccia and sediments contain low concentrations of Au ( $\leq 5\text{--}61$  ppb) and Ag ( $< 1$  ppm; table 1-8). All samples contain tens to  $> 100$  ppm Sb, and several samples contain elevated concentrations of Hg (6–15 ppm), As (hundreds to several thousand parts per million), Bi ( $\sim 2\text{--}135$  ppm), and Pb (hundreds of parts per million); one sample contains 18 ppm Te.

## ASTER Imagery

No hydrothermal minerals were identified from ASTER imagery.

## SWIR Spectra

Based on SWIR analyses, two samples of red clay underlying the breccia outcrops contain montmorillonite and kaolinite. Silicified breccias locally are coated by orange-colored jarosite±montmorillonite.

## Hydrothermal Mineral Ages

Hydrothermal minerals in the FC AZ have not been dated. Field relations indicate that the alteration zone is younger than  $\sim 15\text{--}14$  Ma trachyandesite of Masonic and older than the 10.6–10.3 Ma trachyandesite of Aurora Canyon (table 1).

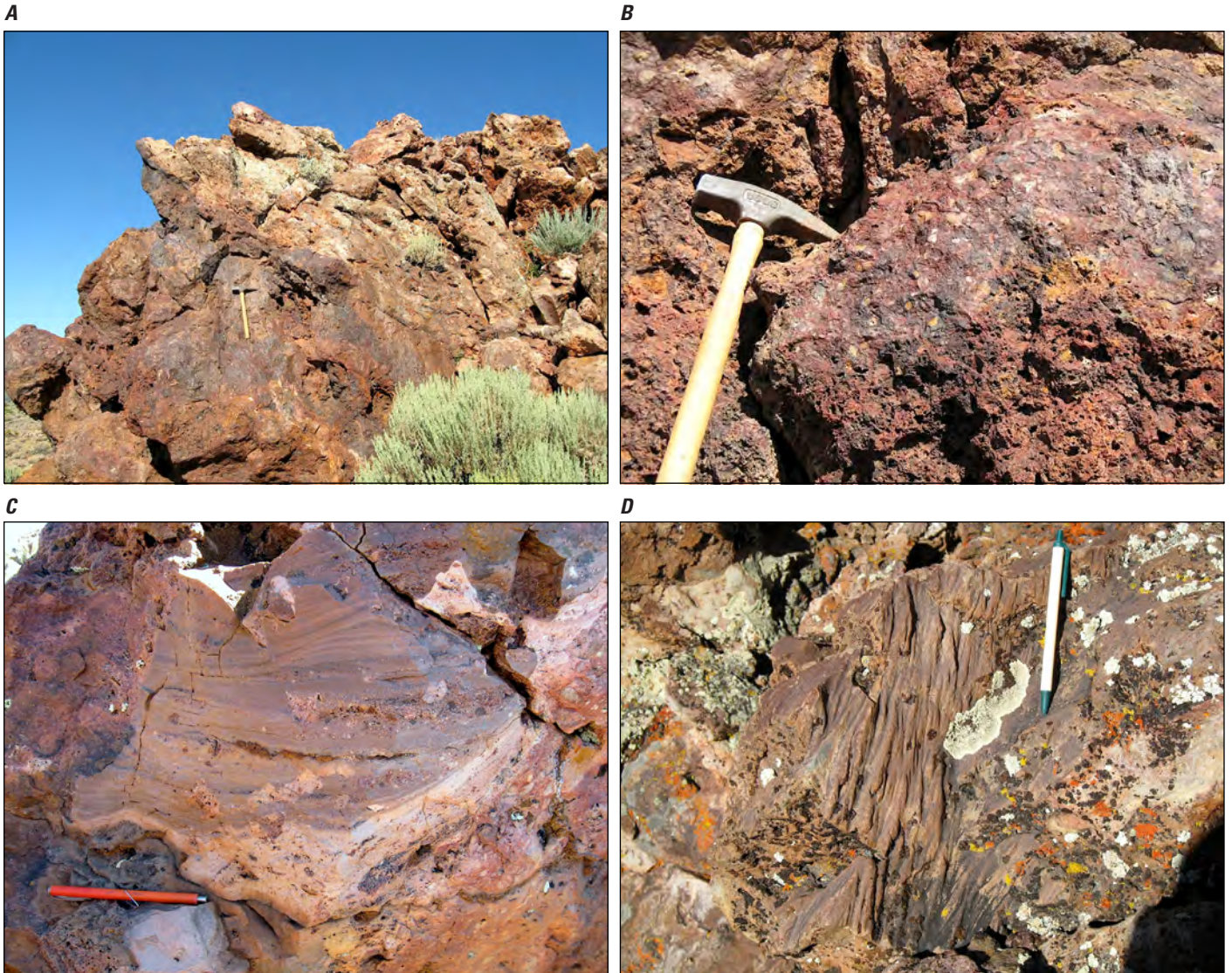
## Paramount-Bald Peak Alteration Zone

### Location

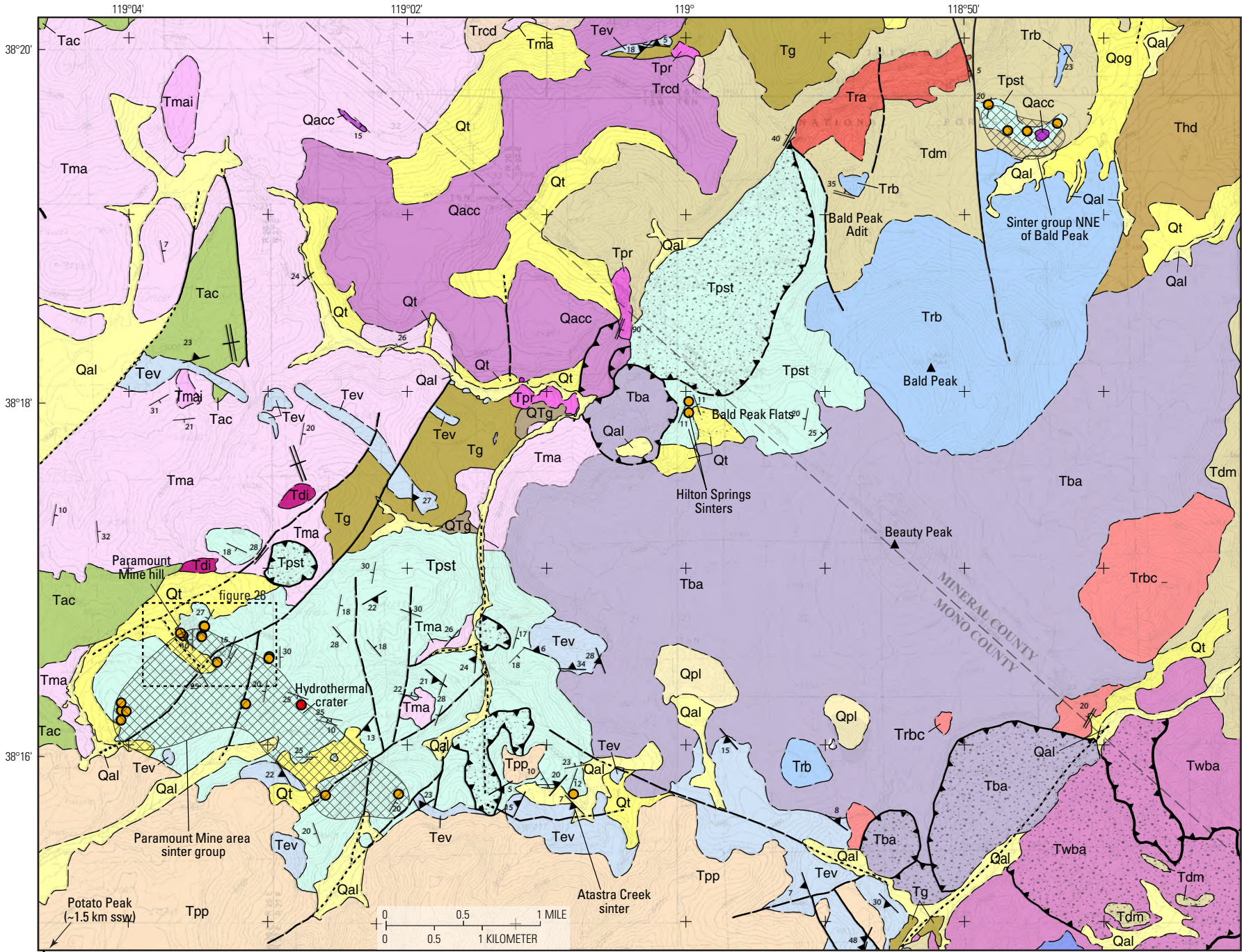
Tps. 5 and 6 N., Rs. 26 and 27 E., mostly unsurveyed, Mono County, California, and Mineral County, Nevada (fig. 1)

### Definition

The Paramount-Bald Peak alteration zone (PBP AZ) is in the central and northeastern part of the Bodie Hills volcanic field and mostly coincides with the sedimentary rocks and tuff of Paramount (Tpst, fig. 27). The alteration zone includes three principal exposures of strongly altered rocks in a 1- to 3-km-wide, northeast-elongate area that extends about 12 km from the northeast flank of Potato Peak to the north side of Bald Peak. The largest exposure is in the southwestern part of the alteration zone, covers about 12 km<sup>2</sup>, and includes the Paramount Hg Mine. The southwest and central exposures most likely are contiguous beneath lava flows of the Pliocene Beauty Peak volcano.




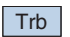
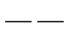

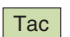

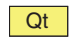
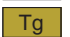

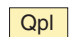
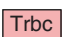
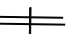
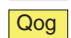
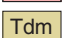
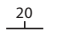

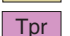
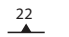
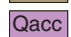
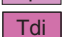

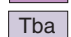
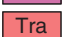

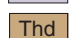
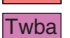

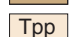

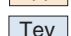
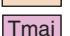
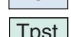
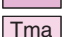
**Figure 26.** Images of hydrothermal features, Four Corners alteration zone. *A*, Outcrop of crudely bedded silicified breccia. Lower part of outcrop is hematite-rich and massive, whereas upper part contains layers of gray, finely bedded sedimentary strata. *B*, Close up view of massive hematite-rich silicified breccia in lower part of outcrop. *C*, Finely crossbedded, chemical and clastic sedimentary beds filling cavity in silicified breccia. *D*, Silicified hematitic mud coating cavity surface. Branching texture of grooves and ridges suggests flow from top to bottom.

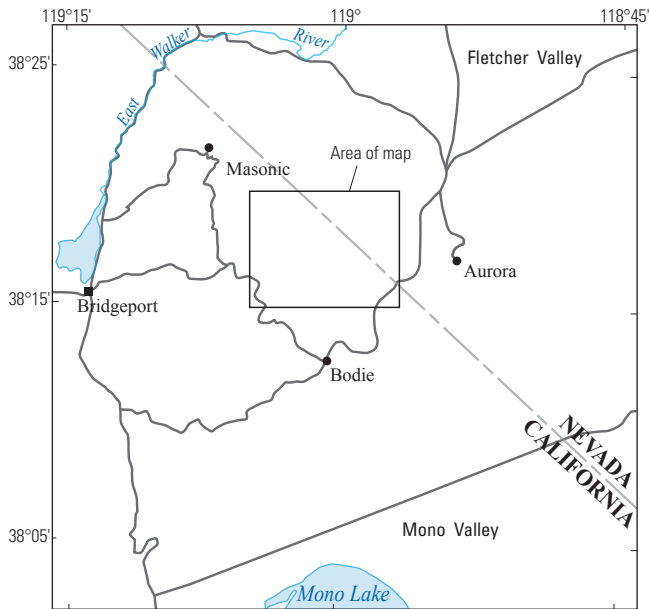


Base modified from U.S. Geological Survey  
Dome Hill, Calif.-Nev., and Aurora, Nev.-Calif., 1989, 1:24,000



EXPLANATION

	<b>Landslide deposits</b>		<b>Rhyolite of Bald Peak</b>		<b>Contact</b>
	<b>Alluvium</b>		<b>Trachyandesite of Aurora Canyon</b>		<b>Fault</b> —Dashed where approximated, dotted where concealed
	<b>Talus deposits</b>		<b>Gravel deposits</b>		<b>Landslide</b> —Head or main scarp of landslide. Hachures point down-slide
	<b>Playa deposits</b>		<b>Rhyolite of Bodie Creek</b>		<b>Vertical dike</b>
	<b>Older gravel deposits</b>		<b>Trachyandesite of Del Monte</b>		<b>Bedding</b>
	<b>Gravel deposits</b>		<b>Pyroxene rhyolite</b>		<b>Foliation</b>
	<b>Trachyandesite of Cow Camp Creek</b>		<b>Dacite intrusions</b>		<b>Sinter</b>
	<b>Basaltic trachyandesite of Beauty Peak</b>		<b>Rhyolite of Aurora Creek</b>		<b>Group of sinters at common elevation</b>
	<b>Hornblende trachydacite</b>		<b>Trachyandesite of West Brawley Peak</b>		<b>Hydrothermal crater</b>
	<b>Trachydacite of Potato Peak</b>		<b>Trachydacite of Rough Creek</b>		
	<b>Eureka Valley Tuff</b>		<b>Trachyandesite intrusion of Masonic</b>		
	<b>Sedimentary rocks and tuff of Paramount</b>		<b>Trachyandesite of Masonic</b>		



**Figure 27. (Facing page)** Geologic map of the Paramount-Bald Peak alteration zone, Mono County, California, and Mineral County, Nevada, showing sinters, sinter groups, and prospects discussed in the text (modified from John and others, 2012).

## History and Production

The Paramount Hg Mine is in the southwestern part of the alteration zone (sec. 13 [projected], T. 5 N., R. 26 E.). Numerous small prospects, trenches, and drill roads have been excavated near the Paramount Mine and in the vicinity of Bald Peak in the central part of the zone. Although Homestake Mining Company explored the area in the 1980s, drill roads and cuttings west of Bald Peak may include pre-1976 Federal Land Policy and Management Act (FLPMA) exploration because of limited to no site reclamation. At the Paramount Mine, Hg was recovered from a chalcedonic quartz vein exposed by two adits, tens of meters of underground workings, and two large trenches (fig. 28). The vein was mined about 1878 (Whiting, 1888), and from 1941 to 1944 at a reported grade of 1.5–5 pounds (lbs) of Hg per ton (Holmes, 1965). According to an unpublished historical compendium filed with regulatory agencies for drilling permitting in 2009, 400 t were also mined and processed in 1968. The volume of calcines associated with a dismantled retorting facility at the lower adit and reported mercury grades indicate that total Hg production was probably tens of flasks. The historical compendium also lists trench excavation in the late 1960s, and drilling programs by Homestake, Molycorp, Noranda, and Equinox from ~1981 to 1991. From 2006 to 2010, approximately 10 holes were permitted and (or) drilled by Cougar Gold at the mine and at various sites on the hill southwest of the mine.

## Stratigraphy

Sedimentary rocks and tuff of Paramount cover most of the PBP AZ (John and others, 2012). This stratigraphic sequence lies on the north and west flanks of the ~9.7 Ma rhyolite of Bald Peak dome. It includes abundant rhyolite tuffs inferred to have erupted from Bald Peak, and rhyolite-rich detritus shed from the dome into the shallow, northeast-elongate Paramount basin (fig. 27). The sequence unconformably overlies ~15 to 14 Ma trachyandesite of Masonic, ~11.3 Ma trachydacite intrusions, ~11 Ma trachyandesite of Del Monte, ~11.3 Ma trachydacite intrusions, and ~10.6 to 10.4 Ma domes of the trachyandesite of Aurora Canyon. Altered sedimentary rocks of the sequence may be temporally equivalent to unaltered coarse gravel deposits that extend northeastward into Fletcher Valley (Tg, fig. 27). A prominent dark-red paleosol developed locally on rocks underlying the sequence is exposed ~0.75 km northeast of the Paramount Mine. The sequence is overlain by ~9.4 Ma Eureka Valley Tuff, by lava flows of ~9 to 8.7 Ma trachydacite of Potato Peak, and by basaltic trachyandesite lava flows of the Pliocene Beauty Peak volcano.

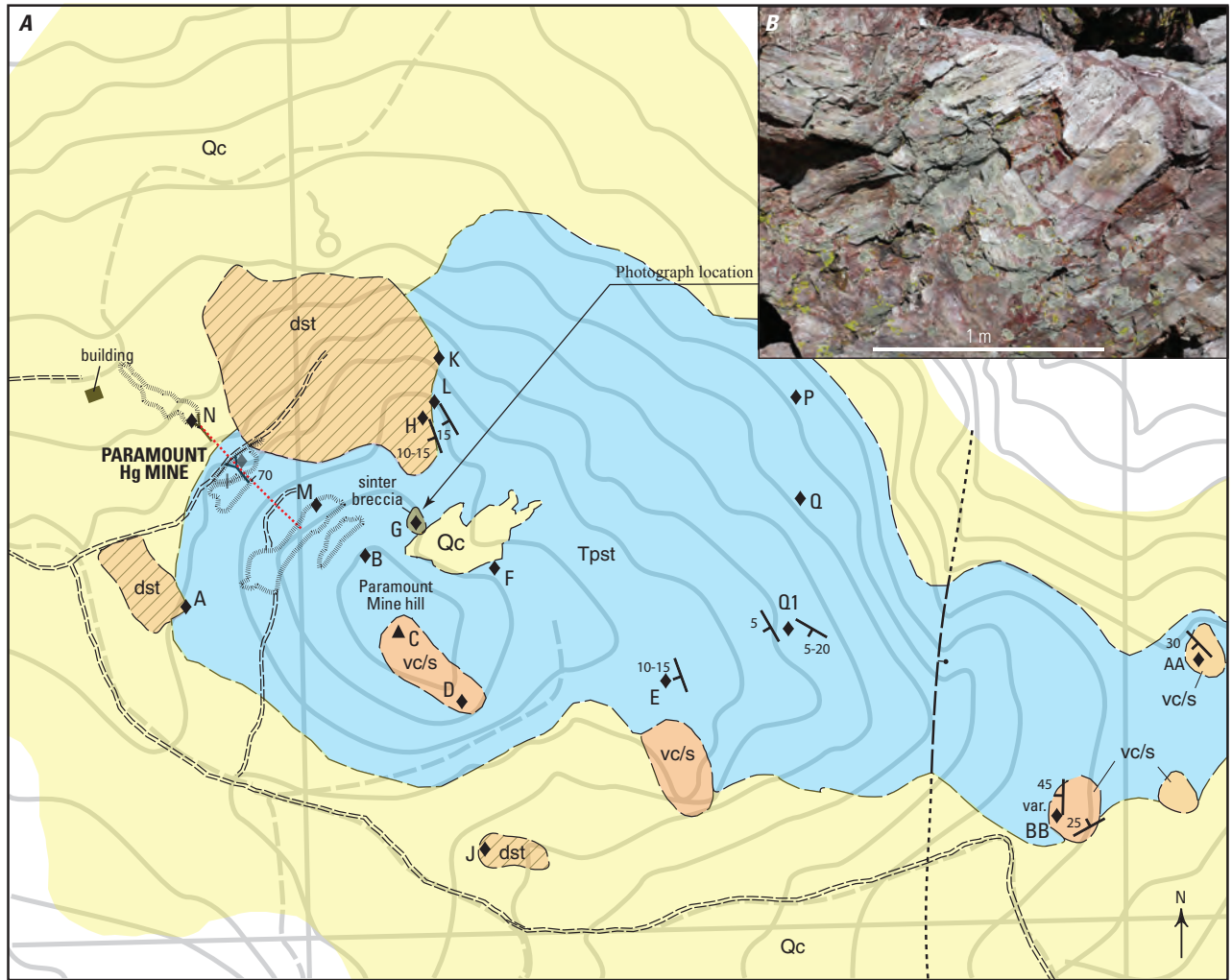
The sedimentary rocks and tuff of Paramount consist of interbedded, crystal-poor, lithic-rich and pumice-rich rhyolite tuff, minor, sparsely porphyritic, flow-banded rhyolite

(possibly intrusive), and poorly sorted volcanoclastic rocks that include volcanic conglomerate, sandstone, and siltstone. Several sinter terraces and numerous sinter beds are dispersed throughout the alteration zone (figs. 27, 28, 29, 30). Pyroclastic rocks vary from unwelded, pumice-rich ash flows that locally contain abundant clasts of nearly aphyric flow-banded rhyolite and porphyritic trachyandesite and dacite lavas, to finely bedded, possibly water lain, crystal-poor air fall tuffs. Clastic sedimentary rocks contain clasts of porphyritic volcanic rocks, including quartz-bearing dacite(?), and less-abundant sparsely porphyritic, flow-banded rhyolite. The sequence may be as much as 200 m thick on the west side of Rough Creek, although irregular dips and complex structure preclude an accurate estimate of thickness in most locations. The sedimentary rocks and tuff are pinkish-gray to pale-red-purple, nearly aphyric, weakly to strongly hydrothermally altered and locally iron stained. Pyroclastic rocks contain trace amounts of plagioclase and quartz phenocrysts in a recrystallized ashy groundmass. The tuff contains abundant, 0.5–10 cm unflattened pumice blocks and exotic lithic fragments composed of porphyritic, intermediate-composition lava and nearly aphyric rhyolite lava.

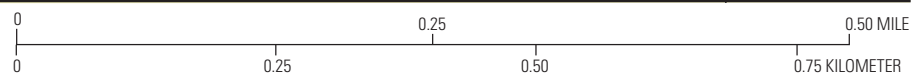
The rhyolite of Bald Peak contains trace to 10 volume percent fine-grained phenocrysts of quartz, sanidine, and lesser biotite and clinopyroxene in hydrated to devitrified glass.

## Structure

The structure of the PBP AZ is poorly understood because of discontinuous stratigraphy within the sequence, pervasive hydrothermal alteration, numerous large landslides, and lack of a detailed geologic map of most of the alteration zone. Faults on figure 27 are inferred on the basis of offset contacts between the sedimentary rocks and tuff of Paramount and underlying lava flows (trachyandesites of Masonic and Del Monte), prominent linear zones of silicification, and variable elevations of sinter terraces. The sedimentary rocks and tuff of Paramount appear to fill a shallow northeast-trending basin (Paramount basin) on the northern and western flanks of the Bald Peak rhyolite dome which probably formed during emplacement of the dome (fig. 27; John and others, 2012). The Paramount basin appears to be bounded by northeast-striking growth(?) faults that were active during sediment deposition in the basin. A series of north-striking faults apparently displaces sinter terraces to progressively lower elevations from about 9,090 ft on the hill southwest of the Paramount Mine, to 8,700 ft at the Paramount Mine, 8,080 ft in Atastracreek, 7,800 ft on the west side of Bald Peak, and ~7,200 ft on the north side of Bald Peak (fig. 27). The pattern of inferred northeast and north-striking faults is similar to fault patterns observed in the Masonic and Aurora Mining Districts (John and others, 2012).

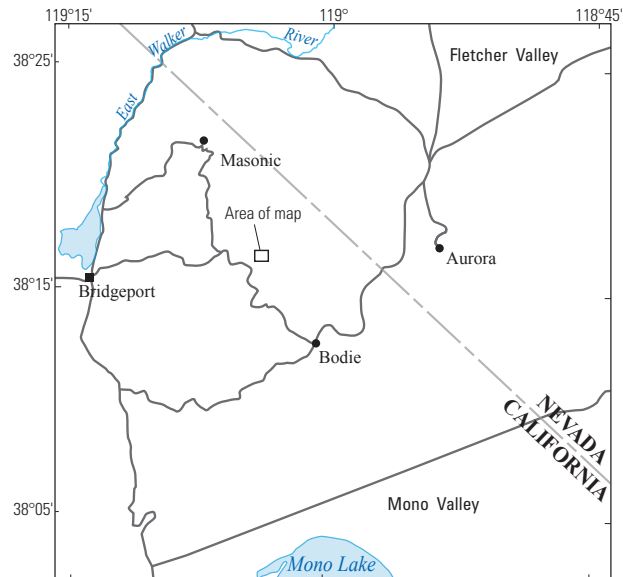


Base modified from U.S. Geological Survey  
Dome Hill, Calif.-Nev., 1989, 1:24,000

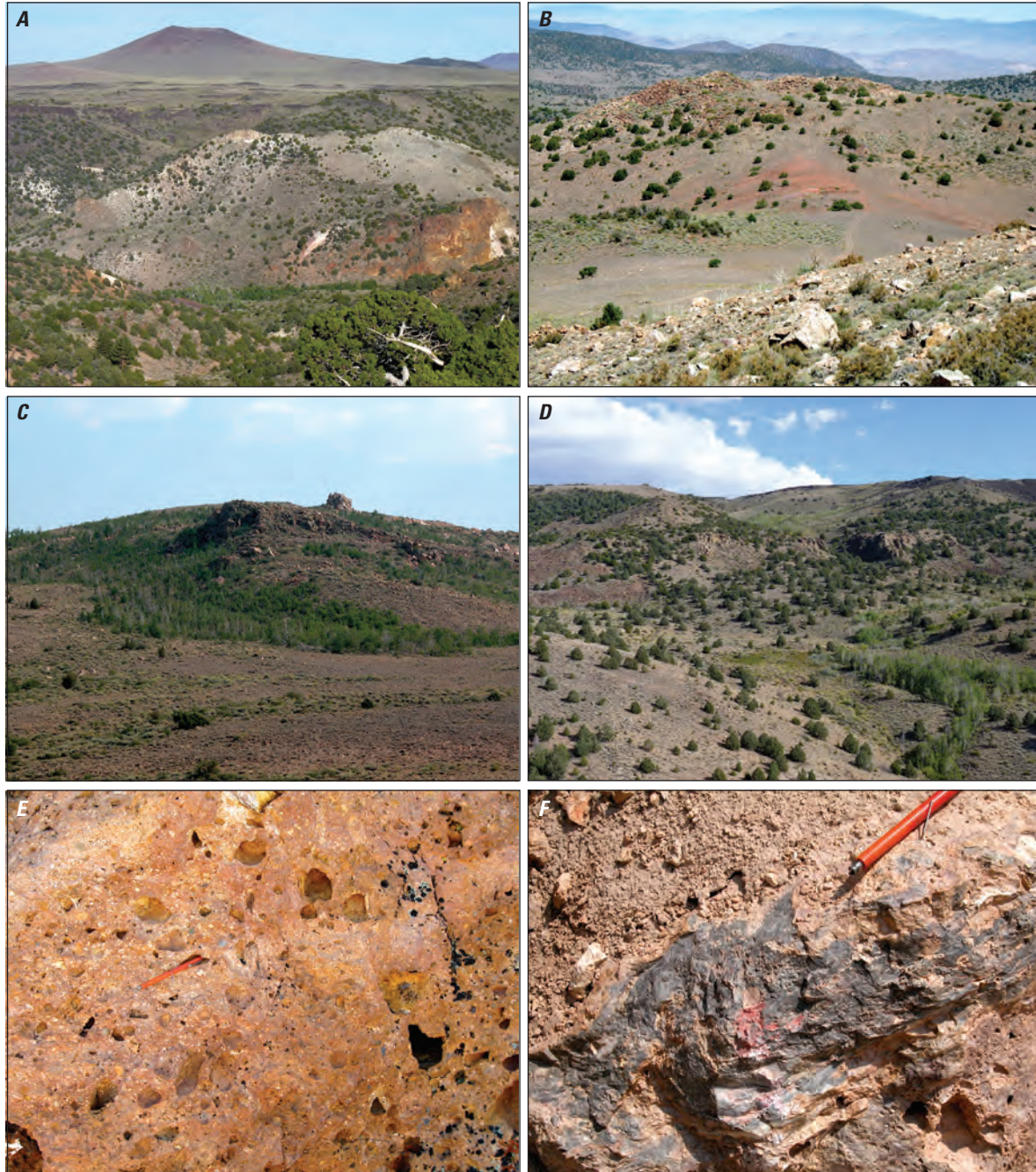


**EXPLANATION**

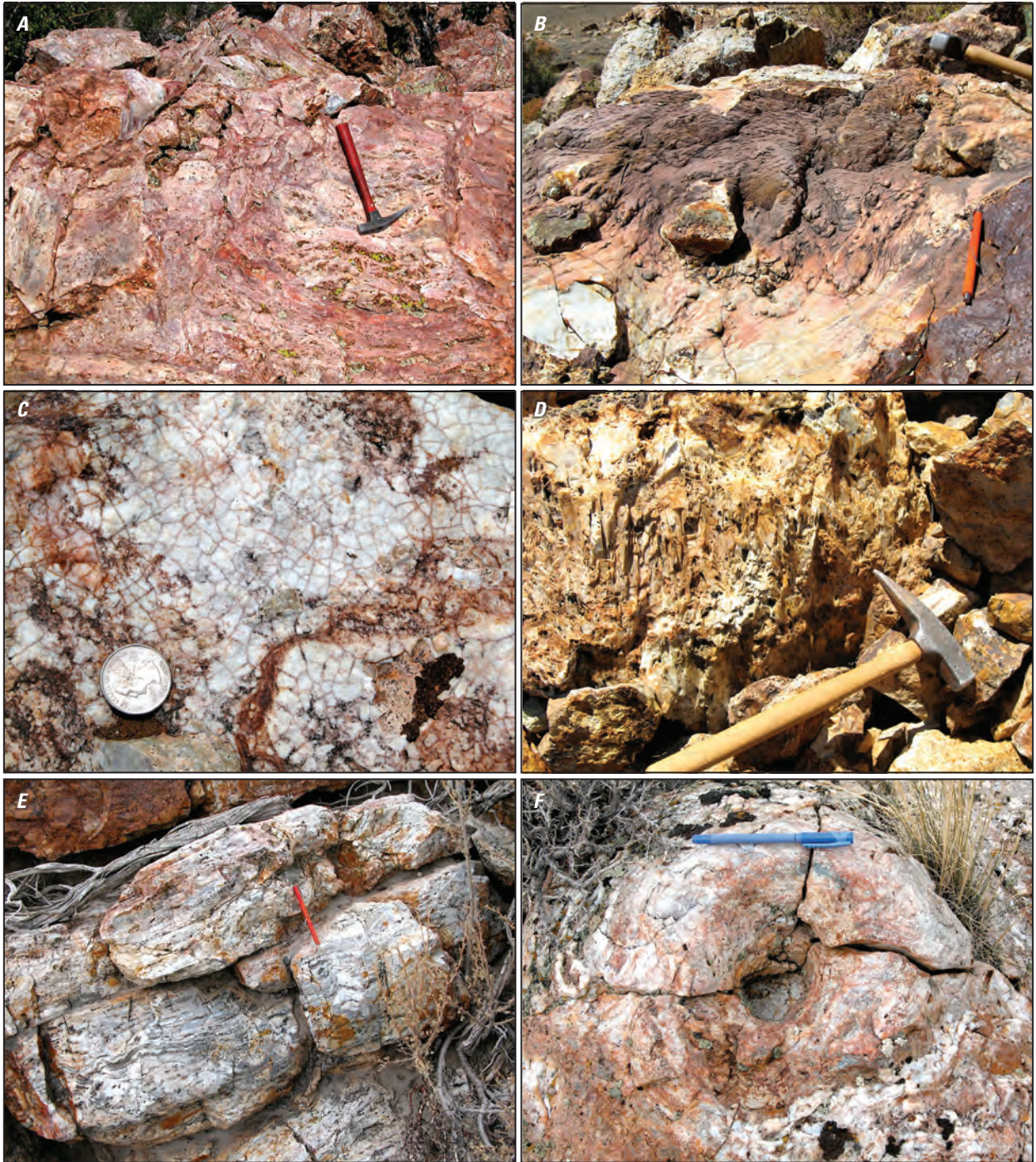
- Qc** Colluvium
- dst** Dismembered sinter terrace
- vc/s** Strongly silicified volcaniclastic rocks (Tpst) ± sinter
- Tpst** Sedimentary rocks and tuff of Paramount (John and others, 2012)—Pervasively altered to quartz, montmorillonite, and lesser kaolinite and pyrite
- Quartz-cinnabar-pyrite vein**
- Contact**—Dashed where approximated
- Fault**—Dashed where approximated, dotted where concealed
- High-angle normal fault**—Bar and ball on downthrown block
- Bedding**
- Mine dump or trench**
- ◆K** Sample site and letter



**Figure 28.** A, Geologic map of the Paramount Hg Mine area, Mono County, California. B, Image showing unoriented, multisized blocks of terrace sinter cemented by fine-grained quartz and minor iron oxide minerals (similar to figure 30G).



**Figure 29.** Images of Paramount-Bald Peak alteration zone. *A*, View looking east at altered rocks in the southwest part of the Paramount basin overlain by unaltered lava flows from Pliocene Beauty Peak volcano (Tba). *B*, View looking northeast from Paramount Mine at a hill composed of altered sedimentary rocks and tuff of Paramount (Tpst) unconformably overlying a red paleosol developed in underlying trachyandesite of Masonic (Tma). *C*, View looking southwest at Paramount Mine hill from the hill in center of *B*. Paramount Mine hill consists of dismembered sinter terraces and altered volcaniclastic rocks. *D*, View of silicified ledges of the Hilton Springs prospect overlain by Beauty Peak lava flows (Tba) at upper right. Most of the rocks in the foreground are part of a large landslide. *E*, Typical leached, argillically altered, pumiceous volcaniclastic deposits in sedimentary rocks and tuff of Paramount (Tpst). *F*, Cinnabar in a chalcedonic quartz vein at the Paramount Mine.



**Figure 30.** Images of hydrothermal features in the Paramount-Bald Peak alteration zone. *A*, Brecciated sinter recemented with red chaledonic quartz on the northwest side of Paramount Mine hill. *B*, Flow textures in siliceous, hematitic, mud-sized sedimentary strata that coat silicified volcanoclastic rocks about 1 km southeast of the Paramount Mine. *C*, Desiccation cracks in thin pool(?) sinter bed in silicified volcanoclastic rocks on top of Paramount Mine hill. *D*, Quartz vein showing replacement texture of coarse bladed carbonate on south side of hill about 1 km southwest of the Paramount Mine. *E*, Sinter beds in Atastra Creek. *F*, Hydrothermal fluid vent on the sinter terrace in Atastra Creek.

## Hydrothermal Alteration

Sedimentary rocks and tuff of Paramount are pervasively altered throughout the Paramount basin. Older units underlying and along margins of the basin also are altered locally, whereas younger units surrounding or overlying the basin generally are unaltered (small exposures of the basal(?) member of the Eureka Valley Tuff are locally altered in Atastr Creek). Three types of alteration affected sedimentary rocks and tuff of Paramount (1) silicification, (2) advanced argillic (kaolinite±dickite) alteration, and (3) intermediate argillic (montmorillonite±kaolinite) alteration. Propylitic alteration assemblages (montmorillonite, illite/smectite, chlorite(?), and calcite) occur locally in underlying, intermediate composition lava flows and volcanoclastic rocks. Variable amounts of iron oxide minerals and jarosite are widespread, and relict pyrite is present in some silicified rocks.

Intermediate argillic alteration assemblages, the most common assemblages in strata of the Paramount basin, are manifested by variable leaching of pumice and volcanic rock clasts that left a porous residue of silica and clay minerals (fig. 29E). SWIR spectrographic analyses indicate that the clay minerals are montmorillonite and lesser kaolinite. These leached and clay-altered rocks are white, beige, or pale green. Pyrite casts are scarce to absent suggesting that this alteration type included little pyrite. With increasing silica content, intermediate argillic alteration grades into silicification as exposed in the bluffs on the southeast side of Paramount Hill (fig. 28).

Smaller areas of intense silicification and advanced argillic alteration occur locally within the broad expanse of strata that are altered to intermediate argillic assemblages. Silicified rocks consist of variably colored, commonly iron oxide-stained, chalcedonic silica and lesser quartz. Domains that contain relict, disseminated, fine-grained pyrite occur locally. Silicified rocks generally form bold outcrops and comprise both elongate cliff-forming ledges and more tabular bodies. Breccia zones are common within silicified rocks. Small zones of advanced argillic alteration locally surround or underlie zones of silicified rock, notably near sinters. Kaolinite is the predominant clay mineral, although dickite is present in several locations including in narrow veins beneath the sinter terrace on Atastr Creek. Alunite was not confirmed in hand samples, although interpretation of ASTER imagery shows alunite occurrences in several places on the southwest side of the Paramount basin (Rockwell, 2010).

Sinter occurs in thin beds (<0.3 m) interstratified with strongly silicified volcanoclastic rocks, and forms terraces, several meters in thickness, that generally overlie silicified volcanoclastic rocks (figs. 27, 28, 29). The largest exposures of sinter are near the Paramount Mine (below). Another large sinter terrace, ~5 m thick, crops out on the west side of Atastr Creek about 1.25 km southeast of its confluence with Rough Creek. This terrace overlies kaolinite-altered volcanoclastic rocks. A small funnel-shaped vent, desiccation cracks, and filamental bacteria mats are exposed on the upper surface of the terrace (fig. 30). Dark-gray siltstone that underlies

part of the terrace may represent mud pot deposits. A third, large terrace is exposed in cliffs above Rough Creek about 2.7 km north-northeast of Bald Peak at the northeast end of the alteration zone (fig. 27). Porous, poorly indurated sinter ~5 m thick is exposed for ~50 m along strike. More strongly indurated sinter, locally containing fossilized reeds, forms thin terraces and clusters of sinter blocks at several other locations in this area of volcanoclastic rocks (fig. 27).

Quartz veins, and quartz-chalcedony veins and stockworks are broadly distributed in the Paramount basin (fig. 27). Veins and stockworks occur (1) at the Paramount Hg Mine, (2) on the top and south side of the hill 1.5 km southwest of the Paramount Mine, (3) on the east side of Atastr Creek east of the sinter terrace, (4) near sinter beds on the west side of Bald Peak (Hilton Springs or Golden Beauty prospect), (5) on the west side of Bald Peak along the California-Nevada state boundary (Bald Peak Flats prospect), and (6) about 1.2 km northwest of Bald Peak (Bald Peak Adit prospect).

## Paramount Mine Area

The chalcedonic quartz vein mined for mercury in the Paramount Mine trends N50°W, dips 70°NE, and is as much as 2 m wide. It is exposed in mine workings on the west side of a low domal hill composed of silicified and illite-clay mineral-altered volcanoclastic rocks (Paramount Hill; fig. 28). The vein consists of dense chalcedonic quartz and lesser clay minerals, and small amounts of pyrite, cinnabar, and metacinnabar. The clay minerals, mostly montmorillonite and kaolinite, occur in irregular, millimeter-wide seams and in centimeter-sized pockets that represent partially leached wall-rock fragments. Clasts and matrix of volcanoclastic deposits exposed in trenches across the vein and at the upper adit are altered to kaolinite and lesser opaline silica and montmorillonite for several meters on both sides of the vein. Remnants of at least five sinter terraces, and a sixth disaggregated and silicified terrace (figs. 28, 29), are adjacent to the vein on the west and north sides of the hill, at the southeast base of the hill, and ~0.8 km east of the mine. The former terraces have been dismembered by substrate deflation and freezing; they are represented by areas of closely spaced, rotated blocks of sinter and volcanoclastic strata, many of which are meters in dimension. Occurrences of disaggregated and silicified sinter are indicative of gravitational instability during terrace construction.

## Minor Elements in Rocks

Samples from the sinter terraces on the north and west side of Paramount hill contain variably elevated concentrations of Au (as much as 32 ppb), Ag (<1 ppm), Hg (≤2.7 ppm), As (≤90 ppm), Sb (≤396 ppm), and W (≤14.4 ppm; table 1-9). Two samples of finely laminated, dark-gray chalcedonic pool sinter(?) from the top of Paramount Hill contain elevated concentrations of Au (0.92; 3.57 ppm), Ag (3; 6 ppm), Hg (1.5; 4.3 ppm), As (19; 38 ppm), Sb (82; 130 ppm)

and Tl (1.8; 4.7 ppm). Samples of quartz-chalcedony veins and altered wall rocks from the flat ridge southeast of Paramount hill contain locally elevated concentrations of Au (7–740 ppb), Ag (<1–13 ppm), Hg (<1,600 ppm), As (<170 ppm), Ba (217–1,500 ppm), Sb (<916 ppm), and W (<28.9 ppm).

Minor element concentrations along a continuous traverse orthogonal to sinter beds (determined by LA ICP-MS; fig. 31), include local (submillimeter) enrichment of Hg, Ag, Bi, As, Pb, and Cu. Bulk analyses of the traversed beds show a slightly elevated Hg concentration; concentrations of other elements are within the range of other bulk sinter samples. Minor element concentrations along a continuous traverse across the chalcedonic quartz vein mined for Hg (fig. 32) include local (submillimeter) enrichment of Au, Ag, S, Hg, Fe, As, Sb, Cu, Mo, Sn, and Zn. Bulk analyses of the traversed vein indicate elevated concentrations of Hg, Au, Sb, and S that are within the range of other vein samples, but many other elements have elevated concentrations at the millimeter scale (for example, Cu, Mo, and Zn) that are not elevated in bulk samples.

A rotary drill hole sited in the vicinity of the Paramount Mine encountered “volcanic breccias and pyroclastic rocks to a depth of 230 feet”, and “dacite and andesite flows” from 230 to 425 ft, the total depth of the hole (Silberman and Berger, 1985). The andesite and dacite flows are likely either the trachyandesite of Masonic or trachyandesite of Aurora Canyon (fig. 27). Alteration of these rocks includes “moderate to intense silicification, argillic alteration, and chloritization” with 2–10 volume percent pyrite. Minor element concentrations in cuttings include intervals of >1 ppm Au (maximum 1.9 ppm) from 100 to 160 ft above the oxide-sulfide boundary, and 0.5–1 ppm Au from 215 to 240 ft. These intervals partly coincide with chalcedonic quartz veins. Other elevated element concentrations include As (mostly hundreds to >1,000 ppm), Sb (mostly hundreds of parts per million), Tl (parts per million to tens of parts per million), Ag (mostly parts per million), and Hg (parts per million to several tens of parts per million; Silberman and Berger, 1985). These and other element concentrations (B, Mn, Sr, Ba, Cr, Mo, Ni, Zn, Pb, V, Co, and Cu) have marginal to no clear relationship to the >1 ppm Au zone, the oxide-sulfide interface, and to the total sulfide content.

Veins as much as 0.3 m wide on the hill 1.5 km southwest of the Paramount Mine contain internal fragments of volcanoclastic wall rocks. These veins are enveloped by centimeter-wide selvages of wall rocks altered proximally to kaolinite and distally to illite/montmorillonite, both of which occur with minor amounts of pyrite; these minerals are interpreted as hypogene. The veins are prominently to indistinctly layered. The centers of most veins are elongate voids partly filled with tabular encrustations of submillimeter, euhedral quartz crystals on relict bladed calcite crystals (perimorphs), most of which have been leached. Vein samples contain variably elevated concentrations of Au (<2 ppm), Ag (<7 ppm), Hg (<34 ppm), As (tens to hundreds of parts per

million), Ba (<2,500 ppm), Sb (tens to hundreds of parts per million), and Tl (<13.7 ppm; table 1-9).

## Atastra Creek Area

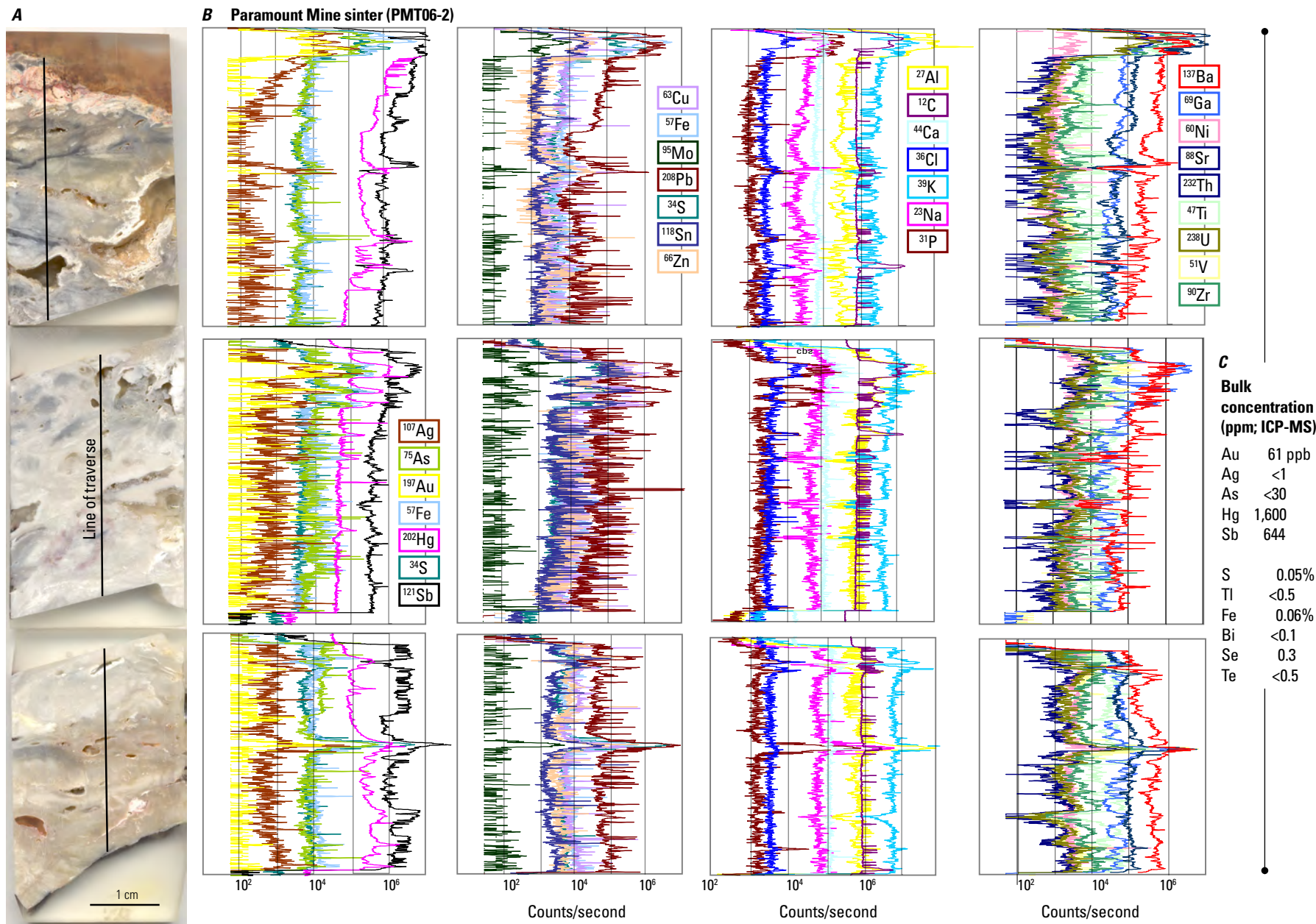
In the Atastra Creek sinter terrace, minor element concentrations, determined by LA ICP-MS, along a continuous traverse orthogonal to sinter beds (fig. 33) include local (submillimeter) enrichment of Sb, As, Ag, Hg, Tl, Sr, Ba, Cu, Pb, and Fe. Bulk analyses of the traversed beds also show slightly elevated concentrations of some of these elements (As, Hg, Sb, and Tl).

In a road bed east of the Atastra Creek sinter terrace, blue-gray, pyritic, chalcedonic quartz veins are poorly exposed in a window of Miocene rocks beneath Pliocene basaltic trachyandesite of Beauty Peak lava flows. The veins are as much as 4 cm wide, contain 5–10 percent pyrite, and are within kaolinite-montmorillonite-altered lower(?) member rocks of the Eureka Valley Tuff. Vein samples contain low concentrations of Au (<5 ppb), and Ag (<1 ppm), and elevated concentrations of Hg (4.7–13.4 ppm), As (47–122 ppm), Sb (96–255 ppm), and W (70–123 ppm; table 1-9).

## Bald Peak Area

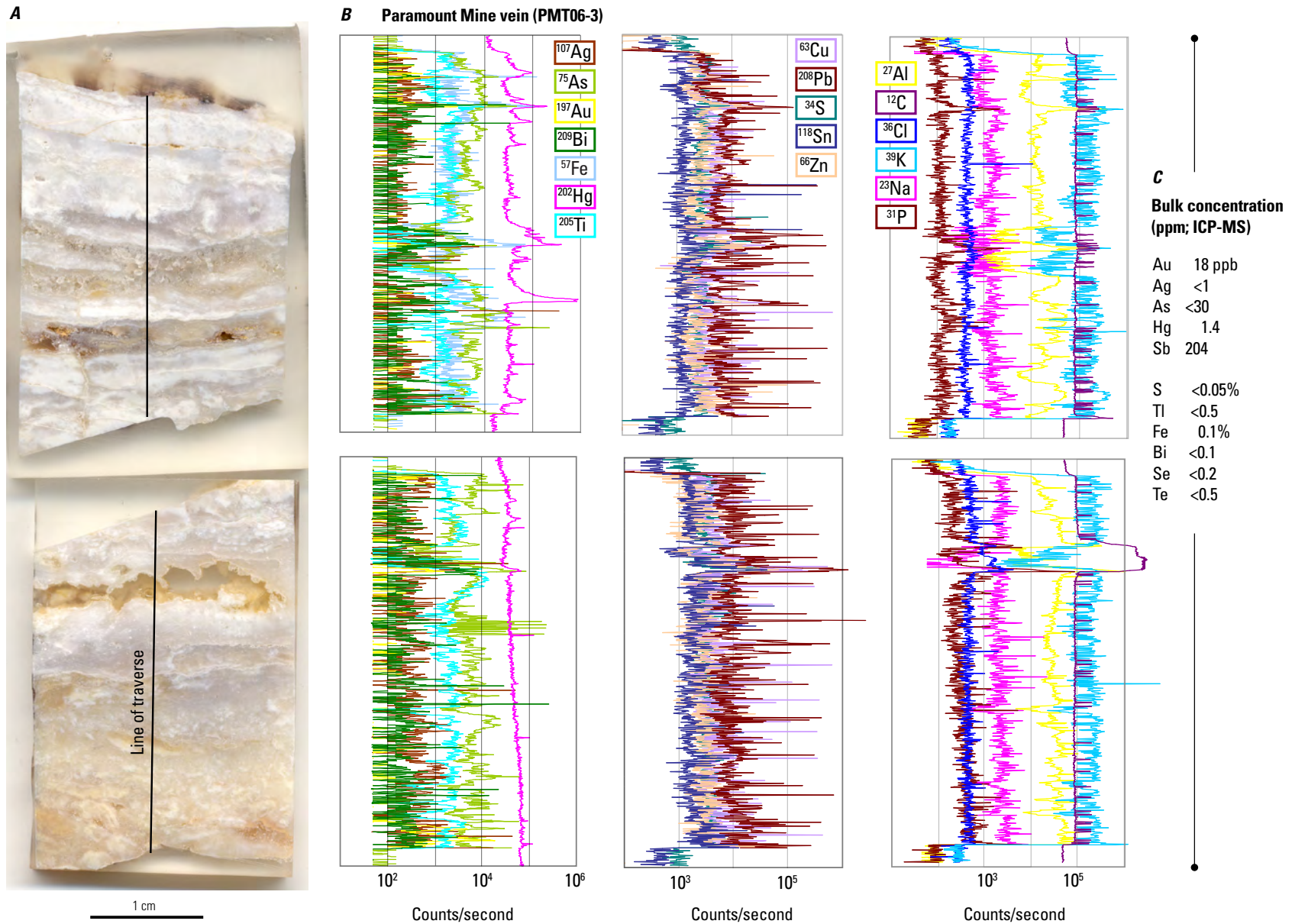
Chalcedony veins and thin beds of sinter are exposed at the Hilton Springs (Golden Beauty) prospect on the west side of Bald Peak overlooking Rough Creek (fig. 27). Several narrow zones of centimeter-wide, sheeted chalcedony-pyrite veins cut strongly argillized and silicified sedimentary rocks and tuff of Paramount that underlie Pliocene Beauty Peak lava flows. The veins strike north-northeast and dip 75–90°NW. Samples of vein and silicified, pyritic wall rock contain elevated concentrations of Au (1.6–2.6 ppm), Ag (7–18 ppm), Hg (4–44 ppm), As (290–640 ppm), Ba (<2,800 ppm), Sb (55–77 ppm), and W (5–16 ppm; table 1-9). Several thin (≤2 cm) beds of dark-gray to black, very finely laminated chalcedonic sinter are interbedded with or overlie silicified sedimentary rocks of the unit (figs. 29, 30). Samples of the silicified sedimentary rocks and sinter contain variably elevated concentrations of Au (0.02–0.5 ppm), Ag (1–8 ppm), Hg (0.2–5 ppm), As (40–380 ppm), Ba (<2,500 ppm), Sb (220–370 ppm), and W (3–21 ppm; table 1-9).

Beds of silicified sedimentary rocks and tuff of Paramount are cut by narrow (mostly <2 cm) opal-chalcedony veins at the Bald Peak Flats prospect along the California-Nevada boundary about 1 km west-southwest of Bald Peak (fig. 27). Several zones (meters wide) containing banded veins (centimeters thick) strike north-northeast to northeast and dip steeply to the southeast. L.J. Peters (written commun., 2004) reported partial chemical analyses for six vein samples from the Bald Peak Flats prospect: Au (<3–106 ppb), Ag (0.08–0.54 ppm), As (99–1,290 ppm), and Hg (1.6–49 ppm).

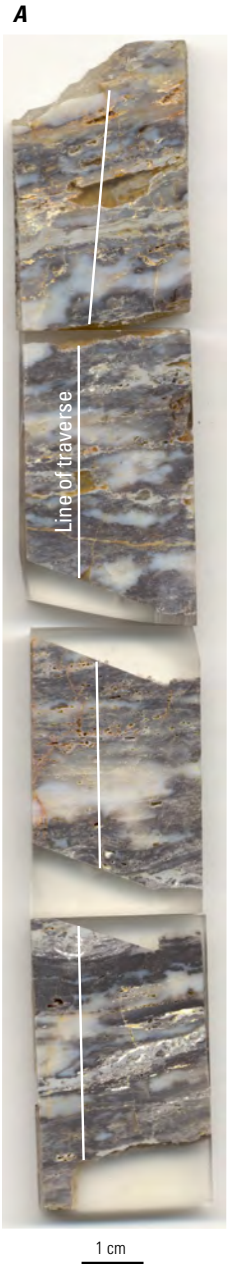


**Figure 31.** *A*, Image showing oriented consecutive sections of sinter from a dismembered terrace at the western base of Paramount Mine hill, Paramount-Bald Peak alteration zone. *B*, Graphs showing relative element concentrations in sinter measured in counts per second (counts/second) by laser ablation inductively coupled plasma-mass spectrometry (LA ICP-MS). *C*, Bulk sample element concentrations determined by inductively coupled plasma-mass spectrometry (ICP-MS). Locally elevated (millimeter-scale) element concentrations include Au, Ag, S, Hg, Fe, As, Sb, Mo, Cu, Pb, Zn, and numerous other elements, only some of which are elevated in the bulk sample.

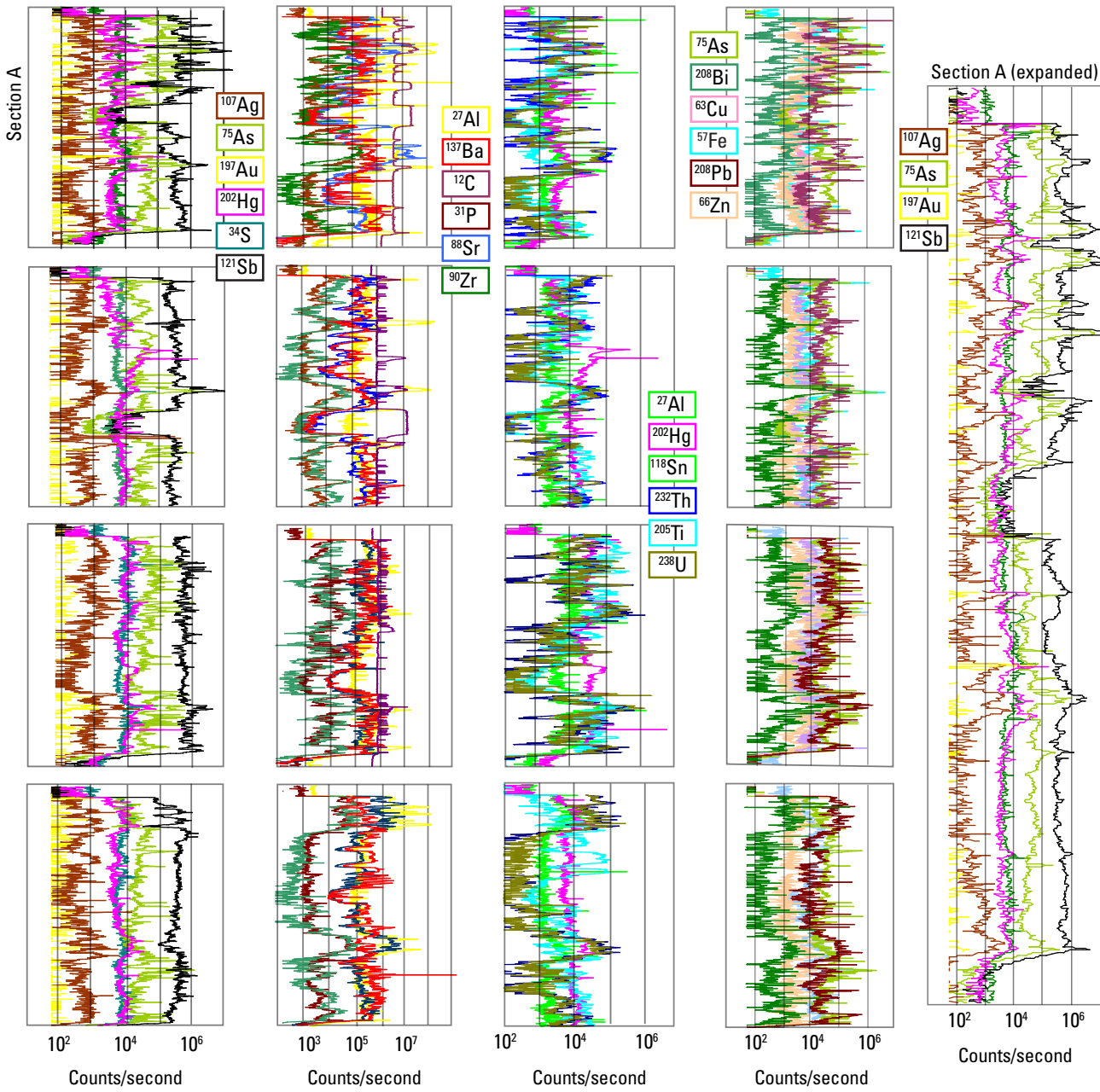




**Figure 32.** A, Image showing oriented consecutive sections of a chalcedonic quartz vein exposed at the upper adit of the Paramount Mine, Paramount-Bald Peak alteration zone (fig. 28). B, Graphs showing relative element concentrations in quartz vein measured in counts per second (counts/second) by laser ablation inductively coupled plasma-mass spectrometry (LA ICP-MS). C, Bulk sample element concentrations determined by inductively coupled plasma-mass spectrometry (ICP-MS). Locally elevated (millimeter-scale) element concentrations include Au, Ag, Hg, Bi, Fe, As, S, Sn, Cu, Pb, Zn, and other elements, only some of which are elevated in the bulk sample.



**B** Atastra Creek sinter (ATAS06-1)



The Bald Peak adit prospect lies about 1.2 km northwest of Bald Peak and encompasses a discontinuously exposed, north-northeast-trending zone of quartz-chalcedony veins and stockworks as much as 700 m long by 250 m wide (fig. 27; L.J. Peters, written commun., 2004). Veins and silicified breccia zones are within porphyritic trachyandesite of Del Monte lava flows. The Bald Peak adit is near the south end of the prospect, where a cliff-forming silicified fault zone contains an ~2-m-wide, massive to banded, locally brecciated, milky white quartz vein. The vein strikes ~N15°E, dips 80°SE–80°NW, and splits into several thinner veins that pinch out at the south end of the cliff face. Several other zones of narrow (centimeters wide) north-northeast-striking, steeply dipping, chalcedonic quartz-pyrite veins are exposed near the south end of the prospect. Wall rocks of these veins are altered to montmorillonite±kaolinite. Quartz veins exposed in bulldozer cuts in the northern part of the prospect consist of brecciated, iron oxide stained, white chalcedonic quartz as much as 0.3 m wide. Some veins are banded with vuggy centers and bladed textures that suggest quartz replacement of carbonate minerals. Vein samples from the Bald Peak adit prospect contain as much as 5.4 ppm Au, 12.3 ppm Ag, 1,900 ppm As, and 6.6 ppm Hg (L.J. Peters, written commun., 2004).

### Sulfur Isotope Compositions

Two samples of cinnabar from the Paramount Mine have similar  $\delta^{34}\text{S}$  values of  $-5.3$  and  $-4.7$  ‰ (PM08-1A; PM08-1B; table 2). These values are slightly higher than some  $\delta^{34}\text{S}$  values of sulfide minerals in the Aurora Mining District, and slightly lower than values of cinnabar in the Cinnabar Canyon-US 395 alteration zone, and most values of sulfide minerals in Bodie district veins. Paramount Mine cinnabar  $\delta^{34}\text{S}$  values may reflect sulfide-sulfate fractionation. However, the presence of sulfate minerals is unsubstantiated; additional sulfur isotope analyses are required to adequately characterize sulfur geochemistry of this very large alteration zone.

### ASTER Imagery

ASTER imagery (Rockwell, 2010) of the PBP AZ shows widely scattered pixels and five fairly contiguous pixel clusters that correspond to groups of hydrothermal minerals.

Pixel clusters that coincide with northeast-elongate, silicified outcrops along upper Rough Creek about 2.5–3 km southeast of the Paramount Mine contain abundant alunite and kaolinite. The largest contiguous cluster of pixels (~0.35 by 0.2 km) on the west side of Atastra Creek west of the sinter terrace corresponds to leached tuff containing abundant smectite and (or) kaolinite and quartz. Other pixel clusters near the confluence of Atastra and Rough Creeks, and on the west side of Rough Creek, correspond to leached tuff that contains quartz, smectite, and kaolinite, and to kaolinite and alunite, respectively. However, no alunite was identified by PIMA spectroscopy in samples collected from several of these clusters.

### SWIR Spectra

SWIR spectra of ~50 hydrothermally altered and mineralized hand samples from the PBP AZ show that montmorillonite and kaolinite are the dominant clay minerals, and that mixed-layer illite/smectite is less common. Kaolinite is most abundant near sinter outcrops. Alunite, illite, and chlorite were not identified in the analyzed hand samples.

### Hydrothermal Mineral Ages

No hydrothermal minerals in the PBP AZ have been dated. However, based on  $^{40}\text{Ar}/^{39}\text{Ar}$  ages of underlying and overlying rock units, sedimentary rocks and tuff of Paramount were hydrothermally altered between ~9.7 and 9.3 Ma. The pervasively altered sedimentary rocks contain abundant clasts of flow-banded, nearly aphyric rhyolite that may have been derived from the ~9.7 Ma Bald Peak lava dome (John and others, 2012). In most parts of the Paramount basin, altered sedimentary rocks and tuff of Paramount are overlain by unaltered ~9.4 Ma Eureka Valley Tuff. The lower part of the Eureka Valley Tuff near Atastra Creek is altered, but that alteration occurred after emplacement of the older, >9.7 Ma Tollhouse Flat member (Pluhar and others, 2009) of the Eureka Valley Tuff. In Atastra Creek and in other parts of the southwestern Paramount basin, unaltered lava flows of ~9.0 to 8.8 Ma trachydacite of Potato Peak overlie altered Paramount basin rocks.

**Figure 33. (Facing page)** *A*, Image showing oriented consecutive sections of sinter with black beds from the sinter terrace on Atastra Creek, Paramount-Bald Peak alteration zone (fig. 27). *B*, Graphs showing relative element concentrations in sinter measured in counts per second (counts/second) by laser ablation inductively coupled plasma-mass spectrometry (LA ICP-MS). *C*, Bulk sample concentrations determined by inductively coupled plasma-mass spectrometry (ICP-MS). Sinter section *A* is expanded at right to show (millimeter-scale) elevated concentrations of Au, Ag, Hg, Sb, and As. These elements and other elements that are locally concentrated (including Sn, Tl, Cu, Pb, Zn, and Fe) are mostly not elevated in the bulk sample.

## Cinnabar Canyon-US 395 Alteration Zone

### Location

Secs. 2, 3, 4, 9, 10, 11, 13, 14, 15, 16, 23, 24, 25, 26, 36, T. 4 N., R. 25 E. (unsurveyed); secs. 19, 29, 30, 31, T. 4 N., R. 26 E. (unsurveyed), Mono County, California (fig. 1)

### Definition

The Cinnabar Canyon-US 395 alteration zone (CC-395 AZ) is defined by a contiguous volume of rock, mostly volcanoclastic deposits and lesser porphyritic volcanic rocks, which have been pervasively hydrothermally altered to quartz, chalcedony, opaline silica, clay minerals, alunite, and pyrite. Altered rocks extend north and west from the mouth of Cinnabar Canyon to highway US 395, and are partly covered by unaltered trachyandesite of Willow Springs (fig. 34). The alteration zone may be several times larger (approaching 30 km<sup>2</sup>) than exposed. Along and south of Clearwater Creek, alteration intensity decreases abruptly at the contacts of altered rocks and Paleozoic metasedimentary rocks and at contacts of younger rhyolite domes. Much of the alteration zone in secs. 23, 24, 25, T. 4 N., R. 25 E., including the sulfur resource, is covered by colluvium.

### History and Production

Production recorded from the CC-395 AZ consists of 10 flasks of mercury recovered in 1923 at the Calmono (Old Timer) Mine (Holmes, 1965), 0.3 km south of Cinnabar Hill (sec. 19, T. 4 N., R. 26 E.; sec. 24, T. 4 N., R. 25 E.; fig. 34). A nearby drill-defined sulfur resource, known as the Cinnabar Canyon sulfur deposit, contains 16.1 Mt at 17.9 weight percent S<sup>o</sup> (sec. 19, T. 4 N., R. 26 E.; sec. 24, T. 4 N., R. 25 E.; Ward, 1992; Vikre and Henry, 2011).

### Stratigraphy

The oldest rocks in the CC-395 AZ, exposed at the mouth of Cinnabar Canyon, are Paleozoic metasedimentary rocks (Chesterman and Gray 1975; fig. 34). In the vicinity of Cinnabar Canyon, Paleozoic metasedimentary rocks are unconformably overlain by a sequence of altered volcanoclastic deposits and largely coextensive porphyritic lava flows (volcanoclastic-flow sequence) in low-relief, domelike landforms. This sequence, which comprises most of the CC-295 AZ, was included in the Willow Springs Formation of Chesterman and Gray (1975), but has been correlated with sedimentary rocks and debris flows of Mount Biedeman (~9.9–8.9 Ma; table 1). Unaltered and variably altered flows that unconformably overlie altered sequence strata are included in trachyandesite of Willow Springs and dacite of Hot Springs Canyon, respectively (fig. 34; John and others,

2012). In the CC-395 AZ, altered sequence strata, trachyandesite, and dacite have been intruded and partly covered by rhyolite of Big Alkali (John and others, 2012), which includes rhyolites in the Mount Biedeman and Willow Springs Formations of Chesterman and Gray (1975). Within the CC-395 AZ, trachyandesite of Willow Springs is ~8.6–8.0 Ma, and dacite of Hot Springs Canyon is ~8.1 Ma. Rhyolite of Big Alkali, north of Cinnabar Hill, is ~5.5 Ma (fig. 34; table 1).

The Paleozoic metasedimentary rocks are dark-gray to black, hornfels and quartzite (Chesterman and Gray, 1975). These Ordovician and Silurian strata are likely correlative with similar rocks exposed in the Log Cabin Mine and Ritter Range roof pendants in the Sierra Nevada (Kistler, 1966; Chesterman and Gray, 1975). Sedimentary rocks and debris flows of Mount Biedeman consist of poorly sorted lahar, block-and-ash flow, and associated sedimentary deposits shed from the flanks of the Mount Biedeman stratovolcano ~8 km east-southeast of the CC-395 AZ. To the south, these strata are intercalated with trachyandesite of Mount Biedeman lava flows. Clast populations in sedimentary rocks and debris flows are dominated by trachyandesite of Mount Biedeman. Most block-and-ash flow deposits are brownish-black, clast supported, and include an ashy matrix. Light-gray, recessively weathering lahar deposits are massive, poorly sorted, and contain silt- to boulder-size clasts in an ash- to clay-rich matrix. The sedimentary facies of this unit consists of matrix-supported deposits that contain rounded, compositionally diverse clasts several centimeters to 0.5 m in diameter.

In the CC-395 AZ, volcanoclastic deposits of the volcanoclastic-flow sequence have been pervasively altered and weather recessively except where silicified. Exposures on the hill marked by conspicuous cuts in clay-altered volcanoclastic deposits (clay-cut hill; fig. 34), and in drainages 1 km west of Cinnabar Canyon and ~0.2 km north of Clearwater Creek, consist of chaotic to well-sorted, subrounded to subangular, centimeter- to millimeter-sized clasts of porphyritic volcanic rocks in soft gray-green to beige matrices composed of sand to ash-sized particles (figs. 34, 35). Conformable porphyritic flows occur mostly near the top of the sequence as blocky to locally tiered outcrops. Flows contain variable abundances of partly altered to relict phenocrysts of plagioclase, hornblende, and biotite in a green-gray to beige aphanitic matrix.

Based on the abundance of altered colluvial clasts, deflated surfaces in sec. 24, T. 4 N., R. 25 E., and stratigraphic sections (Ward, 1992), surficial deposits that cover altered volcanoclastic rocks in areas of low relief in the CC-395 AZ are likely meters to a few tens of meters thick.

### Structure

The distribution of exposed altered rocks indicates that the CC-395 AZ is elongate northwest-southeast. However, alteration was strongly controlled by lateral permeability in the volcanoclastic-flow sequence, much of the alteration zone is partly covered by unaltered trachyandesite of Willow Springs, and the overall extent of the alteration zone may be more

equidimensional. Faults that may have served as conduits for hydrothermal fluid circulation in sequence strata are not widely evident. Northwest-striking faults that bound the sulfur resource near Cinnabar Hill presumably have controlled alteration of sequence strata that contain the resource (Ward, 1992). Normal displacement along the northern fault, which corresponds to a northwest-trending linear escarpment of silicified sequence strata, is interpreted to have down-dropped sequence strata to the south. This fault apparently served as a conduit for hydrothermal solutions; displacement along it confined all sulfur to the footwall block. Lineaments on color air photos suggest that this fault extends to highway US 395. Two west-east-trending structures may slightly displace altered and postalteration rocks near Cinnabar Canyon (fig. 34). Other predominantly north- and northwest-striking faults were mapped by Chesterman and Gray (1975) in the vicinity of the S° resource and north and northwest of the resource.

The west side of the alteration zone is bordered by surficial deposits of Bridgeport Valley. These basin-fill deposits unconformably overlie altered sequence strata and are juxtaposed against them along a northwest-striking fault that is subparallel to US 395 (fig. 34).

## Forms of Mercury and Sulfur Mineralization

The Calmono (Old Timer) Hg Mine, in the drainage at the south base of Cinnabar Hill (fig. 34), consists of shallow pits, cuts, a caved shaft, and remnants of a retorting (recovery) facility. Based on examination of dump samples, cinnabar occurs in thin veins and coats fractures in clay-altered porphyritic flows, and was likely the source of Hg production.

The Cinnabar Canyon sulfur resource, located immediately northwest of Cinnabar Hill, is ~60–135 m below the surface (figs. 34, 36). Its lateral dimensions are ~545 m northwest to southeast, and ~275 m southwest to northeast. The resource was identified in core and reverse circulation holes drilled for gold by Homestake Mining Company and Amselco Minerals Inc. in the late 1980s. The resource occurs in volcanoclastic-flow sequence strata that are altered to stratiform, subhorizontal assemblages of silica, clay minerals, pyrite, sulfur, and minor amounts of gypsum, barite, and cinnabar.

The following description of the sulfur resource is condensed from Ward (1992) and supplemented by observations derived from mapping and examination of discarded pieces of core at drill sites (Vikre and Henry, 2011). Several tens to >100 m of sequence strata are replaced by fine-grained quartz over the sulfur resource (fig. 36). These resistant rocks crop out on and northwest of Cinnabar Hill but rarely contain sulfur. Below and lateral to the stratiform silicification, sequence strata are partially to entirely replaced by clay minerals and opaline silica. Beneath opaline silica-clay alteration is a section of sequence strata ~35–60 m thick that is replaced by fine-grained quartz, 0 to >20 volume percent pyrite, and 0 to

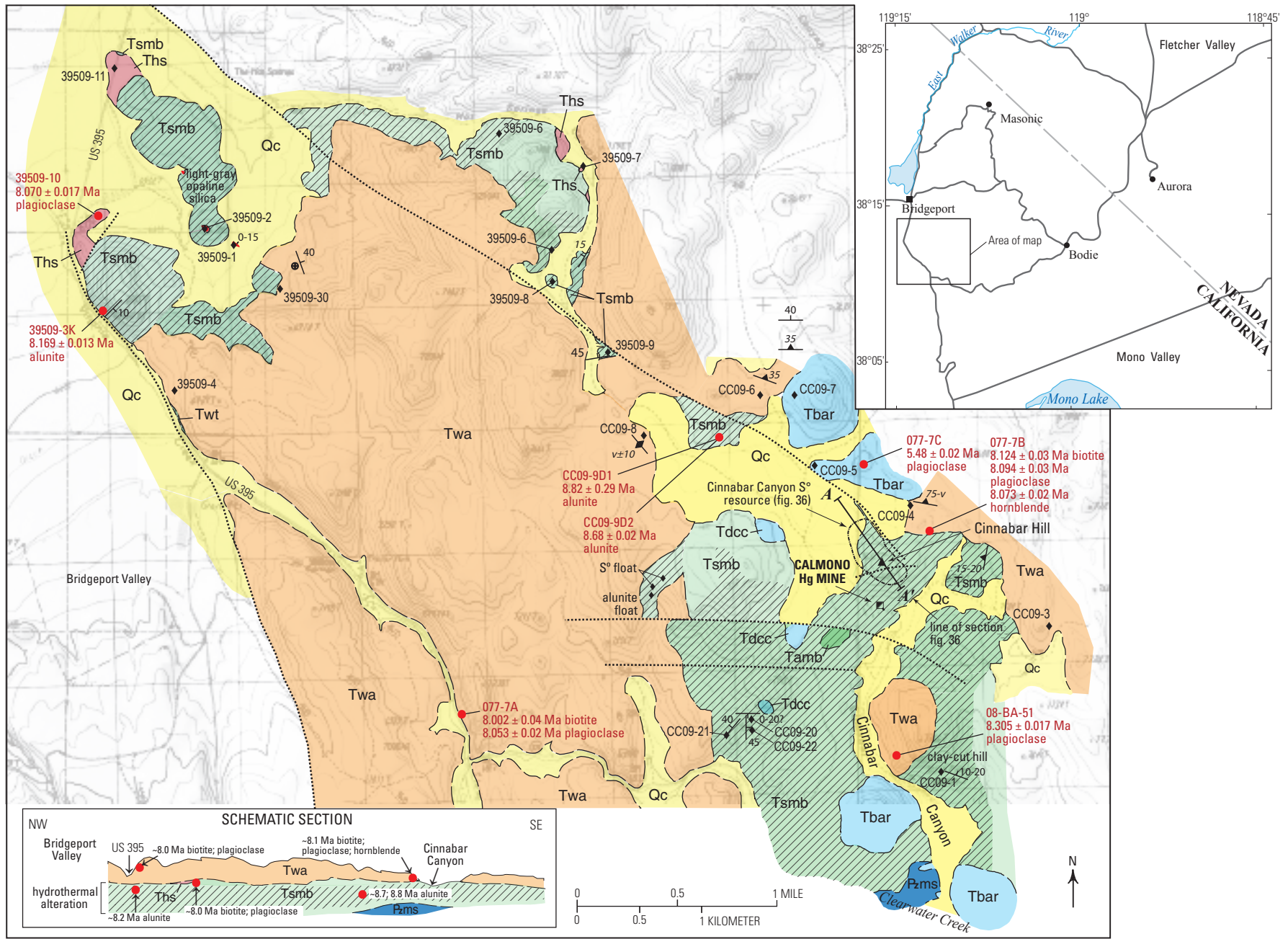
>20 weight percent sulfur. Based on IR and XRD analyses, and on petrographic examination of discarded drill core, these altered strata also contain small amounts of anatase, gypsum, barite, and cinnabar. The paragenetically late gypsum, barite, and cinnabar encrust fractures and voids that represent leached rock fragments and phenocryst sites in sequence strata. Sulfur-mineralized sequence strata grade downward into “weakly argillized” sequence strata that contain significant sulfur in several drill holes. Sulfur occurs in several forms (1) replacements of plagioclase phenocrysts and matrices of lava flows and volcanoclastic deposits, with variable amounts of quartz and pyrite, and (2) open-space filling of fractures and breccia matrices. Sulfur grades are highest in the upper and lower parts of the resource, possibly reflecting lithologic control (contrasting fluid permeability). The resource is confined on the northeast and south by faults. To the southwest and northwest, decreasing sulfur/pyrite defines a gradational limit to the resource.

## Hydrothermal Alteration

Adjacent to and distal from the sulfur resource, volcanoclastic deposits of the volcanoclastic-flow sequence have been pervasively altered to quartz, chalcedony, opaline silica, clay minerals, alunite, pyrite (iron oxides), and small amounts of sulfur (figs. 34, 35). Interbedded porphyritic flows are variably altered; thin flows are pervasively altered and thick flows are less altered. This lithologic control of fluid circulation is evident in numerous places including the area immediately south of the Calmono Hg Mine, and on the south side of the clay-cut hill where altered volcanoclastic deposits and lesser porphyritic flow rocks have been excavated for clay minerals (fig. 34). The predominant mineral in white-colored excavations on the clay-cut hill is montmorillonite, as determined by XRD.

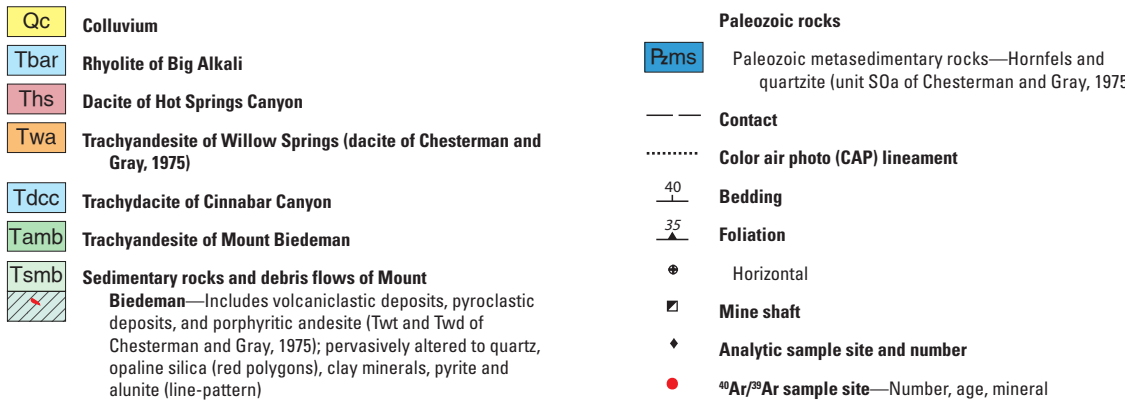
Volcanoclastic deposits on the upper part of Cinnabar Hill are white to beige where they are completely replaced by fine-grained quartz with local iron oxide minerals on fractures; millimeter to centimeter-wide voids from leached clasts and phenocrysts are common in these resistant exposures. At lower elevations on Cinnabar Hill and throughout most of the CC-395 AZ, volcanoclastic deposits are gray-green and beige to yellow-brown to red-brown, depending on proportions of clay minerals (montmorillonite, kaolinite), iron oxide minerals (limonite, hematite, jarosite), and alunite (fig. 35). On the east side of Cinnabar Canyon, east and south of Cinnabar Hill, volcanoclastic deposits locally form resistant knobs of opaline silica that also contain clay minerals and alunite.

Breccias and veins crop out at several locations northwest and west of Cinnabar Hill. Brecciated porphyritic volcanic rocks within the volcanoclastic-flow sequence (NW¼NE¼NW¼ sec. 24, and SE¼SW¼/SW¼ sec. 13, T. 4 N., R. 25 E.) consist of subrounded, centimeter-sized clasts of partly leached vuggy silica in a white matrix of fine-grained to microcrystalline quartz, alunite, and kaolinite



Base modified from U.S. Geological Survey  
Big Alkali, Calif., 1989, 1:24,000

EXPLANATION

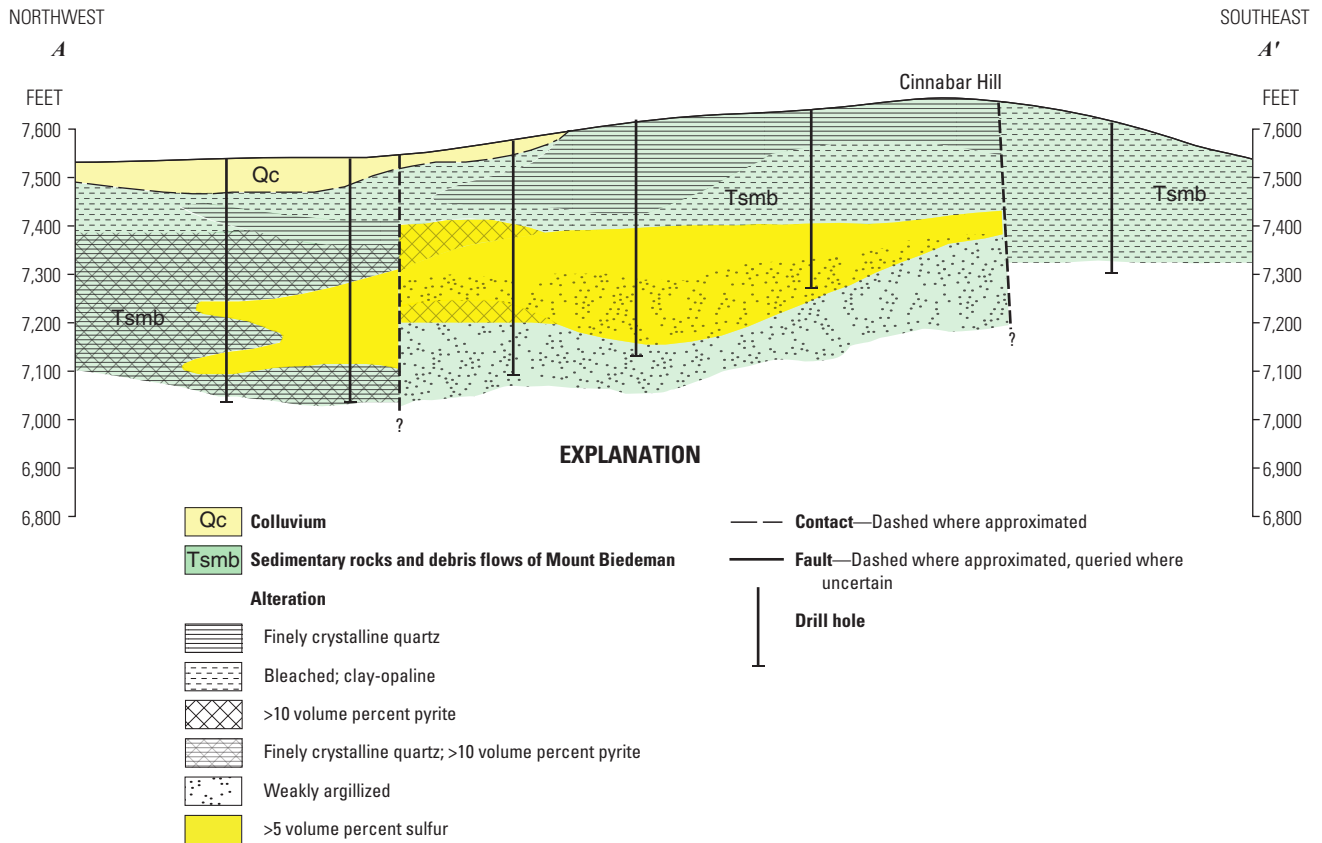


**Figure 34. (Facing page)** Geologic map and schematic stratigraphic section of the Cinnabar Canyon-US 395 alteration zone, Mono County, California, in part modified after Chesterman and Gray (1975) and John and others (2012).



**Figure 35.** Images showing volcaniclastic deposits from the Cinnabar Canyon-US 395 alteration zone. *A*, Volcaniclastic deposits on clay-cut hill, Cinnabar Canyon, altered to montmorillonite, kaolinite, and lesser illite. *B*, Sorted and bedded volcaniclastic deposits in a drainage 1 km west of Cinnabar Canyon, 0.2 km north of Clearwater Creek, altered to montmorillonite and kaolinite; beds strike N-S, dip 65°E; attitude of indistinctly bedded overlying debris flows 30 m (~100 ft) uphill is ~W-E, 0–20°S. *C*, Debris flows exposed in a layback along US 395, ~8 km (~5 mi) south of Bridgeport, California, altered mostly to alunite, kaolinite, and quartz; vertical face is ~4 m.





**Figure 36.** Cross section (northwest-southeast) through the Cinnabar Canyon elemental sulfur resource (after Ward, 1992), Cinnabar Canyon-US 395 alteration zone, Mono County, California. Location of section is shown on figure 34.

in variable proportions. Narrow veins, millimeters wide, consist of the same minerals as the breccia matrix. Similar brecciated rocks within the volcaniclastic-flow sequence in the north-south drainage, about 2 km west-southwest of Cinnabar Hill, contain small amounts of sulfur in leached clasts.

Vegetation contrasts partially delineate the alteration zone. Pervasively and intensely altered volcaniclastic deposits support piñon pine but relatively little ground cover. Ponderosa pine trees near Cinnabar Hill grow in soils derived from opaline silica-clay-alunite-altered volcaniclastic strata, but are rare elsewhere in the Bodie Hills except in the Red Wash-East Walker River alteration zone. Unaltered trachyandesite of Willow Springs that partially overlies the altered volcaniclastic-flow sequence is relatively densely covered by piñon pine.

### Minor Elements in Rocks

Thirty-eight samples of altered rocks and core scraps from the sulfur resource drill sites (table 1-10) contain variably elevated concentrations of Hg (1–337 ppm), Ag (2–20 ppm), As (92–396 ppm), Bi (~11–216 ppm), Pb (~71–7,510 ppm), Sb (~14–231 ppm), and Te (1–8.7 ppm). A few samples contain elevated Co, Ni, and Sr concentrations. The highest Au concentration is 0.084 ppm; Au concentrations in most samples are at or below the ~0.005 ppm detection limit. Barium concentrations exceed 1,000 ppm in many samples; a number of samples contain several percent S, apparently reflecting the presence of barite, alunite and other sulfate minerals, and sulfur. Elevated As, Bi, Pb, and Sb concentrations also allow for the presence of metallic sulfide minerals.

## Sulfur Isotope Compositions

Sulfur isotope ( $\delta^{34}\text{S}$ ) values of sulfur, cinnabar, and pyrite in altered sequence strata (encountered in drill holes) that contain the sulfur resource, vary from  $-5.2$  to  $-4.7$  ‰,  $-0.7$  to  $-0.2$  ‰, and  $-9.8$  to  $-8.0$  ‰, respectively (table 2; Vikre and Henry, 2011). The  $\delta^{34}\text{S}$  value of barite in drill core is 1.1 ‰. Alunite in an altered sequence sample from the drainage ~2 km west of Cinnabar Hill has a  $\delta^{34}\text{S}$  value of 2.5 ‰. These sulfur isotope compositions are difficult to interpret because of paragenetic and age differences among analyzed minerals, and possible sample impurity. Disproportionation of magmatic  $\text{SO}_2$  most likely caused alteration of sequence strata, but the  $\delta^{34}\text{S}$  values allow variable parent sulfur isotope compositions and (or) equilibrium temperatures. Further, the ~0.65 m.y. spread of  $^{40}\text{Ar}/^{39}\text{Ar}$  ages of alunite implies that several separate magmatic-hydrothermal events altered sequence strata. Interpretation of sulfur isotope chemistry requires additional, paragenetically controlled analyses of minerals throughout the CC-395 AZ.

## ASTER Imagery

ASTER imagery (Rockwell, 2010) of the CC-395 AZ shows spatial associations of alunite, kaolinite, illite, montmorillonite, and quartz. The distribution of these minerals is discontinuous because of spectral resolution, colluvium, trees, and unaltered trachyandesite of Willow Springs that cover altered sequence strata. Surficial deposits in low relief parts of the alteration zone overlie clay-alunite-altered sequence rocks; spectral reflectance of altered colluvial clasts mimics that of altered sequence rocks.

Alteration mineral abundances and associations are variable within the CC-395 AZ. Breccias and sequence strata that underlie Cinnabar Hill and the low-relief hills south of the Calmono Hg Mine and east of Cinnabar Canyon contain alunite, kaolinite, montmorillonite, and lesser illite. Alteration minerals on the east slope of Cinnabar Hill and on hills underlain by porphyritic flows west of Cinnabar Hill are mostly kaolinite and montmorillonite. Alteration minerals in the drainage parallel to and ~2 km west of Cinnabar Canyon, on the south slope of the clay-cut hill, and in volcanoclastic

strata south of this hill, are mostly kaolinite and montmorillonite with lesser illite and alunite. Cinnabar Hill, which consists of fine-grained quartz and chalcedony, and the sulfur resource to the northwest that is covered by surficial deposits, are coincident with spectral responses indicative of very sparse illite and montmorillonite. These variable alteration mineral associations, coupled with alunite ages and sulfur isotope analyses, are consistent with several alteration events in the CC-395 AZ.

## SWIR Spectra

Based on SWIR analyses, hydrous minerals in hand samples of altered volcanoclastic strata and porphyritic flows in the CC-395 AZ include montmorillonite, illite, kaolinite, alunite, and opal, supporting field observations and ASTER imagery.

## XRD Mineralogy

Two samples of core scraps from drill sites over the Cinnabar Canyon sulfur deposit consist of quartz, pyrite, sulfur, and trace amounts of anatase.

## Hydrothermal Mineral Ages

The  $^{40}\text{Ar}/^{39}\text{Ar}$  dates of alunite in the matrix of brecciated porphyritic rocks within the volcanoclastic-flow rock sequence ~1 km northwest of the sulfur resource, and of alunite in veins cutting porphyritic rocks (NW $\frac{1}{4}$ NE $\frac{1}{4}$ NW $\frac{1}{4}$  sec. 24, and SE $\frac{1}{4}$ SW $\frac{1}{4}$ SW $\frac{1}{4}$  sec. 13, T. 4 N., R. 25 E.; fig. 34), are  $8.82 \pm 0.29$  Ma and  $8.68 \pm 0.02$  Ma, respectively (fig. 34; table 1). Alunite that has partly replaced fragments in volcanoclastic strata in the US 395 layback ~8 km south of Bridgeport, California, is  $8.17 \pm 0.01$  Ma (fig. 34; table 1).

Although no sulfur isotope analyses are available, the alunite dates are consistent with stratigraphic ages (table 1), and the dated alunites are considered hypogene. The range in alunite dates indicates that sequence strata were altered two or more times. The alunite dates are broadly contemporaneous with magmatism represented by 8.6–8.0 Ma trachyandesite of Willow Springs (table 1).

## Bodie Mining District

### Location

Secs. 9, 10, 16, 17, 20, 21, 28, 29, T. 4 N., R. 27 E., Mono County, California (fig. 1)

### History and Production

The Bodie Mining District has a storied history because of very rich Au-Ag ore and a citizenry that often was indifferent to law. The district and town that provided services were named by companions of one of the discoverers, W.S. Bodey, who died in 1860, the year following discovery. A later intentional misspelling, Bodie, was permanently adopted for both.

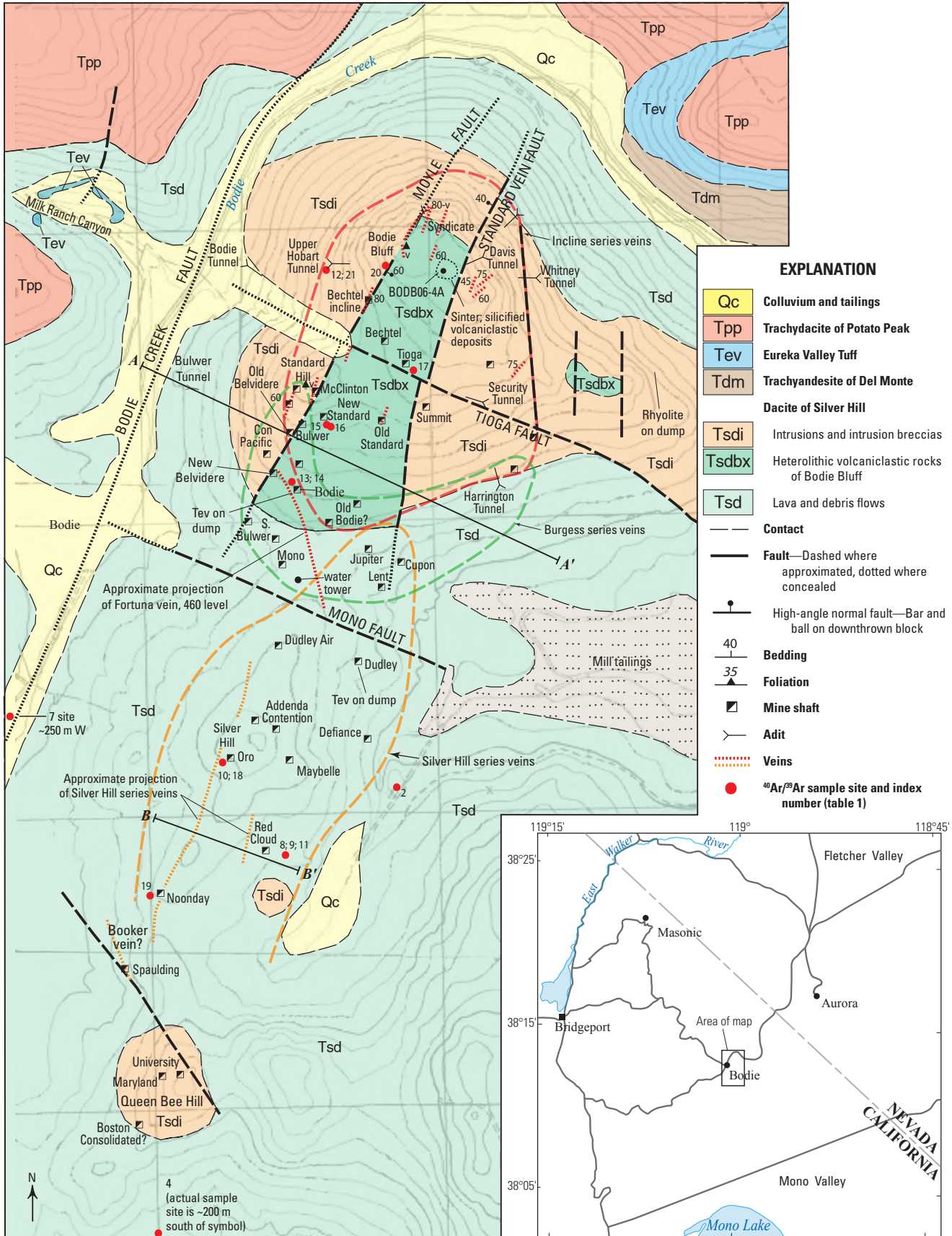
Bodie history has been recounted by Browne (1865), Wasson (1878), Burchard (1881), Wedertz (1969), and Piatt (2003). Placer Au, discovered in 1859 in the shallow drainage east of the Red Cloud Mine dump, led to the location of Au-Ag veins shortly thereafter. In the early 1860s, veins on Standard Hill (earlier named Bunker Hill and High Peak Hill) and Bodie Bluff were mined seasonally because of inaccessibility during winter, summer, and fall water shortages, and perception that the Aurora Mining District was more prospective, even though Bodie veins were extolled by mining notables B. Silliman and W.P. Blake (Wasson, 1878). The small amounts of ore produced from these veins were initially hauled kilometers west for processing in perennial Rough Creek, and some ore was processed at Aurora. The Empire (stamp) mill, constructed in 1864 at the base of the north slope of Bodie Bluff, processed ore from veins that became the Syndicate Mine, and from the Bullion née Bunker Hill vein on Standard Hill, which in 1877 was renamed the Standard vein of the Standard Mine (figs. 37, 38). In that year, 1,000 tons of Standard vein ore, processed at the Empire mill, averaged \$45 per ton (~2.3 opt Au at the prevailing price of ~\$20/oz); a subsequent lot of 10,000 tons netted \$428 per ton (~21.4 opt Au). Rapid development of the Standard and other veins ensued in late 1877, and the Standard mill was built. In 1878, the high-grade Fortuna, Burgess, and Bruce veins were discovered in the adjacent Bodie Mine. Some ores from these veins averaged \$600 per ton (~30 opt Au) and electrum clogged stamps in the Empire mill. Over the next three years, large volumes of very rich ore were produced from the Standard vein, which became the largest source of ore in the district, and from veins in the Bodie Mine. In the early 1880s the population of Bodie was an estimated 8,000.

From 1877 to 1882, numerous additional mines were developed on veins on Bodie Bluff, Silver Hill, and Queen Bee Hill, and in lower ground between these hills. Despite locally high assays and higher expectations (for example, Burchard, 1881; 1882; 1884), little to no ore was found in most mines. Insufficient milling capacity or water shortages

delayed ore processing, which led to owner impatience, investor pressure, and construction of numerous mills, most of which were idled within one year. Optimism, neighbor envy, stock manipulation, and assessments also empowered mining companies to excavate shafts and exploration crosscuts well below the water table, which was encountered at ~400–780 ft. The costs of water control and deep exploration turned most mining companies into assessment companies whose main legacies were multicompartment shafts, mammoth Comstock Lode-scale pumping and hoisting facilities, and fleeced investors. Small amounts of ore were recovered from the dewatered Fortuna vein on the 700, 800, and 1,000 levels of the Lent shaft (fig. 37), but most nonproductive mines had ceased operating by the end of 1884. The Lent and another deep water-control shaft, the Red Cloud (fig. 37), were deepened and dewatered several times during the 1880s, but little to no ore was found at depth. The virtual absence of ore ~600 ft below the surface on Bodie Bluff and Standard Hill is attributed to relatively low Au-Ag grades, narrow vein widths, and the high cost of mining in water at depth.

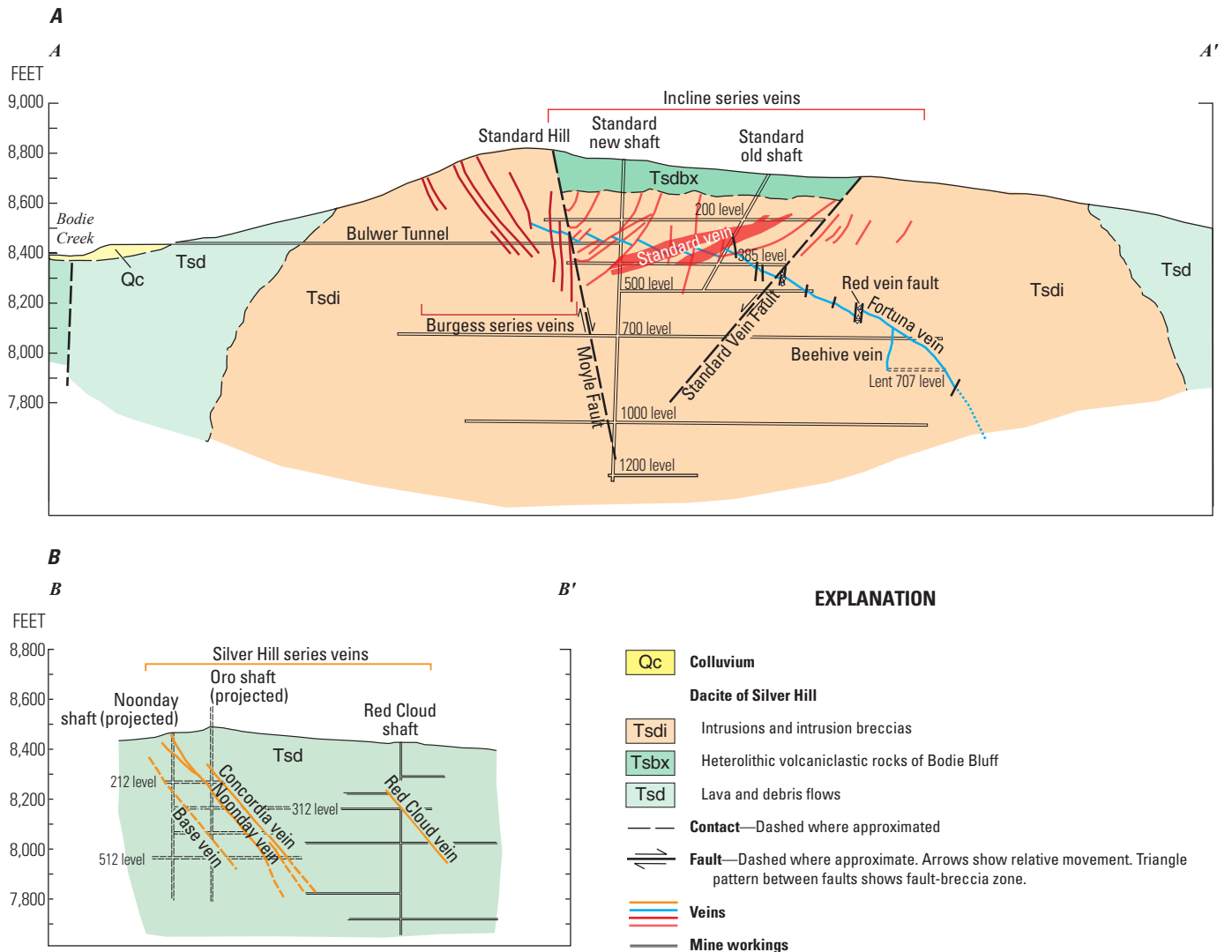
In the 1890s, mining was revived when electricity replaced wood-fueled steam power, and gravity-Washoe pan processing was converted to cyanidation. Efficiencies and lower operating costs derived from these technologies enabled profitable reworking of tailings and dumps, and production from low-grade narrow veins (1–4 inches) above the 500 level of the Standard Mine until 1913, when narrow-vein ore was depleted. After closure of the Standard Mine, cyanidation of mine waste and leasing (Eakle and McLaughlin, 1919) resulted in episodic production through the 1930s, including a short-lived attempt by the Treadwell-Yukon Company, Ltd. in 1929–32, to mill dumps and dewatered sulfide veins in the connected Red Cloud-Noonday-Oro Mines. From 1936 to 1942, the Roseklip Mining Company processed 346,000 tons of dumps from the Bulwer Tunnel (used to access the Standard Mine; fig. 37), Standard and Bodie Mine dumps, and tailings from Silver Hill mills. The company also mined ~55,000 tons of narrow veins from surface excavations in the vicinity of the Standard, Bodie, and Con Pacific shafts, and produced ~21,170 oz Au and ~562,000 oz Ag (estimated from bullion value at gold=\$35/oz, and silver=\$0.70/oz; tables 6 and 7; Chesterman and others, 1986).

Based on bullion value and weight of Au and Ag produced from 1877 to 1882, ore grades in mines on Standard Hill and Bodie Bluff varied from ~1 to several opt Au, and contained several opt Ag. During this period, parts of veins that contained less than ~1 opt Au were often not mined. Gold grades in ore produced from mines near Silver Hill were in the same range, but Ag grades were tens or more opt. However, Silver Hill vein ore was seldom defined by Ag values, in part because some to most Ag was in sulfide minerals and not economically recoverable. Most ore mined after the mid-1890s was lower grade because electrification, cyanidation, and surface mining decreased extraction and processing costs, and because high-grade ore had been depleted.



Base modified from U.S. Geological Survey Bodie, Calif., 1998, and Kirkwood Spring, Calif.-Nev. 1989, 1:24,000

**Figure 37. (Facing page)** Geologic map of the Bodie Mining District, Mono County, California, modified from Chesterman and others (1986), and John and others (2012). Cross section sections A–A' and B–B' shown in figure 38A,B, respectively.



**Figure 38.** Geologic cross sections of the Bodie Mining District. *A*, West-northwest to east-southeast cross section through the Standard Mine, modified from Chesterman and others (1986), Whiting (1888), Brown (1908), and Piatt (2003), showing distribution of Incline and Burgess series veins, and the Fortuna vein. Eureka Valley Tuff on the Bodie Mine dump (fig. 37) indicates that the stratigraphy on the west side of the section is incompletely represented. *B*, Approximately west-northwest to east-southeast cross section through the Red Cloud shaft, modified from sections in the Bodie Consolidated Mining Company Collection (2003; University of Nevada Reno, Special Collections), showing distribution of Silver Hill series veins. Mine workings, veins, and faults are approximately positioned because of inconsistencies among source sections. Section locations are shown in figure 37. Vertical and horizontal scales are equivalent. Proj., projected.

Recorded production from 1859 to 1955 is 1.456 Moz Au, and 7.280 Moz Ag recovered from 1.5 Mt of ore (Long and others, 1998). Significant amounts of ore (>10,000 oz Au) were produced from the Standard, Bodie, Noonday, and Bulwer Mines. Smaller production (tens to several thousand ounces of Au, estimated from production values in Burchard, 1881) came from the Bechtel, Red Cloud, Syndicate, Belvidere, Bodie Tunnel, and Oro Mines. The Tioga, Mono, and Lent Mines produced no or small amounts of ore despite extensive workings and large dumps. Primary functions of the Lent and Red Cloud Mines were to dewater and provide access to productive neighboring mines. Based on maps of underground workings (Chesterman and others, 1986), other sizeable mines on and near Silver Hill, including the Contention, Addenda, and Maybelle, accessed veins encountered in the Noonday and Oro Mines. No production has been verified for mines south of the Noonday Mine (fig. 37).

A resource of ~24.6 Mt @ 0.07 opt Au and 0.42 opt Ag was identified in the 1980s (Long and others, 1998) by drilling on Standard Hill and Bodie Bluff. A larger but lower grade resource estimate of 75 Mt @ 0.037 opt Au and 0.08 opt Ag is reported by Hollister and Silberman (1995a). This resource includes ~25 Mt @ 0.04–0.05 opt Au in oxidized rocks (Chesterman and others, 1986; Hollister and Silberman, 1995a) that could be mined by open pit and processed by heap leaching. These resources consist of closely spaced narrow veins, vein stockworks, and breccias between and branching from larger veins that were mined from ~1877 to 1942 (Hollister and Silberman, 1995a). In 1997, the mining claims that include the resources and nearly all old mines were added to the Bodie State Historic Park (Bodie Consolidated Mining Company Collection, 2003), which is managed by the California Department of Parks and Recreation.

## Stratigraphy

Veins are nearly entirely within dacitic to andesitic intrusions, flows, debris flows, block-and-ash flows, and other volcanoclastic deposits (Silver Hill volcanic series of Chesterman and others, 1986; dacite of Silver Hill of John and others, 2012; other stratigraphic units are described by Gumble and others, 1991); these host rocks are collectively referred to hereinafter as dacite of Silver Hill. According to Brown (1908), wall-rock fragments internal to veins that were encountered during mining include a fine-grained, coal-black lithology. These fragments are likely Eureka Valley Tuff, which comprises some of the Bodie and Dudley Mine dumps on the south slope of Standard Hill and northeast of Silver Hill, respectively (fig. 37). The 9.5–9.3 Ma Eureka Valley Tuff (John and others, 2012) on these dumps is cut by quartz-adularia veins and breccias that are ~8.9–8.1 Ma elsewhere in the district (table 1). Eureka Valley Tuff on Standard Hill and Bodie Bluff is entirely concealed by flows, debris flows, and talus adjacent to domes of dacite of Silver Hill that comprise these landforms.

Domical intrusions and associated debris flows of dacite of Silver Hill were emplaced over a short time interval, 9.1–8.9 Ma (table 1). Bodie Bluff, Standard Hill, Queen Bee Hill (fig. 37), and Sugarloaf (Sugarloaf is ~0.1 km south of fig. 37) are cored by flow-banded dacite intrusions (dacite plugs of Chesterman and others, 1986); the most productive veins occur in these intrusions on Standard Hill and Bodie Bluff. Veins on Silver Hill, and other veins between Standard Hill, Queen Bee Hill, and Silver Hill, occur in biotite-hornblende dacite flows, associated block-and-ash flows, and debris flows. Biotite-hornblende flows also are exposed on the south slopes of Bodie Bluff and Standard Hill, and south of Queen Bee Hill. In mine workings, endogenous flow-domes are reportedly as much as 700 ft thick (Chesterman and others, 1986).

The dacite of Silver Hill is medium-light-gray to light-brownish-gray, moderately porphyritic, and commonly massive but locally flow laminated. It contains 15–30 percent phenocrysts of plagioclase, hornblende, and biotite, and trace amounts of quartz and (or) sanidine in a moderately devitrified (rarely glassy) groundmass. Regionally, the dacite forms a series of lava domes that coalesce to a roughly circular area. Debris flows associated with the dacite of Silver Hill are light-gray to very pale-orange, recessive-weathering, poorly sorted, matrix-supported deposits that were shed during the lateral collapse of lava domes. Clast populations are dominated by dacite of Silver Hill blocks as much as several meters in diameter that commonly are prismatically jointed, but include clasts of older volcanic rocks of the Bodie Hills volcanic field, especially trachyandesite of Mount Biedeman. A weakly consolidated ash and clay-rich matrix is present in isolated outcrops, yielding residual surfaces strewn with large-boulder lag deposits.

Heterolithic volcanoclastic deposits on the top and south slope of Bodie Bluff are bounded to the west and east by northeast-trending, graben-forming faults, which both offset and contain mineralized veins. These deposits, as much as 60 m thick, are composed of subangular, altered clasts of dacite, mostly centimeters in dimension, and other, uncorrelated volcanic rocks in a fine-grained matrix of comminuted rock fragments and ash (figs. 37, 38). On the summit of Bodie Bluff, the deposits include a dismembered sinter terrace and local sinter fragments. Adjacent to, between, and above veins, dacite intrusions, dacite flows, and volcanoclastic deposits have been altered to zoned associations of hydrothermal minerals.

Porphyritic lavas and block-and-ash flows of trachydacite of Potato Peak (9.1 to 8.8 Ma; John and others, 2012) overlie dacite of Silver Hill to the north and west of the district. Eureka Valley Tuff is exposed ~1 km northeast of Bodie Bluff and in Milk Ranch Canyon west of Bodie Bluff where it underlies dacite of Silver Hill and trachydacite of Potato Peak (fig. 37). Based on exposures of Eureka Valley Tuff in Milk Ranch Canyon, Eureka Valley Tuff in the Bodie and Dudley Mines is ~5–8 m thick.

## Structure

In the Bodie Mining District, flows and volcanoclastic strata of dacite of Silver Hill originated from, and were domed by, three or more dacite intrusions, creating a north-northeast-trending landform that extends from Bodie Bluff south to Sugarloaf (Wisser, 1960; Chesterman and others, 1986). Tensional fissures and fan-pattern sheeting created by flexure are thought to have localized veins (Whiting, 1888; Wisser, 1960; Chesterman and others, 1986), at least on Bodie Bluff.

The landform is segmented by northeast-striking and west-northwest-striking fault sets (Whiting, 1888; McLaughlin, 1907; Brown, 1908; Chesterman and others, 1986; fig. 37). Two northeast-striking faults with opposing dips, the Moyle and Standard vein faults, define the graben on Bodie Bluff. The graben contains volcanoclastic deposits that cover much of the summit and south slope of Bodie Bluff. The normal Moyle Fault strikes N38°E, dips 60–70°SE, is 0.6 m wide according to Chesterman and others (1986), and had combined pre and postmineralization displacement of at least 60 m based on the thickness of volcanoclastic deposits in the graben. According to Brown (1908), the Moyle Fault is 10–40 ft wide and is represented on the surface by a northeast-striking, 3–4.5 m high scarp west of the Standard Mine shaft. The Standard Vein Fault strikes ~N10–20°E, dips 60–70°NW, and apparently had pre and postmineralization displacement similar to the Moyle Fault (Chesterman and others, 1986). These synmineral faults contain and displace mineralized veins; they also offset sinter in volcanoclastic deposits and veins in the subsurface from adjacent veins in dacite of Silver Hill (figs. 37, 38). Atop Bodie Bluff, volcanoclastic deposits include a small, dismembered sinter terrace, small pool sinters, and angular clasts of sinter (fig. 39G). These structural and stratigraphic relationships attest to at least two periods of vein and sinter deposition, and demonstrate that volcanoclastic deposits on Bodie Bluff accumulated during hydrothermal events.

The west-northwest-striking, near-vertical Tioga and Mono Faults, on and south of Bodie Bluff, respectively, are also marked by topographic depressions. Normal, down-to-the-south displacement of as much as 150 m along the Tioga Fault occurred prior to mineralization (Chesterman and others, 1986). Along the Mono Fault, flows and volcanoclastic deposits of dacite of Silver Hill have been displaced 150 m right-laterally and down-to-the-south. The Mono Fault is ~30 m wide and altered to montmorillonite near the Bodie State Park water tower (Chesterman and others, 1986). Distribution of altered rocks and absence of the Fortuna and other veins on Standard Hill and Bodie Bluff south of the Mono Fault, suggested to Chesterman and others (1986) that displacement on the Mono Fault predates mineralization. However, temporal relationships among vein types and associated wall-rock alteration, do not clearly constrain timing and magnitude of fault displacements. Other unnamed faults, including a northwest-striking, 60°E-dipping, premineralization fault that extends from Queen Bee Hill to the Spaulding Mine, offset stratigraphy of dacite of Silver Hill (Chesterman and others, 1986).

North-northeast-trending normal faults, one of which projects through the Bodie town site (Bodie Creek Fault, fig. 37), may offset trachydacite of Potato Peak and Eureka Valley Tuff from dacite of Silver Hill. Although the elevations of Eureka Valley Tuff in the Bodie and Dudley Mines, and of possible Eureka Valley Tuff fragments in veins (Brown, 1908), are unknown, Eureka Valley Tuff encountered underground is apparently above 8,200 ft, the lowest elevation of stoping in nearly all mines. Displacement of Eureka Valley Tuff in mines relative to Eureka Valley Tuff in Milk Ranch Canyon at 8,500–8,400 ft cannot be verified, but is probably not more than tens of meters.

## Forms of Silver-Gold Deposits

All precious metal production was derived from veins, vein stockworks, and fault breccias that were mined underground prior to ~1936, and from small open cuts in the late 1930s and early 1940s. Different vein types were initially recognized by Whiting (1888), and further characterized by Brown (1908), Chesterman and others (1986), and Hollister and Silberman (1995b). Three vein types, distinguished by mineralogy, textures, Au/Ag, distribution, and to an extent, age, have been termed the Incline, Burgess, and Silver Hill series veins (figs. 37, 38). Brown (1908) classified a fourth vein type, based in part on attitudes and relative ages, that is represented by the Fortuna vein, although differences between Burgess series veins and the Fortuna vein, based on mine dump and archival specimens, are not straightforward. Incline series veins are prominently exposed on Bodie Bluff and Standard Hill, whereas Silver Hill series veins, which mostly occur south of the Mono Fault, rarely crop out. Some Incline and Burgess series veins are exposed in stopes, and in (1930s) open cuts on the south slope of Standard Hill. However, most Burgess veins and the Fortuna vein were encountered underground and do not crop out, or are covered by detritus and mine waste. Characteristics of these four vein types, synthesized from incomplete exposure, dump samples, archival specimens, adularia ages (table 1), and published descriptions, reveal marked to subtle differences among the vein types, summarized in table 4.

A small group of veins in the vicinity of Queen Bee Hill (fig. 37) was extensively developed, produced little to no ore, and appears to be entirely oxidized by weathering. The relationship, other than spatial, of these veins to other vein types is incompletely known, and published descriptions are limited; dump samples provide some vein characteristics that are briefly described.

Based on textures of mineral assemblages, adularia dates, sulfur isotope compositions, and the absence of copper and other oxide minerals, the sulfide, selenide, telluride, and silicate minerals, and electrum, described below and imaged, are nearly entirely hypogene. Iron oxide minerals that marginally replace pyrite are interpreted to have formed during weathering, and mineral assemblages in veins that formed during weathering are not described.

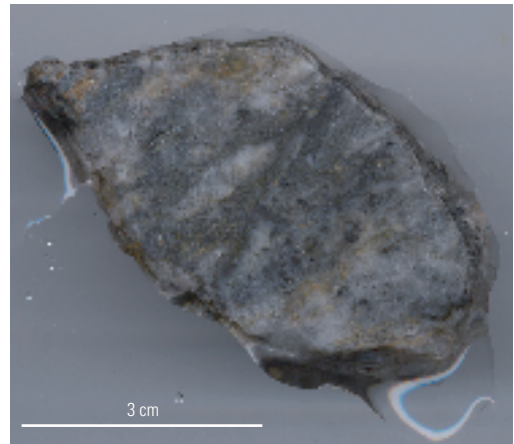
A. Bodie Tunnel Dump



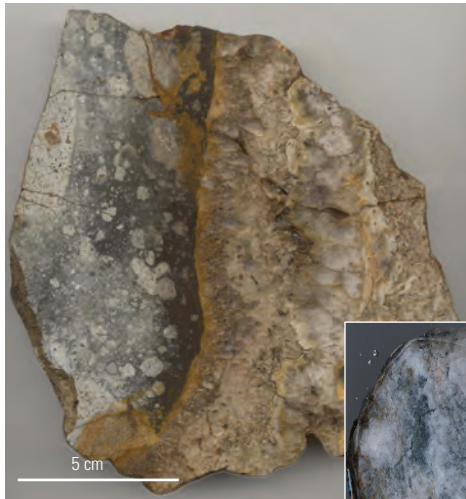
Standard Mine



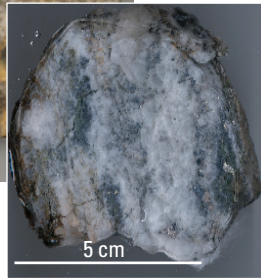
B. Belvedere Mine



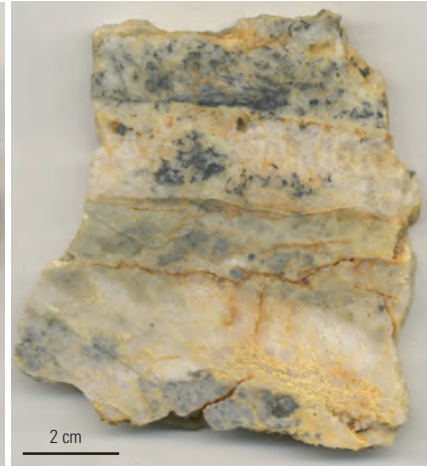
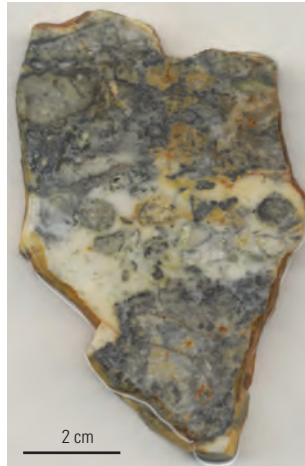
C. Fortuna Vein, Standard Mine



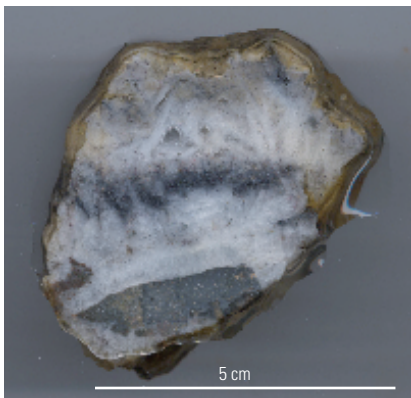
Fortuna vein,  
Mono Mine



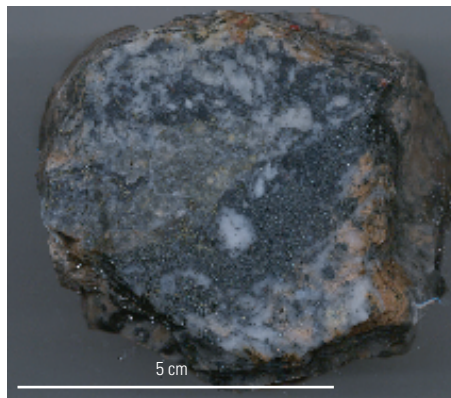
D. Red Cloud Mine



E. Oro Mine, 520 level



F. Addenda Mine, 560 level



G. Sinter clast in volcaniclastic deposits, Bodie Bluff





**Figure 39. (Facing page)** Images of veins in the Bodie Mining District. *A*, Incline series veins, Bodie Tunnel dump, and Standard Mine (inset image; California State Mining and Mineral Museum collection specimen 660). *B*, Burgess series vein, Belvidere Mine (California State Mining and Mineral Museum collection specimen 7638). *C*, Fortuna vein, Standard Mine, 528 level (Mackay-Stanford collection specimen OD 7604) and Mono Mine (inset image; California State Mining and Mineral Museum collection specimen 7045). *D*, Silver Hill series veins, Red Cloud Mine dump, east of Silver Hill. *E*, Silver Hill series vein (Oro vein), Oro Mine, 520 level (California State Mining and Mineral Museum collection specimen 5304). *F*, Silver Hill series vein (Oro vein), Addenda Mine, 560 level (California State Mining and Mineral Museum collection specimen 2009). *G*, Sinter fragments in volcanoclastic deposits, Bodie Bluff summit. Mine locations and veins shown on figures 37 and 38.

**Table 4.** Characteristics of Incline, Burgess, and Silver Hill series veins in the Bodie Mining District. Distribution of vein series is shown on figures 37 and 38.

[Ag, silver; Au, gold; As, arsenic; Cu, copper; Fe, iron; S, sulfur; Sb, antimony; Se, selenium; Sn, tin; Te, tellurium; FeOx, iron oxides; wt, weight; v, vertical]

Vein series	Distribution	Attitude; width	Au/Ag (wt)	Textures and minerals	Wall-rock alteration	Age (Ma)
Incline	Bodie Bluff; Standard Hill; Noonday Mine	Mostly N–N20±5°E, v–40°W and E; mostly ≤1.2 m	≥0.4	Tens to hundreds of ≤1 mm-thick, planar to slightly undulating layers of fine-grained quartz, lesser adularia, and less than 1 percent electrum, acanthite, and other sulfide minerals; minor paragenetically late calcite (mostly quartz perimorphs)	9,000–8,600 ft: centimeters-thick selvages of quartz, K-feldspar, illite, minor pyrite (FeOx); distal illite, chlorite, montmorillonite, calcite	~8.3–8.1
Burgess	South slope of Standard Hill and Bodie Bluff below 8,700 ft elevation and north of Mono Fault	N25°E, v–70°E; ~4–0.1 m	>0.5(?)	Pronounced to indistinct, several to tens of submillimeter to centimeter-thick layers of quartz, adularia (often quartz perimorphs), and lesser calcite (mostly quartz perimorphs), and as much as several percent electrum, sphalerite, galena, and Ag-Au-Cu-As-S-Se phases mostly in quartz layers; some layers consist of millimeter to centimeter euhedrons/subhedrons of quartz, adularia, and calcite (quartz perimorphs)	8,700–8,400 ft: centimeters-thick selvages of K-feldspar, quartz, clinochlore, pyrite (FeOx); distal illite, chlorite, montmorillonite, calcite	8.5–8.4
Silver Hill	Vicinity of Silver Hill; north to Bodie Bluff below ~8,500 ft; south to Queen Bee Hill	Mostly N–N20°E, ~50°E; <2 m	≤0.04	Fault breccia fragments replaced by quartz and minor sulfide minerals, and cemented by fine-grained to vuggy quartz, adularia, several to greater than 10 percent opaque minerals, clay minerals, barite, and calcite; opaque minerals include electrum, sphalerite, galena, pyrite, acanthite, tetrahedrite, chalcocopyrite, bornite, hessite, and numerous Ag-Au-Sb-As-S-Te-Se and Cu-Fe-Sn-S-Ag-As phases	8,500–8,400 ft: meters-thick selvages of quartz, illite, kaolinite, montmorillonite, pyrite	8.9–8.5

## Incline Series Veins

Incline series veins include the main Standard vein, the most productive vein in the district, and other productive veins in the Standard, Bodie, Bulwer, Bechtel, and Syndicate Mines on Standard Hill and Bodie Bluff (Whiting, 1888; Brown, 1908; figs. 37, 38). Based on vein texture, Au/Ag, adularia dates, and mineralogy, some veins on the Noonday and Oro Mine dumps south of Silver Hill are similar to Incline series veins. However, Silver Hill series veins were also developed in the Noonday Mine, and variable Au/Ag (weight; table 5A) may reflect mining economics and different vein types. From 1877 to 1881, ore was produced from several tens of individual Incline series veins, or segments thereof. By 1908, more than 100 narrow and low-grade veins had been identified between wider, stoped veins (Brown, 1908); some of these veins were mined prior to closure of the Standard Mine in 1913. On Standard Hill and Bodie Bluff, Incline series veins are distributed from the Moyle Fault, where they occur only in the hanging wall, to east of the Standard vein Fault, whereas spatially associated but older Burgess series veins are largely confined to the footwall of the Moyle Fault in Standard Hill according to Brown (1908; fig. 38). Incline series veins apparently accounted for most district Au and Ag production, although Burgess series veins were also highly productive. Ore produced simultaneously from both vein series in mines on Standard Hill was not recorded separately.

Incline series veins predominantly strike  $N20\pm 5^\circ E$ , most are vertical or dip steeply east and southeast on the west side of Bodie Bluff and on Standard Hill, and most dip steeply to moderately ( $85\text{--}40^\circ$ ) west and northwest on the east side of Bodie Bluff (figs. 37, 38; table 6). The Standard vein on the section in Chesterman and others (1986) dips  $\sim 20^\circ W$ ; other sources assign dips of  $\sim 40\text{--}80^\circ W$ , and the vein as portrayed (fig. 38) may consist of closely spaced, more steeply dipping vein segments. In the early years of mining, these inwardly opposing dips engendered the concept of a central Veta Madre (Mother Vein; promoted by B. Silliman and W.P. Blake), the mythical large vein at depth from which narrower, nearer-surface veins branch. A Veta Madre was never found but became a rationale for deep exploration.

The Standard vein and other high-grade Incline and Burgess series veins stoped in the Standard and adjacent mines extend for as much as 900 m along strike, but were mined no deeper than  $\sim 150$  m below the surface (90 m in the Bodie Mine). Incline series veins that were mined during the most productive period, 1877–81, varied in width from  $<1$  to 27 m (McLaughlin, 1907; Brown, 1908; figs. 37, 38; table 5). Multiple closely spaced veins, and brecciated and mineralized wall rock on both sides of some veins, or segments thereof, often enabled mining (Whiting, 1888). Two or more parallel to subparallel veins as much as 1 m wide and separated by centimeter- to meter-thick wall-rock septa are commonly exposed in shaft collars and stopes. “Enrichers” or small veins that crossed thicker veins or branched into the footwall and contained high-grade Au, also enhanced minability; however,

enrichers generally followed larger veins, were not spatially associated with intramineralization faults, and may represent a younger vein series. Based on surface stopes and mine dumps, Incline series veins in dacite of Silver Hill on Bodie Bluff and Standard Hill are competent with sharp, planar, and often unshaped wall-rock contacts. Mining of these veins required little timbering, except where veins and vein sets exceeded several meters in width (for example, the Standard vein).

South of the Standard Mine, Incline series veins were stoped in the Bodie Mine, but farther south on Standard Hill, and at depths below  $\sim 150$  meters, veins narrowed to unmineable low-grade or unmineralized fissures and seams. Productive Incline series veins also declined in width and grade north and northeast of the Standard Mine where they were stoped in the Bechtel, Upper Hobart, Syndicate, and other mines near the summit and on the north and northwest slopes of Bodie Bluff (fig. 37). Combined production of these mines was small (several tens of thousands of ounces of Au).

Many Incline series veins on Bodie Bluff and Standard Hill were covered by colluvium. Other veins represented by thin seams at the surface were identified first by subsurface mining. Upward stoping of Incline series veins terminated at the contact of dacite and volcanoclastic deposits because relatively wide veins in dacite below the contact branched into unmineable, thin veins and seams in volcanoclastic deposits, or could not be followed into volcanoclastic deposits (Whiting, 1888; fig. 38). The stratigraphic control of hydrothermal mineral assemblages by physical properties of host rocks has been documented elsewhere in the Great Basin (for example, Vikre, 2007; Vikre and Henry, 2011). The restricted vertical interval of ore in Incline series veins, and smaller grain size of quartz in veins on the summit of Bodie Bluff relative to grain size of quartz in veins encountered in the Bodie and Bulwer Tunnels  $\sim 180$  m deeper (fig. 38), are cited as evidence for vertical zonation of vein mineral assemblages (Silberman and Chesterman, 1991; Wisser, 1960; Gumble and others, 1991).

Incline series veins are composed predominantly of fine-grained quartz, variable amounts of adularia, and minor metallic minerals (mostly  $<1$  volume percent) in planar to slightly undulating layers (millimeters wide) that parallel wall-rock contacts (fig. 39A). Narrow veins (millimeters to a few centimeters wide) consist of several parallel and symmetrical layers, whereas wider veins consist of tens to  $>100$  layers; the frequency of layers containing metallic minerals determined minability of veins. Central quartz layers in some veins enclose lenticular vugs lined with quartz pseudomorphs and perimorphs that replace or encrust bladed calcite. Less commonly, central layers (millimeters to centimeters thick) consist of relatively coarse-grained calcite that locally constitutes several to tens of volume percent of veins. These calcite layers are mostly, if not entirely, paragenetically later than quartz ( $\pm$ adularia  $\pm$ sulfide mineral) layers.

Metallic minerals include electrum, acanthite, and other sulfide minerals; iron and manganese oxides in weathered veins mark sites of sulfide minerals and attest to former calcite. Anhydrous electrum and sulfide minerals occur in

**Table 5.** Gold and silver production and precious metal grades for mines and veins in the Bodie Mining District from 1875 to 1942, and relative value of gold and silver in bullion from 1878 to 1881.

[Gold and silver production and precious metal grades converted, in part, from gold and silver bullion values using \$20.67/oz gold (Au) and \$1.29/oz silver (Ag) (average or single assay values from Addenda, Jupiter and Noonday Mines; Burchard, 1882; 1884; Whiting, 1888; Eakle and McLaughlin, 1919; Chesterman and others, 1986; University of Nevada Reno library special collections NC323). Some vein type assignments are based on mine location and dump/archival vein sample characteristics. Relative value of gold and silver in bullion, 1878–1881 is as reported in Burchard (1881) and King and others (1885). Au, gold; Ag, silver; e, estimated; oz, ounce]

Gold and silver production and precious metal grades from 1875 to 1942				
Period/ year	Mine, vein	Au	Ag	Au/Ag
Incline series veins				
1875–76	Syndicate Mine	1,788 oz	4,332 oz	0.41
1879	Noonday Mine, Keystone vein	543 oz	1,349 oz	0.40
1883	Syndicate Mine	4,143 oz	4,940 oz	0.84
1883	Standard main vein	49,100 oz	258,937 oz	0.45
1883	Standard main vein	1.65 oz/ton	3.14 oz/ton	0.53
1900	Standard Mine, above 500 level	e20,160 oz	e28,160 oz	0.72
1912	Standard Mine	5.43 oz/ton	0.35 oz/ton	15.5
Burgess series veins				
1879	Bulwer Mine	737 oz	1,089 oz	0.68
1879	Bodie Mine	656 oz	1,269	0.52
1936–42	Roseclip cuts, tailings and dumps	21,171 oz	561,904 oz	0.04
Fortuna vein				
1883	Bodie Mine, Fortuna vein	5,085 oz	109,800 oz	0.05
Silver Hill series veins				
1881	Noonday Mine, Concordia vein	2.3 oz/ton	361 oz/ton	0.006
1881	Noonday Mine, Concordia vein	6 oz/ton	53 oz/ton	0.11
1881	Red Cloud Mine, Concordia vein	13.5 oz/ton	2,679 oz/ton	0.005
1881	Red Cloud Mine, Red Cloud vein	1 oz/ton	32.3 oz/ton	0.03
1881	Addenda Mine	5.4 oz/ton	130 oz/ton	0.04
1881	Jupiter Mine	7.25 oz/ton	3,333 oz/ton	0.002
Relative value of gold and silver in bullion from 1878 to 1881				
Year	Mine, vein	Au %	Ag %	Au/Ag
Incline and Burgess series veins				
1878	Standard main vein	92.3	7.5	12.3
1879	Standard	92	8	11.5
1880	Standard	93	7	13.3
1879	Syndicate	93	7	13.3
1880	Syndicate	93	7	13.3
Burgess series veins				
1879	Bulwer	92	8	11.5
1880	Bulwer	93	7	13.3
1880	Belvidere	37?	63?	0.59?
Fortuna vein				
1879	Bodie	85	15	5.7
1880	Bodie	59.5	41.5 [sic]	1.4
Silver Hill series veins				
1879	Noonday	70	30	2.3
1880	North Noonday	41	59	0.6
Queen Bee Hill veins				
1881	Boston Consolidated	75	25	3

**Table 6.** Vein attitudes and widths derived from surface mapping and published descriptions.

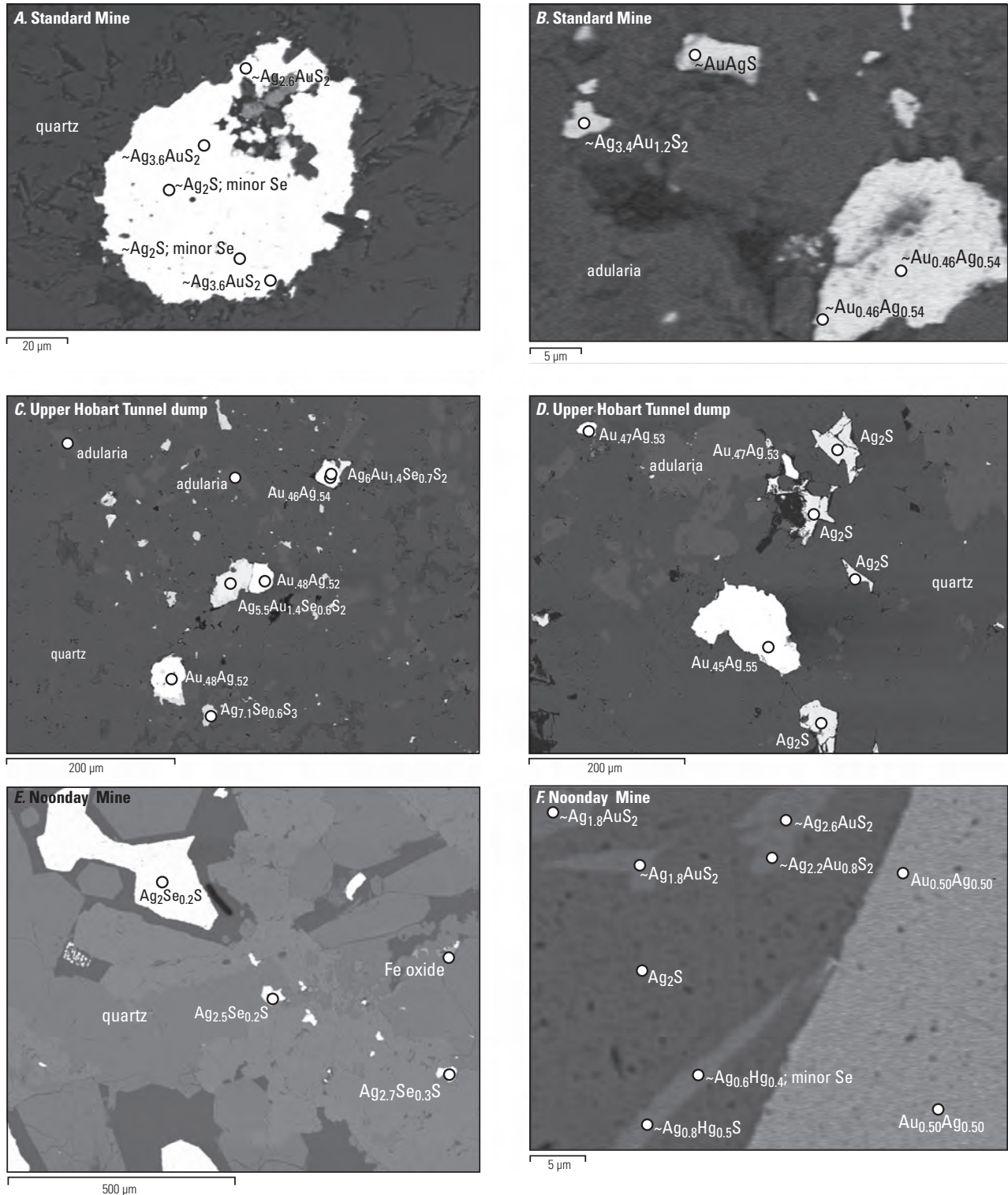
[Burchard, 1881, 1882, 1884; Whiting, 1888; Brown, 1908; Wedertz, 1969; Chesterman and others, 1986; Piatt, 2003). Some veins are shown on figures 37 and 38. ave., average; ft, feet; v, vertical; —, no data; <, less than]

Mine	Vein	Level	Strike (°)	Dip (°)	Width (ft)
<b>Incline series veins</b>					
Standard	Main vein	Surface	N20E±5	60W	4
		200	—	78W	15–25
		385	—	40W	<90
		—	—	—	ave. 20
		700	—	—	8
North Standard	—	—	—	—	3.5–6
Bechtel	—	440	—	—	3–5
		512	—	steep W	3–12
Bodie Tunnel	—	—	—	—	6
<b>Burgess series veins</b>					
Bodie	Burgess; Bruce	—	N25E	75–85E; v	—
Belvedere	—	600	—	—	14
Con Pacific	—	400	—	—	5
Bulwer	Ralston; Stonewall	400	—	—	2–4
South Bulwer	—	550	—	steep E–v.	6
<b>Fortuna vein</b>					
Bodie	Fortuna	300	N10–20W	20–30E	0.2–12
		600	—	45E	ave. 20
<b>Silver Hill series veins</b>					
Jupiter	—	500	—	—	2
Goodshaw	—	600	—	—	4
Red Cloud	Red Cloud; Packard & Morton	—	N20E	steep E	—
		400	—	—	2–10
		600	—	—	6
Noonday	Keystone	—	N10–40E	80E	2–5
		—	—	—	5–20
Addenda/Contention	—	500	—	—	7–8
<b>Queen Bee Hill veins</b>					
Boston Consolidated	—	200	—	—	2–5
		400	—	—	2–4
University	—	382	—	—	2–22
Champion	—	400	—	—	ave. 5

discrete crystals and in submillimeter aggregates that appear to be texturally coeval with quartz. In low-grade samples of multilayer veins, these crystals and aggregates form small dark specks that are sparsely distributed in one or a few layers of fine-grained white quartz. In samples with elevated Au and Ag grades, larger clots (millimeters to centimeters in size) and small dendrites of electrum and sulfide minerals accentuate quartz layers (fig. 39A, inset image). Metallic minerals identified and semiquantified by optical and scanning electron microscopy include electrum with subequal proportions of Au and Ag, Ag-Au-S-Se minerals (including possible uytendogaardtite, Ag<sub>3</sub>AuSSe<sub>2</sub>, and AuAgS (Barton and others, 1978; Barton, 1980), acanthite with minor Se, and chalcopyrite (fig. 40). A few bulk vein samples contain

elevated concentrations of As and Sb (table 1-11), suggesting the local presence of Ag-As-Sb-S minerals. Vein minerals, including molybdenite and scheelite, previously identified on mine dumps on Bodie Bluff and Standard Hill (Hollister and Silberman, 1995a; 1995b), were not found during this investigation.

Gold/silver by weight and value in Incline (and Burgess) series veins are relatively high ( $\geq 0.40$  and  $>11$ , respectively) compared to Silver Hill series veins and the Fortuna vein (mostly  $<0.1$  and  $<6$ , respectively; table 5). The Au and Ag contents of veins correspond spatially to associated placer deposits in that high Au/Ag placers were mined on the slopes of Bodie Bluff and Standard Hill, whereas low Au/Ag placers were recovered from Silver Hill slopes (Whiting, 1888).



**Figure 40.** Secondary and backscatter electron images of samples representative of Incline series veins on Bodie Bluff, and of vein samples from the Nooday Mine near Silver Hill, Bodie Mining District. Mineral identifications and approximate atomic proportions for these images, and for images in figures 41, 42, 43, 44, and 45, were determined petrographically and by scanning electron microscopy algorithms. *A* and *B* correspond to specimen CSMMM-660, Standard Mine (California State Mining and Mineral Museum collection; fig. 38). *C* and *D* correspond to sample 11-BA-26B, Upper Hobart Tunnel dump (fig. 37). *E* and *F* correspond to specimens 5074 and KM-952, respectively, Nooday Mine (Keck museum collection, University of Nevada, Reno; fig. 37). Imaged phases include quartz, adularia, acanthite (some with minor Se), electrum with subequal Au and Ag, Ag-Au-S minerals (~Ag<sub>3</sub>AuS<sub>2</sub>, possibly uytenbogaardite; ~AuAgS; ~Ag<sub>2</sub>AuS<sub>2</sub>), Ag-S-Se minerals (~Ag<sub>7.1</sub>Se<sub>0.6</sub>S<sub>3</sub>; ~Ag<sub>2.5</sub>Se<sub>0.2</sub>S; ~Ag<sub>2.7</sub>Se<sub>0.3</sub>S), and Ag-Hg-S-Se minerals. Mine locations are shown on figure 37.

Incline series veins are, in part, parallel to northeast-striking tabular breccias that offset the Fortuna vein and may constitute intrusive breccias or decomposed dikes (Whiting, 1888; Brown, 1908; Gumble and others, 1991; for example, Red vein Fault, also known as “Red ledge”, or “Red vein” fig. 38). These high-angle, meter-wide, iron oxide-rich breccias, encountered in the Standard, Bodie, Bulwer, and other mines on Standard Hill and Bodie Bluff, may be coeval with overlying volcanoclastic deposits. Based on composition (Turner, 1908), the Red ledge/vein could be altered rhyolite in which  $K_2O$  has been added (potassic alteration) and  $CaO$  and  $Na_2O$  were reduced by hydrolysis of plagioclase. Spatial relationships among breccias encountered underground and potassically altered breccias that cut dacite, described by Silberman and Berger (1985), Silberman and Chesterman (1991), Gumble and others (1991), and Herrera and others (1993), are uncertain. These latter breccias consist of rock fragments partially replaced by K-feldspar, and matrices composed of quartz, adularia, and hematite. Matrices of other breccias at higher elevations consist of quartz, adularia, illite, calcite, and zeolites. Some of these breccias are parallel and adjacent to veins, and locally include mineralized quartz-adularia vein clasts (Silberman and Berger, 1985; Silberman and Chesterman, 1991; Gumble and others, 1991; Herrera and others, 1993); however, paragenetic relationships among these breccias and specific vein series are also uncertain.

## Burgess Series Veins

Burgess series veins, based on underground exposures, were originally thought to exist exclusively on the south and west slopes of Standard Hill west of the Moyle Fault (Brown, 1908; Chesterman and others, 1986). However, samples of veins similar to Burgess series veins occur on mine dumps on the south slope of Bodie Bluff north of the Mono Fault, suggesting wider distribution (figs. 37, 38). Burgess series veins were stoped in the Standard, Bodie, Belvidere, Con Pacific, Bulwer, and other mines where they are cut by Incline series veins. Burgess series veins (individually named Bruce, Burgess, Incline, Gildea, Bullion, Ralston, and Cook) strike  $N25^\circ E$ , dip steeply southeast or are vertical, and extend as much as 900 m along strike, although profitable segments had strike lengths of 180 m or less (Brown, 1908). They were stoped no deeper than ~180 m below the summit of Standard Hill (fig. 38). Burgess series veins exposed in the open cut on the south slope of Standard Hill are mostly centimeters wide, and many veins contained sufficient Au to be mineable at widths of ~2 cm. Gold in some veins occurred in “hard quartz” cohesive with wall rock, or in shaley clay-sand partings (Whiting, 1888; Brown, 1908), increasing ore widths as much as ~4.2 m (table 6).

Most Burgess series veins consist of relatively coarse-grained quartz and adularia (compared to Incline series vein minerals) in indistinct or pronounced layers that parallel wall-rock contacts and that may be defined by thin seams and septa (<1 mm) of micaceous minerals (fig. 39B). Some

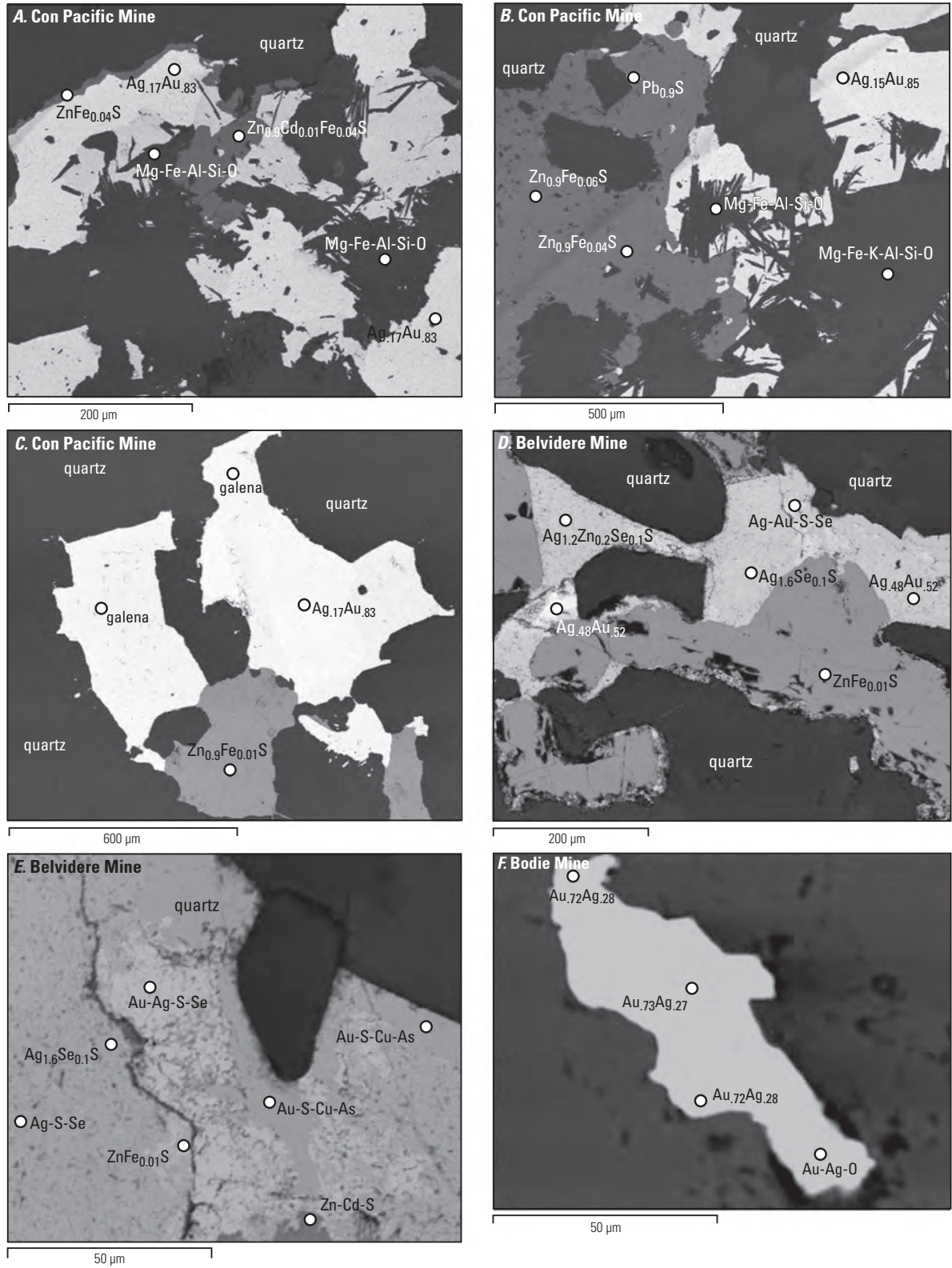
layers contain as much as several volume percent of relatively coarse-grained metallic minerals and “axial comb-textured” quartz layers (Brown, 1908; Chesterman and others, 1986). Vein interstices of dump samples on upper elevations of Standard Hill are commonly vuggy, and some are encrusted by quartz and (or) euhedral adularia crystals with dimensions of as much as several centimeters. These euhedral crystals further distinguish Burgess series veins from Incline and Silver Hill series veins.

Vein minerals identified and semiquantified optically and by SEM include quartz, adularia, an euhedral to subhedral Mg-Fe-Al-Si-O mineral (possibly clinocllore), Au-rich electrum, low Fe- and low-Cd sphalerite, and galena—all of which are intergrown in apparent textural equilibrium (fig. 41A, B, C). Other metallic minerals, some in submicrometer mineral aggregates, include electrum with subequal proportions of Au and Ag, acanthite with minor Se and Zn, and mixed Ag-Au-S-Se and Au-S-Cu-As phases (fig. 41D, E, F). A few bulk vein samples contain elevated abundances of As, Sb, and other elements (table 1-11), suggesting the local presence of Ag-As-Sb-S and other minerals.

The Fortuna vein, which was the source of most production from the Bodie Mine and likely the only source of production from the Mono Mine, is not exposed at the surface. In mine workings it is cut by numerous faults (described in previous section “Incline Series Veins”) and by Incline and Burgess series veins (fig. 38). The Fortuna vein strikes  $N10-20^\circ W$ , dips  $20-30^\circ NE$  on the 300 level of the Bodie Mine, and  $\sim 45^\circ NE$  on the 600 level (table 6). It varies in width from centimeters to ~6 m, as brecciated and mineralized wall rocks often enabled thin vein segments to be mined. It was stoped for as much as ~110 m along strike and ~300 m downdip, but below the 600 level it was mostly unmineable. On the 600 level of the Bodie Mine, the centimeter-wide, Ag-rich Beehive vein splits from the Fortuna vein (fig. 38). The Beehive vein was mined for ~45 vertical meters, and apparently is the deepest stoped vein in the northern part of the district. About 230 m below the surface, the Beehive vein narrowed to seams and thin veins of weakly mineralized quartz enclosed by wall rocks more decomposed than at higher levels (Brown, 1908).

To the southeast, the Fortuna vein was intersected on the 1000 level of the Standard Mine, and in the Lent (707 and 1200 levels) and Dudley Mines (figs. 37, 38). Deep vein segments consisted of isolated bunches and narrow veins of quartz in sheeted zones of clay-altered, pyritic wall rocks (Brown, 1908). Although Au-Ag minerals and relatively abundant sphalerite were encountered locally, few of the deep segments contained sufficient Au and Ag to warrant mining. Wall rocks of the Fortuna vein are described as pyritic and “much decomposed” compared to wall rocks adjacent to Incline series veins (Brown, 1908).

Archival specimens of the Fortuna vein from the Standard and Mono Mines (fig. 39C) include two texturally distinct zones. A 5-cm-wide zone in the Standard Mine specimen consists of wall-rock fragments (centimeters to millimeters in size) cemented by very fine-grained adularia,



**Figure 41.** Secondary electron images of samples representative of Burgess series veins on Standard Hill, Bodie Mining District. *A*, *B*, and *C* correspond to specimen 4260, Con Pacific Mine (Keck museum collection, University of Nevada, Reno). *D* and *E* correspond to sample BOD11-4A, Belvidere Mine dump. *F* corresponds to sample BOD11-13, Bodie Mine dump. Imaged phases include quartz, electrum with variable Au and Ag, sphalerite with minor Fe and Cd, a Mg-Fe-Al-Si-O mineral (possibly clinocllore), galena, a Ag-S-Se mineral (~Ag<sub>1.6</sub>Se<sub>0.1</sub>S), and a Ag-Au-S-Se mineral or mineral intergrowth. Mine locations are shown on figure 37.

quartz, and minor pyrite. This zone sharply borders a complex zone of similar width (represented in both specimens) that consists of distinct layers of fine-grained quartz (millimeters to centimeters thick), euhedral quartz crystals, adularia, finely dispersed electrum and Ag sulfide minerals, and wavy layers of chalcedonic quartz (millimeters to centimeters wide). An irregular, centimeter-wide layer of brown and white chalcedonic quartz borders the zone of brecciated wall-rock fragments. In addition to the observed minerals, reported metallic minerals include magnetite, chalcocopyrite, pyrrargyrite, Ag, kerargyrite [sic], iron oxides, and copper oxides (Brown, 1908), some of which were apparently produced by weathering. Argentite was described as occurring, in part, in thin films between apices of quartz crystals in druses.

## Silver Hill Series Veins

Silver Hill series veins include veins on and near Silver Hill (fig. 37), only a few of which crop out. Maps and sections of underground workings (Chesterman and others, 1986; Bodie Consolidated Mining Company Collection, 2003) indicate that most Silver Hill series veins trend N–N20°E, and dip 50°E (fig. 38), although the near-vertical Booker(?) vein exposed in workings of the Spaulding Mine south of Silver Hill trends N15°W. Silver Hill series veins were extensively developed in the Noonday, Oro, Contention, Maybelle, Addenda, Dudley, and Red Cloud Mines. Small amounts of ore were recovered in the Oro, Addenda and Red Cloud Mines, but only the Noonday Mine had significant production. However, some Noonday Mine production apparently was derived from Incline series veins. Based on mine dumps, Silver Hill series veins may have been mined at the south base of Bodie Bluff several hundred meters north of the Mono Fault. If this interpretation is correct, then significant displacement along the Mono Fault apparently predates formation of Silver Hill series veins.

Compared to Incline and Burgess series veins, Silver Hill series veins are distinctly Ag-rich. Gold/silver by weight and value in Silver Hill veins are  $\leq 0.04$  and  $\leq 3$ , respectively, although ratios are based mostly on ore grades and small production (table 5). Gold/silver and other characteristics (including adularia dates) of veins on the Noonday Mine dump suggest that ore mined in 1879 (Keystone vein) was derived from veins similar to Incline series veins, whereas ore mined in 1880–81 (Concordia vein) was derived from Silver Hill series veins (table 5). Alternatively, high Au/Ag in ore mined prior to 1880 and lower Au/Ag in ore mined 1–2 in later years may attest to ore selectively mined for high gold content, because mills were not designed to recover silver in sulfide minerals, or to possible supergene enrichment.

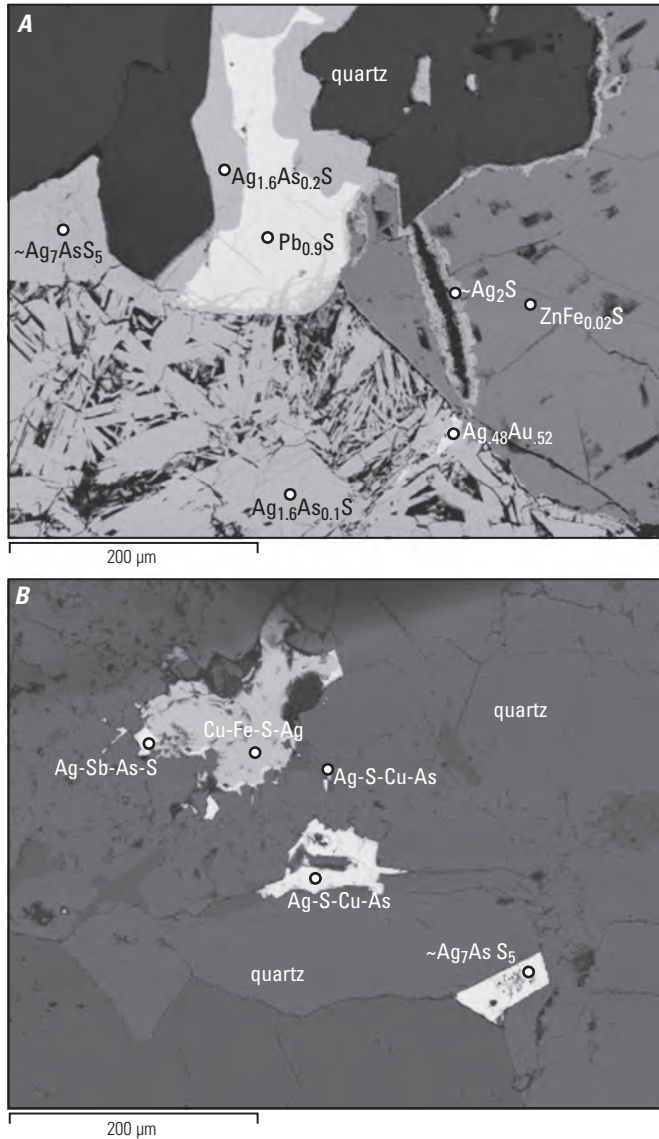
Ore in Silver Hill series veins was mostly recovered from a >1-m-wide segment of the Concordia vein (fig. 38; table 4). Reported stope dimensions between the 450 and 700 levels are ~120 meters along strike, and ~75 meters downdip (Chesterman, and others, 1986). Small amounts of ore were recovered

from a 1.2-m-wide segment of the Red Cloud vein with reported stope dimensions between the 256 and 592 levels of ~35 meters along strike and ~350 ft downdip (Chesterman, and others, 1986).

Vein textures and minerals in the Concordia, Red Cloud, and Oro veins are described by Whiting (1888), Brown (1908), Chesterman and others (1986), and Hollister and Silberman (1995a). The Concordia vein consists of fragments of dacite cemented by fine-grained and vuggy white quartz, coarse-grained calcite, quartz pseudomorphs after calcite, clay gouge, tetrahedrite, pyrrargyrite, and pyrite. The Red Cloud vein is mostly gouge and crushed quartz, but varies along strike from narrow, parallel, anastomosing veins to contiguous “ribbon” quartz and calcite a few centimeters to 1.2 m wide. On the 700 ft level, the Red Cloud vein consists of quartz, quartz after calcite, coarse-grained calcite, and fine-grained adularia, tetrahedrite, pyrite, galena, pyrite, chalcocopyrite, and minor amounts of sphalerite and pyrrargyrite (fig. 39D). The Oro vein in the Oro and Addenda Mines consists of quartz, coarse-grained calcite, tetrahedrite, stephanite, pyrrargyrite, pyrite, and galena, and minor barite (fig. 39E, F). Major oxides in bulk samples of Silver Hill series veins vary from 4.2 to 21.9 weight percent  $\text{Al}_2\text{O}_3$ , 1.2–11.3 weight percent  $\text{K}_2\text{O}$ , 0.1–7.1 weight percent FeO, and <1 weight percent MgO, CaO,  $\text{Na}_2\text{O}$ , and  $\text{TiO}_2$  (calculated from element concentrations, table 1-11).

Vein minerals identified and semiquantified by optical and SEM (fig. 42) include quartz, mica-clay minerals, adularia, and metallic minerals in aggregates of anhedral crystals. The mineralogy of the aggregates varies somewhat between mines and among samples from individual mines. Samples from the Oro Mine dump consist of quartz, adularia, minor amounts of barite, low Fe-sphalerite, galena, acanthite, Ag-Sb-As-S minerals, Cu-Fe-S-Ag-As minerals, and electrum with subequal proportions of Au and Ag. Silver minerals, some of which are euhedral, and electrum are paragenetically later than sphalerite and galena (fig. 42A, B). In an archival specimen from the Addenda Mine, anhedral intergrowths of hessite ( $\text{Ag}_2\text{Te}$ ), electrum with subequal proportions of Au and Ag, tetrahedrite, chalcocopyrite, bornite (not imaged), and an Ag-Te-Cu-S phase are intergrown with euhedral and subhedral quartz crystals (fig. 43A, B, C). Samples from the Red Cloud and Contention Mine dumps (figs. 44A, B, C; 45A, B, C) consist of assemblages that are similar to the Addenda Mine specimen, but also include galena, sphalerite, acanthite, and Ag-Au-Te, Cu-Fe-Sn-S, and Ag-S-Fe minerals. Sylvanite, acanthite, and bornite (not imaged) were identified in separate Red Cloud Mine samples. A dump sample from the Maybelle Mine consists of quartz, acanthite with minor Se, naumannite, an Ag-Sb-S mineral, an Ag-Sb-Se-Fe-S phase, and low Fe-sphalerite; silver minerals are paragenetically later than sphalerite and some fill spaces between euhedral quartz crystals (fig. 45D). Bulk samples of veins contain markedly elevated concentrations of elements of these minerals and phases as well as high concentrations of Hg, Bi, Cd and numerous other chalcophile elements (table 1-11). Tellurium concentrations are markedly anomalous in most samples.





**Figure 42.** Secondary electron images of samples representative of Silver Hill series veins on and near Silver Hill, Bodie Mining District. *A* and *B* correspond to samples BOD11-1D and BOD11-1H, respectively, Oro Mine dump. Imaged phases include quartz, galena, sphalerite, acanthite, electrum with subequal Au and Ag, Ag-As-S minerals ( $\sim\text{Ag}_{1.6}\text{As}_{0.2}\text{S}$ ;  $\sim\text{Ag}_7\text{AsS}_5$ ), and several Ag-Sb-As-Fe-Cu-S minerals or mineral intergrowths. Mine locations are shown on figure 37.

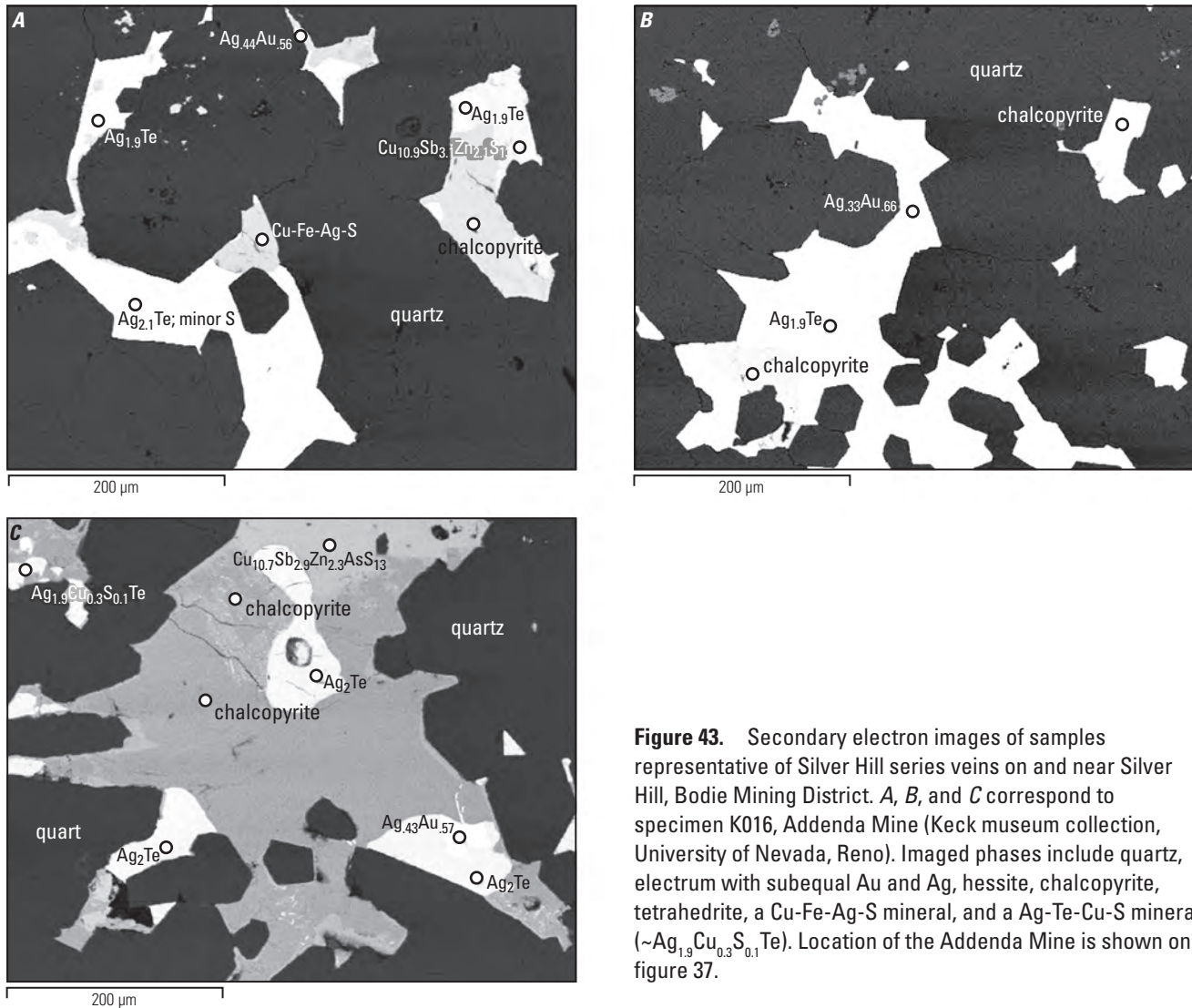
In addition to low Au/Ag and textures, vein mineralogy clearly distinguishes Silver Hill series veins from all other vein types. Dump samples of Silver Hill veins with elevated Au and Ag concentrations typically contain several percent to >10 percent sulfide minerals, predominantly sphalerite, galena, tetrahedrite, and chalcopyrite, whereas other vein types rarely contain more than 1 percent metallic minerals. Other common and distinguishing minerals in Silver Hill series veins are electrum, pyrite, acanthite, bornite, hessite, and sylvanite. Hessite and other Te minerals, tetrahedrite and other Cu-Ag-Sb-As-S sulfosalt minerals, bornite, and possibly barite occur exclusively in Silver Hill series veins.

### Veins On and Near Queen Bee Hill

No production is recorded for veins in the vicinity of Queen Bee Hill in the southern part of the district (fig. 37). Small amounts of \$30–150 per ton ore were found on the 300 and 500 levels of the Maryland Consolidated Mine (Queen Bee Hill), but quantities apparently were insufficient to mill (Chesterman and others, 1986). Limited Au and Ag data suggest that Au/Ag in these veins is similar to Au/Ag of Silver Hill series veins (table 5; Hollister and Silberman, 1995b). The Booker(?) vein, between Queen Bee Hill and the Noonday Mine, and vein pieces on the University, Maryland, and Boston Consolidated Mine dumps, consist of quartz, calcite, quartz pseudomorphs after calcite, and pyrite. Veins on Queen Bee Hill are <1 m wide and extend to at least 800 ft below the surface, but at depth are mostly composed of calcite, based on the prevalence of calcite in pieces of vein on dumps.

### Wall-Rock Alteration

Alteration of volcanic rocks varies with elevation, latitude, vein series, and proximity to veins. It is, in part, lithologically controlled. Matrix of lag blocks of volcanoclastic deposits on the summit of Bodie Bluff (9,000 ft) has been pervasively replaced by very fine-grained quartz and lesser pyrite (iron oxides). Small embayments in some blocks are filled with thin deposits of finely layered, microcrystalline quartz, some of which are draped over rock fragments. The blocks are adjacent to partially excavated clasts of sinter (probably the sinter with reed casts described by Herrera and others, 1993). They represent silicification of volcanoclastic matrices and pool sinter subjacent to a small sinter terrace that subsequently has been dismembered by deflation and frost heaving. Clasts in volcanoclastic deposits include dacite of Silver Hill, uncorrelated porphyritic volcanic rocks, and small (centimeter-sized) angular to tabular, layered fragments of very fine-grained white quartz. Although the white quartz fragments resemble layered Incline series veins at the same elevation (fig. 37, 39A), they contain concentrations of Au, Ag, As, Sb, Rb, and Sr that are indistinguishable from those in terrace sinter, but differ distinctly from those in adjacent Incline series veins (fig. 39; table 1-11). The silicified volcanoclastic



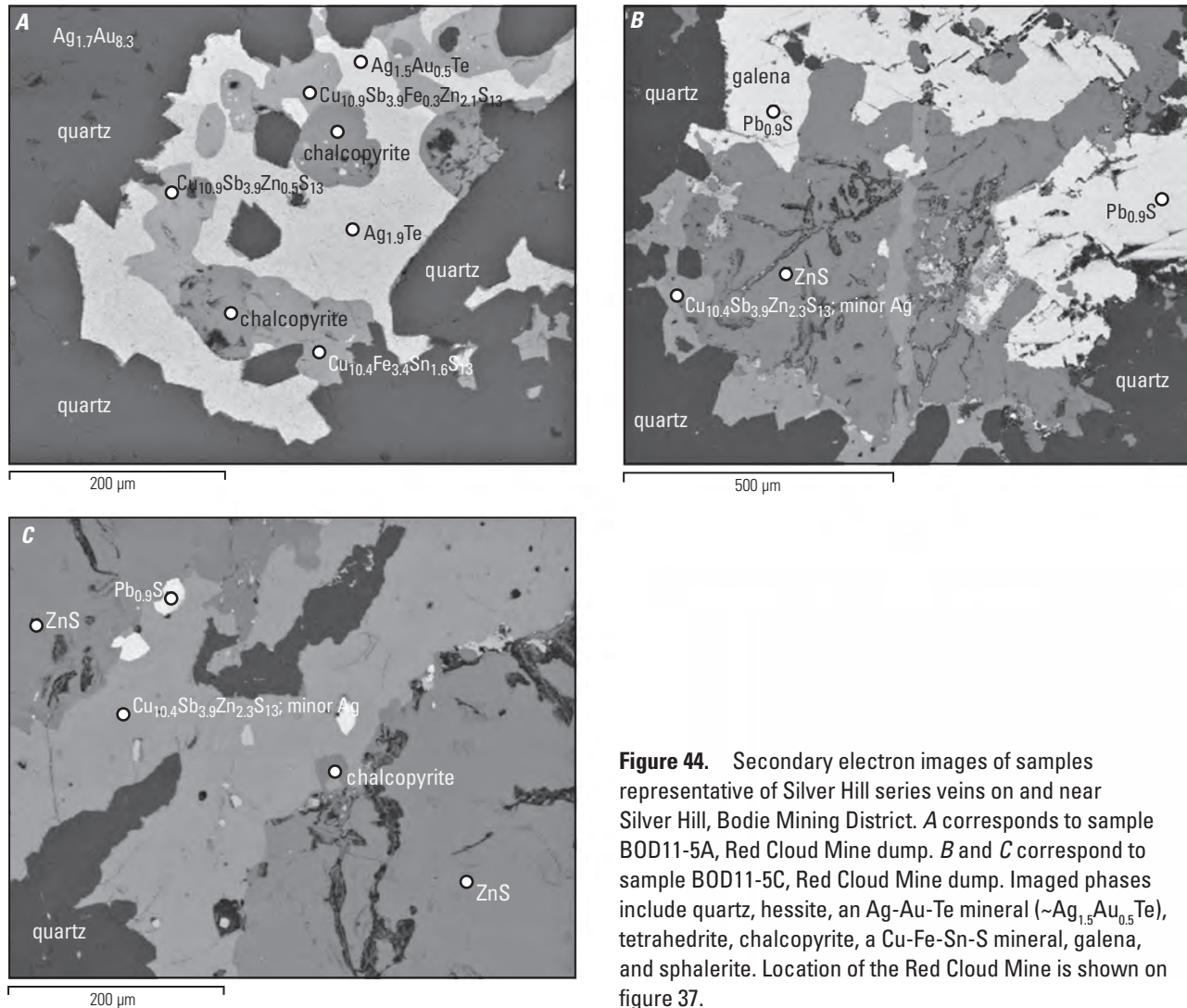
**Figure 43.** Secondary electron images of samples representative of Silver Hill series veins on and near Silver Hill, Bodie Mining District. *A*, *B*, and *C* correspond to specimen K016, Addenda Mine (Keck museum collection, University of Nevada, Reno). Imaged phases include quartz, electrum with subequal Au and Ag, hessite, chalcopyrite, tetrahedrite, a Cu-Fe-Ag-S mineral, and a Ag-Te-Cu-S mineral ( $\sim\text{Ag}_{1.9}\text{Cu}_{0.3}\text{S}_{0.1}\text{Te}$ ). Location of the Addenda Mine is shown on figure 37.

deposits and sinter are the upper strata of the ~60-m-thick sequence of volcanoclastic deposits that accumulated in the graben on Bodie Bluff (fig. 38; Chesterman and others, 1986; Silberman and Berger, 1985; Silberman and Chesterman, 1991; Herrera and others, 1993).

Volcanoclastic deposits in near-surface mine workings on Bodie Bluff, including the upper 100 ft of the old Standard shaft, were reportedly soft and decomposed, and covered veins in underlying dacite (Whiting, 1888; Brown, 1908). Brown (1908) described “dead zones” of fractured and decomposed (“pulpy”) andesite on Bodie Bluff that predated veins but did not maintain open conduits for mineralizing fluids. It is unclear from Brown’s descriptions whether “dead zones” included decomposed volcanoclastic deposits. Matrix, and to a lesser extent, clasts of volcanoclastic deposits on mine dumps at lower elevations on the south slope of Bodie Bluff have been altered to K-feldspar, illite, and montmorillonite, but primary clastic textures are preserved.

A few meters east and tens of meters west of the blocks of silicified volcanoclastic deposits and sinter, dacite, at approximately the same elevation, contains Incline series veins (centimeters to tens of centimeters thick). The veins consist of layers of very fine-grained quartz and lesser adularia. Some narrow veins contain internal voids lined with euhedral quartz and lesser adularia crystals. Adjacent to veins, centimeter-thick selvages of altered dacite consist of quartz, subequal amounts of illite and K-feldspar, and several percent iron oxide that have replaced phenocrysts and matrix without substantially modifying primary texture.

At elevations several hundreds of meters below the summit of Bodie Bluff, vein selvages and brecciated dacite adjacent to Incline and Burgess series veins on the south slope of Standard Hill (8,588 ft) consist of aggregates of quartz and K-feldspar in which grain sizes approach 1 mm. Adjacent to Incline series veins, illite partially replaces K-feldspar in some aggregates, occurs in small seams between quartz



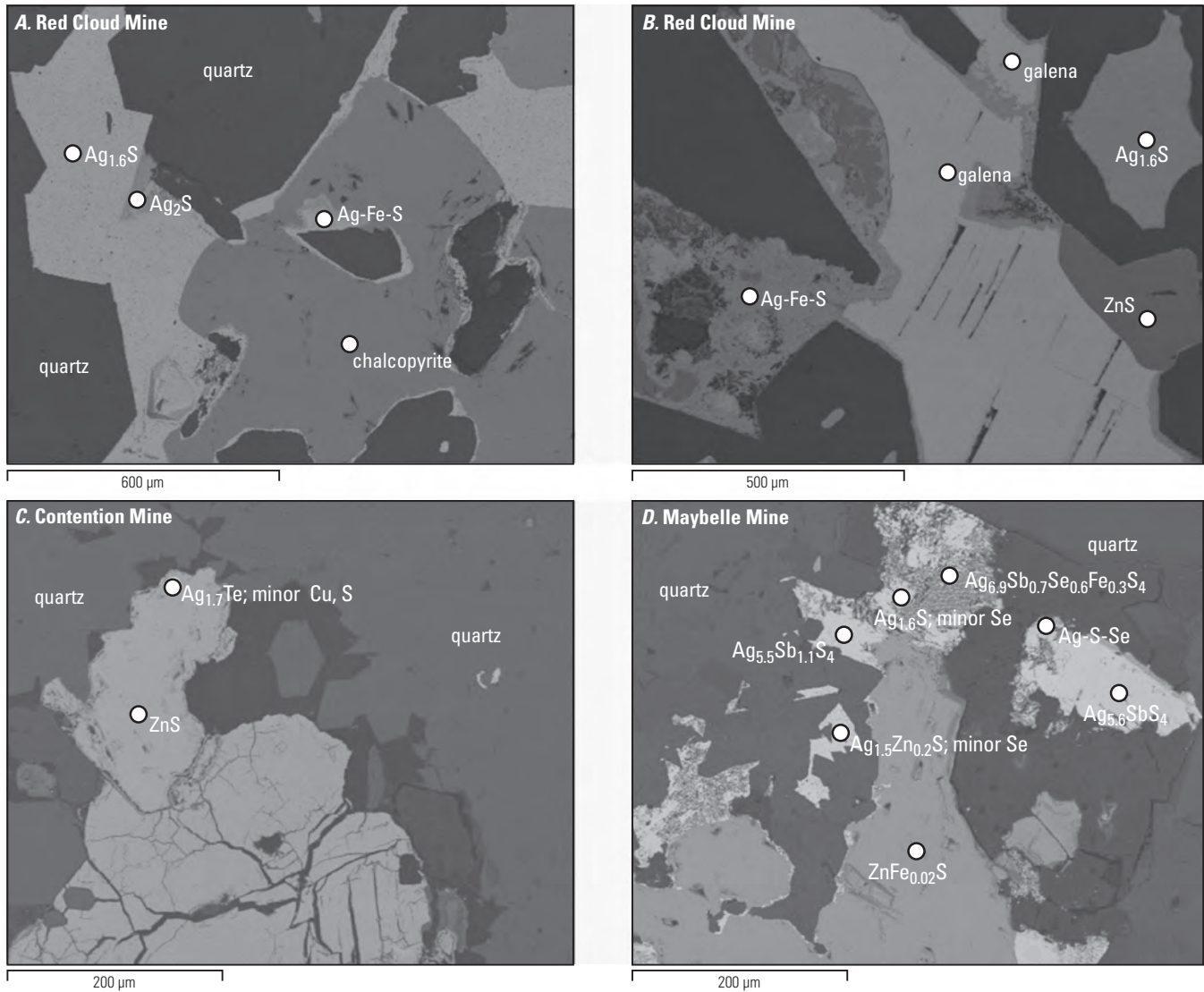
**Figure 44.** Secondary electron images of samples representative of Silver Hill series veins on and near Silver Hill, Bodie Mining District. *A* corresponds to sample BOD11-5A, Red Cloud Mine dump. *B* and *C* correspond to sample BOD11-5C, Red Cloud Mine dump. Imaged phases include quartz, hessite, an Ag-Au-Te mineral ( $\sim\text{Ag}_{1.5}\text{Au}_{0.5}\text{Te}$ ), tetrahedrite, chalcopyrite, a Cu-Fe-Sn-S mineral, galena, and sphalerite. Location of the Red Cloud Mine is shown on figure 37.

layers in veins, and with quartz, K-feldspar, and pyrite, partially replaces dacite fragments in veins and breccias. Centimeter-thick wall-rock selvages adjacent to Burgess series veins consist predominantly of K-feldspar, subequal to lesser amounts of quartz and clinocllore (XRD analysis), and <2 volume percent pyrite (weathered to iron oxide minerals or jarosite). These minerals also cement brecciated dacite near veins. An archival sample of dacite adjacent to the Fortuna vein on the 526 level of the Standard Mine consists mostly of K-feldspar, with lesser quartz and  $\sim 2$  volume percent pyrite.

Vertical zonation of alteration mineral assemblages has been described by O'Neil and others (1973) and Herrera and others (1993). Pervasive K-feldspar-dominant alteration assemblages extend about 100–150 m beneath Bodie Bluff. Mass balance calculations based on major oxide and minor element analyses of unaltered and altered rocks (O'Neil and others, 1973) demonstrate enrichment of K and Rb and depletion of Na, Ca, Mg, and Sr in dacite adjacent to veins

on Bodie Bluff; Si and Al abundances were not changed significantly by alteration processes at these high elevations. Wall-rock selvages of altered dacite adjacent to veins narrow with increasing depth. At depth, selvages include sericite that has replaced K-feldspar, and below  $\sim 8,500$  ft may include kaolinite in addition to quartz and pyrite. Distal to veins, feldspar and mafic phenocrysts in dacite are variably altered to chlorite, illite, montmorillonite, calcite, and lesser pyrite and zeolite minerals. Epidote is uncommon and spatially unrelated to veins, but may be coeval with these distal propylitic alteration minerals.

Alteration mineral associations in dacite spatially associated with Silver Hill series veins consist of quartz, illite, kaolinite, montmorillonite, and pyrite (iron oxides). Variable proportions of these minerals have replaced phenocrysts and matrices as much as tens of meters from veins. Although few veins are exposed near Silver Hill, wall rocks on mine dumps display more pervasive clay-mica alteration than altered



**Figure 45.** Secondary electron images of samples representative of Silver Hill series veins on and near Silver Hill, Bodie Mining District. *A* and *B* correspond to sample BOD09-3C, Red Cloud Mine dump. *C* corresponds to sample BOD09-4A, Contention Mine dump. *D* corresponds to sample BOD09-6, Maybelle Mine dump. Imaged phases include quartz, acanthite with minor Se, chalcopyrite, galena, sphalerite, hessite, a Ag-Fe-S mineral, Ag-Sb-S minerals, a Ag-Zn-S mineral, a Ag-S-Se mineral, and a Ag-Sb-Se-Fe-S mineral or mineral intergrowth. Mine locations are shown on figure 37.

wall rocks associated with other vein series. The smooth, beige-colored dumps in the vicinity of Silver Hill contrast sharply with dumps on Standard Hill and Bodie Bluff, which are dominated by reddish-brown to green, angular blocks of K-feldspar- and illite-altered dacite.

## Absolute and Relative Vein and Sinter Ages

Based on  $^{40}\text{Ar}/^{39}\text{Ar}$  adularia dates, Incline series veins vary in age from ~8.3–8.1 Ma (table 1). They are exposed mostly on Bodie Bluff and Standard Hill (fig. 37), but also are represented on the Noonday Mine and Oro Mine dumps which are linked by underground workings. Burgess series veins and Silver Hill series veins, which are distinguished from Incline series veins by textures, vein mineral assemblages, and wall-rock alteration, vary in age from ~8.5 to 8.4 Ma and ~8.9 to 8.5 Ma, respectively (table 1). However, there are no exposures from which the relative vein ages assigned by Brown (1908), or those determined by  $^{40}\text{Ar}/^{39}\text{Ar}$  geochronology, can be verified. Based on adularia dates, contrasting minor element concentrations (fig. 46; table 1-11), and common elevations (fig. 37), Incline series veins postdate sinter atop Bodie Bluff, and sinter may be temporally equivalent to Burgess or Silver Hill series veins. The Fortuna vein has not been dated. If the crosscutting relationships among veins shown on figure 38 are valid, then the Fortuna vein is older than Incline and Burgess series veins.

Narrow veins (millimeters to centimeters wide) on Bodie Bluff that are juxtaposed with mined Incline and Burgess series veins consist of quartz and adularia layers with internal lenticular vugs containing millimeter quartz and adularia crystals. Adularia dates of 8.4 Ma and 8.2 Ma (table 1, uncorrelated veins), and to an extent, wall-rock alteration suggest that these veins are temporally associated with Burgess and Incline series veins, respectively, although there are no metallic minerals that might confirm associations. The narrow vein ages, coupled with the spread in adularia dates within vein series, imply that a succession of hydrothermal events followed eruption of dacite of Silver Hill at ~9.1–8.9 Ma (table 1). The ~8.9–8.1 span of hydrothermal events in the Bodie Mining District is partly contemporaneous with ~8.6–8.0 Ma trachydacite of Willow Springs, and with the Cinnabar Canyon-US 395 alteration zone (~8.8–8.2 Ma; table 1), ~8 km or more west of the district (fig. 1).

## Minor Elements in Veins and Wall Rocks

The distribution of minor elements and oxygen isotope values in veins and wall rocks has been determined in numerous investigations (Silberman and Berger, 1985; O'Neil and others, 1973; Silberman, 1991; Silberman and Chesterman, 1991; Herrera and others, 1993; Hollister and Silberman, 1995a; 1995b). Concentrations of As, Zn, Sb, Mn, Ba, and Sr in veins vary from low parts per million to hundreds of parts per million, whereas Au, Hg, Ag, Tl, B, Co, Cu, Ni, and Pb

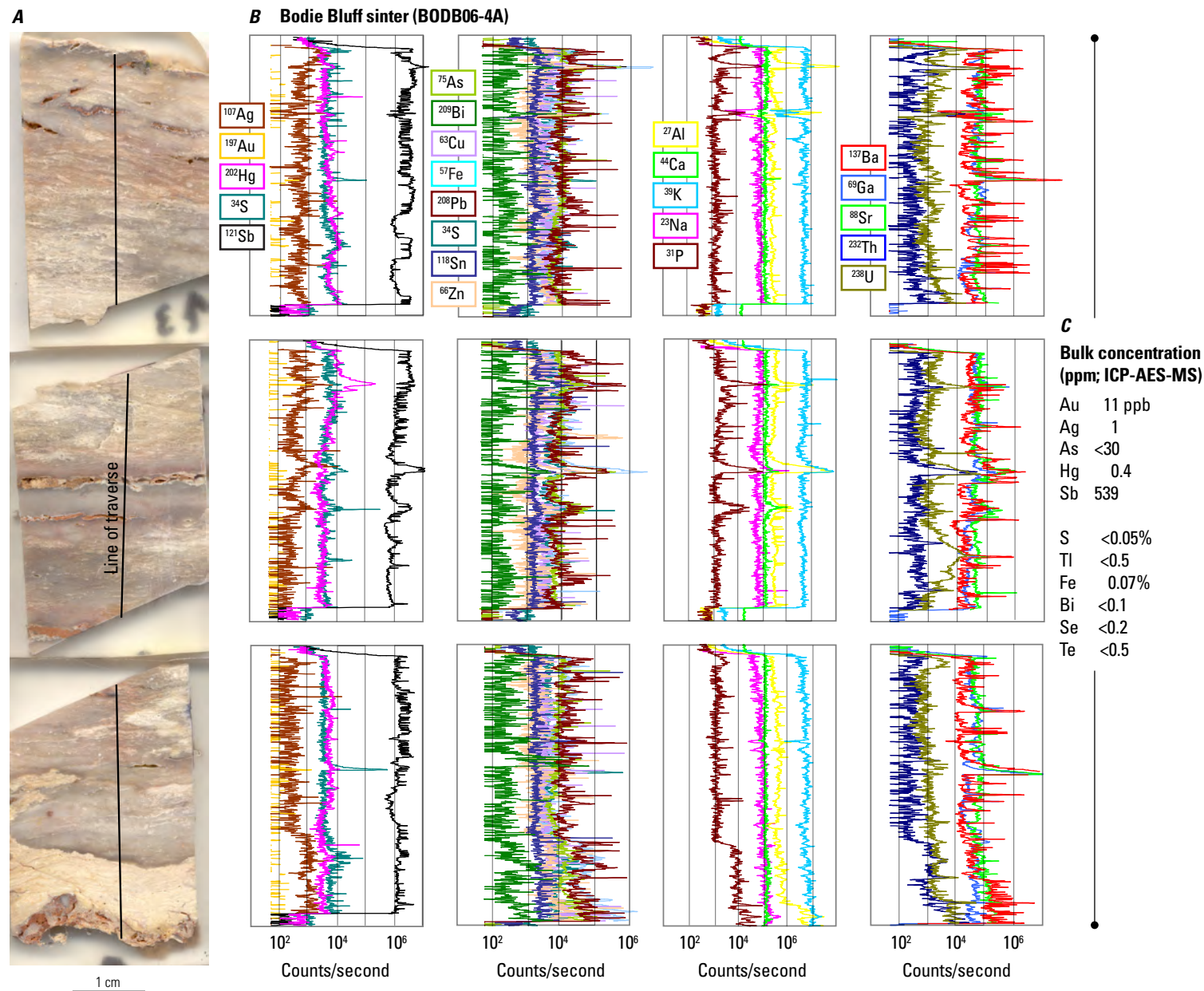
concentrations vary from low parts per million to tens of parts per million. Many published analytical data sets overlap and spatial gradients among element concentrations are mostly inconsistent or difficult to recognize. Minor element distributions from numerous sources are synthesized as follows.

The vertical distribution of minor elements in sinter and Incline series veins from the top (~9,000 ft) to the base (~8,400 ft) of Bodie Bluff shows both variation and relative constancy. Sinter (9,000 ft) contains <1 ppm Au, Hg, and Tl, ~180 ppm As, ~280 ppm Sb, and low ppm concentrations of Cu, Pb, and Zn. At ~8,720 ft (Upper Hobart Tunnel), Au and Ag concentrations in Incline series veins (~0.1–100 ppm) are 10 or more times higher than at 8,400 ft (Bodie Tunnel), whereas concentrations of Sb (1–~60 ppm), Hg (0.01–~11 ppm), Tl (<7.5 ppm), Cu (~2–70 ppm), Zn (~10–100 ppm), and Sr (~100–800 ppm) are broadly similar. Arsenic (~2–490 ppm), Mn (~8–10,000 ppm), Pb (~2–80 ppm), and Ba (10–1,100 ppm) concentrations are generally elevated in Bodie Tunnel samples relative to samples from higher elevations.

Gradients in the vertical distribution of minor elements in altered dacite are more difficult to interpret because all high-elevation samples contain quartz veins, whereas samples from lower elevations do not. Elements that display relatively consistent concentrations at 9,000 and 8,400 ft include As (190 to 6 ppm, respectively), Zn (low to 110 ppm), and Sb (130 to low ppm). Gold, Ag, Tl, and Hg concentrations vary little with elevation. Other minor element concentrations are elevated locally, but variations show minimal or no correlation with elevation.

Lateral distribution of Sr, Rb, Au, and oxygen isotopes in dacite wall rocks and a 0.6-m-wide Incline series vein in the Upper Hobart Tunnel show higher Sr (~100–700 ppm) and Rb (~130–400 ppm) concentrations, and higher  $^{18}\text{O}$  values (~–0.1 to –2.1 ‰) in dacite, and higher Au concentrations (0.04–4.2 ppm) in the vein. Slight gradients are implied by decreasing Sr and Rb and increasing  $^{18}\text{O}$  values with distance from the vein, although sample density is inadequate to substantiate trends. Concentrations of Zn, Ag, As, and Tl in dacite either decrease abruptly with distance from the dacite-vein contact (Ag, Tl), or display no systematic trend (Zn, As).  $\delta^{18}\text{O}$  values in other whole rock and phenocryst samples from Bodie Bluff and Standard Hill indicate variable exchange between dacite and meteoric water.

Concentrations of Au, Ag, Cu and other elements in veins on Bodie Bluff and Standard Hill, in Silver Hill series (“polymetallic”) veins, in veins on Queen Bee Hill, and in wall rocks have been compared by Hollister and Silberman (1995b). Silver-gold ratios in veins and wall rocks at 9,000 ft on Bodie Bluff (presumably Incline series veins) are 2.3 and 21, respectively, and at 8,400 ft are 19 and 31. Silver-gold ratios in Silver Hill series veins and wall rocks are 244 and 43, respectively, and in veins and wall rocks on Queen Bee Hill are 6.6 and 104, respectively. Cu-Au ratios in Silver Hill series veins are several orders of magnitude higher than in Bodie Bluff and Queen Bee Hill veins. These element

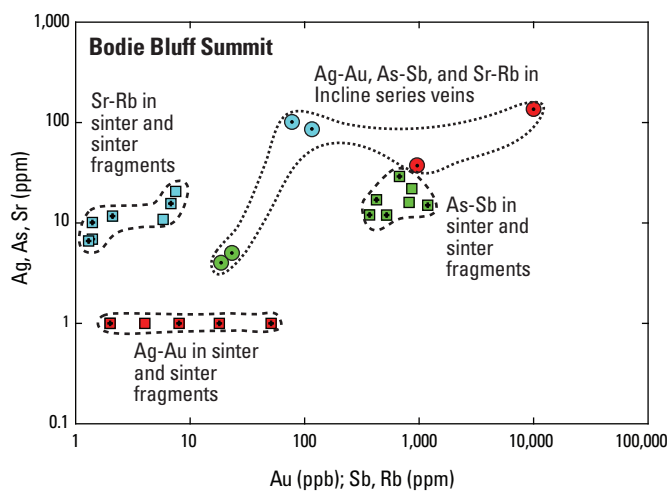


**Figure 46.** *A*, Image showing oriented consecutive sections of sinter from Bodie Bluff summit, Bodie Mining District (BODB06-4A; fig. 37). *B*, Graphs showing relative element concentrations in sinter measured in counts per second (counts/second) by laser ablation inductively couple plasma-mass spectrometry (LA ICP-MS). *C*, Bulk sample element concentrations determined by inductively coupled plasma-atomic emission spectrometry-mass spectrometry (ICP-AES-MS). Locally elevated (millimeter-scale) element concentrations include Au, Ag, Hg, S, Sb, Cu, As, Fe, Sn, Bi, Zn, Pb, and Ba, most of which are not elevated in the bulk sample.

concentrations and ratios in veins, at least, are corroborated by vein mineralogy described previously, and by production records (table 5).

Minor element concentrations in sinter atop Bodie Bluff (9,000 ft; fig. 37) were determined for possible element correlations between sinter and veins (Vikre, 2007). Element concentrations, determined by LA ICP-MS along a continuous traverse orthogonal to sinter beds, include local (submillimeter scale) enrichment of Ag, Sb, Hg, S, Bi, As, Fe, Cu, Pb, Ba, and other elements (fig. 46). Bulk analyses of the traversed sinter beds, and of other sinter samples (table 1-11), show elevated concentrations of Sb, Hg, As, Tl, and Se, but some elevated concentrations at the millimeter scale (for example, Ag, Bi) are not elevated in bulk samples. Based on these analyses, sinter cannot be correlated unequivocally with any specific vein series (table 1-11).

Elevated concentrations of Sb, Hg, As, and Pb in some bulk sinter samples and in Silver Hill series veins broadly correspond, whereas Au, Ag, Bi, Cu, Se, Sn, Te, and Zn are enriched in Silver Hill series veins but not in sinter. Element concentration correlations between Incline and Burgess series veins and sinter are fewer and include similar As, Pb, and Sb concentrations in some samples (table 1-11). Sinter and Incline series veins at the same elevation on the summit of Bodie Bluff contain, in part, similar As, Sr, and Sb concentrations, but Au and Ag concentrations in sinter are as much as two orders of magnitude lower than those in veins (fig. 47).



#### EXPLANATION

- Sinter (dismembered sinter terrace)
- ▣ Sinter fragments (in volcanoclastic deposits)
- Incline series veins

**Figure 47.** Graph of Ag, As, Sr concentrations versus Au, Sb, Rb concentrations in sinter from the dismembered sinter terrace, sinter fragments in volcanoclastic deposits, and Incline series veins, Bodie Mining District, Bodie Bluff summit. Elevation of all samples is 8,960±20 ft.

## Fluid Inclusion Microthermometry

Limited fluid inclusion microthermometric analyses and petrographic descriptions of fluid inclusions have been published. A fluid inclusion “filling temperature” of 245 °C and salinity of 0.3 weight percent NaCl equivalent in a sample of vein quartz from the McClinton Mine dump (atop Standard Hill, ~8,720 ft; presumably an Incline series vein), were determined by J.T. Nash and reported by O’Neil and others (1973). Hollister and Silberman (1995b) described saturated fluid inclusions (containing as many as four daughter minerals) in a polymetallic vein sample from the vicinity of Silver Hill (presumably a Silver Hill series vein), but provided no microthermometric data.

## Oxygen and Hydrogen Isotope Compositions of Vein Minerals and Fluid Inclusion Water

Oxygen isotope values of vein quartz±adularia, and hydrogen isotope values of fluid inclusion water in vein quartz±adularia, were determined by O’Neil and others (1973) and O’Neil and Silberman (1974) for samples from the McClinton Mine dump and Upper Hobart Tunnel (fig. 37; presumably Incline series veins), Red Cloud Mine dump (presumably Silver Hill series veins), and of the Fortuna vein (fig. 38). The  $\delta^{18}\text{O}$  values of water in equilibrium with quartz, calculated at an assumed fractionation temperature of 250 °C, vary from -3.0 to -0.1 ‰; the  $\delta\text{D}$  values of water vary from -108.1 to -97.6 ‰. These isotope values imply that vein components were transported by, and deposited from, meteoric water-dominated fluid, and very high water-rock ratios during hydrothermal events. The  $\delta\text{D}$  values of kaolinite and K-mica, -133.2 and -127.3 ‰, respectively, are also compatible with meteoric water-mineral equilibration. Lower equilibrium temperatures of 228 °C and 123 °C were calculated for coexisting quartz and calcite in a vein sample from the Red Cloud Mine dump; the temperature differences reflect different experimentally determined quartz-water fractionations (O’Neil and others, 1973; O’Neil and Silberman, 1974).

## Sulfur Isotope Compositions of Vein Minerals

The  $\delta^{34}\text{S}$  values of sulfide minerals in Bodie district veins were determined for comparison with those of hydrothermal minerals in other mining districts and alteration zones in the Bodie Hills volcanic field (table 2). In Bodie district veins,  $\delta^{34}\text{S}$  values vary by ~6 ‰ (-4.7 to 1.4 ‰) with a mode of ~0 ‰, indicative of a reduced and fairly isotopically homogenous source; the values are broadly similar to values of sulfide melt inclusions in mantle rocks (Chaussidon and others, 1989) and are consistent with a magmatic source of sulfur. The ~0 ‰ mode and near absence of hypogene sulfate minerals distinguish Bodie district veins from sulfide-sulfate mineral assemblages in the Masonic Mining District, and in the Red Wash-East Walker River, Sawtooth Ridge, Potato

Peak, and Cinnabar Canyon-US 395 alteration zones. The  $\delta^{34}\text{S}$  values of sulfide and sulfate minerals at Masonic and most alteration zones reflect disproportionation of magmatic  $\text{SO}_2$  (Rye, 2005). The  $\delta^{34}\text{S}$  values of Bodie district veins have much less variance than those of Aurora district veins. The larger range in values at Aurora may reflect unrecognized sulfate minerals, or more than one sulfur source.

## ASTER Imagery

ASTER imagery of the Bodie Mining District (Rockwell, 2010) shows a fairly contiguous cluster of pixels in the area between the Mono Fault and Silver Hill that corresponds to kaolinite, smectite, smectite/montmorillonite, and quartz. Less dense pixel clusters, coincident with Standard Hill and Bodie Bluff, correspond to illite, smectite/montmorillonite, and quartz. Diffuse pixels, coincident with the area between Bodie Bluff and Queen Bee Hill, correspond to illite.

## SWIR Spectra; XRD Analyses

SWIR and XRD analyses of hand samples and subsamples show that altered dacite, adjacent to Incline series veins on Standard Hill, contains illite, K-feldspar, quartz, and small amounts of pyrite (iron oxides). Dacite adjacent to Burgess series veins contains clinocllore, and possible montmorillonite, in addition to quartz, K-feldspar, and small amounts of pyrite (iron oxides). Altered volcanoclastic strata and dacite on Bodie Bluff (Tioga Mine dump) contain illite/smectite, and montmorillonite. Hydrothermal minerals in dump samples of Silver Hill series veins include adularia and illite in addition to quartz.

## Spring Peak Sinter

### Location

Sec. 34, T. 5 N., R. 28 E., Mineral County, Nevada (fig. 1)

### Definition

The Spring Peak sinter consists of a partially dissected sinter terrace with west-east and north-south dimensions of ~0.2 and 0.1 km, respectively (0.02 km<sup>2</sup>; fig. 48). The terrace overlies altered volcanoclastic deposits and Cretaceous granitic and Mesozoic metamorphic rocks on a low west-east ridge. The ridge is near the eastern margin of an area of erratically altered trachyandesite of Aurora, Pliocene volcanic rocks, and Cretaceous granitic rocks that extends south and east from the Aurora Mining District and East Brawley Peak (figs. 16, 48). Temporal relationships between the Aurora Mining District, the East Brawley Peak alteration zone, Spring Peak sinter, and the west-east zone of altered rocks that underlie the Spring Peak sinter have not been completely determined.

## History and Production

No production is recorded from the Spring Peak sinter terrace or subjacent rocks. Small prospect pits were excavated in altered volcanic and pre-Tertiary rocks west, northwest, and east of the terrace, and a small prospect pit in the terrace exposes opaline silica with minor amounts of cinnabar. Cinnabar also occurs in chalcedonic and opaline sinter at the eastern edge of the terrace. Small pieces (centimeters in dimension) of layered vein, some of which contain elevated gold and silver values, lie on the south slope of the sinter-capped, west-east ridge. Nineteen, relatively shallow holes ( $\leq 505$  ft deep; Kinetic Gold Corp., 2013) were drilled in the 1980s to determine if precious metal deposits occur beneath or lateral to the sinter terrace. Recent geological mapping, geochemical analyses, and geophysical interpretation have been used to correlate layered vein float with sinter and other alteration mineral assemblages (Kinetic Gold Corp., 2013). The Spring Peak sinter and subjacent rocks represent a relatively intact sinter-vein system that contains elevated concentrations of Au, Ag, Hg, Sb, and As.

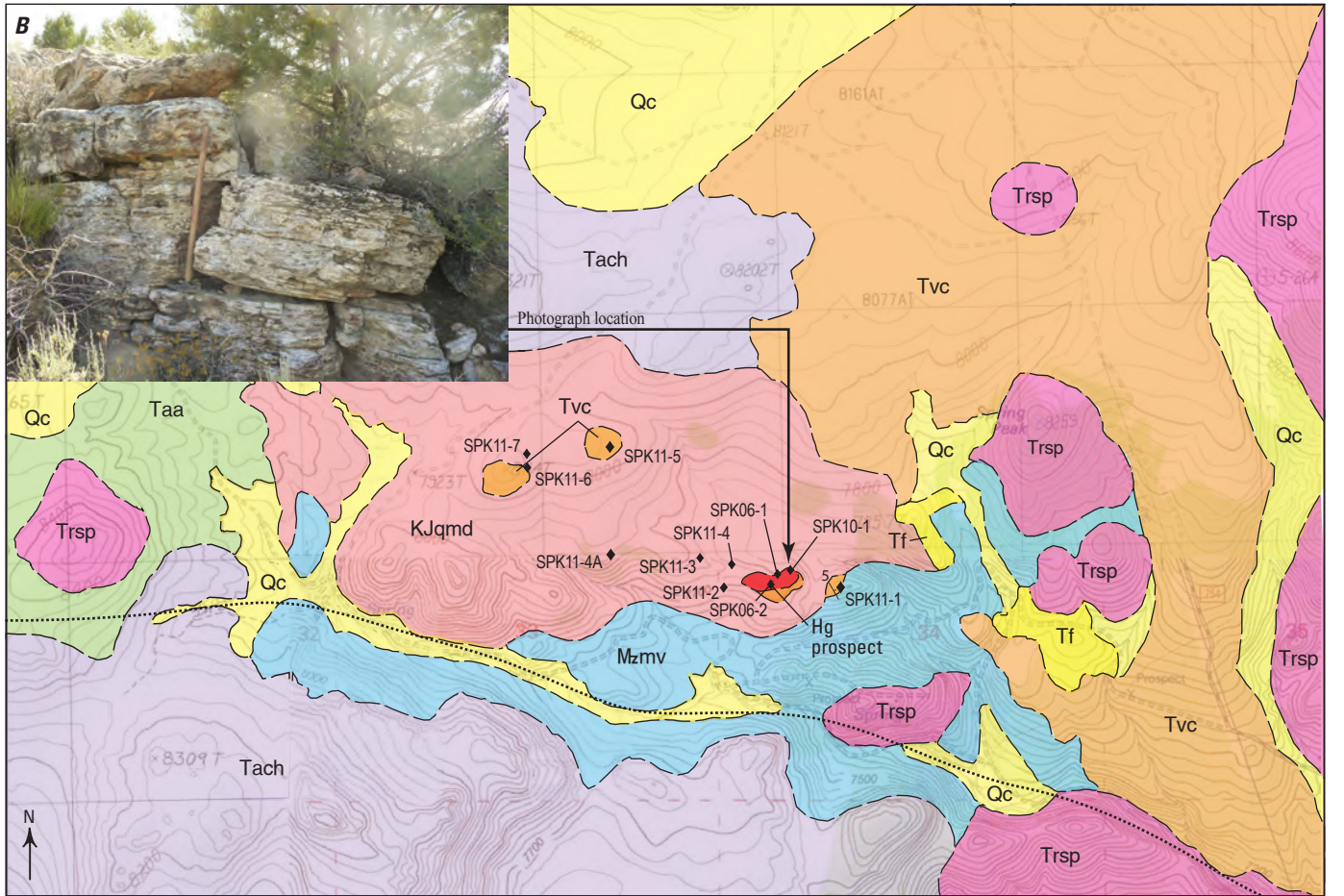
## Stratigraphy

The oldest rocks in the vicinity of the Spring Peak sinter are Cretaceous granitic rocks, and Mesozoic metamorphic rocks, presumably correlative with rocks of the Excelsior Formation (Al-Rawi, 1969; Silberman and others, 1995; Breit, 2000; divided by Speed, 1977 into the Mina, Gold Range, and Black Dyke formations). Thin (meters-thick) altered volcanoclastic strata underlie the sinter terrace and unconformably overlie pre-Tertiary rocks on the west end of a small hill tens of meters (>100 ft) east of the terrace. The terrace has a maximum thickness of ~5 m at its northeastern edge, but is <1 m thick elsewhere where it is largely dismembered into meter-sized blocks and smaller clasts of float. Much of the northeastern terrace margin consists of large to small blocks (meters in dimension) that are slightly tilted (fig. 48). The gray- to brown-weathering volcanoclastic substrate is moderately well-sorted and bedded, sand and silt. Larger feldspar and quartz fragments (centimeter-sized) in sand beds were apparently derived from subjacent Cretaceous granitic rocks.

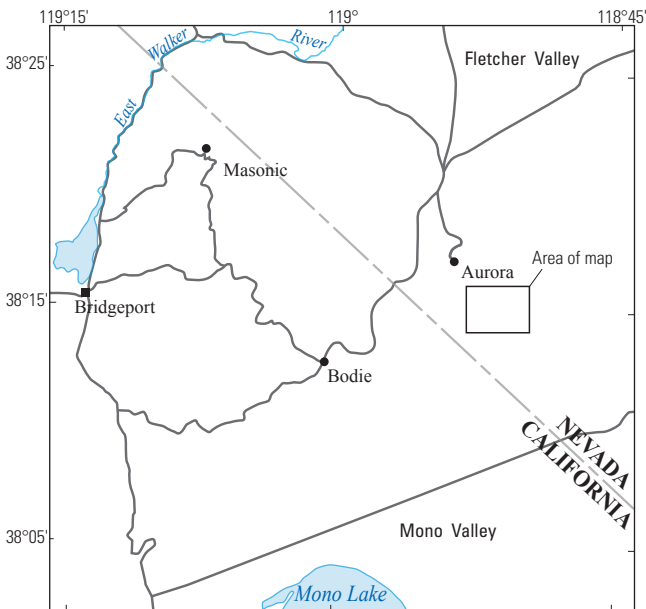
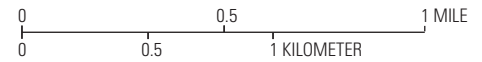
Cretaceous granitic rocks consist of very light-gray to yellowish-gray hypidiomorphic granular, porphyritic quartz monzodiorite with prominent, euhedral, perthitic, pink potassium feldspar megacrysts 2–3 cm long. The medium-grained quartz monzodiorite contains about two percent tan- to greenish-brown biotite, mostly replaced by chlorite. Mesozoic metamorphic rocks intruded by quartz monzodiorite in the Spring Peak sinter area are similar to those in the Masonic Mining District.



A



Base modified from U.S. Geological Survey  
 Mount Hicks, Nev., 1989, Aurora, Nev.-Calif., 1989,  
 Cedar Hill, Calif.-Nev., 1994, and Kirkwood Spring, Calif.-Nev., 1989, 1:24,000



**EXPLANATION**

<b>Qc</b>	<b>Colluvium</b>	<b>KJqmd</b>	<b>Granitic and metamorphic rocks</b> Quartz monzodiorite of Aurora (Cretaceous or Jurassic)—Quartz veined and altered to kaolinite near sinter (line-pattern on map) Trachyandesite of Cedar Hill (Pleistocene)
<b>Qmh</b>	<b>Aurora Volcanic Field</b> Trachyandesite of Mount Hicks (Pleistocene)	<b>Mzmv</b>	Metavolcanic rocks (Mesozoic)
<b>Trsp</b>	Rhyolite of Spring Peak (Pliocene)	<b>Contact</b>	Dashed where approximated
<b>Tach</b>	Trachyandesite of Cedar Hill (Pliocene)	<b>5</b>	<b>Bedding</b>
<b>Tsi</b>	Sinter	<b>Color air photo (CAP) lineament</b>	Dotted line
<b>Tvc Tf</b>	Silicified volcaniclastic rocks (Tvc) and silicified fanglomerate (Tf)	<b>Analytic sample site and number</b>	Diamond symbol
<b>Taa</b>	<b>Bodie Hills Volcanic Field</b> Trachyandesite of Aurora (Miocene)		

**Figure 48.** A, Geologic map of the Spring Peak sinter, Mineral County, Nevada, modified from Breit (2000) and John and others (2012). B, Image showing nearly intact sinter beds from the northern margin of the terrace.

## Structure

No obvious structures control the morphology of the Spring Peak sinter terrace. A prominent west-east lineament on color air photos (CAP lineament; fig. 48) borders the terrace to the south. This lineament extends to the west through the southern part of the East Brawley Peak alteration zone (fig. 16), and may have regionally displaced veins in the Aurora Mining District.

## Hydrothermal Alteration

Sinter consists of bedded chalcedonic quartz, opaline silica, and hackly voids (former rock fragments and bioherms) that contain small amounts of illite and montmorillonite. Minor cinnabar and a dark-green mineral, possibly nontronite ( $\text{Na}_{0.3}\text{Fe}^{3+}_2\text{Si}_3\text{AlO}_{10}(\text{OH})_2 \cdot 4(\text{H}_2\text{O})$ ), occur locally in bedding planes and along fractures, and are finely dispersed in chalcedonic silica. Volcaniclastic strata beneath the sinter have been pervasively silicified, and contain as much as several percent pyrite, small amounts of kaolinite, and a few <1 mm-thick quartz veins.

Quartz monzodiorite, along the western part of the low west-east ridge that is partially covered by the sinter terrace, has been altered to opaline silica and kaolinite. Local exposures of quartz monzodiorite with disrupted texture apparently represent a weathering surface that predates hydrothermal alteration. Layered quartz veins (centimeters wide) occur in float at sub-sinter elevations on the south side of the ridge of quartz monzodiorite. These veins consist of fine-grained quartz, K-feldspar, and minor sericite.

Samples of sinter and subjacent rocks contain as much as 27 ppm Hg, tens to >1,000 ppm As, and hundreds to >1,000 ppm Sb (table 1-12). A few samples contain elevated concentrations of Au (tens to >126 ppb), Ag, Ba, Mo, and W. Higher Au concentrations (several parts per million) were encountered in drill holes and in samples of layered vein float (Kinetic Gold Corp., 2013). Minor element concentrations, determined by LA ICP-MS, along continuous traverses orthogonal to sinter beds (figs. 49, 50, 51) define local (submillimeter) enrichments of Au, Ag, Hg, S, As, Bi, Tl, Fe, and other elements. Bulk analyses of the traversed beds indicate slightly to markedly elevated concentrations of Au, Sb, Hg, and Fe, but many elements with elevated concentrations at the millimeter scale (for example, As, Bi, Tl, and Ag) are not anomalously concentrated in bulk samples.

## Hydrothermal Mineral Ages

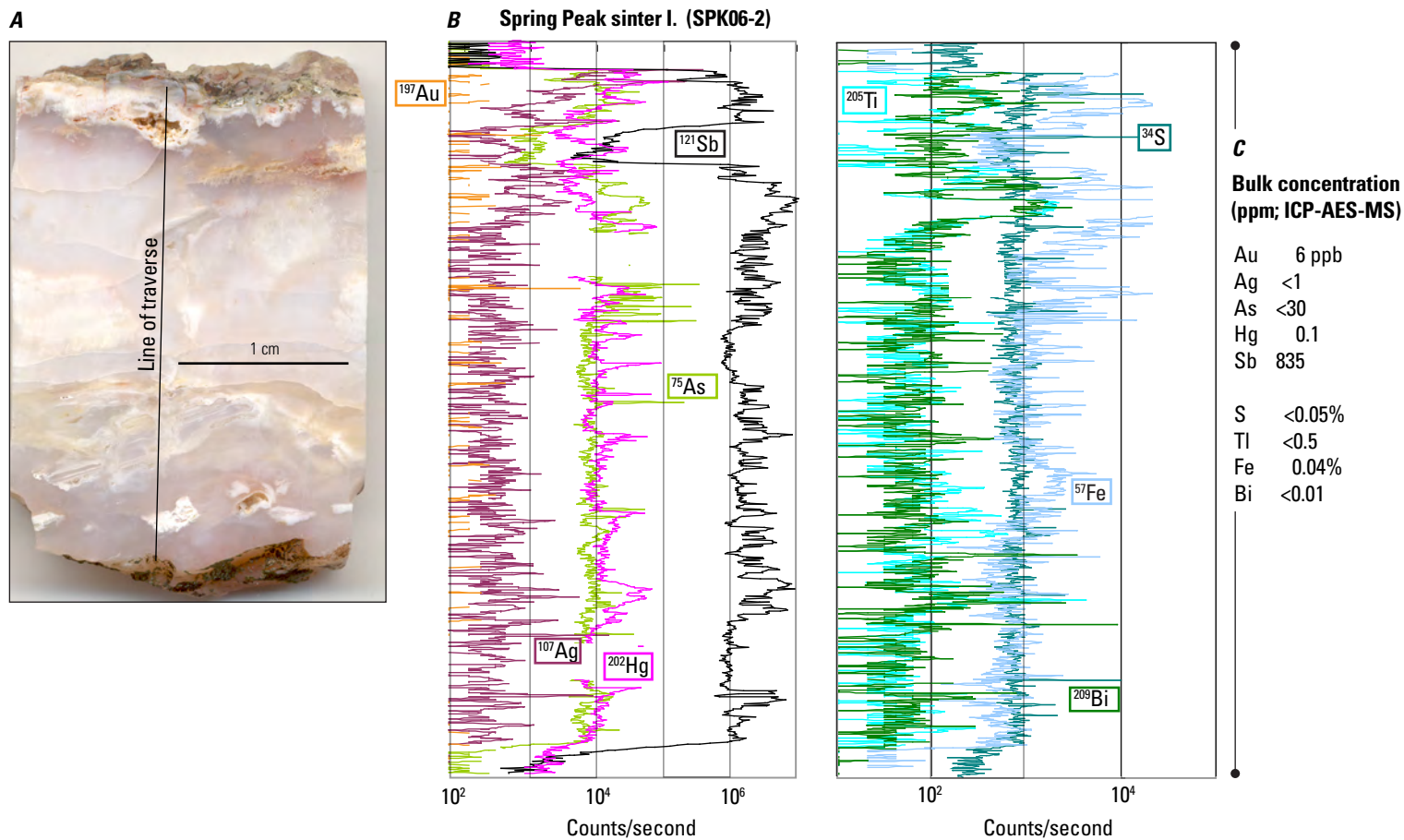
Spring Peak sinter has not been dated directly, but its age is somewhat constrained stratigraphically. Altered rhyolite (possibly Pliocene rhyolite of Spring Peak) and silicified Tertiary fanglomerate in the west-east zone of altered rocks that includes the sinter terrace (fig. 48) imply that the sinter is Pliocene or younger.

## Evolution of Landforms During Assembly and Alteration of the Miocene Bodie Hills Volcanic Field

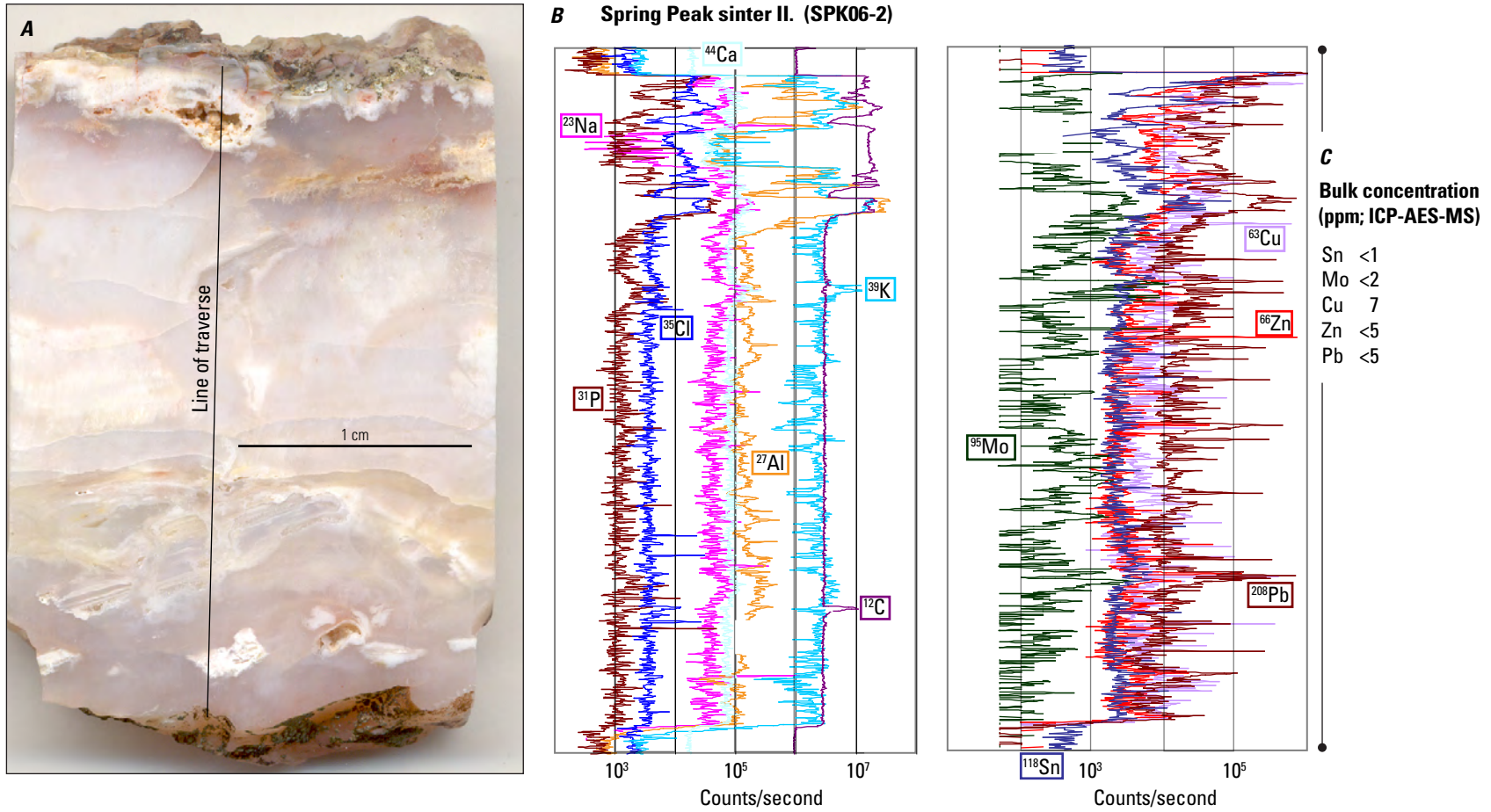
Characteristics of mining districts and alteration zones, coupled with volcanic stratigraphy and geochronology, can be used to reconstruct Miocene landform evolution during the assembly, alteration, and erosion of the Bodie Hills volcanic field. Detailed mapping and dating of volcanic rocks, Au-Ag-Cu deposits, and alteration zones has enabled identification of erosional paleosurfaces (lithologic contacts between volcanic flows and volcaniclastic deposits) closest in age to the hydrothermal systems. In several mining districts and alteration zones, hydrologic paleosurfaces (surfaces during hydrothermal activity) are marked by remnant terrace and pool sinters. In eroded mineralized and altered areas, the relative elevations of paleopotentiometric surfaces (groundwater saturation surfaces) can be estimated from vein fluid inclusion microthermometry, vein sulfur isotope equilibrium temperatures, and more generally, alteration mineral assemblages. Based on climatic evidence (Aldrich Station flora), potentiometric surfaces in the Bodie Hills during the middle Miocene were largely equivalent to hydrologic surfaces. Comparison among present elevations of erosional paleosurfaces, hydrologic paleosurfaces, and paleopotentiometric surfaces above exposed veins can be used to estimate (1) thicknesses of host rocks, veins, and mineralized and altered rocks that have been eroded; (2) postmineralization fault displacements; and (3) depths at which high-grade sections of veins and mineral deposits formed. The restoration of paleosurfaces and paleotopography within mining districts and alteration zones, based on fluid dynamics, volcanic stratigraphy, and geochronology, enables larger scale reconstruction of landforms as they evolved during assembly and alteration of the entire volcanic field (fig. 52). Key datums for this reconstruction are the Aldrich Station flora and Eureka Valley Tuff.

## Aldrich Station Flora and Fossils in the Bodie Hills

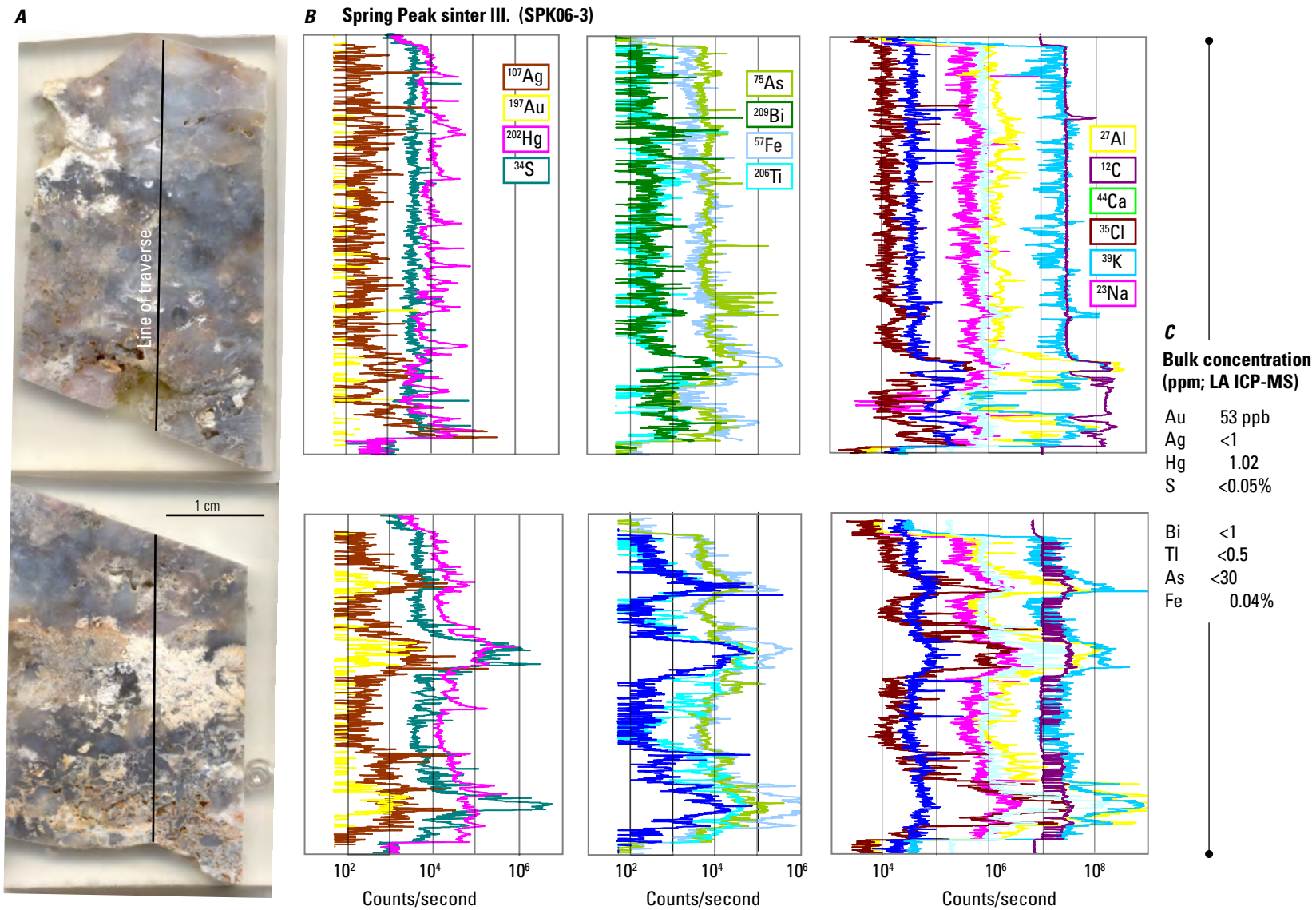
The ~11 Ma Aldrich Station flora (Axelrod, 1956; Evernden and James, 1964; Gilbert and Reynolds, 1973; Millar, 1996), ~22.5 km north of the Aurora Mining District, occurs in tuffaceous shales that accumulated during Bodie Hills volcanism (fig. 52B). The flora consists of riparian species that grew in fluviallacustrine basins, and species representative of conifer forests and live oak woodlands that grew on bordering volcanic uplands with hundreds of feet of relief. The prevailing subhumid climate was more equable than present climate with ~64 cm or more of winter and summer precipitation. In basins, groundwater saturation was at or above land surface, whereas in volcanic uplands, groundwater saturation was apparently within meters below the surface.



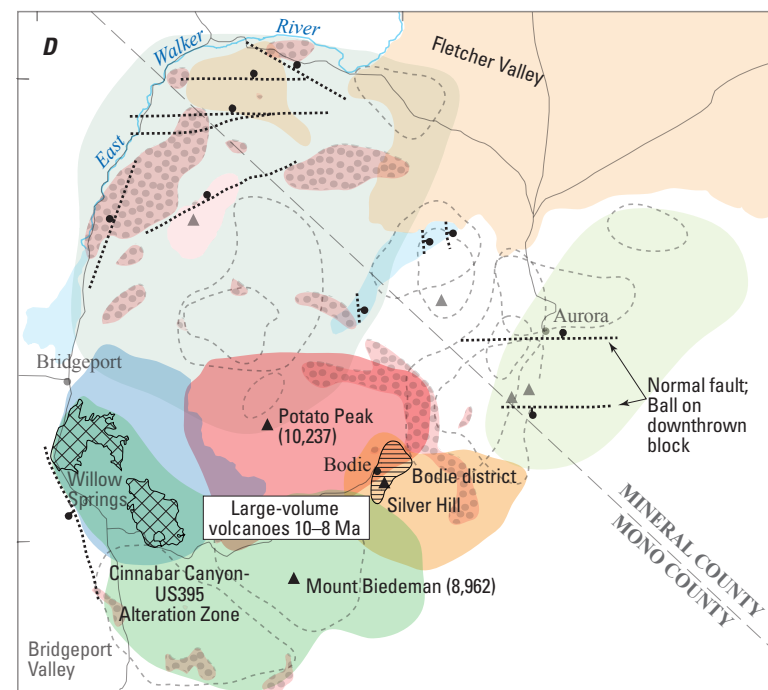
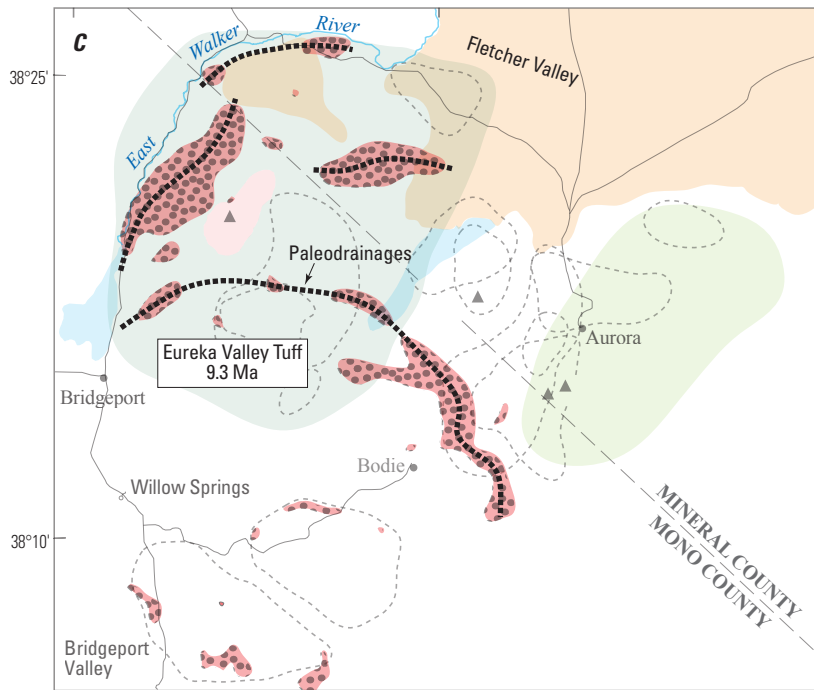
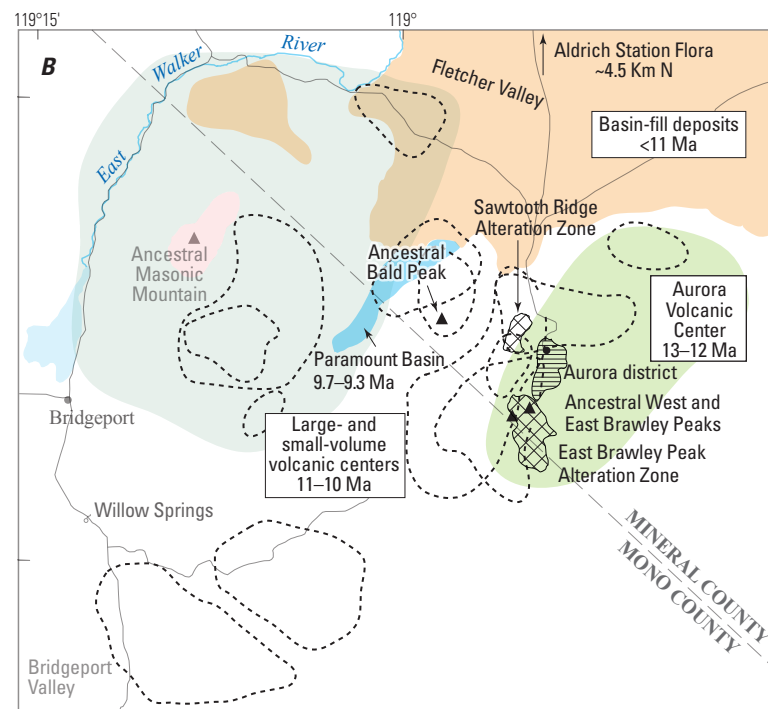
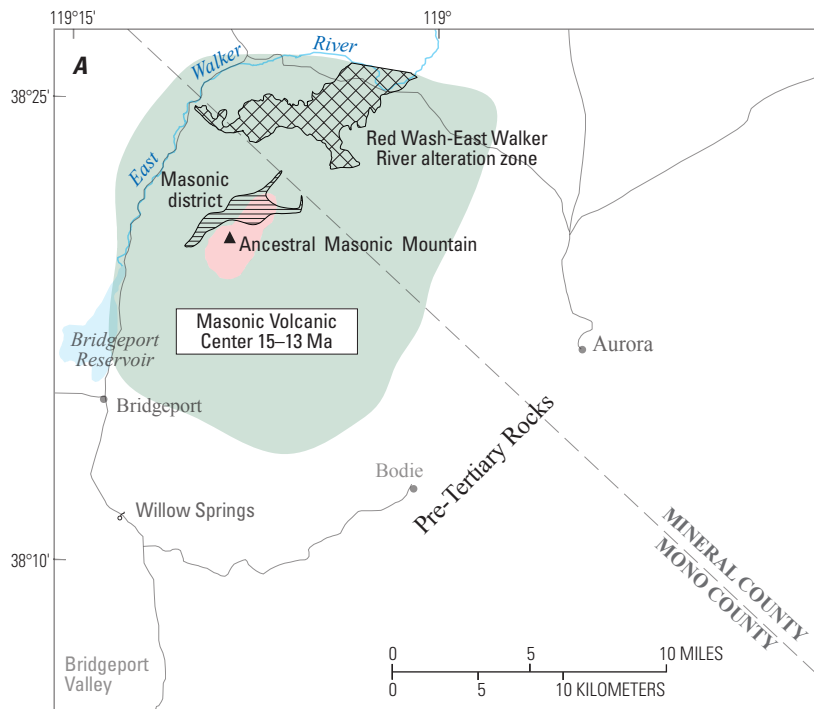
**Figure 49.** A, Image of sample of Spring Peak sinter from the Hg prospect in the sinter terrace, Spring Peak alteration zone (fig. 48). B, Graphs showing relative element concentrations in sinter measured in counts per second (counts/second) by laser ablation inductively coupled plasma-mass spectrometry (LA ICP-MS). C, Bulk sample element concentrations determined by inductively coupled plasma-atomic emission spectrometry-mass spectrometry (ICP-AES-MS). Locally elevated (millimeter-scale) element concentrations include Au, Hg, Ag, Sb, Fe, and S.



**Figure 50.** A, Image of sample of Spring Peak sinter from the Hg prospect in the sinter terrace, Spring Peak alteration zone (fig. 48). B, Graphs showing relative element concentrations in sinter measured in counts per second (counts/second) by laser ablation inductively coupled plasma-mass spectrometry (LA ICP-MS). C, Bulk sample element concentrations determined by inductively coupled plasma-atomic emission spectrometry-mass spectrometry (ICP-AES-MS). Same section as in figure 49 showing additional elements. Locally elevated (millimeter-scale) element concentrations include Sn, Mo, Cu, Zn, Pb, K, Al, Ca, and P.



**Figure 51.** *A*, Image of oriented consecutive sections of sinter from the northern edge of the Spring Peak sinter terrace (fig. 48). *B*, Graphs showing relative element concentrations in sinter measured in counts per second (counts/second) by laser ablation inductively coupled plasma-mass spectrometry (LA ICP-MS). *C*, Bulk sample element concentrations determined by inductively coupled plasma-atomic emission spectrometry-mass spectrometry (ICP-AES-MS). Locally elevated (millimeter-scale) element concentrations include Au, Ag, Hg, S, As, Bi, Tl, Fe, K, Al, Na, and Ca.



**Figure 52. (Facing page)** Maps showing assembly of the Miocene Bodie Hills volcanic field, California and Nevada, from 15 to 8 Ma based on volcanic stratigraphy (John and others, 2012), mineral deposits, alteration zones, and geochronology. *A*, Northwestern part of the field, 15–13 Ma, consisting of the Masonic volcanic center (green-gray), which includes 15–14 Ma trachyandesite of Masonic and associated volcanoclastic strata, 13.5–12.9 Ma trachyandesite domes, 13.4–13.3 and 13 Ma Au-Ag-Cu deposits of the Masonic Mining District (horizontal line pattern), and the 13.3 Ma Red Wash-East Walker River alteration zone (cross-hatch pattern). Pre-Tertiary rocks are uncolored. *B*, Eastern, central, southwestern, and northeastern parts of the field, 13–9.3 Ma, and the Masonic volcanic center (from *A*; subdued green-gray). The Aurora volcanic center (yellow-green) includes 13–12 Ma trachyandesite of Aurora, ~12 Ma East Brawley Peak alteration zone (cross-hatch pattern), and ~10.5 Ma Au-Ag vein deposits of the Aurora Mining District (horizontal line pattern). The 11.1 Ma Sawtooth Ridge alteration zone (cross-hatch pattern) is adjacent to the Aurora volcanic center to the northwest. Central and southwestern parts of the field (uncolored) include ~11–10 Ma large- to small-volume flows and domes of trachyandesite, rhyolite, and trachydacite (dashed-line enclosures), some of which cover rocks of the Masonic and Aurora volcanic centers, and ~9.7–9.3 Ma Paramount basin (Paramount-Bald Peak alteration zone; blue). Basin-fill deposits of ancestral Fletcher Valley (brown) north of the Aurora volcanic center, and covering parts of the Masonic volcanic center are ~11 Ma. *C*, Northwestern, central, and southwestern parts of the field at 9.3 Ma, and the Masonic volcanic center (subdued green-gray), Aurora volcanic center (subdued yellow-green), large- to small-volume flows and domes (subdued dashed line enclosures), the Paramount basin (subdued blue,) and ancestral Fletcher Valley (brown; from *A* and *B*). Eureka Valley Tuff (Eureka Valley Tuff; 9.5–9.3 Ma; red with dot pattern), derived from the Little Walker caldera ~20 km to the west of Bridgeport, filled depressions and paleochannels (dark, short dashed lines), defined by semialigned Eureka Valley Tuff remnants, in the Masonic volcanic center, and among large- and small-volume flows and domes. *D*, Southeastern part of the field, 10–8 Ma, older volcanic and sedimentary strata (from *A*, *B*, and *C*, subdued), and <9.3 Ma normal faults. Large-volume stratovolcano and flow-dome complexes include 10–9 Ma trachyandesite of Mount Biedeman (green), ~9 Ma trachydacite of Potato Peak (red), ~9 Ma dacite of Silver Hill (orange), and 8.6–8 Ma trachyandesite of Willow Springs (blue), and contain the 8.8–8.2 Ma Cinnabar Canyon alteration zone (and S° resource; cross-hatch pattern), and the 8.5–8.1 Ma Au-Ag vein deposits of the Bodie Mining District (horizontal line pattern).

Although Aldrich Station sediments and flora may not have been derived directly from Bodie Hills volcanism and vegetation, they broadly reflect climate and geography of the region as evidenced by stratigraphic relationships and by three occurrences of plant litter in the northern part of the Bodie Hills. (1) North and northwest of the Aurora Mining District, at elevations of ~7,900 ft (~2.39 km), petrified wood fragments in sedimentary rocks of Fletcher Valley (Tfv of John and others, 2015), deposited on ~11 Ma trachyandesite of Del Monte and beneath 9.3 Ma Eureka Valley Tuff, are contemporaneous with Aldrich Station flora. (2) A cored drill hole ~6.4 km north of the Aurora townsite (fig. 20) encountered gold-bearing sand and gravel beneath ~0.5–0.1 Ma trachyandesite of Aurora Crater (Lange and others, 1993; Lange and Carmichael, 1996), and overlying altered lacustrine sediments that contain carbonized plant fragments (Nevada Exploration Inc., 2013). The cored stratigraphy, which ranges in elevation from 5,470 to ~6,100 ft (<1.66 to ~1.85 km), corresponds to sedimentary rocks of Fletcher Valley; the gold-bearing sand and gravel apparently record erosion of Aurora Mining District Au-Ag veins, and the altered sediments may be similar in age to those veins (~10.5 Ma). (3) In the Bodie Mining District, a 14-in.-diameter silicified tree trunk was found in the drainage west of the Bulwer shaft at ~8,400 ft (~2.45 km; Brown, 1908; fig. 37).

Bodie Hills fossils attest to the presence of woody plants and near-surface groundwater saturation from ~11 Ma, the initial sedimentation of Fletcher Valley, to ~8.5 Ma, the formation of the youngest veins in the Bodie Mining District. Fossil elevations indicate either (1) hundreds to more than 2,000 ft of relief in the Bodie Hills during this period, or (2) differential displacement of fossil-bearing strata since ~11 Ma by magmatic inflation and (or) faults. Paleoelevation estimates of the Aldrich Station flora, which vary by method, are 2,000 to 2,500 ft (~0.6 to 0.8 km; Axelrod, 1956) and ~4,300 to 6,900 ft (~1.3 to 2.1 km; Wolfe, 1995; Wolfe and others, 1997), implying that paleoelevations in the Bodie Hills during flora accumulation, and initial Fletcher Valley sedimentation, were either entirely lower than present elevations, or near present elevations.

## Eureka Valley Tuff in the Bodie Hills

There are few stratigraphic markers among the domes, lavas, debris flows, and sedimentary strata that make up the Bodie Hills volcanic field, and none is regionally distributed. Remnants of externally sourced, ~9.5–9.3 Ma Eureka Valley Tuff in the western and central parts of the field (fig. 52) provide critical stratigraphic, structural, and age datums. Dense to moderate welding, high glass content, confinement of thickest exposures (tens of meters) to the deeply incised East Walker River drainage, and distance from source vents (20–40 km) east of the Little Walker caldera; Pluhar and others, 2009), attest to the low viscosity (high fluidity) of the ash flows. Although fluidal ash flows can be deposited on slopes

(Fisher and Schmincke, 1984), Eureka Valley Tuff exposures in the Bodie Hills are the farthest east from their source, and waning momentum mostly confined deposition to drainages and depressions. Meandering alignments of thinner remnants at higher elevations likely reflect paleotributaries, and isolated remnants mark depressions or eroded channels. Coarse gravel deposits beneath some Eureka Valley Tuff remnants suggest locally steep pre-Eureka Valley Tuff drainage gradients. Therefore, it is assumed that Eureka Valley Tuff filled drainages and depressions to an approximately common elevation, and that basal contacts of Eureka Valley Tuff provide a broad, 9.3 Ma elevation datum. Present elevations of remnants span ~3,550 ft from the East Walker River west of the Elbow (~5,600 ft; fig. 1) to the north slope of Potato Peak (~9,150 ft). This relief was imposed since 9.3 Ma, and indicates that most present relief in the Bodie Hills was caused by magmatic inflation and (or) fault displacement since 9.3 Ma.

## Landforms in Mining Districts and Alteration Zones

### Masonic Mining District

The Au-Ag-Cu deposits at Masonic occur in a sequence of Miocene volcanoclastic deposits and trachyandesite lavas (trachyandesite of Masonic), and in Mesozoic rocks. Deposit ages comprise two groups, one ~13.4–13.3 Ma, and the other ~13 Ma. Both groups of deposits are younger than trachyandesite lavas (~15–14 Ma, fig. 2; table 1) but are similar to the ages of nearby trachyandesite intrusions (~13.5–13.4 and 12.9 Ma, table 1), demonstrating that the deposits formed nearly simultaneously with emplacement of intrusions.

Eureka Valley Tuff (9.5–9.3 Ma) overlies Mesozoic rocks and trachyandesite of Masonic in the southwestern and northwestern parts of the district, and constrains relative elevations of erosional paleosurfaces and fault displacements in the northwestern part of the Bodie Hills. Eureka Valley Tuff lies on granodiorite and metavolcanic rocks on the northwest and south slopes of Masonic Mountain at ~8,600 and 8,775 ft, respectively (fig. 2). It lies on trachyandesite of Masonic at 7,000 to 7,100 ft near the 13.5–13.4 Ma trachyandesite domes (fig. 14). These contacts, which represent a common 9.3 Ma erosional paleosurface, imply ~1,800 ft of down-to-the-north displacement of the domes since ~9.3 Ma, relative to Eureka Valley Tuff on Masonic Mountain. This displacement can be attributed to mapped (figs. 2, 14) and unrecognized, down-to-the-north faults, and (or) to domical uplift of the southern part of the district. About 600–800 ft of normal displacement occurred along a northeast-striking fault that extends through the Chemung Mine and across Masonic Gulch at the site of Masonic middle town (fig. 2). This fault separates Eureka Valley Tuff at 8,600 and 8,775 ft on Masonic Mountain east and southeast of the Chemung Mine from Eureka Valley Tuff at 8,000 ft, 0.8 km (0.5 mi) north-northwest of the Chemung Mine.



Movement on west-east-striking faults on the north side of the 13.5–13.4 Ma trachyandesite domes has displaced trachyandesite of Masonic several hundreds of feet down-to-the-north (fig. 14). This estimate is based on the difference in elevation of moderately extensive exposures of Eureka Valley Tuff near the domes (7,000 to 7,100 ft) and a small exposure of Eureka Valley Tuff in the Red Wash-East Walker River alteration zone (6,695 ft). Therefore, post-9.3 Ma displacement of the Red Wash-East Walker River alteration zone relative to Masonic Mountain could exceed 2,100 ft (fig. 14). This cumulative estimate of post-Eureka Valley Tuff displacement is comparable to the elevation differences between Eureka Valley Tuff on Masonic Mountain and Eureka Valley Tuff at 6,400 to 6,600 ft along the East Walker River west of Masonic Mountain. The deposition of Eureka Valley Tuff on Mesozoic granodiorite indicates that pre-Tertiary rocks of Masonic Mountain were exposed at 9.3 Ma and possibly earlier. However, granitic and metamorphic clasts have not been recognized in 15–14 Ma altered volcanoclastic-flow sequences in the Masonic Mining District.

In the southwestern part of the district, a hydrologic paleosurface is represented by 13.4–13.3 Ma volcanoclastic-pool sinter deposits at the Sarita Mine (fig. 5). The present elevation of these sinters, ~8,400 ft, is as much as 200 ft higher than altered volcanoclastic strata at the Red Rock, Lakeview, and Chemung Mines, ~400 ft higher than the intrusive contact of 12.9 Ma Lakeview Spring domes and trachyandesite of Masonic, and ~400 ft higher than the 9.3 Ma erosional paleosurface at 8,000 ft represented by Eureka Valley Tuff on trachyandesite of Masonic, 0.5 km west of the domes (fig. 2). Although the dome-trachyandesite contact is intrusive, the nearby 9.3 Ma erosional paleosurface implies little erosion of domes and adjacent trachyandesite of Masonic between 12.9 and 9.3 Ma. The elevation differences among the volcanoclastic-pool sinter deposits, volcanoclastic strata, and slightly younger domes have several possible explanations (1) displacement of the Lakeview Spring domes and volcanoclastic strata at the Red Rock, Lakeview, and Chemung Mines relative to the volcanoclastic-pool sinter deposits at the Sarita Mine by faulting; (2) emplacement of Lakeview Spring domes after displacement of the volcanoclastic-pool sinter deposits by faulting; and (3) volcanoclastic-pool sinter landforms with hundreds of feet of relief. Several lines of evidence, including temporal and elevational relationships among Lakeview Spring domes and Eureka Valley Tuff, and sulfur isotope equilibrium temperatures of hydrothermal mineral assemblages, suggest that fault displacement, explanation (1), accounts best for the elevation differences.

Sulfur isotope equilibrium temperatures of coexisting pyrite and alunite at four mines range from 188 to 231 °C (table 2). These temperatures equate to minimum hydrologic paleodepths of ~430–1,000 ft, respectively (estimated graphically from figure 2 in Haas, 1971), assuming that pyrite and alunite precipitated simultaneously in low-salinity water. Relative to the Sarita Mine hydrologic paleosurface, present elevations of mineral pairs at the Pittsburgh-Liberty Mine

(–720 ft), aspen grove prospect (–840 ft), and Perini Mine (–1,040 ft), are broadly similar to estimated paleodepths regardless of alunite age, implying that deposits north and east of the Sarita Mine have not been greatly displaced relative to the Sarita Mine since ~13 Ma, the age of the youngest alunite. However, if the relative hydrologic paleodepth (~1,000 ft) based on the Red Rock Mine isotope equilibrium temperature (231 °C) is accurate, then the Sarita Mine sinters (elev ~8,400 ft) have been displaced down-to-the-northeast as much as 250 m (~800 ft), relative to volcanoclastic strata at the Red Rock Mine (elev 8,200 ft), since ~13.3 Ma.

The terraces of landslide debris and fanglomerate ~0.5 km northwest of the Lakeview Mine (TIs, fig. 2) include weathered clasts of Eureka Valley Tuff (at least on present surfaces), indicating that some, if not all, mass wasting represented by landslide debris has taken place since 9.3 Ma. Deformation and mass wasting are also recorded by relatively steep and variable west-southwest dips (>40°) of originally near-horizontal, 13.4–13.3 Ma volcanoclastic-pool sinter deposits at the Sarita Mine, and by large slide blocks and slope wash of altered volcanoclastic strata immediately north of the Sarita Mine (fig. 2). Although the timing of mass wasting at Sarita relative to the displacement and erosion of Eureka Valley Tuff is unconstrained, these catastrophic erosion features reflect unstable edifices of altered, volcanoclastic, pool sinter deposits that were episodically(?) created by uplift. Based on displacement of Eureka Valley Tuff, uplift of Masonic Mountain relative to volcanoclastic strata at the Red Rock, Lakeview, Chemung, and Sarita Mines primarily occurred since 9.3 Ma along the normal, northeast-striking fault on the northwest side of Masonic Mountain. However, between 12.9 and 9.3 Ma, Sarita Mine sinters may have been displaced downward relative to Lakeview Spring domes and volcanoclastic strata at the Red Rock, Lakeview, and Chemung Mines along a north-trending fault provisionally located between the domes and the Sarita Mine (fig. 2). This fault could account for the disparity among hydrologic paleodepths derived from sulfur isotope equilibrium temperatures.

## Synthesis

Paleosurfaces, stratigraphy, structure, and ages of hydrothermal and igneous minerals enable conditional reconstruction of the geologic and geomorphic evolution of the Masonic Mining District. The volcanoclastic rocks and lavas (trachyandesite of Masonic) that accumulated in depressions or on slopes northwest of Masonic Mountain from ~15 to 14 Ma were altered and Au-Ag-Cu-mineralized at 13.4–13.3 Ma. These strata were bordered to the southeast by an upland of Mesozoic granodiorite and metamorphic rocks, and to the west, northwest, and south by trachyandesite lavas and domes, the sources of volcanoclastic detritus that filled depressions. At 13 Ma, similar Au-Ag-Cu mineralization formed in high-angle fault zones north of Masonic Mountain. The vertical extent of mineable deposits range from the

paleosurface (marked by the volcanoclastic-pool sinter deposits at the Sarita Mine) to ~300 m (~1,000 ft) below the surface in the Pittsburg-Liberty Mine. Uplift of the Masonic Mountain landform by fault displacement may have begun at ~13 Ma, but present relief largely reflects uplift since 9.3 Ma. Post-9.3 Ma differential displacement of volcanoclastic rocks and lavas (trachyandesite of Masonic), volcanoclastic-pool sinter deposits, trachyandesite intrusions, and Eureka Valley Tuff in the district relative to Eureka Valley Tuff along the East Walker River north and west of Masonic Mountain, cumulatively totals at least 640 m (~2,100 ft).

### Aurora Mining District

The ~10.5 Ma Au-Ag veins at Aurora are nearly entirely in ~13.1–12.6 Ma trachyandesite of Aurora; a few veins are in 11.2 Ma rhyolite of Aurora Creek (table 1). Other premineralization eruptive rocks that overlie trachyandesite of Aurora on the north and west sides of the district are 11.5–11.0 Ma trachyandesite of West Brawley Peak and 11 Ma trachyandesite of Del Monte. Rhyolite of Bodie Creek (10.2–9.7 Ma), which partly coincides in age with veins, unconformably overlies trachyandesite of Del Monte ~5 km west of the district. Pliocene and Pleistocene eruptive rocks (3.4–0.1 Ma) unconformably overlie trachyandesite of Aurora and Mesozoic rocks on the northeast, east, and south sides of the district.

Pre and postmineralization landform aspect and relief can be broadly estimated from (1) paleohydrology implied by vein textures, dimensions, and abundance, and by wall-rock alteration; (2) fluid inclusion microthermometry of vein quartz; (3) comparison among several erosional paleosurface elevations (contacts) during vein mineralization and present elevations of premineralization rocks; and (4) postmineralization fault displacement. Vein textures represent open-space filling of tabular conduits that, based on present vein elevations of ~7,200 to 8,400 ft, may have had vertical dimensions of >360 m (>1,200 ft). Vertical dimensions of veins, high vein density, pervasive alteration between veins, and large water/rock volumes implied by quartz  $\delta^{18}\text{O}$  and fluid inclusion  $\delta\text{D}$  values (O'Neil and Silberman, 1974), collectively imply water saturation of trachyandesite of Aurora hundreds of meters below the paleosurface during mineralization.

Low-salinity fluid inclusion populations in veins are interpreted to represent boiling at ~230 °C (and lower temperatures; Osborne, 1985; Knudsen and Prens, 2002), which requires a potentiometric surface ~300 m (~1,000 ft) above fluid inclusion sample elevations (Haas, 1971). Although elevations of some fluid inclusion samples are not well documented, the paleopotentiometric surface elevation above located Juniata vein samples in the northeastern part of the district (present elevation ~7,400 ft; fig. 20), relative to present vein elevations, was ~8,400 ft. If the trachyandesite of Aurora was water-saturated at the surface, as implied by paleohydrologic evidence and Miocene climate, then potentiometric surfaces and erosional paleosurfaces were at the same elevation during mineralization. If similar fluids formed

the Esmeralda-Radical vein, with a present upper elevation of ~8,400 ft, then paleosurface elevations in the southwestern part of the district would have exceeded 9,000 ft. Present maximum elevations of ~11 Ma premineralization volcanic rocks (rhyolite of Aurora Creek; trachyandesite of Del Monte; trachyandesite of West Brawley Peak), those rocks closest in age to vein age (John and others, 2012), vary from ~7,800 to 9,400 ft. The premineralization trachyandesite of Aurora that underlies East Brawley Peak (9,400 ft) was altered to resistant quartz±alunite assemblages at ~12 Ma. If premineralization volcanic rocks were not displaced by postmineralization faults, and if resistant rocks atop East Brawley Peak were not eroded significantly, then paleosurface elevations above veins ranged from ~180 m (~600 ft) higher than volcanic landforms north and west of the district to the approximate elevation of East Brawley Peak in the southwest part of the district.

These lines of evidence and assumptions imply that Aurora district veins formed in a prominent northeast-trending ridge of trachyandesite of Aurora. The ridge extended northeast from East Brawley Peak at least 14 km to the New Esmeralda veins. Adjacent volcanic landforms to the west and northwest were as much as 180 m (~600 ft) lower than ridge elevations. To the north, northeast, and east of the ridge, terrain sloped downward to the lower elevations in Fletcher Valley, which began filling with detritus at ~11 Ma (table 1). The upper elevation of gold-bearing sand and gravel beneath 0.5–0.1 Ma trachyandesite of Aurora Crater (~6,100 ft; Nevada Exploration, Inc. 2013) is similar to elevations in Fletcher Valley 2 km north of Aurora Crater. These colluvial deposits are interpreted to postdate ~10.5 Ma Aurora veins, and support relatively low elevation surfaces north of Aurora during vein erosion.

Oncoidal thermal vents in altered rhyolite of Aurora Creek (fig. 17) ~0.5 km northwest of the Aurora town site (fig. 20), also support the existence of a ridgelike landform during vein formation. These vents, at ~7,600 ft elevation, are ~120 m (~400 ft) above, and presumably coeval with, steam-heated 11.1 Ma alunite (SAW11-9; table 1). They are ~60 m (~200 ft) below the highest present elevation of rhyolite of Aurora Creek. The vents mark a hydrologic paleosurface along the northwest margin of the district that existed ~0.6 m.y. before vein formation. The Juniata vein system potentiometric surface (interpreted as equivalent to the paleosurface; present elevation ~8,400 ft) on the northeast-trending Aurora paleoridge was ~240 m (~800 ft) higher than the oncoidal thermal vents, and at least 120 m (400 ft) higher than rhyolite of Aurora Creek.

Although the extent and orientation of an Aurora paleoridge are constrained by vein distribution and paleohydrology, the proposed relief among 11–10 Ma volcanic landforms is less well constrained because of possible postmineralization fault displacement and erosion. No fluid inclusion microthermometry is available for the Esmeralda-Radical and other Silver Hill veins; these veins may have been displaced upward relative to veins to the northeast by one or more faults. A west-east lineament, prominent on color

air photography and marked by topographic gradients and stream course deflections on Silver, Middle, and Last Chance Hills (CAP lineament, fig. 20), may correspond to a fault that extends west from the district to Beauty Peak. The lineament apparently offsets ~2.5 Ma(?) sedimentary rocks of Martinez Hill that are exposed north of Martinez Hill and in mine open pits from rhyolite of Martinez Hill (Osborne, 1991; Knudsen and Prens, 2002; fig. 20). Down-to-the-north displacement along this inferred fault may have offset vein systems on Humboldt Hill and Last Chance Hill to elevations lower than those of veins on Silver Hill and Middle Hill. Therefore, the original vertical extent of veins may have been <360 m (<1,200 ft). Right-lateral displacement along this prospective fault also may have displaced veins to the northeast, increasing areal vein distribution, although other west-east faults in the Bodie Hills have left-lateral displacement. A second, prominent west-east air-photo lineament south of Brawley Peaks coincides with the stream course south of Spring Peak sinter (fig. 48). This inferred fault may mark the southern margin of a postmineralization, fault-elevated structural block that contains East Brawley Peak and Silver and Middle Hill veins. Restoration of displacement on the west-east faults would decrease elevation differences between the Aurora paleoridge and adjacent premineralization volcanic rocks as well as among veins. Accounting for postmineralization erosion could further reduce the estimated 11–10 Ma relief at Aurora by tens to more than one hundred meters.

The absence of significant placer gold in the district suggests that the present level of erosion, or as much as 300 m (~1,000 ft) below the paleosurface, approximately coincides with the top of high-grade (Au-Ag) vein mineral assemblages. Most ore was mined from within ~150 m (~500 ft) below the present surface, indicating that the vertical interval of elevated Au-Ag grades was ~300–450 m (~1,000–1,500 ft) below the paleosurface. Alternatively, gold in veins was too fine-grained to form mineable placer deposits, and the absence of placer has little relationship to depths of ore formation.

## Synthesis

Landforms in the Aurora Mining District at 10.5 Ma during Au-Ag vein formation consisted of a northeast-elongate, ~14 km ridge of 13.1–12.6 Ma trachyandesite of Aurora. Based on characteristics of veins and altered wall rocks, and relative elevations of contacts, hydrologic paleosurfaces, and paleopotentiometric surfaces among trachyandesite of Aurora and adjacent volcanic rocks, the ridge stood as much as several hundreds of meters above flow-domes of 11.5–11.0 Ma rhyolite and trachyandesite to the west, north, and east. Present relief, the distribution and elevation of veins, and the absence of Au placer deposits, may be partly attributed to antithetical displacement along two west-east faults that elevated ancestral West and East Brawley Peaks, and caused ~300 m (~1,000 ft) of erosion of the trachyandesite paleoridge and veins to the tops of high-grade Au-Ag mineral assemblages.

## Bodie Mining District

The 8.9–8.1 Ma Au-Ag veins at Bodie are ~1.0–0.4 Ma younger than dacite of Silver Hill (9.1–8.9 Ma; table 1), the host rock of all Bodie veins. Dacite of Silver Hill is overlain by slightly younger trachydacite of Potato Peak (9.1–8.7 Ma) within 1 km west, north, and northeast of the district (fig. 37). Trachydacite of Potato Peak is unaltered, lacks veins, and is not known to cover veins. Veins and remnant sinter are exposed at the top of Bodie Bluff at ~9,000 ft. Trachydacite of Potato Peak exposures near Bodie vary in elevation from ~8,200 to 10,168 ft, on the summit of Bodie Mountain. These elevations are ~800 ft lower and nearly 1,200 ft higher than the highest veins on Bodie Bluff. Eureka Valley Tuff (9.5–9.3 Ma) in Milk Ranch Canyon, ~1 km north of the town of Bodie, underlies dacite of Silver Hill, although the substrate is not exposed. Approximately 1 km northeast of Bodie Bluff, it overlies 11 Ma trachyandesite of Del Monte, indicating that dacite of Silver Hill does not extend very far north of Bodie Bluff. At both locations, Eureka Valley Tuff is overlain by trachydacite of Potato Peak.

Sinter atop Bodie Bluff formed on, and possibly within, a 60 m-thick sequence of volcanoclastic deposits that accumulated in a graben between north-northeast-striking, antithetically dipping faults (figs. 37, 38). Open tensional fractures with opposing dips, flanking and beneath the graben, were filled by Incline series and Burgess series veins. Incline series veins occur in dacite of Silver Hill on both sides of the graben at the same elevation as sinter. If sinter is coeval with adjacent veins, then it has been displaced downward relative to veins along the graben faults, and Incline series veins formed within ~60 m (the thickness of volcanoclastic deposits) of the paleosurface marked by the sinter. Alternatively, if sinter is younger than Incline series veins, then sinter and graben-filling volcanoclastic rocks are ~<8.2 Ma, the youngest age of adularia in Incline series veins on Bodie Bluff (table 1). This latter interpretation requires that Incline series veins on Bodie Bluff have been significantly eroded, sinter is temporally associated with Silver Hill series veins (~≤8.2 Ma) or a younger hydrothermal event, and the graben formed between 8.2 and <8.1 Ma.

Regardless of relative and absolute ages of veins and sinter atop Bodie Bluff, the association of sinter and veins, and nearly identical ages of dacite of Silver Hill and trachydacite of Potato Peak, require that Potato Peak rocks either (1) thinly covered dacite of Silver Hill on Bodie Bluff and were eroded prior to sinter deposition, or (2) never covered Bodie Bluff. These possible stratigraphic relationships, and the absence of dacite of Silver Hill north of the district, imply that present relief of the Bodie Bluff landform, considered an intrusion by Chesterman and others (1986), ostensibly reflects eruptive topology. On a regional scale, the Bodie Mining District formed near the northwestern edge of the dacite of Silver Hill dome field where the field is partly overlapped by the eastern extent of Potato Peak flows. Faulting may have elevated Bodie Bluff somewhat along hypothesized bounding faults

(for example, Bodie Creek and Mono faults; fig. 37) but fault displacement, other than graben-forming faults, has not been quantified. Incline series veins occur on both side of the Tioga Fault, and Silver Hill series veins occur on both sides of the Mono Fault, suggesting that displacement along these faults was small.

Domal uplift has been proposed to explain Bodie Bluff relief (Wisser, 1960); episodic doming could account for both tensional fractures filled by Incline series veins, and the apical graben. However, the attitudes of the Fortuna vein and Silver Hill series veins, which consist mostly of replaced fault breccia and gouge and lesser open-space filling, are not plausibly explained by tensional strain. The Fortuna vein may be related to a transtensional structural regime that preceded doming, although a relatively abrupt stress field transition is required given the small differences in vein ages.

High-grade (Au-Ag) Incline series veins on Standard Hill (elev ~8,840 ft) are ~50 m (~160 ft) lower than veins and sinter atop Bodie Bluff. Although temporal relationships between veins and sinter are imprecisely known, the vertical distance between sinter and ore-grade veins in other Tertiary vein districts varies considerably (compare Sherlock, 2005; Vikre, 2007). If sinter atop Bodie Bluff postdates Incline series veins and older Burgess series veins, then vein ore on Standard Hill formed >50 m (>165 ft) below the paleosurface. Since little ore was mined deeper than ~150 m (~500 ft), the vertical range of ore in Incline series and Burgess series veins (fig. 38) was >50–200 m (>165–660 ft) below the paleosurface. Silver Hill series veins, with the exception of veins mined in the Noonday Mine, contained small quantities of ore, and archival samples from the Noonday, Addenda, Oro, and Red Cloud Mines (fig. 40) were all obtained within 600 ft of the surface. If vein samples on the Jupiter, Cupon, and other mine dumps on the south slope of Bodie Bluff (fig. 37) are the same age as Silver Hill series veins, then ore-grade mineralization in Silver Hill series veins formed at least 200–360 m (~660–1,200 ft) below the paleosurface (fig. 38). Fluid inclusion microthermometry could provide paleoelevational control among vein types that would constrain (1) temporal and spatial relationships of sinter to veins, (2) paleodepths of ore deposition, and (3) quantification of postmineralization erosion and fault displacement.

## Synthesis

Time-space relations among volcanic stratigraphy, vein types, and sinter support the following succession of magmatic and hydrothermal events in the Bodie Mining District (1) eruption of dacite flows that covered the southern part of the district; (2) intrusion of dacite into older dacite flows to form Bodie Bluff and other topographically high domes; (3) fracture-filling along the southern margin of the dacite intrusion at Bodie Bluff by Burgess series veins; (4) doming of the dacite intrusion by magmatic inflation, creating tensional fractures that were filled by Incline series veins; (5) transtensional faulting of dacite flows; some faults

became Silver Hill series veins; and (6) further doming of Bodie Bluff, creating an extensional depression that filled with volcanoclastic deposits and sinter. Magmas younger than dacite of Silver Hill that could have domed Bodie Bluff prior to, and after deposition of Incline series veins are not represented in the Bodie Mining District. The nearest volcanic rocks coeval with veins are flows and domes of 8.6–8.0 Ma trachyandesite of Willow Springs, ~10 km to the west. Igneous rocks that are somewhat older than veins include 9.9–8.9 Ma trachyandesite of Mount Biedeman, ~10 km (~6.3 mi) to the southwest, and 9.1–8.7 Ma trachydacite of Potato Peak that borders the western side of the district.

## Alteration Zones

Variable evidence within alteration zones constrains paleosurfaces, paleolandforms, fault displacements, and erosion depths. The relationship of a paleosurface in the Sawtooth Ridge alteration zone to paleolandforms in the Aurora Mining District is described in previous sections of this report. Paleolandforms and postalteration evolution of the Red Wash-East Walker River, Four Corners, Paramount-Bald Peak, Aurora Canyon, Potato Peak, and Cinnabar Canyon-US 395 alteration zones can be reconstructed broadly from stratigraphy, geochronology, and characteristics of hydrothermal mineral assemblages.

The Red Wash-East Walker River alteration zone includes two temporal markers and hydrothermal mineral assemblages that somewhat constrain landforms. The zone formed at ~13.3 Ma, based on alunite ages, mostly in a volcanoclastic-flow sequence within ~15–14 Ma trachyandesite of Masonic (table 1). Altered volcanoclastic-flow rocks were partially covered at 9.5–9.3 Ma by Eureka Valley Tuff, a remnant of which is on the top east side of hill 6,696 (elevation 6,696 ft; fig. 14). Pervasive lateral silicification of permeable volcanoclastic strata presumably minimized erosion of these rocks during the ~3.7 m.y. of exposure prior to deposition of Eureka Valley Tuff. Landforms at 9.3 Ma are envisioned as a series of low hills and shallow depressions aligned in a ~20 km west-east zone with north-south dimensions of 2–5 km (Rockwell, 2010). These low hills were underlain by debris and lavas flows that were variably leached and clay-altered by steam and other gases that condensed in matrices and discontinuous fissures. Depressions among hills consisted of bleached and unvegetated flows that were saturated with groundwater acidified by gas condensation. Fissures (fluid conduits) were most prevalent in the central part of the zone, where lateral permeability in volcanoclastic strata led to pervasive precipitation of silica minerals in leached rocks and fissures, and in subsurface water-saturated flows. Adjacent, less-fractured lavas were variably altered to clay-mica minerals and lesser pyrite.

Variable permeability in the Red Wash-East Walker River alteration zone is reflected by present inverse topography of the resistant, flat-topped hills of quartz-alunite-clay-altered debris flows that have deflected drainages. The resistant hills are flanked by recessively weathering, clay-altered lavas partially covered by gravel terraces (fig. 14). The erosional

surface represented by the Eureka Valley Tuff contact (~6,650 ft elevation) on hill 6,696 is several hundreds of feet (tens to >100 m) higher than elevations of Eureka Valley Tuff (5,600 to 6,200 feet; John and others, 2015) along the East Walker River north of the alteration zone. These elevation differences (at least 135 m; ~450 ft) imply that the present elevation of the alteration zone, and incisement by the north-trending Masonic Gulch, Sonoma Canyon, and Red Wash drainages, occurred since ~9.3 Ma. Dissection of fluvio-lacustrine sediments that overlie the northwestern part of the alteration zone, and gravel terraces south of the resistant central part of the zone (fig. 14), demonstrate that the Fletcher Valley basin was well established by 9.3 Ma.

Paleolandforms in the Paramount-Bald Peak alteration zone can be provisionally reconstructed from groups of sub-aerial terrace and pool sinters in the southwestern, central, and northeastern parts of the alteration zone. These sinter groups occur among upper strata of the ~9.7–9.3 Ma sedimentary rocks and tuff of Paramount (Tpst; fig. 27), which is constrained in age by overlying 9.3 Ma Eureka Valley Tuff and by blocks of 9.7 Ma rhyolite of Bald Peak (John and others, 2012) within the strata. In the southwestern part of the alteration zone, sinters on Paramount Mine hill and hills to the southwest and southeast (Paramount Mine area sinter group; fig. 28) have present elevations of 9,040–8,400 ft. The sinter terrace at Atastra Creek, ~4.2 km southeast of Paramount Mine hill, is at 8,000 ft. Sinters near Hilton Springs in the central part of the alteration zone (Hilton Spring sinters; fig. 28) are at ~7,800 ft. The group of sinters ~2.5 km north-northeast of Bald Peak have present elevations of ~7,200–7,080 ft. Locally, as on Paramount Mine hill, sinter terraces protruded from slopes and do not necessarily represent maximum local paleoelevations. Furthermore, the elevationally tiered sinter groups may not be coeval or represent common paleoelevations. However, the groups formed within several hundreds of thousands of years, they occur at or near the top of sedimentary rocks and tuff of Paramount, and they likely represent a small range in paleoelevation.

Present elevation differences among sinter groups may partially reflect downward displacement to the northeast along faults. Several mapped faults offset sinter groups (fig. 27) but fault displacement may not entirely account for the nearly 2,000 ft of elevation range among sinter groups. Alternatively, elevation differences may reflect magmatic inflation centered on Potato Peak, ~5.5 km south-southwest of Paramount Mine hill, during voluminous Potato Peak trachydacite volcanism at ~9 Ma. The ~1,500 ft elevation difference between the nearly simultaneously formed Potato Peak and Aurora Canyon alteration zones (10.8 and 10.7 Ma, respectively; table 1), ~1.2 km and ~4.2 km northwest, respectively, of Potato Peak, also is not clearly related to fault displacement. Therefore, elevation differences among sinter groups and coeval altered rocks on the north and northwest sides of Potato Peak are provisionally attributed both to fault displacement and landform inflation associated with Potato Peak magmatism. If this interpretation is correct, then much of the present relief of the southern part of the Bodie Hills volcanic field was attained by ~9 Ma.

The Four Corners alteration zone contains small pockets of chemical and clastic sediments that fill depressions in silicified breccia (fig. 20) and resemble similar deposits at the Sarita Mine. Although undated, this small alteration zone is on the range divide at an elevation of 8,600 ft and its preservation supports a young age relative to the ages of larger alteration zones at lower elevations, which are >8 Ma. Exposures in the Four Corners alteration zone apparently have not been modified significantly by erosion or fault displacement.

In the Cinnabar Canyon-US 395 alteration zone, a >8 Ma volcanoclastic-flow sequence was altered to quartz, alunite, kaolinite, and pyrite at 8.8–8.2 Ma (table 1). The altered sequence strata are ~60 m thick where they overlie pre-Tertiary rocks along Clearwater Creek near the mouth of Cinnabar Canyon, but could be somewhat thicker to the north and northwest (possibly 400 ft in the Cinnabar Canyon sulfur resource; fig. 36). Trachyandesite of Willow Springs (~8.6–8.0 Ma) overlies altered sequence strata in numerous places including Cinnabar Canyon (clay-cut hill) and Hot Springs Canyon (fig. 34). Although sequence strata are correlated with 9.9–8.9 Ma sedimentary rocks and debris flows of Mount Biedeman, the slightly younger and similar age ranges of alunite in altered sequence strata (8.8–8.2 Ma; table 1) and unaltered trachyandesite of Willow Springs indicate that exposed sequence surfaces represent a marginally eroded paleosurface. Landforms prevailing during this time resembled those of the Red Wash-East Walker River alteration zone, which consisted of lowlands and depressions of soggy, steaming ground, amidst low hills of variably leached and silicified sequence strata. Cyclic leaching and silicification in parts of the alteration zone reflect a hydrologic regime of fluctuating groundwater saturation levels into which gases derived from cooling magma(s) condensed and oxidized. The Cinnabar Canyon S<sup>o</sup> resource formed in this dynamic environment subjacent to silicified volcanoclastic strata that underlie Cinnabar Hill (Vikre and Henry, 2011). Similar to the Red Wash-East Walker River alteration zone, significant erosion of the Cinnabar Canyon alteration zone was confined to larger drainages (Cinnabar Canyon; Hot Springs Canyon; fig. 34).

### Evolution of Landforms in the Bodie Hills Volcanic Field, 15–3.9 Ma

Evolution of landforms can be broadly reconstructed from several lines of evidence variously described in previous sections of this report (1) paleotopography of the Aldrich Station flora north of the Bodie Hills and provisional correlation of the flora with older sedimentary deposits of Fletcher Valley; (2) paleolandforms and paleosurfaces in mining districts and alteration zones; (3) distribution and elevations of 9.5–9.3 Ma Eureka Valley Tuff; and (4) distribution, elevations, and ages of volcanoes and associated sedimentary rocks that are older and younger than Eureka Valley Tuff. Faults demonstrably older than Eureka Valley Tuff are those filled with 13.3–10.5 Ma veins and altered breccias in the Masonic and Aurora Mining Districts. Common hangingwall

and footwall strata in these districts preclude estimation of displacement along these structures. Veins and faults in the Bodie Mining District, which are younger than Eureka Valley Tuff, have measured and suspected displacements of tens of meters or less. Most mapped or proposed faults that offset Eureka Valley Tuff also have common wall rocks. Estimates of displacement, tens of meters, are derived from elevations of contacts of Eureka Valley Tuff and underlying strata. Because of the structural and stratigraphic significance of Eureka Valley Tuff, which is distributed throughout much of the Bodie Hills, landform evolution has been reconstructed here relative to this marker.

### Northwestern Bodie Hills, 15–9.3 Ma

Based on paleosurfaces and paleolandforms in the Masonic Mining District and Red Wash-East Walker River alteration zone, the northwestern part of the Bodie Hills volcanic field at 12.9 Ma consisted of a broad upland (~500 km<sup>2</sup>) of 15–12.9 Ma trachyandesite flows, volcaniclastic strata, and domes (Masonic volcanic center; fig. 52A). The domes (15–14, 13.5–13.4, and 12.9 Ma), included a prominent edifice south of Masonic Mountain, and protrusions of Mesozoic granitic and metamorphic rocks (ancestral Masonic Mountain) punctuated by relatively subdued upland topography. Basin-fill deposits, which contain 11–10 Ma tephra, partly cover strata of the Masonic volcanic center (fig. 52B), indicating that a depression (ancestral Fletcher Valley) existed north and northeast of Masonic Mountain by 11 Ma. By 9.5 Ma, numerous water courses incised the upland, some of which drained north to northeast toward ancestral Fletcher Valley. Paleodrainages, including the present East Walker River, subparallel water courses, and depressions west, southwest, and northwest of ancestral Masonic Mountain, are now marked by relatively thick and contiguous deposits of 9.5–9.3 Ma Eureka Valley Tuff (fig. 52C). The lowest elevation exposure of Eureka Valley Tuff, ~5,600 ft along the East Walker River north of the Masonic volcanic center, implies that detritus in the western part of Fletcher Valley was derived from uplands in the vicinity of Masonic Mountain. Present elevations of domes and Masonic Mountain relative to the highest elevation of Eureka Valley Tuff suggest that relief in the northwestern Bodie Hills at 9.5 Ma was tens to hundreds of meters (hundreds of feet), and probably ≤20 percent of present relief.

### Eastern Bodie Hills, 13–9.5 Ma

In the eastern part of the Bodie Hills volcanic field, the prominent paleolandform in the Aurora Mining District and East Brawley Peak alteration zone at ~10.5 Ma was an elongate ridge of 13.1–12.6 Ma trachyandesite of Aurora (Aurora volcanic center; ~130 km<sup>2</sup>; 51 mi<sup>2</sup>; fig. 52B). The ridge extended ~14 km northeast from ancestral East Brawley Peak, and was flanked to the north and west by relatively small-volume trachyandesite and rhyolite flow-dome fields (~≤50 km<sup>2</sup>) at similar to lower elevations. No Eureka Valley Tuff exists near Aurora to mark drainages and depressions

that developed by 9.5 Ma. Basin-fill deposits that overlie 13–11 Ma eruptive rocks north of Aurora, coupled with the 11.1 Ma age of unwelded tuff in Fletcher Valley sedimentary strata (table 1), confirm that Fletcher Valley bordered the volcanic field to the north by 11 Ma. Gold-bearing sand and gravel deposits that overlie altered lacustrine strata beneath Holocene trachyandesite of Aurora Crater (Nevada Exploration Inc., 2013) also support low elevations north of the Aurora Mining District by 10.5 Ma. Relative to the basin-fill deposits, relief in the eastern Bodie Hills at 9.5 Ma was tens to hundreds of meters (hundreds of feet), probably ≤25 percent of present relief.

### Central and Southern Bodie Hills, 15–9.5 Ma

From ~15 to 12 Ma, Mesozoic rocks were apparently exposed between the Masonic and Aurora volcanic centers because only small-volume (~13 km<sup>2</sup>) trachydacite of Rough Creek was erupted between those centers. From ~11 to 10 Ma, numerous large- (~30–50 km<sup>2</sup>) to small-volume (<20 km<sup>2</sup>) flows and domes of trachyandesite, rhyolite, and trachydacite erupted between, north, and south of the Masonic and Aurora centers. Several large-volume flow sequences and lava domes partly covered the Masonic and Aurora centers, and contributed detritus and tuff to a central depression, the 9.7–9.3 Ma Paramount basin (fig. 52B). These permeable volcaniclastic strata were pervasively altered (Paramount-Bald Peak alteration zone) by artesian hydrothermal fluids that built numerous sinter terraces (fig. 27), several of which are associated with the Hg deposit at the Paramount Mine (fig. 28). Fluid circulation may have been driven by a concealed intrusion spatially related to ~9.7 Ma Bald Peak rhyolite.

### Eureka Valley Tuff, 9.5–9.3 Ma

By 9.3 Ma, drainages and depressions among 15–10 Ma eruptive rocks and Mesozoic rocks in the central and western parts of the Bodie Hills volcanic field had been at least partly filled with ash flows and reworked tephra deposits of the externally sourced Eureka Valley Tuff (fig. 52C). Semialigned remnants and elongate exposures of Eureka Valley Tuff mark paleochannels, several of which are subparallel to the East Walker River. Present elevations of Eureka Valley Tuff exposures, contiguous with large- and small-volume volcanic centers, indicate relief of tens of meters (tens to hundreds of feet) at the time of Eureka Valley Tuff eruption.

### Southeastern Bodie Hills, 10–8 Ma

Four large-volume, coalesced volcanic centers (~150–70 km<sup>2</sup>) were emplaced in the southern Bodie Hills at 10–8 Ma (fig. 52D). From 10–9 Ma, trachydacite and associated volcaniclastic deposits formed a large flow-dome complex centered on Potato Peak while trachyandesite lava and associated debris flows were erupted from the Mount Biedeman stratovolcano, in part simultaneously with eruption of Eureka Valley Tuff. Rocks from these volcanic centers

partly covered strata of the Masonic volcanic center, and 11–10 Ma large- and small-volume volcanoes. From 9 to 8 Ma, extensive flow-dome complexes were emplaced east (dacite of Silver Hill) and west (trachyandesite of Willow Springs) of Potato Peak. These volcanic edifices were partly altered by hydrothermal systems that formed Bodie district Au-Ag veins (8.5–8.1 Ma), the extensive Cinnabar Canyon alteration zone (8.8–8.2 Ma; fig. 52D), and the S° resource in the Cinnabar Canyon alteration zone.

### Bodie Hills Landforms, 8–3.9 Ma

At 8 Ma, landforms in the central and southern parts of the Bodie Hills volcanic field were dominated by the 10–8 Ma volcanoes centered on Potato Peak and Mount Biedeman, and by adjacent, small-volume volcanoes. Since 8 Ma, only a few small-volume landforms (~6.2–5.4 Ma rhyolite and dacite flow-domes; John and others, 2012) have been added to the Bodie Hills volcanic field. Since 8 Ma, the 10–8 Ma volcanoes have been marginally eroded, and vent-filling plugs of trachydacite on Potato Peak (10,237 ft) and Mount Biedeman (8,962 ft) are among the highest elevations in the Bodie Hills. At ~8 Ma, the elevation difference between the top of the Potato Peak volcano and Eureka Valley Tuff beneath trachydacite of Potato Peak lava flows in the Bodie Mining District (~8,500 ft, fig. 37), was at least 1,737 ft, discounting unquantified post-8 Ma erosion of ancestral Potato Peak. The difference in elevation between the Potato Peak volcano and Fletcher Valley at 8 Ma, assuming a common paleoelevation for Eureka Valley Tuff at Bodie, along the East Walker River, and in Fletcher Valley, would also have been 1,737 ft (or more). The present elevation difference between Potato Peak, East Walker River, and Fletcher Valley, ~4,600–4,200 ft, suggests that most prevailing relief (>60 percent) in the Bodie Hills has developed since 8 Ma. Given the absence of significant faults in the southern part of the volcanic field (John and others, 2012), this relief largely reflects magmatic inflation during growth of 10–8 Ma volcanoes in the southern part of the volcanic field.

Small increments of relief have been added to northwestern and eastern parts of the field by displacement along west-east, and north-northeast-striking normal faults that have been mapped or are expressed by lineaments on color air photographs (fig. 52D), although stratigraphic displacement along lineaments is not always evident. A north-northwest-trending fault that apparently borders the east side of Bridgeport Valley also contributed to relief of the volcanic field. The west-east and northeast-striking faults have displaced trachyandesite north of Masonic (fig. 14) and at Aurora (fig. 20), mostly by down-to-the-north movement of tens of meters. North of Masonic, displacement along west-east faults perched fluvial lacustrine deposits relative to Fletcher Valley basin-fill. Elevations of sinter groups in the Paramount basin differ by tens to hundreds of meters (<2,000 ft; fig. 27). These elevation differences reflect both post-9.3 Ma, down-to-the-east displacement along north-striking faults (fig. 52D), and magmatic

inflation during construction of the 9 Ma Potato Peak volcano. The volcanic centers at Masonic and Aurora also may have acquired additional relief by magmatic inflation during construction of the 10–8 Ma Mount Biedeman stratovolcano, and by flow-dome complex development in the southern part of the volcanic field. Distribution of Pliocene-Holocene volcanic rocks of the Aurora volcanic field in the eastern Bodie Hills does not appear to have been significantly modified by faults, although these rocks are cut by numerous northeast-striking faults in the eastern and southeastern parts of the Bodie Hills (John and others, 2015). Other landform modifications since 8 Ma include incision by drainages that mostly originated in the trachyandesite uplands at Masonic, Aurora, Potato Peak, and Mount Biedeman.

### Relief and Absolute Paleoelevations

Pre-Eureka Valley Tuff relief in the 15–10 Ma Masonic and Aurora volcanic centers is estimated at tens to hundreds of meters (tens to >1,000 ft). The highest and lowest remnants of Eureka Valley Tuff, on Potato Peak (~9,150 ft) and near the confluence of the East Walker River and Red Wash (~5,600 ft), respectively, differ in elevation by ~3,550 ft. Potato Peak, which formed after emplacement of Eureka Valley Tuff, is at least 4,600 ft higher than the lowest Eureka Valley Tuff, and ~4,200 ft higher than Fletcher Valley (present elevation ~6,100–6,000 ft). The smaller elevation difference between Potato Peak and Fletcher Valley, ~4,200 ft, apparently reflects ~400 ft of basin fill added since 9.3 Ma. This estimate is supported by ~600 ft (~180 m) of gold-bearing sand and gravel deposits in drill holes beneath Holocene trachyandesite of Aurora Crater (Nevada Exploration Inc., 2013). The colluvial deposits overlie altered lacustrine strata that may be the same age as, or older than, ~10.5 Ma Aurora district veins ~4 km to the south. Therefore, relief within the Bodie Hills volcanic field, created by volcano construction, magmatic inflation, fault displacement, and erosion since 15 Ma, totaled at least 4,200 ft and likely exceeded 4,600 ft.

Absolute elevations during landform evolution in the Bodie Hills volcanic field can be estimated from paleoelevations of the 11 Ma Aldrich Station flora. If elevations in the Masonic and Aurora volcanic centers at 11 Ma were 2,500–2,000 ft (Axelrod, 1956), then elevations have increased by at least 6,100 ft (~1,850 m) in the northwestern and eastern parts of the volcanic field (present elevation of Eureka Valley Tuff remnants on Masonic Mountain are 8,600 and 8,775 ft), and elevations have been increased by ~8,000 ft (~2,425 m) to account for the present elevation of Potato Peak. If paleoelevations of Aldrich Station flora were 4,300–6,900 ft (Wolfe, 1995; Wolfe and others, 1997), then elevations at Masonic increased by ~1,700–4,300 ft (~515–1,300 m), and at Potato Peak by ~3,300–5,900 ft (~1,000–1,790 m) since 11 Ma. If ~11 Ma sediments containing fossils in the northern Bodie Hills are stratigraphically equivalent to Aldrich Station flora, then the Bodie Hills have been elevated an additional 1,700 ft (515 m), or ~3,400–7,600 ft (~1,030–2,300 m), since 11 Ma.

Therefore, based on present elevations of Eureka Valley Tuff remnants, Potato Peak, Fletcher Valley, and fossil-bearing sediments, the higher paleoelevation range estimate (4,300–6,900 ft) for Aldrich Station flora is more consistent with relief developed in the Bodie Hills since 9.3 Ma (at least 4,200–4,600 ft; ~1,279–1,400 m). Relative to Aldrich Station flora, elevations in the northwestern part of the Bodie Hills volcanic field at 9.3 Ma were ~4,300–6,900 ft, and possibly hundreds to more than 1,000 feet higher in the eastern part of the volcanic field. At 8 Ma, after eruption of large-volume stratovolcanoes and flow-dome complexes in the southern part of the Bodie Hills volcanic field, maximum elevations exceeded 8,500 ft, and could have approached 10,000 ft (ancestral Potato Peak).

## Summary

Significant conclusions of this investigation are summarized as follows:

1. The 15–6 Ma Bodie Hills volcanic field consists of coalescing stratovolcanoes and lava domes that were assembled on an irregular pre-Tertiary surface of Paleozoic and Mesozoic metamorphic and Cretaceous granitic rocks. The field is part of a subduction-related alignment of predominantly andesitic eruptive rocks that parallels the western margin of North America. Volcanic rocks are predominantly trachyandesite, lesser trachydacite, and subordinate rhyolite that commonly contain phenocrysts of plagioclase, pyroxene, hornblende, biotite, sanidine, and quartz, and have compositions similar to subduction magmas elsewhere. Three Au-Ag-Cu mining districts and nine aerially extensive alteration zones, one of which contains a significant sulfur (S<sup>o</sup>) resource, occur mostly in the volcanic rocks.
2. The Masonic Au-Ag-Cu Mining District (production of 0.056 Moz Au, 0.04 Moz Ag, and minor Cu) includes two styles of mineralization, ~13 Ma fault breccia and vein deposits, and ~13.3 Ma clastic and hydrothermal sedimentary deposits. Deposits occur in ~15–14 Ma trachyandesite of Masonic and pre-Tertiary rocks, and are temporally associated with ~13.5 and ~13 Ma trachyandesite and andesite domes. Both types consist of quartz, alunite, lesser kaolinite, pyrophyllite and sericite, pyrite, enargite, Au-rich electrum, and numerous Cu-As-Sb-Fe-Bi-Au-Ag-S-Se-Te minerals.
3. The Aurora Au-Ag Mining District (estimated production of 1.91 Moz Au and 21 Moz Ag production) includes ~10.5 Ma layered quartz-adularia-sericite-electrum-sulfide veins in ~13.1–12.6 Ma trachyandesite of Aurora that is altered to sericite, K-feldspar, pyrite, chlorite, albite, calcite, and montmorillonite.
4. The Bodie Au-Ag Mining District (production of 1.46 Moz Au and 7.3 Moz Ag) includes at least three, ~8.9–8.1 Ma quartz-adularia-sericite-sulfide-telluride vein series that are distinguished by textures, ages, and mineralogy. The vein series occur in ~9 Ma dacite of Silver Hill.
5. Alteration zones include quartz-alunite-pyrite(iron oxide)-dominant assemblages that vary in age from ~13.3 to 8.2 Ma, and quartz-kaolinite-montmorillonite-dominant assemblages that are ~9.7–9.3 Ma and include sinter. The alteration zones occur in rocks that are the same age to ~2 m.y. older than hydrothermal minerals. Small amounts of Hg were recovered from deposits in several alteration zones (Potato Peak; Paramount-Bald Peak; Cinnabar Canyon-US 395; Spring Peak), a sulfur resource occurs in the Cinnabar Canyon-US 395 alteration zone.
6. The evolution of landforms during the assembly, alteration, and erosion of the volcanic field, based on volcanic stratigraphy, geochronology, and hydrothermal mineral assemblages, began with construction of the large 15–13 Ma Masonic and 13–12 Ma Aurora volcanic centers that mark the northwestern and northeastern parts of the field. Smaller volcanoes erupted at ~11–10 Ma in, between, and south of these centers as erosional detritus accumulated north of the field in Fletcher Valley. Distally sourced, 9.7–9.3 Ma Eureka Valley Tuff filled drainages and depressions among older volcanoes and was partly covered by nearly synchronous eruptives during construction of four large 10–8 Ma volcanoes, which comprise the southern part of the field. The scarcity of significant internal fault displacement, distribution of Eureka Valley Tuff, and elevation estimates derived from floras, suggest that the Bodie Hills volcanic field attained present elevations mostly through volcano construction and magmatic inflation, and that maximum paleoelevations (>8,500 ft) at the end of large volume eruptions at ~8 Ma are similar to present elevations.

## Acknowledgments

Numerous individuals and institutions provided maps, reports, specimens, and site access that greatly enhanced description of mining districts and alteration zones, and characterization of ores. Unpublished mine maps, geologic maps, and reports from the Masonic, Aurora, and Bodie Mining Districts by Page Blakemore, Robert Hatch, C. Hogge, Richard Kern, Peter Knudsen, Edmond Lawrence, N. Lehman, Anthony Payne, Neil Prenn, William Rehrig, David Shaddrick, Miles Silberman, Amer Smailbogevic, Scott Tregaskis, and Robert Wilson significantly supplemented published accounts. Archival mining district files maintained on-line by the



Nevada Bureau of Mines and Geology were the source of some of these unpublished reports and maps. Simon Poulson provided some sulfur isotope analyses, Larry Snee provided several  $^{40}\text{Ar}/^{39}\text{Ar}$  dates, and Jim Rytuba provided some geochemical analyses. LA ICP-MS traverses of sinter and vein sections were done under the guidance of Alan Koenig in his laboratory. Discussions and field tours of several districts and alteration zones with Ken Brook, Tony Eng, and Greg Kouzma led to productive sharing of geologic information and perspectives. Rachel Dolbier and D.D. LaPointe of the Keck Museum, University of Nevada Reno (Reno, Nevada), and Darci Moore of the California State Mining and Mineral Museum (Mariposa, California) graciously loaned archival specimens from the Aurora and Bodie Mining Districts. Mark Langner, Thomas Gunther, Joshua Heitzmann, and Tamara Sasaki of the Department of Parks and Recreation, State of California, provided ready access to Bodie State Historic Park and permission to collect samples. Thorough reviews of a draft manuscript by John Slack and Jeff Mauk led to many improvements in the final version.

## References Cited

- Al-Rawi, Y.T., 1969, Cenozoic history of the northern part of Mono Basin, California and Nevada: Berkeley, University of California, Ph.D. dissertation, 163 p.
- Angel, M., ed., 1881, History of Nevada with illustrations and biographical sketches of its prominent men and pioneers: Oakland, Calif., Thompson and West, 680 p.
- Archbold, N.L., 1966, Industrial mineral deposits of Mineral County, Nevada: Nevada Bureau of Mines and Geology Report 14, 32 p.
- Atwater, Tanya, and Stock, J., 1998, Pacific-North America plate tectonics of the Neogene southwestern United States—An update: *International Geology Review*, v. 40, p. 375–402.
- Axelrod, D.I., 1956, Mio-Pliocene floras from west-central Nevada: *University of California Publications in Geological Sciences*, v. 33, 322 p.
- Barton, M.D., 1980, The Ag-Au-S system: *Economic Geology*, v. 75, p. 303–316.
- Barton, M.D., Kieft, C., Burke, E.A.J., and Oen, I.S., 1978, Uytendogaardtite—A new silver-gold sulfide: *Canadian Mineralogist*, v. 16, p. 651–657.
- Blake, W.P., 1869, Report upon the precious metals: Being statistical notices of the principal gold and silver producing regions of the world represented at the Paris Universal Exposition: Washington, D.C., Government Printing Office, 369 p.
- Bodie Consolidated Mining Company Collection, 2003, California Department of Parks and Recreation, Sacramento, California; microfilm copy in Special Collections, University of Nevada Reno, available at <http://innopac.library.unr.edu/search~S6?/dBodie+Consolidated+Mining+Company/dbodie+consolidated+mining+company/-3%2C-1%2C0%2CB/frameset&FF=dbodie+consolidated+mining+company&1%2C1%2C>.
- Brady's map of Aurora and Esmeralda, 1862, E.J. Mathews and Company, Aurora, and Wakelee and Charles, San Francisco, available at <http://www.delamare.unr.edu/Maps/digitalcollections/nvmaps/histgeo>.
- Breit, F.J., 2000, Structural and temporal relationship and geochemical characteristics of the East Brawley Peak acid-sulfate prospect and the adjacent Aurora adularia-sericite system: University of Nevada Reno, M.S. thesis, 219 p.
- Brown, H.G., 1908, The vein-system of the Standard Mine, Bodie, Calif.: *Transactions of the American Institute of Mining Engineers*, v. 38, p. 343–357.
- Browne, J. R., 1865, A trip to Bodie Bluff and the Dead Sea of the West: *Harper's New Monthly Magazine*, p. 274–284, p. 411–419.
- Burchard, H.C., 1881, Report of the Director of the Mint: Washington, D.C., Government Printing Office, p. 38–47.
- Burchard, H.C., 1882, Report of the Director of the Mint upon the statistics of the production of the Precious metals in the United States: Washington, D.C., Government Printing Office, p. 51–60.
- Burchard, H.C., 1884, Report of the Director of the Mint upon the statistics of the production of the Precious metals in the United States during the calendar year 1883: Washington, D.C., Government Printing Office, p. 173–176.
- Chaussidon, M., Albarede, F., and Sheppard, S.M.F., 1989, Sulphur isotope variations in the mantle from ion microprobe analyses of micro-sulphide inclusions: *Earth and Planetary Science Letters*, v. 92, p. 144–156.
- Chesterman, C.W., Chapman, R.H., and Gray, C.H., 1986, Geology and ore deposits of the Bodie mining district, Mono County, California: *California Division of Mines and Geology, Bulletin 206*, 36 p.
- Chesterman, C.W., and Gray, C.H., Jr., 1975, Geology of the Bodie 15-minute quadrangle, Mono County, California: *California Division of Mines and Geology, Map Sheet 21*, scale 1:48,000.
- Clarke, H.G., 1882, Aurora, Nevada—A little of its history, past and present: *The School of Mines Quarterly*, v. 3, p. 133–136.

- Couch, B.F., and Carpenter, J.A., 1943, Nevada's metal and mineral production: Nevada Bureau of Mines and Geology Bulletin 37, 159 p.
- Dalrymple, G.B., and Lanphere, M.A., 1974,  $^{40}\text{Ar}/^{39}\text{Ar}$  age spectra of some undisturbed terrestrial samples: *Geochimica et Cosmochimica Acta*, v. 38, p. 715–738.
- du Bray, E.A., John, D.A., Box, S.E., Vikre, P.G., Fleck, R.J., and Cousens, B.L., 2013, Petrographic and geochemical data for Cenozoic volcanic rocks of the Bodie Hills, California and Nevada: U.S. Geological Survey Data Series 764, 10 p., <http://pubs.usgs.gov/ds/764/>.
- Eakle, A.S., Huguenin, E., McLaughlin, R.P., and Waring, C.A., 1917, Mines and mineral resources of Alpine County, Inyo County, Mono County: California State Mining Bureau, Fifteenth annual report of the State Mineralogist, p. 5–175.
- Eakle, A.S., and McLaughlin, R.P., 1919, Mono County: California State Mining Bureau, Report XV of the State Mineralogist, Sacramento, p. 135–175.
- Eaton, G.P., Wahl, R.R., Prostka, H.J., Mahey, D.R., and Kleinkopf, M.D., 1978, Regional gravity and tectonic patterns—Their relation to late Cenozoic epeirogeny and lateral spreading in the western Cordillera, *in* Smith, R.B., and Eaton, G.P., eds., *Cenozoic tectonics and regional geophysics of the Western Cordillera*: Geological Society of America Memoir 152, p. 51–91.
- Etoh, J., Izawa, E., Watanabe, K., Taguchi, S., and Sekine, R., 2002, Bladed quartz and its relationship to gold mineralization in the Hishikari low-sulfidation epithermal gold deposit, Japan: *Economic Geology*, v. 97, p. 1841–1851.
- Evernden, J.F., and James, G.T., 1964, Potassium-Argon dates and the Tertiary florae of North America: *American Journal of Science*, v. 262, p. 945–974.
- Faulds, J.E., and Henry, C.D., 2008, Tectonic influences on the spatial and temporal evolution of the Walker Lane—An incipient transform fault along the evolving Pacific – North American plate boundary, *in* Spencer, J.E., and Tittley, S.R., eds., *Ores and orogenesis—Circum-Pacific tectonics, geologic evolution, and ore deposits*: Arizona Geological Society Digest 22, p. 437–470.
- Ferguson, H.G., 1929, The mining districts of Nevada: *Economic Geology*, v. 24, p. 115–148.
- Field, C.W., and Fifarek, R.H., 1985, Light stable-isotope systematics in the epithermal environment, *in* Berger, B.R., and Bethke, P.M., eds., *Geology and geochemistry of epithermal systems*, *Reviews in Economic Geology*, v. 2, p. 99–128.
- Fisher, R.V., and Schmincke, H.-U., 1984, *Pyroclastic rocks*: New York, Springer-Verlag, 472 p.
- Fleck, R.J., du Bray, E.A., John, D.A., Vikre, P.G., Cosca, M.A., Sneek, L.W., and Box, S.E., 2015, Geochronology of Cenozoic rocks in the Bodie Hills Volcanic Field, California and Nevada: U.S. Geological Survey Data Series 916, 26 p., <http://dx.doi.org/10.3133/ds916>.
- Fleck, R.J., Sutter, J.F., and Elliot, D.H., 1977, Interpretation of discordant  $^{40}\text{Ar}/^{39}\text{Ar}$  age-spectra of Mesozoic tholeiites from Antarctica: *Geochimica et Cosmochimica Acta*, v. 41, p. 15–32.
- Giesemann, A., Jager, H.J., Norman, A.L., Krouse, H.P., and Brand, W.A., 1994, On-line sulfur-isotope determination using an elemental analyzer coupled to a mass spectrometer: *Analytical Chemistry*, v. 66, p. 2816–2819.
- Gilbert, C.M., Christiansen, M.N., Al-Rawi, Y., and Lajoie, K.R., 1968, Structural and volcanic history of Mono Basin, California-Nevada, *in* Coats, R.R., and others, eds., *Studies in volcanology*: Geological Society of America Memoir 116, p. 275–329.
- Gilbert, C.M., and Reynolds, M.W., 1973, Character and chronology of basin development, western margin of the Basin and Range Province: *Geological Society of America Bulletin*, v. 84, p. 2489–2510.
- Gilbert, J.R., 1976, .42 minerals inventory and analysis of the Walker Planning Unit, Carson City District, Nevada and California: Bureau of Land Management Report, document 00400009, 149 p., accessed June 2013 at <http://www.nbmj.unr.edu/mdfiles/mdfiles.php>.
- Grassineau N.V., Matthey D.P. and Lowry D., 2001, Sulfur isotope analysis of sulfide and sulfate minerals by continuous flow-isotope ratio mass spectrometry: *Analytical Chemistry*, v. 73, p. 220–225.
- Green, W.R., 1964, Structural control of mineralization at the Aurora mining district: University of Nevada Reno, M.S. thesis, 41 p.
- Gumble, G.E., Warren, R., Whitehead, M.L., and Enders, M.S., 1991, Summary of the geology of the northern part of the Bodie mining district, Mono County, California, *in* Schafer, R.W., Bonham, H.F., and Silberman, M.L., eds., *Diverse tectonic setting for epithermal volcanic-hosted precious metal deposits along the Nevada-California border*, Great Basin Symposium Field Trip 9, Geological Society of Nevada, Reno, Nevada, p. 619–623.
- Haas, J.L., 1971, The effect of salinity on the maximum thermal gradient of a hydrothermal system at hydrostatic pressure: *Economic Geology*, v. 66, p. 940–946.

- Hardyman, R.F., and Oldow, J.S., 1991, Tertiary tectonic framework and Cenozoic history of the central Walker Lane, Nevada, *in* Raines, G.L., Lisle, R.E., Schafer, R.W., and Wilkinson, W.H., eds., *Geology and ore deposits of the Great Basin: Geological Society of Nevada, Symposium Proceedings*, Reno, Nev., p. 279–301.
- Herrera, P.A., Closs, L.G., and Silberman, M.L., 1993, Alteration and geochemical zoning in Bodie Bluff, Bodie mining district, eastern California: *Journal of Geochemical Exploration*, v. 48, p. 259–275.
- Hill, J.M., 1915, Some mining districts in northeastern California and northwestern Nevada: *U.S. Geological Bulletin* 594, 200 p.
- Hollister, V.F., and Silberman, M.L., 1995a, Geology and epithermal silver-gold bulk-mining targets, Bodie district, Mono County, California: *Nonrenewable Resources*, v. 42, p. 129–137.
- Hollister, V.F., and Silberman, M.L., 1995b, Silver-gold and polymetallic quartz veins in the Bodie mining district east-central California—Are they related to a porphyry Cu-Mo system at depth?, *in* Pierce, F.W., and Bolm, J., eds., *Porphyry copper deposits of the American Cordillera*, Arizona Geological Society Digest 20, p. 297–305.
- Holmes, G.H., 1965, Mercury in California, *in* *Mercury potential of the United States: U.S. Bureau of Mines Information Circular* 8252, p. 87–206.
- Jenkins, O.P., 1951, Mono County: *California Journal of Mines and Geology*, v. 47, no. 2, p. 342–343.
- John, D.A., du Bray, E.A., Blakely, R.J., Fleck, R.J., Vikre, P.G., Box, S.E., and Moring, B.C., 2012, Miocene magmatism in the Bodie Hills volcanic field, California and Nevada: A long-lived eruptive center in the southern segment of the ancestral Cascades arc: *Geosphere*, v. 8, p. 44–97.
- John, D.A., du Bray, E.A., Box, S.E., Vikre, P.G., Rytuba, J.J., Fleck, R.J., and Moring, B.C., 2015, Geologic map of the Bodie Hills, California and Nevada: *U.S. Geological Survey Scientific Investigations Map* 3318, 64 p., 2 sheets, scale 1:50,000, <http://dx.doi.org/10.3133/sim3318>.
- Johnson, R.F., 1951, *Geology of the Masonic mining district, Mono County, California: University of California, M.A. thesis*, 51 p.
- Kinetic Gold Corp., 2013, Spring Peak Project, accessed December 14, 2013, at <http://www.kineticgold.com/s/SpringPeak.asp>.
- King, C., Emmons, S.F., and Becker, G.F., 1885, *Statistics and technology of the precious metals: Washington, D.C., Department of the Interior, Census Office, Government Printing Office*, 541 p.
- Kister, R.W., 1966, Structure and metamorphism in the Mono Craters Quadrangle, Sierra Nevada: *U.S. Geological Survey Bulletin* 1221-E, 53 p.
- Kleinhampl, F.J., Davis, W.E., Silberman, M.L., Chesterman, C.W., Chapman, R.H., and Gray, C.H., 1975, Aeromagnetic and limited gravity studies and generalized geology of the Bodie Hills region, Nevada and California: *U.S. Geological Survey Bulletin* 1384, 38 p.
- Knudsen, P., and Prenn, N., 2002, Technical report on the Esmeralda Project, Mineral County, Nevada U.S.A.: *Mine Development Associates*, 121 p., available at <http://www.secinfo.com/dVut2.215aw.htm>.
- Lange, R.A., and Carmichael, I.S.E., 1996, The Aurora volcanic field, California-Nevada: oxygen fugacity constraints on the development of andesitic magma: *Contributions to Mineralogy and Petrology*, v. 125, p. 167–185.
- Lange, R.A., Carmichael, I.S.E., and Renne, P., 1993, Potassic volcanism near Mono Basin, California—Evidence for high water and oxygen fugacities inherited from subduction: *Geology*, v. 21, p. 949–952.
- Lawrence, E.F., 1987, Geologic report on the southern half of the Aurora mining district, Mineral County, Nevada: *Bureau of Land Management Report*, document 04100099, 118 p., available at <http://data.nbmj.unr.edu/Public/MiningDistricts/0410/04100099.pdf>.
- Le Bas, M.J., Le Maitre, R.W., Streckeisen, A., Zanettin, B.A., and IUGS Subcommittee on the Systematics of Igneous Rocks, 1986, Chemical classification of volcanic rocks based on the total alkali-silica diagram: *Journal of Petrology*, v. 27, p. 745–750.
- Long, K.R., DeYoung, J.H., and Ludington, S.D., 1998, Database of significant deposits of gold, silver, copper, lead, and zinc in the United States: *U.S. Geological Survey Open-File Report* 98-206 A, B, 33 p., available at <http://pubs.usgs.gov/of/1998/0206a-b/>.
- McDougall, L., and Harrison, T.M., 1999, *Geochronology and thermochronology by the <sup>40</sup>Ar/<sup>39</sup>Ar method (2d ed.): Oxford, Oxford University Press*, 269 p.
- McLaughlin, R.P., 1907, *Geology of the Bodie district, California: Mining and Scientific Press*, v. 94, p. 795–796.
- McLaughlin, R.P., 1915, *Masonic mining district, Mono County, California: Mining Press*, p. 27–29.
- Millar, C.I., 1996, Tertiary vegetation history, *in* *Sierra Nevada Ecosystem Project, Final report to Congress, Volume II, Assessments and Scientific Basis for Management Options, Centers for Water and Wildland Resources, Report No. 37, University of California, Davis, Calif.*, p. 71–122.

- Mono County Historical Society 2004 Newsletter, Masonic Mining District, 4 p.
- Morton, J.L., Silberman, M.L., Bonham, H.F., Garside, L.J., and Noble, D.C., 1977, K-Ar ages of volcanic rocks, plutonic rocks, and ore deposits in Nevada and eastern California—determinations run under the USGS-NBMG cooperative program: *Isochron/West*, no. 20, p. 19–29.
- Nash, J., 1972, Fluid inclusion studies of some gold deposits in Nevada: U.S. Geological Survey Professional Paper 800-C, p. 15–19.
- Nevada Bureau of Mines and Geology, 2009, *The Nevada Mineral Industry 2009: Special Publication MI-2009*, 180 p.
- Nevada Exploration Inc., 2013, Fletcher Junction Project, accessed October 14, 2013, at <http://www.nevadaexploration.com/properties/fletcher/overview/>.
- Oldow, J.S., 1992, Late Cenozoic displacement partitioning in the northwestern Great Basin, in Craig, S.D., ed., *Structure, tectonics, and mineralization of the Walker Lane: Walker Lane Symposium, proceedings volume*, Geological Society of Nevada, Reno, Nev., p. 17–52.
- Oldow, J.S., 2003, Active transtensional boundary zone between the western Great Basin and Sierra Nevada block, western U.S. Cordillera: *Geology*, v. 31, p. 1033–1036.
- O’Neil, J.R., and Silberman, M.L., 1974, Stable isotope relations in epithermal Au-Ag deposits: *Economic Geology*, v. 69, p. 902–909.
- O’Neil, J.R., Silberman, M.L., Fabbi, B.P., and Chesterman, C.W., 1973, Stable isotope and chemical relations during mineralization in the Bodie mining district, Mono County, California: *Economic Geology*, v. 68, p. 765–784.
- Osborne, M.A., 1985, Alteration and mineralization of the northern half of the Aurora mining district, Mineral County, Nevada: University of Nevada Reno, M.S. thesis, 93 p.
- Osborne, M.A., 1991, Epithermal mineralization at Aurora, Nevada, in Raines, G.L., Lisle, R.F., Schafer, R.W., and Wilkinson, W.H., eds., *Geology and ore deposits of the Great Basin*, Geological Society of Nevada, Symposium Proceedings, Reno, Nevada, p. 1097–1110.
- Payne, A., 1965, Geologic report Wasp and Hornet claims, Aurora mining district, Mineral County, Nevada: Bureau of Land Management Report, document 04100095, 26 p., available at <http://data.nbmgu.unr.edu/Public/MiningDistricts/0410/04100095.pdf>.
- Piatt, M.H., 2003, Bodie “The mines are looking well...”, a history of the Bodie mining district, Mono County, California: El Sobrante, Calif., North Day Books, 288 p.
- Pluhar, C.J., Deino, A.L., King, N.M., Busby, Cathy, Huasback, B.P., Wright, Tracy, and Fischer, Collin, 2009, Lithostratigraphy, magnetostratigraphy and radio-isotopic dating of the Stanislaus Group, CA, and the age of the Little Walker caldera: *International Geology Review*, v. 51, p. 873–899.
- Renne, P.R., Deino, A.L., Hames, W.E., Heizler, M.T., Hemming, S.R., Hodges, K.V., Koppers, A.A.P., Mark, D.F., Phillips, D., Singer, B.S., Turin, B.D., Villa, I.M., Villeneuve, M., and Wijbrans, J.R., 2009, Data reporting norms for  $^{40}\text{Ar}/^{39}\text{Ar}$  geochronology: *Quaternary Geochronology*, v. 4, p. 346–352.
- Rhoden, H.N., 1992, Exploration of Silver Hill, Aurora district, Mineral County, Nevada: Bureau of Land Management Report, document 04100087, 5 p., available at <http://data.nbmgu.unr.edu/Public/MiningDistricts/0410/04100087.pdf>.
- Robinson, A.C., and Kistler, R.W., 1986, Maps showing isotopic dating in the Walker Lake 1° by 2° quadrangle, California and Nevada: U.S. Geological Survey Miscellaneous Field Studies Map MI-1382-N, scale 1:250,000.
- Rockwell, B.W., 2010, Mineral and vegetation maps of the Bodie Hills, Sweetwater Mountains, and Wassuk Range, California/Nevada, generated from ASTER satellite data: U.S. Geological Survey Scientific Investigations Map 3104, scale 1:62,000, 4 plates, pamphlet, 5 p., available at <http://pubs.usgs.gov/sim/3104/>.
- Ross, D.C., 1961, Geology and mineral deposits of Mineral County, Nevada: Nevada Bureau of Mines and Geology Bulletin 58, 98 p.
- Rye, R.O., 2005, A review of the stable-isotope geochemistry of sulfate minerals in selected igneous environments and related hydrothermal systems: *Chemical Geology*, v. 215, p. 5–36.
- Sampson, R.J., 1940, Mineral resources of Mono County: State Mineralogist’s Report XXXVI, *California Journal of Mines and Geology*, v. 36, no. 2, p. 117–156.
- Shaddrick, D.R., 1989, The Aurora district, Nevada—Nevada Goldfields Inc. reserves and potential—A critical review, document 04100091, 49 p., available at <http://data.nbmgu.unr.edu/Public/MiningDistricts/0410/04100091.pdf>.
- Sherlock, R.L., 2005, The relationship between the McLaughlin gold-mercury deposit and active hydrothermal systems in the Geysers-Clear Lake area, northern Coast Ranges, California: *Ore Geology Reviews*, v. 26, p. 349–382.

- Silberman, M.L., and Berger, B.R., 1985, Relationship of trace-element patterns to alteration and morphology in epithermal precious-metal deposits, *in* Berger, B.R., and Bethke, P.M., eds., *Geology and Geochemistry of epithermal systems: Reviews in Economic Geology*, v. 2, p. 203–232.
- Silberman, M.L., Breit, F., and Lawrence, E.F., 1995, *Geology and ore deposits of Bodie Hills, Northern Mono Basin Region: 1996 Fall Field Trip Guidebook*, Geological Society of Nevada, Reno, Nevada, Special Publication No. 22, 65 p.
- Silberman, M.L., and Chesterman, C.W., 1991, A description of the Bodie Hills and Bodie mining district, Mono County, California with annotated road log from Bridgeport to Bodie, *in* Schafer, R.W., Bonham, H.F., and Silberman, M.L., eds., *Diverse tectonic setting for epithermal volcanic-hosted precious metal deposits along the Nevada-California border*, Great Basin Symposium Field Trip 9, Geological Society of Nevada, Reno, Nev., p. 601–618.
- Silberman, M.L., and McKee, E.H., 1972, A summary of radiometric age determinations on Tertiary volcanic rocks from Nevada and eastern California: part II, western Nevada: *Isochron-West*, no. 4, p. 7–28.
- Smailbegovic, Amer, 2002, *Structural and lithologic constraints to mineralization in Aurora, Nevada and Bodie, CA mining districts, observed and interpreted with aerospace geophysical data*: University of Nevada Reno, Ph.D. dissertation, 261 p.
- Speed, R.C., 1977, Excelsior Formation, west central Nevada—Stratigraphic appraisal, new divisions, and paleogeographic interpretations, *in* Stewart, J.H., Stevens, C.H., and Fritsche, A.E., eds., *Paleozoic paleogeography of the western United States: Society of Economic Paleontologists and Mineralogists, Pacific Coast Paleogeography Symposium 1*, p. 325–336.
- Stanford Geological Survey, 1961, *Geologic map of Swauger Creek-Masonic Mountain area, Mono County, California*: Stanford, Calif., Stanford University, scale 1:31,680, available at <http://www-sul.stanford.edu/depts/branner/images/maps/JamesGsmith-BIG.jpg>.
- Stewart, J.H., 1988, Tectonics of the Walker Lane belt, western Great Basin: Mesozoic and Cenozoic deformation in a zone of shear, *in* Ernst, W.G., ed., *Metamorphism and crustal evolution of the western United States: Englewood Cliffs*, N.J., Prentice Hall, p. 681–713.
- Stewart, J.H., 1992, Walker Lane belt, Nevada and California—an overview, *in* Craig, S.D., ed., *Walker Lane Symposium proceedings volume*, Geological Society of Nevada, Reno, Nev., p. 1–16.
- Stone, J.G., 1982, Siskon Corporation assets, document 04100018, 6 p., available at <http://data.nbmng.unr.edu/Public/MiningDistricts/0410/04100018.pdf>.
- Streckeisen, A., 1976, To each plutonic rock its proper name: *Earth-Science Reviews*, v. 12, p. 1–33.
- Stretch, R.H., 1867, *Annual report of the State Mineralogist of the State of Nevada for 1866: Carson City, Nev.*, Joseph E. Eckley, State Printer, 151 p.
- Sylvester, A.G., 1988, Strike-slip faults: *Geological Society of America Bulletin*, v. 100, p. 1666–1703.
- Tingley, J.V., 1990, *Mineral resource inventory*, Bureau of Land Management, Carson City District, Nevada: Nevada Bureau of Mines and Geology Open-File Report 90–1, 257 p.
- Turner, H.W., 1908, The vein-system of the Standard Mine, Bodie, Cal.: *Bi-Monthly Bulletin of the American Institute of Mining Engineers*, no. 22, July, p. 12.
- Vanderburg, W.O., 1937, *Reconnaissance of mining districts in Mineral County, Nevada*: U.S. Bureau of Mines Information Circular 6941, 79 p.
- Vikre, P.G., 1989, Fluid-mineral relations in the Comstock Lode: *Economic Geology*, v. 84, p. 1574–1613.
- Vikre, P.G., 2000, Elemental sulfur (S<sup>0</sup>) deposits and S<sup>0</sup> associated with precious metals, mercury, and thermal springs in the Great Basin, *in* Cluer, J.K., Price, J.G., Struhsacker, E.M., Hardyman, R.F., and Morris, C.L., eds., *Geology and Ore Deposits 2000: Geological Society of Nevada Symposium Proceedings*, Reno, Nev., p. 735–767.
- Vikre, P.G., 2007, Sinter-vein correlations at Buckskin Mountain, National district, Humboldt County, Nevada: *Economic Geology*, v. 102, p. 193–224.
- Vikre, P.G., and Henry, C.D., 2011, Quartz-alunite alteration cells in the southern segment of the ancestral Cascades magmatic arc, *in* Steininger, R., and Pennell, B., eds., *Symposium Proceedings, Great Basin Evolution and Metallogeny: Geological Society of Nevada, Reno, Nev.*, p. 701–745.
- Ward, J.M., 1992, The Cinnabar Canyon sulfur deposit, *in* Wessel, G.R., and Wimberly, B.H., eds., *Native sulfur developments in geology and exploration: Society for Mining, Metallurgy, and Exploration, Inc.*, p. 159–164.
- Wasson, J., 1978, *Bodie and Esmeralda: San Francisco, Spaulding, Barto and Co., Steam Book and Job Printers*, 60 p.
- Wedertz, F.S., 1969, *Bodie 1859–1900: Bishop, Calif.*, Community Printing and Publishing, 211 p.

**120 Gold-Silver Mining Districts, Alteration Zones, and Paleolandforms in the Miocene Bodie Hills Volcanic Field**

Wesnousky, S.G., 2005, Active faulting in the Walker Lane: Tectonics, v. 24, no. 3, DOI 10.1029/2004TC001645, 35 p.

Whiting, H.A., 1888, Mono County: California State Mining Bureau, Eighth Annual Report of the State Mineralogist, p. 382–401.

Wisser, E., 1960, Relation of ore deposition to doming in the North American cordillera: Geological Society of America Memoir 77, 177 p.

Wolfe, J.A., 1995, Paleoclimatic estimates from Tertiary leaf assemblages: Annual Review of Earth and Planetary Sciences, v. 23, p. 119–142.

Wolfe, J.A., Schorn, H.E., Forest, C.E., and Molnar, P., 1997, Paleobotanical evidence for high altitudes in Nevada during the Miocene: Science, v. 276, p. 1672–1675.

# Appendixes

---

- 1-1. Minor element concentrations in rock samples from the Masonic Mining District.
- 1-2. Minor element concentrations in rock samples from the Red Wash-East Walker River alteration zone.
- 1-3. Minor element concentrations in rock samples from the East Brawley Peak alteration zone.
- 1-4. Minor element concentrations in rock samples from the Sawtooth Ridge alteration zone.
- 1-5. Minor element concentrations in rock samples from the Aurora Canyon alteration zone.
- 1-6. Minor element concentrations in rock samples from the Potato Peak alteration zone.
- 1-7. Minor element concentrations in rock samples from the Aurora Mining District.
- 1-8. Minor element concentrations in rock samples from the Four Corners alteration zone.
- 1-9. Minor element concentrations in rock samples from the Paramount-Bald Peak alteration zone.
- 1-10. Minor element concentrations in rock samples from the Cinnabar Canyon-US 395 alteration zone.
- 1-11. Minor element concentrations in rock samples from the Bodie Mining District.
- 1-12. Minor element concentrations in rock samples of Spring Peak sinter.





**Table 1-1.** Minor element concentrations in rock samples from the Masonic Mining District.—Continued

[—, no data]

Sample number	As ppm	Ba ppm	Be ppm	Bi ppm	Cd ppm	Ce ppm	Co ppm	Cr ppm	Cs ppm	Cu ppm	Ga ppm	In ppm	La ppm	Li ppm	Mn ppm	Mo ppm	Nb ppm
2007–12 samples																	
MAS09-3	1,040	1,530	1.1	1,050	0.6	5.18	0.3	3	<5	3,140	3.49	0.35	2.8	2	14	15.5	8.4
MAS09-3A	>10,000	242	<0.1	4,310	0.7	5.54	0.6	2	<5	>50,000	3.68	0.49	3.5	3	15	6.91	<0.1
07-BA-39A	145	478	0.6	189	<0.1	8.53	6	7	<5	179	11.8	0.08	4.4	16	95	5.13	1.9
07-BA-39B	146	548	0.2	57.1	<0.1	12.8	0.4	8	<5	72.8	22.6	0.17	7	12	78	1.74	2.2
12-BA-21A	549	652	0.7	2,780	0.5	7.05	3.3	6	<5	1,310	4.83	0.27	3.8	7	50	15.4	8.6
12-BA-21B	315	562	0.8	2,610	0.5	4.31	0.6	5	<5	325	3.91	0.17	2.3	4	45	3.04	13.9
07-BA-35	256	1,230	0.4	0.06	0.3	35.1	6.1	8	<5	25.1	10.4	0.07	18	18	56	4.54	7.7
07-BA-35B	81	547	0.2	0.1	0.2	27.5	2.4	9	<5	15.9	13.7	0.02	16.1	1	20	0.41	8
07-BA-36	50	2,750	0.4	0.56	<0.1	30.4	0.8	15	<5	16.9	29	0.1	16.7	4	26	5.03	3.7
07-BA-37	40	1,940	0.4	1.25	<0.1	11.5	0.8	7	<5	11.2	8.98	<0.02	6.7	7	42	3.19	3.5
07-BA-40	12	535	0.3	0.92	<0.1	9.74	0.3	2	<5	4.8	20.9	0.31	4.9	11	14	0.3	3.7
07-BA-41	66	693	<0.1	7.06	0.3	12.1	5.5	8	<5	49.5	53.2	0.46	7.7	3	9	0.38	0.3
07MS5	59	1,020	0.6	15.8	<0.1	18	0.6	5	<5	15.8	2.18	0.04	8.9	4	30	4.18	3.1
07MS3	35	6,120	0.3	24.7	<0.1	17.8	0.7	5	<5	7.9	1.28	0.02	10	2	52	5.73	4.5
07MS2	67	244	0.4	0.06	<0.1	22.5	4.2	6	<5	11	11	<0.02	10.6	4	25	2.4	2.5
MAS11-11	46	209	0.2	13.3	<0.1	32.9	3.3	7	<5	68.8	31.8	0.06	17.4	5	28	0.89	4.5
MAS11-11A	788	97	0.3	4,340	0.3	49.8	0.3	15	<5	191	66.5	0.31	26	3	29	4.37	8.1

	As ppm	Bi ppm	Cu ppm
1988 samples			
MD88-1	592	1	1,270
MD88-1C	588	24.8	2,700
MD88-3C	526	0.3	56
MD88-4	680	0.034	163
MD88-4A	3,107	0.093	2,900
MD88-4C	174	916	600
MD88-5A	265	2,900	3,500
MD88-5B	370	3,110	1,230

**Table 1-1.** Minor element concentrations in rock samples from the Masonic Mining District.—Continued

[—, no data]

Sample number	Ni ppm	P ppm	Pb ppm	Rb ppm	Sb ppm	Sc ppm	Se ppm	Sn ppm	Sr ppm	Te ppm	Th ppm	Tl ppm	U ppm	V ppm	W ppm	Y ppm	Zn ppm
2007–12 samples																	
MAS09-3	<0.5	60	92.1	0.8	1,120	2.6	—	26.9	106	>500	3.5	0.5	2.8	13	73.8	3.5	4
MAS09-3A	<0.5	490	149	0.8	>10,000	1.2	—	461	429	>500	1.1	4.2	3.1	8	0.6	2.5	11
07-BA-39A	4.9	270	132	1.4	99.9	1.3	17.5	0.9	162	296	1.2	0.2	1	46	9.7	1.2	6
07-BA-39B	1.3	630	216	2.2	114	2.5	5.9	0.3	625	166	1.7	0.2	1.5	85	31.3	2.7	3
12-BA-21A	8.5	100	97.6	1.4	479	2.3	198	1.9	168	>500	4.3	1.1	2.9	20	138	5.3	11
12-BA-21B	0.7	<50	115	0.9	857	3.6	43.2	4.7	32.6	>500	5.6	0.4	2.8	21	135	3.5	5
07-BA-35	6.4	1,150	93.3	2.2	71.9	4.4	5.3	0.6	1,080	3.1	6.4	2.9	6.6	45	40.6	4.5	19
07-BA-35B	3.2	300	25	2.7	51.3	4.4	8.1	0.9	304	2.1	6.2	10.4	3.2	66	36.8	3	128
07-BA-36	2.7	790	278	1.9	45	5.5	2.5	1	592	2.6	5	0.3	10.3	132	21.9	4.8	6
07-BA-37	1.7	310	61.6	2.3	11.3	1.9	3.4	1	258	2.2	2.6	0.2	2.7	45	10.7	2.4	7
07-BA-40	2.2	210	131	3.6	5.57	4.2	0.8	0.8	219	1.7	12	0.1	1.7	39	4.9	0.4	15
07-BA-41	13.7	960	1,640	1.8	76.3	3	17.6	0.8	641	4.8	4.7	1.5	0.9	113	23.6	0.3	31
07MS5	1.7	370	80.7	3.6	97.9	2.8	—	1.8	306	200	3.1	0.5	6.6	12	22.3	3.4	7
07MS3	1.7	350	116	2.3	96.7	2.5	—	1.2	335	25	4.2	0.4	8.6	13	25.8	3.2	9
07MS2	2.9	310	14.2	2	63.4	1.9	—	0.8	303	3.7	3.5	1.2	1.7	42	39.1	1.6	3
MAS11-11	3.9	1,800	308	4.5	42.9	4.3	28.9	1.6	2,850	10.1	4.1	0.2	7.5	77	24.5	5.5	3
MAS11-11A	<0.5	2,000	1,070	3	3,180	6.3	43.9	74.3	1,520	287	5	0.6	2.1	143	130	4.8	4
1988 samples																	
MD88-1					3,500			10		0.8							
MD88-1C					780			16		300							
MD88-3C					20			10		2.5							
MD88-4					4,600			57		3,220							
MD88-4A					1,710			3		483							
MD88-4C					480			3		547							
MD88-5A					119			48		346							
MD88-5B					550			52		617							

**Table 1-2.** Minor element concentrations in rock samples from the Red Wash-East Walker River alteration zone.

[Fe, iron; FeOx, iron oxide; —, no data]

Sample number	Description	Latitude	Longitude	Au ppm	Hg ppm	Al %	Ca %	Fe %	K %	Mg %	Na %	S %	Ti %	Ag ppm
09-E02	—	—	—	—	1.42	4	—	—	0.03	0.01	0.02	0.96	0.22	1.2
09-E04	—	—	—	—	2.7	4.86	—	—	0.05	0.02	0.02	0.11	0.28	1.2
09-E09	Silicified with quartz veins	—	—	<0.005	0.35	7.15	0.23	4	2.04	0.02	0.67	>5	0.19	<1
09-E10	—	—	—	—	0.4	2.14	—	—	0.35	0.1	0.08	0.93	0.07	<0.5
09-E11	Vuggy, silica-cut quartz veins	—	—	<0.005	0.07	5.86	0.17	0.44	1.39	<0.01	0.67	4.32	0.29	<1
09-E12	Clastic sediment; Fe-cemented	—	—	<0.005	0.2	0.62	0.19	12	0.08	0.03	0.02	0.19	0.15	<1
09-E13	Volcaniclastic silicified rib with Fe	—	—	0.006	0.09	0.36	0.16	12	0.02	0.03	<0.01	0.14	0.06	<1
09-E14	—	—	—	—	0.45	0.19	—	—	0.02	0.01	0.01	0.1	0.32	<0.5
09-E015	—	—	—	—	1.68	0.14	—	—	0.01	0.01	<0.01	0.04	0.26	<0.5
09-E16	Fe-rich volcaniclastic sediment; silicified	—	—	0.01	0.01	0.42	0.18	2.21	0.05	0.01	0.01	0.24	0.13	<1
09-E18	Fe on fractures in volcaniclastic; sediment silicified	—	—	<0.005	0.07	4.99	0.45	13	1.05	0.01	0.56	3.94	0.1	<1
09-E19	Breccia with silicified quartz vein	—	—	<0.005	<0.01	8.43	7.76	4.34	1.13	1.69	2.05	0.03	0.34	<1
09-E20	Breccia with silicified quartz vein	—	—	<0.005	0.82	2.27	0.08	1.35	0.3	<0.01	0.34	1.69	0.14	<1
09-E23	Silicified tuff cut by Fe on fractures	—	—	<0.005	0.38	5.55	0.16	8.85	0.31	0.02	0.1	0.99	0.16	<1
09-E24	Vuggy silica float cut by Fe-stained quartz veins	38.40844	-119.09776	0.006	0.14	4.76	0.14	7.93	1.35	0.02	0.25	2.98	0.28	<1
09-E25	Vuggy silica cut by Fe-stained quartz veins	38.40843	-119.09809	<0.005	0.05	3.81	0.12	5.9	0.71	0.01	0.44	2.81	0.1	<1
09-E27	Silica core of alteration cut by Fe veinlets	38.41013	-119.10394	0.03	5.19	2.3	0.09	>15	0.59	<0.01	0.12	1.43	0.14	<1

		Latitude	Longitude	Au ppb	Pd ppb	Pt ppb	Al %	Ca %	Fe %	K %	Mg %	Na %	S %	Ti %
RW11-1	Brick-red (FeOx), soft, variably leached volcaniclastic deposits	38.40473	-119.06708	21	2	1.6	0.73	0.15	0.63	0.07	0.07	0.03	0.08	0.33
RW11-2ME	Silicified, FeOx-stained volcaniclastics, variably leached, resistant	38.407	-119.07178	4	<1	0.5	5.53	0.39	0.73	1.33	0.01	0.71	4.31	0.47
RW11-3ME	Silicified, FeOx-stained Masonic andesite with clay-altered phenocrysts	38.40191	-119.06982	3	<1	<0.5	7.48	0.27	3.77	0.9	0.02	0.54	3.47	0.41
RW11-4ME	Beige-brick-red, clay-altered, partly silicified volcaniclastics	38.40318	-119.07082	6	<1	0.5	4.81	0.26	3.22	1.4	0.02	0.56	4.35	0.14
RW11-5ME	Silicified, clay-alunite-altered, variably sorted volcaniclastics, some FeOx	38.4006	-119.06973	4	<1	<0.5	6.82	0.16	4.33	2.15	0.02	0.84	>5	0.34

**Table 1-2.** Minor element concentrations in rock samples from the Red Wash-East Walker River alteration zone.—Continued

[Fe, iron; FeOx, iron oxide; —, no data]

Sample number	As ppm	Ba ppm	Be ppm	Bi ppm	Cd ppm	Ce ppm	Co ppm	Cr ppm	Cs ppm	Cu ppm	Ga ppm	In ppm	La ppm	Li ppm	Mn ppm	Mo ppm	Nb ppm	Ni ppm
09-E02	9	560	<0.5	7	0.05	<0.5	2	21	44	0.63	20	—	20	—	11	4	—	1
09-E04	8	130	<0.5	4	0.08	<0.5	3	23	107	2.08	20	—	20	—	41	18	—	1
09-E09	28	181	0.3	1.8	<0.1	42.7	0.9	9	<5	34.7	27.7	0.06	22.5	<1	39	1.98	3.6	1.3
09-E10	65	1,120	0.7	<2	0.27	0.5	<1	76	62	25	20	—	10	—	126	14	—	7
09-E11	8	346	0.5	4.36	<0.1	97.2	0.4	6	<5	7.9	22.2	<0.02	44.3	<1	33	0.96	4.5	0.9
09-E12	47	1,240	0.4	0.69	<0.1	20.6	1.4	10	<5	33.2	2.02	<0.02	11	2	182	6.32	2.4	1
09-E13	42	1,160	0.3	0.66	0.2	4.94	2	8	<5	42.5	4.94	0.03	2.2	1	168	23.5	1.1	2
09-E14	12	2,410	<0.5	2	0.04	<0.5	<1	15	16	0.21	<10	—	<10	—	12	1	—	<1
09-E015	8	360	<0.5	2	0.01	<0.5	1	20	9	0.27	<10	—	<10	—	21	2	—	1
09-E16	34	1,240	0.2	0.59	<0.1	14.8	1.4	3	<5	17.1	2.07	<0.02	7.8	9	109	21.5	2.5	2.1
09-E18	477	385	0.2	0.9	<0.1	82.4	1.2	14	<5	33.4	22.9	0.06	43.8	<1	59	24	1.9	<0.5
09-E19	<1	1,320	1.4	<0.04	<0.1	50.6	30.1	146	<5	33.2	20.3	0.05	30.3	5	789	0.29	5	117
09-E20	11	1,120	0.1	0.96	<0.1	25.8	0.6	5	<5	14.4	4.31	0.04	15.3	<1	25	3.24	4.5	1.2
09-E23	41	1,100	0.3	0.52	<0.1	31.8	0.9	22	<5	148	22.6	0.07	17.6	13	33	68	1.9	<0.5
09-E24	50	512	0.8	1.29	<0.1	80.9	1	30	<5	70.3	26.9	0.12	43.8	2	88	11.5	7.3	1.9
09-E25	43	869	0.5	0.43	0.1	35	2	11	<5	87.7	18.1	0.06	19.6	<1	70	8.33	2.2	3.1
09-E27	205	731	0.2	0.82	0.2	39.5	5.5	93	<5	189	52.1	0.12	23	3	42	168	1.5	8.8

	Ag ppm	As ppm	Ba ppm	Be ppm	Bi ppm	Cd ppm	Ce ppm	Co ppm	Cr ppm	Cs ppm	Cu ppm	Ga ppm	Hg ppm	In ppm	La ppm	Li ppm	Mn ppm	Mo ppm
RW11-1	<1	10	1,000	0.2	0.18	0.1	12	1.2	4	<5	20.7	2.03	0.04	<0.02	6.5	17	131	6.11
RW11-2ME	<1	16	109	0.6	0.2	<0.1	41.3	0.9	15	<5	8	14.9	0.01	0.04	19.9	2	80	3.14
RW11-3ME	<1	31	134	0.3	1.37	<0.1	64.1	0.3	20	<5	39.3	23.5	0.13	0.07	32.6	4	21	2.46
RW11-4ME	<1	21	89	0.2	1.57	<0.1	31.5	0.7	9	<5	6.5	12.7	0.06	0.02	15.3	<1	39	21
RW11-5ME	<1	36	82	0.4	0.6	<0.1	51.4	0.2	22	<5	24.8	22.8	0.09	0.05	26.3	1	20	3.72

**Table 1-2.** Minor element concentrations in rock samples from the Red Wash-East Walker River alteration zone.—Continued

[Fe, iron, FeOx, iron oxide; —, no data]

Sample number	P ppm	Pb ppm	Rb ppm	Sb ppm	Sc ppm	Sn ppm	Sr ppm	Te ppm	Th ppm	Tl ppm	U ppm	V ppm	W ppm	Y ppm	Zn ppm	Se ppm	C %	
09-E02	680	258	—	11	4	—	881	—	<20	<10	<10	76	<10	—	3	—	—	
09-E04	910	136	—	15	5	—	990	—	<20	<10	<10	77	10	—	15	—	—	
09-E09	1,840	16.3	11.3	1.07	4	0.9	815	1	4.9	0.8	0.9	163	0.2	4.1	6	—	—	
09-E10	2,430	21	—	<5	3	—	849	—	<20	<10	10	104	<10	—	47	—	—	
09-E11	2,030	17.7	2.8	1.28	5.5	1.5	1,090	0.4	10.5	<0.1	1	151	0.3	2.9	6	—	—	
09-E12	1,810	7.2	2.4	0.31	1.4	0.4	379	0.1	2.7	<0.1	1.5	31	0.2	2.1	20	—	—	
09-E13	660	5.2	1.1	0.37	0.9	0.8	42.2	0.4	1.6	<0.1	1.1	73	0.3	2.5	16	—	—	
09-E14	40	7	—	7	1	—	38	—	<20	<10	<10	6	<10	—	<2	—	—	
09-E015	30	4	—	8	<1	—	19	—	<20	<10	<10	4	<10	—	<2	—	—	
09-E16	870	23.4	1.5	2.35	0.5	0.6	190	1	4.6	0.2	1.3	38	0.6	1.7	4	—	—	
09-E18	2,290	23.2	3.3	2.67	2.7	0.7	1,390	5.4	10	0.2	1.2	286	0.3	2	7	—	—	
09-E19	1,340	12.3	11	0.16	19.4	0.8	1,060	<0.1	3.1	<0.1	0.9	112	<0.1	13.1	79	—	—	
09-E20	870	15.4	1.4	1.29	2.8	0.7	1,010	0.3	3.2	0.2	1.1	38	0.7	2.9	5	—	—	
09-E23	1,910	66	0.9	0.61	2.7	2.4	2,570	2.3	2	<0.1	0.6	125	0.7	2	22	—	—	
09-E24	2,300	43.1	4.7	1.43	7.4	1.1	1,190	6.6	14.7	<0.1	3.5	137	1.3	6.2	23	—	—	
09-E25	1,260	34.4	2.5	0.55	3.5	0.9	1,120	0.3	3.8	0.2	1.7	122	0.6	3.2	11	—	—	
09-E27	1,670	34.2	0.7	1.85	5.3	1.1	1,210	6.2	3.8	<0.1	0.4	508	47.5	1.6	7	—	—	
	Nb ppm	Ni ppm	P ppm	Pb ppm	Rb ppm	Sb ppm	Sc ppm	Se ppm	Sn ppm	Sr ppm	Te ppm	Th ppm	Tl ppm	U ppm	V ppm	W ppm	Y ppm	Zn ppm
RW11-1	4.5	1.8	490	8.5	2.4	10.7	0.6	0.3	1	139	0.7	2.4	0.2	0.7	20	1.1	1.1	7
RW11-2ME	7.8	0.9	1,260	20.5	4	3.86	7.3	1	1.5	816	1.1	8.1	0.2	2.4	111	1.3	4.2	3
RW11-3ME	5.2	0.6	1,960	15.1	3.2	1.22	5.5	6.6	1.6	1,260	1.6	6.6	0.2	2.2	199	0.5	3.5	3
RW11-4ME	2.1	1	1,800	22.7	8.5	2.52	3.3	1.2	2.3	348	0.7	5.6	0.5	0.9	70	0.5	1.6	11
RW11-5ME	4.9	<0.5	1,630	16.1	5.6	1.36	6.5	7	1.2	952	2.1	8.8	2	1.4	200	0.6	2.7	3

**Table 1-3.** Minor element concentrations in rock samples from the East Brawley Peak alteration zone.

[—, no data]

Sample number	Description	Latitude	Longitude	Au ppm	Hg ppm	Al %	Ca %	Fe %	K %	Mg %	Na %	S %	Ti %	Ag ppm	As ppm	Ba ppm
08-BA-4	Andesite altered to kaolinite	38.25567	-118.90875	<0.005	0.34	5.32	0.17	2.56	0.06	0.02	0.02	0.29	0.31	<1	30	844
10-BA-23	Quartz-dickite altered rhyolite	38.27127	-118.91707	<0.005	1.8	<0.01	<0.01	<0.01	<0.01	<0.01	<0.01	<0.01	<0.01	<1	35	<5
10-BA-24	Quartz-dickite alteration	38.27114	-118.91754	0.009	1.11	5.73	0.01	0.09	0.02	<0.01	<0.01	0.03	0.06	<1	10	458
10-BA-25	Quartz-dickite alteration, head of landslide	38.26963	-118.91960	0.017	0.37	0.91	0.03	0.68	0.03	<0.01	<0.01	0.12	0.43	<1	168	2,500

**Table 1-3.** Minor element concentrations in rock samples from the East Brawley Peak alteration zone.—Continued

[—, no data]

Sample number	Be ppm	Bi ppm	Cd ppm	Ce ppm	Co ppm	Cr ppm	Cs ppm	Cu ppm	Ga ppm	In ppm	La ppm	Li ppm	Mn ppm	Mo ppm	Nb ppm	Ni ppm
08-BA-4	0.3	0.53	<0.1	86.2	0.2	9	<5	28.5	22.5	<0.02	49.6	19	26	2.48	7.8	<0.5
10-BA-23	0.9	0.14	<0.1	46.3	0.1	<1	<5	<0.5	10.1	<0.02	30.7	<1	<5	0.8	9.7	<0.5
10-BA-24	0.2	0.52	<0.1	38.9	0.2	1	<5	3	14	<0.02	24.2	12	8	1.59	12.1	0.5
10-BA-25	0.6	0.12	<0.1	24.9	0.2	3	<5	9.6	4.15	<0.02	16.2	5	9	32.3	9.8	0.6

**Table 1-3.** Minor element concentrations in rock samples from the East Brawley Peak alteration zone.—Continued

[—, no data]

Sample number	P ppm	Pb ppm	Rb ppm	Sb ppm	Sc ppm	Sn ppm	Sr ppm	Te ppm	Th ppm	Tl ppm	U ppm	V ppm	W ppm	Y ppm	Zn ppm	Se ppm
08-BA-4	1,780	49.4	1.4	6.43	3.4	0.8	1,290	1.8	11.1	<0.1	2.1	74	10	4.6	4	—
10-BA-23	<50	11.2	2.1	16	2.1	0.6	<0.5	<0.1	19	0.1	8.6	<1	5.9	9.4	<1	—
10-BA-24	110	7.4	1.2	13	2.4	1	59.3	<0.1	28.6	0.1	10.2	28	4.8	5.5	3	—
10-BA-25	340	19.5	1.2	20.6	1.9	1.3	297	<0.1	4.9	0.1	1.1	38	42.6	2.3	5	—

**Table 1-4.** Minor element concentrations in rock samples from the Sawtooth Ridge alteration zone.

[FeOx, iron oxide; bxd, brecciated; alt, altered; chal, chalcedony; lim, limonite; bx, breccia; hem, hematite; —, no data]

Sample number	Latitude	Longitude	Description	Au ppb	Pd ppb	Pt ppb	Al %	Ca %	Fe %	K %	Mg %	Na %	S %	Ti %	Ag ppm
SAW11-1ME	38.29305	-118.90932	Brecciated, FeOx-stained white rhyolite	16	<1	<0.5	5.96	0.08	0.43	0.11	0.07	0.04	0.07	0.08	3
SAW11-2ME	38.29442	-118.91269	Bxd FeOx-stained (limonite) rhyolite alt to chal, opal	16	<1	<0.5	6.03	0.05	0.11	0.08	0.02	0.03	0.05	0.06	2
SAW11-3ME	38.29452	-118.91475	White-beige bxd rhyolite, alt to chal, opal	6	<1	<0.5	7.42	0.09	0.18	0.19	0.02	0.02	0.31	0.1	<1
SAW11-4ME	38.29772	-118.91724	White-beige bxd rhyolite, minor FeOx (lim+hem)	3	<1	<0.5	11.9	0.16	0.7	3.31	0.06	0.09	>5	0.06	<1
SAW11-5ME	38.30095	-118.91615	Dump; angular rhyolite clasts in heavy FeOx (lim+hem) matrix	9	<1	<0.5	2.33	0.09	21	0.87	0.01	0.05	1.56	0.03	<1
SAW11-7ME	38.29756	-118.91457	White-beige bxd rhyolite, minor FeOx (lim+hem)	3	<1	0.5	9.3	0.1	0.27	0.24	0.04	0.03	0.38	0.08	<1
SAW11-8ME	38.29097	-118.90810	Beige rhyolite flow and flow bx, minor FeOx	7	<1	<0.5	4.92	0.21	0.77	3.47	0.09	0.57	0.12	0.05	<1
SAW11-9ME	38.29036	-118.91657	White bxd rhyolite with chal, opal, alunite matrix and veins	2	<1	<0.5	6.51	0.06	0.1	1.87	0.02	0.05	3.22	0.06	<1
SAW11-10ME	38.29010	-118.91155	Beige-red rhyolite and bxd rhyolite	3	<1	<0.5	5.93	0.07	0.35	0.07	0.01	0.02	0.05	0.05	<1
SAW11-11ME	38.28904	-118.90930	Bxd rhyolite, FeOx-stained	3	<1	<0.5	6.24	0.31	2.14	1.92	0.3	3.32	0.21	0.37	<1
07-BA-33	38.29023	-118.91201	Argillized tuff with secondary silica, Aurora Mine Road	<0.005	—	—	4.38	0.07	0.62	0.06	<0.01	0.01	0.22	0.04	<1

**Table 1-4.** Minor element concentrations in rock samples from the Sawtooth Ridge alteration zone.—Continued

[FeOx, iron oxide; bxd, brecciated; alt, altered; chal, chalcedony; lim, limonite; bx, breccia; hem, hematite; —, no data]

Sample number	As ppm	Ba ppm	Be ppm	Bi ppm	Cd ppm	Ce ppm	Co ppm	Cr ppm	Cs ppm	Cu ppm	Ga ppm	Hg ppm	In ppm	La ppm	Li ppm	Mn ppm	Mo ppm	Nb ppm
SAW11-1ME	42	503	0.9	0.37	<0.1	16.6	0.7	2	7	27.8	14.4	2.11	<0.02	12.5	157	57	5.22	7.7
SAW11-2ME	22	298	0.6	0.49	<0.1	16.3	0.2	1	11	18.3	15.4	0.61	<0.02	14.6	70	14	3.08	9.7
SAW11-3ME	8	720	0.3	0.42	<0.1	31.7	0.3	3	7	15.6	16.6	0.3	0.02	19.8	51	12	1.6	9.3
SAW11-4ME	12	156	0.7	0.38	<0.1	85.2	0.8	45	6	18.3	76.8	0.07	0.03	63.3	44	56	2.38	7.7
SAW11-5ME	354	504	2.6	0.3	<0.1	33.3	0.6	8	7	21.6	11.3	0.51	<0.02	21.5	3	60	25.3	3.7
SAW11-7ME	25	631	0.3	0.49	<0.1	43.2	0.2	4	8	10	18.2	0.12	0.03	27.6	78	18	13.4	10.4
SAW11-8ME	289	901	1.4	0.09	0.1	45	0.6	2	12	10	12.3	1.63	<0.02	25.4	37	62	4.15	8
SAW11-9ME	9	190	0.3	0.36	<0.1	14.3	0.2	3	8	3.5	17.8	1.61	<0.02	10.6	18	<5	1.53	9.2
SAW11-10ME	17	299	1.6	0.1	<0.1	43.9	0.8	<1	<5	5.9	10.3	0.75	<0.02	26.4	53	23	4	7.9
SAW11-11ME	17	1,060	0.9	<0.04	<0.1	13.7	4.8	20	5	28.2	17.7	0.74	0.03	7.1	26	110	0.24	6.2
07-BA-33	33	300	1.9	0.08	<0.1	21.7	0.5	3	<5	7.5	7.88	7.88	<0.02	11	41	35	18.5	6.1

**Table 1-4.** Minor element concentrations in rock samples from the Sawtooth Ridge alteration zone.—Continued

[FeOx, iron oxide; bxd, brecciated; alt, altered; chal, chalcedony; lim, limonite; bx, breccia; hem, hematite; —, no data]

Sample number	Ni ppm	P ppm	Pb ppm	Rb ppm	Sb ppm	Sc ppm	Se ppm	Sn ppm	Sr ppm	Te ppm	Th ppm	Tl ppm	U ppm	V ppm	W ppm	Y ppm	Zn ppm
SAW11-1ME	1.6	270	31.3	7.1	85.3	1.1	0.7	1.2	217	1.6	11.4	0.1	9	31	8.8	3.4	10
SAW11-2ME	<0.5	150	46.4	5	24.4	1.2	0.4	1.3	120	3.8	16.3	0.2	7	14	3.4	2.8	4
SAW11-3ME	1.1	740	30.5	4.9	9.45	1.3	<0.2	1.2	199	0.5	16.6	0.1	9.2	37	10.6	2.9	5
SAW11-4ME	3.1	1,680	25.8	7.6	7	2.1	<0.2	0.9	1,740	0.4	41.9	0.1	7.6	131	16.5	4.9	8
SAW11-5ME	0.6	1,590	27.1	6.4	25.8	1.7	1	0.7	259	0.2	21.3	<0.1	9.1	190	45.2	3.9	16
SAW11-7ME	0.8	550	33.2	4.7	6.08	2	0.4	1.1	417	0.2	23	0.4	12.8	78	11.3	9	7
SAW11-8ME	1.2	380	32.1	138	97.7	0.7	<0.2	0.7	241	0.1	24.8	1.3	7.9	33	11.5	16.1	13
SAW11-9ME	<0.5	210	34.2	6.7	9.24	1.8	<0.2	0.9	113	0.1	9.9	0.1	7.4	30	6	1.3	2
SAW11-10ME	2.5	410	34.2	3.2	10.5	2.7	0.5	0.9	295	1.4	25.6	<0.1	11.7	57	6.1	7	22
SAW11-11ME	19.7	570	9.8	53.6	15.4	9.8	0.3	1.1	531	1	2.9	0.3	1.2	83	28.2	3.3	42
07-BA-33	0.8	120	12.2	2	5.18	1.1	1.8	0.6	56.2	<0.1	32.1	<0.1	10.3	17	2	4	7



**Table 1-5.** Minor element concentrations in rock samples from the Aurora Canyon alteration zone.

Sample number	Latitude	Longitude	Description	Au ppm	Hg ppm	Al %	Ca %	Fe %	K %	Mg %	Na %	S %	Ti %	Ag ppm	As ppm	Ba ppm
PP09-20	38.25336	-119.13584	Quartz-alunite-clay-altered andesite	<0.005	10	3.22	0.07	6.87	1.13	<0.01	0.12	2.55	0.08	<1	67	380
PP09-21	38.26387	-119.12638	Silicified and brecciated andesite	<0.005	3.11	6.63	0.16	4.64	1.71	0.03	0.73	>5	0.1	<1	480	116
PP09-22	38.257	-119.13689	Quartz-alunite-altered andesite	<0.005	0.8	0.44	0.13	0.1	0.04	0.01	<0.01	0.06	0.09	<1	8	221
PP09-23	38.25974	-119.13051	Quartz-clay-altered andesite	<0.005	20.6	0.48	0.03	0.57	0.03	0.01	<0.01	0.09	0.23	<1	192	1,360
08-BA-43	38.25330	-119.13567	Silicified andesite with alunite veins	<0.005	0.23	6.68	0.13	0.3	2.75	<0.01	0.18	>5	0.19	<1	26	106
08-BA-44	38.256910	-119.13795	Quartz-alunite-altered andesite	<0.005	0.59	10.2	0.54	1.32	1.22	0.03	2.19	>5	0.58	<1	25	87
08-BA-45	38.256325	-119.13673	Fine-grained alunite	<0.005	0.09	6.22	0.08	0.53	2.21	0.01	0.36	4.71	0.11	<1	11	135
09-BA-45	38.270139	-119.13000	Silicified hematitic breccia	0.018	1.9	0.22	0.02	0.75	0.01	<0.01	<0.01	0.23	0.1	<1	81	8,870

**Table 1-5.** Minor element concentrations in rock samples from the Aurora Canyon alteration zone.—Continued

Sample number	Be ppm	Bi ppm	Cd ppm	Ce ppm	Co ppm	Cr ppm	Cs ppm	Cu ppm	Ga ppm	In ppm	La ppm	Li ppm	Mn ppm	Mo ppm	Nb ppm	Ni ppm
PP09-20	0.3	2.15	<0.1	49.1	0.9	16	<5	35.1	9.62	0.03	27.9	3	23	4.86	1.9	0.8
PP09-21	0.4	2.18	<0.1	32.6	1	14	<5	19.3	20.9	0.05	17.7	5	64	2.02	1.7	1.7
PP09-22	0.3	1.37	<0.1	7	0.3	3	<5	8.4	0.65	<0.02	3.7	7	28	1.07	1.1	0.6
PP09-23	0.1	4.52	<0.1	10.7	0.5	5	<5	19.6	2.28	0.03	5.9	26	13	1.19	3.3	1.2
08-BA-43	0.4	2.23	<0.1	108	0.6	22	<5	7.7	13.8	0.04	56.7	2	20	2.67	4.6	1.3
08-BA-44	0.4	2.34	0.2	90.4	0.6	37	<5	31.7	26	<0.02	46.2	4	151	3.66	13.8	1.9
08-BA-45	0.2	0.61	<0.1	23.9	0.3	33	<5	2.6	11.7	<0.02	15.3	1	30	1.54	2	<0.5
09-BA-45	0.1	2.37	<0.1	2.51	2	2	<5	15.2	0.58	<0.02	2	<1	73	6.32	1.5	2.2

**Table 1-5.** Minor element concentrations in rock samples from the Aurora Canyon alteration zone.—Continued

Sample number	P ppm	Pb ppm	Rb ppm	Sb ppm	Sc ppm	Sn ppm	Sr ppm	Te ppm	Th ppm	Tl ppm	U ppm	V ppm	W ppm	Y ppm	Zn ppm
PP09-20	1,640	23.5	3	2.39	2.2	0.8	533	0.5	10	0.3	1.5	102	0.5	2.2	8
PP09-21	1,290	13.9	5.6	13.5	3	0.7	827	3.7	3.9	0.2	0.8	164	2.5	2	10
PP09-22	2,240	1.8	1.4	83	1.2	0.4	53.5	0.6	1.5	<0.1	0.7	5	0.6	1.9	11
PP09-23	270	30.5	2.1	33.2	2.8	0.9	205	1.9	3	0.7	2.2	17	6	2.2	4
08-BA-43	2,490	58.2	6.8	2.97	4.9	1	1,020	0.2	18.5	2.2	3.3	104	1	4.4	6
08-BA-44	3,310	17.6	6.8	4.42	6.4	1.8	458	0.5	10.9	0.8	2.5	93	1.7	8.2	13
08-BA-45	570	10.5	4	7.91	4.1	0.9	561	0.4	3.1	<0.1	0.5	67	1.2	2.4	3
09-BA-45	170	3.8	1.1	4.93	1.6	0.6	77.6	4.1	1.8	0.1	1.3	11	0.3	1.8	4

**Table 1-6.** Minor element concentrations in rock samples from the Potato Peak alteration zone.

Sample number	Latitude	Longitude	Description	Au ppm	Hg ppm	Al %	Ca %	Fe %	K %	Mg %	Na %	S %	Ti %	Ag ppm	As ppm	Ba ppm
POTPK08-1	38.24439	-119.10512	Silicified volcanoclastic breccia; vuggy quartz, cinnabar, barite matrix	0.903	171,339	0.62	0.02	2.29	0.12	0.01	<0.01	3.74	0.29	1	281	76
POTPK09-20	38.24398	-119.10379	Volcanoclastic deposits replaced by fine-grained quartz and kaolinite	<0.005	17.4	8.08	0.21	7.58	0.27	0.05	0.02	0.28	0.4	<1	138	832
08-BA-46	38.244298	-119.10385	Silicified volcanoclastic deposits with alunite matrix	<0.005	0.71	3.99	0.11	3.83	1.16	<0.01	0.29	3.22	0.09	<1	79	401
08-BA-47	38.244298	-119.10385	Silicified breccia with cinnabar matrix	0.064	19,400	0.26	0.02	0.54	0.03	<0.01	<0.01	0.27	0.1	<1	51	128
08-BA-48	38.244298	-119.10385	Volcanoclastic deposits altered to dickite	<0.005	9.97	8.89	0.14	0.3	0.08	0.02	<0.01	0.31	0.4	<1	91	1,250
08-BA-49	38.246409	-119.09876	Volcanoclastic deposits altered to dickite and pyrite	0.093	5.15	5.19	0.04	1.79	0.02	<0.01	<0.01	2.09	0.07	1	29	438

**Table 1-6.** Minor element concentrations in rock samples from the Potato Peak alteration zone.—Continued

Sample number	Be ppm	Bi ppm	Cd ppm	Ce ppm	Co ppm	Cr ppm	Cs ppm	Cu ppm	Ga ppm	In ppm	La ppm	Li ppm	Mn ppm	Mo ppm	Nb ppm	Ni ppm
POTPK08-1	0.4	1.32	0.3	37.5	5.9	12	<5	30	2.01	0.12	16.6	22	8	17.2	9.5	12.9
POTPK09-20	1	0.27	<0.1	81.8	0.3	99	<5	29.4	21.1	0.13	41.5	52	9	3.94	8.2	1
08-BA-46	0.3	18.5	<0.1	87.7	0.6	26	<5	13.2	21.7	0.05	39.4	1	6	13	1.6	0.9
08-BA-47	0.2	5.17	<0.1	9.5	0.7	4	<5	27.6	0.7	<0.02	4.5	10	8	12.1	1.7	2.3
08-BA-48	0.4	8.32	<0.1	75.4	0.2	24	<5	6.9	28.4	0.03	35	82	10	12.2	8.6	0.5
08-BA-49	0.3	3.85	<0.1	49.9	4.8	18	<5	17.1	15.7	<0.02	24.6	73	<5	3.43	2.3	13.6

**Table 1-6.** Minor element concentrations in rock samples from the Potato Peak alteration zone.—Continued

Sample number	P ppm	Pb ppm	Rb ppm	Sb ppm	Sc ppm	Sn ppm	Sr ppm	Te ppm	Th ppm	Tl ppm	U ppm	V ppm	W ppm	Y ppm	Zn ppm
POTPK08-1	250	61.4	4.6	98.4	5.3	0.9	172	2.6	10.4	3.8	5.6	14	13.5	15.7	43
POTPK09-20	3,000	59	11.6	10.3	12.4	1.8	1,220	0.8	21	0.8	3.9	265	6.1	4.9	7
08-BA-46	2310	33	4	6.96	8.9	0.9	1,040	0.4	21.4	0.2	2	81	2.5	1.6	2
08-BA-47	230	4.7	1.2	20.3	0.8	1.3	148	0.3	3.2	0.3	1.6	9	1.3	1.8	5
08-BA-48	1,960	17.2	2.4	14.5	6.7	1.7	1,120	1	17.9	0.2	3.6	166	10.1	6.1	15
08-BA-49	850	22.5	1	7.75	2.3	0.7	875	0.8	13.2	0.5	1.2	60	1.9	1.7	2

**Table 1-7.** Minor element concentrations in rock samples from the Aurora Mining District.

[K, potassium; —, no data]

Sample number	Latitude	Longitude	Description <sup>1</sup>	Au ppm	Hg ppm	Al %	Ca %	Fe %	K %	Mg %	Na %	S %	Ti %	Ag ppm	As ppm	Ba ppm
AUR10-1	38.27118	-118.89644	Dream adit dump; Bald Eagle vein?	0.005	0.73	2.77	0.03	0.12	0.93	<0.01	0.17	1.98	0.15	<1	40	550
AUR11-10ME	38.27321	-118.90045	Irregularly banded quartz vein with sulfide streaks, clots; Cortez-Utah	0.121	0.02	0.84	0.06	0.28	0.32	0.05	0.01	0.17	0.02	11	29	72
AUR11-12	38.27019	-118.9017	Irregularly banded quartz vein, minor sulfides; Seminole	2	0.43	0.68	0.03	0.54	0.26	0.04	<0.01	0.57	<0.01	32	17	34
AUR11-15	38.27321	-118.89905	Quartz vein, minor sulfides; Gladiator	0.505	0.61	1.69	0.09	0.39	0.68	0.1	0.02	0.34	0.04	22	87	246
AUR11-16	38.28483	-118.8924	Pyritic quartz stockwork, dump; Wide West	1.62	0.06	1.27	0.04	1.96	0.88	0.08	0.02	1.63	0.04	29	257	245
AUR11-17A	38.27727	-118.88483	Quartz-sulfide vein, mine dump; drainage between Middle-Martinez Hills	8.16	0.03	1.31	0.07	0.67	0.63	0.04	0.02	0.39	0.02	6	4,290	198
AUR11-19ME	38.29572	-118.89484	Quartz-K-mica vein, open cut, rhyolite of Aurora	0.026	0.16	3.07	0.08	0.1	0.17	0.02	<0.01	0.01	0.03	<1	87	229
12-BA-19A	38.26533	-118.90017	Esmeralda vein, sulfide dump sample	84.8	0.29	1.26	0.05	0.44	0.44	0.06	0.02	0.51	0.02	1,110	511	142
12-BA-19B	38.26533	-118.90017	Esmeralda vein, sulfide dump sample	65.1	0.2	0.99	0.05	0.43	0.35	0.06	0.01	0.29	0.01	1,370	438	121
NE-1	38.30685	-118.84810	New Esmeralda Mine, quartz vein with black sulfides	3.42	1.18	0.55	0.09	0.1	0.1	0.03	0.01	0.02	<0.01	42	29	106
NE-2	38.30685	-118.84810	New Esmeralda Mine, quartz vein with black sulfides	0.658	0.23	0.32	0.1	0.09	0.05	0.04	0.01	<0.01	<0.01	20	23	40
11-BA-52C	38.30685	-118.84810	New Esmeralda Mine, quartz vein with black sulfides	0.102	0.09	0.68	0.06	0.21	0.15	0.03	0.02	<0.01	0.02	8	45	80
11-BA-52D	38.30685	-118.84810	New Esmeralda Mine, quartz vein with black sulfides	0.224	0.1	0.89	0.07	0.25	0.2	0.04	0.01	<0.01	0.02	5	56	92

**Table 1-7.** Minor element concentrations in rock samples from the Aurora Mining District.—Continued

[K, potassium; —, no data]

Sample number	Be ppm	Bi ppm	Cd ppm	Ce ppm	Co ppm	Cr ppm	Cs ppm	Cu ppm	Ga ppm	In ppm	La ppm	Li ppm	Mn ppm	Mo ppm	Nb ppm	Ni ppm	P ppm	Pb ppm
AUR10-1	<0.1	1.3	<0.1	9.16	0.2	7	<5	4.2	15.5	<0.02	7.7	<1	<5	0.83	3	<0.5	450	47.6
AUR11-10ME	1.1	0.89	0.3	6.77	0.4	1	<5	36.9	2.39	<0.02	3.5	73	27	111	0.7	2.7	60	19.1
AUR11-12	0.7	0.46	<0.1	2.91	0.1	1	<5	26.4	1.43	<0.02	2.1	66	80	57.8	<0.1	0.9	<50	62.6
AUR11-15	1.6	1.16	0.5	13.1	1	1	13	29.1	6.53	<0.02	5.9	89	39	1,310	1.4	3.1	170	17.3
AUR11-16	1.4	3.58	0.5	20	0.5	3	7	131	4.06	<0.02	13	150	40	924	0.5	0.7	170	56.9
AUR11-17A	1.9	0.17	<0.1	14	0.2	2	<5	13.6	2.36	<0.02	9.4	99	40	129	1.1	1.3	120	7.7
AUR11-19ME	0.9	0.31	<0.1	13	0.2	1	<5	9.6	7.73	<0.02	8.3	107	16	13.5	4.2	1.7	110	17
12-BA-19A	0.8	0.04	3.3	5.06	0.5	1	<5	1,090	2.02	<0.02	2.8	85	51	53.4	0.8	1.3	<50	47.9
12-BA-19B	0.7	0.08	1.8	1.95	0.4	<1	<5	367	1.77	<0.02	1.2	92	49	94.6	0.3	1.2	<50	84.6
NE-1	2	37.4	<0.1	0.48	0.2	<1	8	13.9	1.4	<0.02	<0.5	119	24	12.1	0.1	1.6	<50	5
NE-2	2	13.8	<0.1	0.7	1	<1	<5	7.7	3.92	<0.02	<0.5	63	167	1.1	0.1	12.5	80	1.1
11-BA-52C	1.4	1.85	0.2	2.64	28.7	2	6	10.9	1.52	<0.02	1	130	826	11.1	0.3	93.5	60	2.4
11-BA-52D	1.3	1.34	0.2	3.23	44	2	5	12.9	1.78	<0.02	1.2	123	1,100	17.6	0.3	127	70	1.4

**Table 1-7.** Minor element concentrations in rock samples from the Aurora Mining District.—Continued

[K, potassium; —, no data]

Sample number	Rb ppm	Sb ppm	Sc ppm	Se ppm	Sn ppm	Sr ppm	Te ppm	Th ppm	Tl ppm	U ppm	V ppm	W ppm	Y ppm	Zn ppm
AUR10-1	0.6	8.84	0.8	—	3.4	404	0.6	2.4	<0.1	0.2	18	0.4	0.7	1
AUR11-10ME	24	18.6	0.4	0.4	0.2	23.4	1.1	0.4	0.5	0.7	11	2.7	5	19
AUR11-12	20.5	25.8	0.1	2.9	0.7	14.2	0.4	<0.2	0.3	0.5	9	3.9	7.7	8
AUR11-15	52.9	79	0.6	1	0.4	49.4	1.3	0.7	12.3	1.1	24	6.3	7.4	11
AUR11-16	62.8	64.1	1.3	1.9	0.3	138	3.7	0.2	3.6	0.2	52	10.7	3.5	4
AUR11-17A	34.3	69.8	0.3	2.2	0.3	44.4	0.2	0.6	0.8	0.3	5	0.6	4.6	7
AUR11-19ME	15.3	20.8	1	0.7	0.4	54.1	<0.1	9.3	0.2	4.4	43	3.7	4.7	8
12-BA-19A	20.9	264	0.3	203	0.2	21.8	15.7	0.4	0.3	0.1	8	1	0.6	195
12-BA-19B	20.7	275	0.2	198	0.2	20	7.5	<0.2	0.2	<0.1	8	1.2	0.4	70
NE-1	10.8	267	<0.1	3.7	0.1	35.5	13	<0.2	0.6	<0.1	3	1.3	0.2	4
NE-2	4.9	226	<0.1	0.8	<0.1	47.7	6.6	<0.2	0.6	<0.1	2	0.7	56.5	9
11-BA-52C	12.2	88.7	0.3	0.2	0.1	45.3	0.4	0.2	6	0.1	5	1.7	8.8	70
11-BA-52D	15.3	67.5	0.3	<0.2	0.2	42.6	0.6	0.3	9.4	0.1	7	2.1	7	104

<sup>1</sup>Locations of veins (Bald Eagle, Cortez-Utah, Seminole, Gladiator, Wide West) are on figure 20.

**Table 1-8.** Minor element concentrations in rock samples from the Four Corners alteration zone.

[Fe, iron; Mn, manganese]

Sample number	Latitude	Longitude	Description	Au ppm	Hg ppm	Al %	Ca %	Fe %	K %	Mg %	Na %	S %	Ti %	Ag ppm	As ppm	Ba ppm
08HC1	38.28055	-119.10158	Red mud layer	0.005	0.84	0.77	0.35	1.56	0.07	0.02	0.02	0.2	0.53	<1	19	717
08HC2	38.28055	-119.10158	Silt/sand sediment below mud	<0.005	0.08	0.34	0.1	0.39	0.04	<0.01	0.02	0.06	0.69	<1	8	118
08HC3	38.28055	-119.10158	Red sand below mud	<0.005	0.65	1.4	0.29	0.52	0.11	0.03	0.03	0.23	0.71	<1	12	443
08HC4	38.28067	-119.10175	Coarse pebble/sand	<0.005	0.22	0.2	0.15	1.65	0.02	<0.01	0.01	0.12	0.69	<1	8	730
08HC5	38.28046	-119.10162	Fe and Mn oxide breccia	0.006	6.2	0.51	0.08	12.9	0.05	<0.01	0.02	0.06	0.85	<1	408	327
08HC6	38.28049	-119.10157	White opalite breccia	<0.005	0.39	0.2	0.44	0.19	0.08	0.01	0.02	0.26	0.16	<1	12	114
08HC7	38.28049	-119.10157	Black massive benatite	<0.005	15.1	0.39	0.08	12.5	0.06	<0.01	0.02	0.04	0.55	<1	353	934
08HC8	38.28094	-119.09985	Knob of Fe oxide breccia	<0.005	9.9	1.22	0.44	4.32	0.48	0.05	0.03	0.66	0.31	<1	1,190	2,490
08-BA-30	38.28048	-119.10142	Red hematite silicified breccia with fragments of white silica	<0.005	0.49	0.23	0.02	1.09	0.03	<0.01	0.02	<0.01	0.24	<1	17	52
08-BA-31	38.28062	-119.09941	Silicified jarosite-rich breccia with blocks of flow-banded andesite?	0.061	0.17	1.33	0.12	2.27	0.47	0.07	0.02	0.45	0.39	<1	3,510	1,380

**Table 1-8.** Minor element concentrations in rock samples from the Four Corners alteration zone.—Continued

[Fe, iron; Mn, manganese]

Sample number	Be ppm	Bi ppm	Cd ppm	Ce ppm	Co ppm	Cr ppm	Cs ppm	Cu ppm	Ga ppm	In ppm	La ppm	Li ppm	Mn ppm	Mo ppm	Nb ppm	Ni ppm
08HC1	0.8	1.97	0.7	11.1	6.5	19	8	13.3	1.68	0.02	5.5	86	772	1.02	4.3	4.9
08HC2	0.5	0.63	<0.1	3.77	0.4	11	6	5.3	1.2	<0.02	1.8	77	27	0.21	8.3	0.9
08HC3	0.6	0.59	<0.1	9.42	1.1	18	8	13.7	2.56	<0.02	4.9	81	86	0.71	3.9	2.3
08HC4	0.2	0.93	<0.1	2.33	0.7	11	<5	3.8	1.52	<0.02	1.6	57	43	0.6	7.6	0.7
08HC5	0.6	9.13	<0.1	16.6	2.2	33	7	16.8	4.06	0.98	6.6	68	129	9.72	3.3	1.1
08HC6	0.2	1.54	<0.1	1.85	1.2	8	<5	32.5	0.86	<0.02	0.7	15	82	1.11	0.7	1.6
08HC7	0.8	135	<0.1	14.6	1.4	21	5	25.4	5.48	0.49	6.6	52	75	8	2.9	3
08HC8	1.4	0.2	0.3	21.8	2.1	47	8	6.9	21.9	0.06	15.8	83	279	1.28	3.6	3.1
08-BA-30	0.3	1.6	<0.1	0.77	0.2	3	<5	7.2	1.6	<0.02	<0.5	42	44	0.73	1.7	<0.5
08-BA-31	0.7	0.27	0.1	35	0.6	9	9	20.4	17.6	0.09	20.9	28	46	2.35	4	2

**Table 1-8.** Minor element concentrations in rock samples from the Four Corners alteration zone.—Continued

[Fe, iron; Mn, manganese]

Sample number	P ppm	Pb ppm	Rb ppm	Sb ppm	Sc ppm	Sn ppm	Sr ppm	Te ppm	Th ppm	Tl ppm	U ppm	V ppm	W ppm	Y ppm	Zn ppm
08HC1	1,080	21.7	6.6	52.1	1.8	1	135	2	1.4	0.3	0.7	38	24.3	3	24
08HC2	130	7.1	4.2	42.6	1.2	0.6	33.3	0.6	0.5	0.2	0.2	13	4.6	0.4	4
08HC3	950	10.8	8.5	53.3	2.3	0.7	186	1.3	1.2	0.2	0.6	26	3.3	1.5	14
08HC4	120	2.9	1.9	48.4	0.7	1.4	25.9	0.8	0.3	<0.1	0.4	22	24.6	1	3
08HC5	760	201	4.8	20.6	2.9	2	150	3.3	3.7	0.3	1.3	56	5.3	2.5	10
08HC6	2,080	4.5	2	30.5	0.9	1.2	32.2	1.4	0.3	<0.1	0.3	6	2	0.8	8
08HC7	1,020	421	3.9	109	3.8	3.3	76.9	18.1	3.4	0.3	1.7	24	25.6	3.3	16
08HC8	2,720	84.7	32.3	69.2	9.8	1	559	<0.1	16.6	1.3	1	166	74.5	2.3	15
08-BA-30	<50	3.6	3.2	51	0.5	0.5	8.7	0.2	<0.2	0.1	0.2	22	7.5	0.4	5
08-BA-31	3,850	795	32.5	152	27.6	1.5	826	0.9	41.8	0.7	1.5	28	18.3	3.2	12

**Table 1-9.** Minor element concentrations in rock samples from the Paramount-Bald Peak alteration zone.

[Hg, mercury; HgS, mercury sulfide; mm, millimeter; cb, cinnabar; py, pyrite; —, no data]

Sample number	Latitude	Longitude	Description	Location	Au ppm	Hg ppm	Al %	Ca %	Fe %
ATAS06-1	38.26255	-119.01192	Sinter with mm-thick black layers, intact terrace, Atastra Creek	Atastra Creek	0.004	1.56	0.61	0.03	0.05
06-BA-5	38.2621	-119.0125	Silicified fault underlying sinter terrace; Atastra Creek	Atastra Creek	0.009	0.85	1.02	0.03	0.15
06-BA-6	38.2621	-119.0125	Banded sinter with black bands; Atastra Creek	Atastra Creek	0.005	0.12	0.71	0.03	0.22
06-BA-7	38.2643	-119.0074	Chalcedony veins cutting tuff of Paramount; Atastra Creek	Atastra Creek	<0.005	13.4	3.38	0.13	2.24
06-BA-8	38.2643	-119.0074	Chalcedony veins cutting tuff of Paramount; Atastra Creek	Atastra Creek	<0.005	4.65	3.81	0.09	0.73
11-BA-43	38.26169	-119.00869	Fe-oxide-silica altered lower Eureka Valley Tuff overlying strongly argillized Paramount tuff and sediments	Atastra Creek	0.01	5.94	0.61	0.13	3.9
11-BA-33A	38.34568	-118.98167	Chalcedony-pyrite vein cutting silicified Paramount tuff and sediments	Hilton Springs	2.64	3.94	1.89	0.03	1.38
11-BA-33B	38.34568	-118.98167	Silicified pyritic wall rock from 11-BA-33A	Hilton Springs	1.62	44.1	3.03	0.07	0.71
11-BA-34A	38.29883	-118.99753	Silicified finely laminated sediments in Paramount tuff and sediment sequence	Hilton Springs	0.023	0.23	0.7	0.07	0.26
11-BA-34B	38.29883	-118.99753	Silicified finely laminated sediments in Paramount tuff and sediment sequence	Hilton Springs	0.542	2.25	0.97	0.05	1.82
11-BA-35A	38.29805	-118.99864	Silicified finely laminated sediments in Paramount tuff and sediment sequence	Hilton Springs	0.026	2.06	1.03	0.07	1.38
11-BA-35B	38.29805	-118.99864	Silicified finely laminated sediments in Paramount tuff and sediment sequence	Hilton Springs	0.061	4.17	0.6	0.06	0.51
PMT06-1	38.27787	-119.05766	5-foot chalcedonic quartz vein with white clay pockets, long dozer cut, Paramount Mine	Paramount Mine hill	0.007	137	0.35	0.03	0.12
PMT06-1A	38.27787	-119.05766	5-foot chalcedonic quartz vein with white clay pockets, long dozer cut, Paramount Mine	Paramount Mine hill	0.034	71.5	0.29	0.03	0.08
PMT06-2	38.27823	-119.05859	Dense 7-foot chalcedonic quartz vein with minor cb, py; upper adit, Paramount Mine	Paramount Mine hill	0.061	1,600	0.36	0.01	0.06
PMT06-3	38.27729	-119.06083	Sinter blocks, west dismembered terrace, Paramount Mine hill	Paramount Mine hill	0.018	1.35	0.22	0.02	0.1
07PM1	38.2773	-119.0595	Sinter	Paramount Mine hill	0.017	0.53	0.1	0.07	0.07
07PM2	38.2773	-119.0595	Quartz carbonate breccia	Paramount Mine hill	0.237	1.23	2.2	0.04	0.42
07PM4	38.2777	-119.0577	Chalcedony vein cutting breccia	Paramount Mine hill	0.495	94.2	2.26	0.02	0.51
07PM6	38.2759	-119.0539	Silicified tuff cut by quartz veins	Paramount Mine hill	0.209	16.4	1.63	0.1	1.25
07PM8	38.2779	-119.0566	White to tan chalcedonic sinter	Paramount Mine hill	0.017	2.45	0.3	0.02	0.17
07PM9	38.2778	-119.0566	Sinter cut by red chalcedony	Paramount Mine hill	0.032	1.48	1.18	0.04	0.3
07PM10	38.2778	-119.0566	Red chalcedony in sinter breccia	Paramount Mine hill	0.067	2.71	1.89	0.02	0.62
07PM11	38.2778	-119.0566	White sinter clasts in breccia	Paramount Mine hill	0.011	0.24	0.13	0.02	0.16
07PM14	38.2792	-119.0598	Calcines from Paramount Hg Mine	Paramount Mine hill	0.103	17.4	3.06	0.18	0.5
07PM12	38.2789	-119.0592	HgS in silicified tuff	Paramount Mine hill	0.063	516	0.33	0.02	0.13
07-BA-20	38.2769	-119.0569	Laminated gray silica, possible pool sinter near Paramount Mine	Paramount Mine hill	0.917	1.51	1.05	0.05	0.22
07-BA-20A	38.2769	-119.0569	Laminated gray silica, possible pool sinter near Paramount Mine	Paramount Mine hill	3.57	4.28	2.61	0.09	0.31

**Table 1-9.** Minor element concentrations in rock samples from the Paramount-Bald Peak alteration zone.—Continued

[Hg, mercury; HgS, mercury sulfide; mm, millimeter; cb, cinnabar; py, pyrite; —, no data]

Sample number	K %	Mg %	Na %	S %	Ti %	Ag ppm	As ppm	Ba ppm	Be ppm	Bi ppm	Cd ppm	Ce ppm	Co ppm	Cr ppm
ATAS06-1	0.04	<0.01	<0.01	0.02	0.07	<1	80	1,050	<5	<0.1	<0.2	16.2	<0.5	<10
06-BA-5	0.07	0.02	0.01	0.39	0.12	<1	67	687	7.1	0.13	<0.1	19.6	0.4	26
06-BA-6	0.06	0.01	0.01	0.07	0.07	<1	93	1,060	6.7	0.08	<0.1	13.8	0.2	9
06-BA-7	1.15	0.08	0.21	1.7	0.16	<1	122	340	3.8	<0.04	0.1	51.1	21.3	13
06-BA-8	0.27	0.06	0.05	0.12	0.2	<1	47	1,910	4.5	<0.04	<0.1	37.7	2.1	19
11-BA-43	0.11	0.02	0.02	0.01	0.14	<1	61	407	5.9	0.13	<0.1	69.7	1.2	6
11-BA-33A	1.99	0.02	0.03	1.15	0.04	18	643	602	1.4	0.13	<0.1	15.2	0.6	4
11-BA-33B	2.97	0.02	0.03	0.1	0.05	7	288	2,810	1.4	0.17	<0.1	30.5	0.5	4
11-BA-34A	0.18	0.02	0.01	0.08	0.02	1	37	203	3.5	0.15	<0.1	5.01	0.8	3
11-BA-34B	0.33	0.04	<0.01	0.39	0.04	8	377	2,310	4.5	0.13	<0.1	20.9	0.8	5
11-BA-35A	0.18	0.02	0.01	0.28	0.03	3	236	2,530	6.1	0.1	<0.1	5.72	1.4	4
11-BA-35B	0.12	0.01	0.02	0.24	0.03	1	205	145	4.1	0.06	<0.1	7.31	7.2	3
PMT06-1	0.09	<0.01	<0.01	<0.01	0.02	<1	40	758	9	<0.1	<0.2	1.5	<0.5	<10
PMT06-1A	0.06	<0.01	<0.01	<0.01	0.02	<1	<30	217	8	<0.1	<0.2	1.7	<0.5	<10
PMT06-2	0.06	<0.01	<0.01	<0.01	0.02	<1	<30	863	6	<0.1	<0.2	2.9	0.6	<10
PMT06-3	0.02	<0.01	<0.01	<0.01	<0.01	<1	<30	41.5	25	<0.1	<0.2	0.4	<0.5	10
07PM1	0.03	<0.01	0.01	0.03	<0.01	<1	17	115	9.5	<0.04	<0.1	0.97	0.2	3
07PM2	1.37	0.03	0.03	0.02	0.04	<1	40	268	6.1	0.16	0.1	29.4	0.9	4
07PM4	0.11	<0.01	0.01	0.1	0.06	5	170	931	6.7	0.09	<0.1	26.3	0.2	3
07PM6	1.63	0.02	0.02	0.37	0.11	2	580	621	8.4	<0.04	0.2	23.3	1.3	4
07PM8	0.06	<0.01	0.01	0.02	<0.01	<1	28	412	9.5	<0.04	<0.1	2.12	0.6	4
07PM9	0.08	<0.01	0.01	0.05	0.05	<1	72	506	9.3	<0.04	<0.1	10.7	0.9	6
07PM10	0.16	0.03	0.01	0.04	0.06	<1	90	357	6.5	0.05	<0.1	18.1	0.8	8
07PM11	0.03	<0.01	0.01	<0.01	<0.01	<1	18	56	13.9	<0.04	<0.1	1.09	0.5	3
07PM14	0.17	0.04	0.07	0.03	0.22	<1	55	586	3.6	0.13	<0.1	40.5	2.3	10
07PM12	0.06	<0.01	0.01	0.03	0.24	<1	5	584	2.9	<0.04	<0.1	3.91	0.3	4
07-BA-20	0.78	<0.01	0.02	0.03	<0.01	6	19	559	11.3	0.13	<0.1	2.35	0.8	8
07-BA-20A	2.61	0.06	0.05	0.04	0.04	3	38	883	7.7	0.04	<0.1	7.43	0.4	3



**Table 1-9.** Minor element concentrations in rock samples from the Paramount-Bald Peak alteration zone.—Continued

[Hg, mercury; HgS, mercury sulfide; mm, millimeter; cb, cinnabar; py, pyrite; —, no data]

Sample number	Cs ppm	Cu ppm	Ga ppm	In ppm	La ppm	Li ppm	Mn ppm	Mo ppm	Nb ppm	Ni ppm	P ppm	Pb ppm	Rb ppm	Sb ppm
ATAS06-1	7.9	<5	27	<0.2	9.2	30	—	3	3	<5	—	7	4.6	364
06-BA-5	10	3.6	57.2	<0.02	9.8	34	45	5.82	4.1	12.7	330	9.8	6.3	347
06-BA-6	10	4.9	45.7	<0.02	7	32	32	3.29	2.6	12.5	190	6.8	6	477
06-BA-7	28	23.8	9.01	<0.02	24.3	79	52	2.87	6.1	12.1	140	18.5	66.7	95.6
06-BA-8	20	12.6	9.27	<0.02	19.4	84	46	1.1	6.7	7.5	140	23.6	19.7	255
11-BA-43	25	25.4	2.95	<0.02	33.7	62	56	1.18	7.1	1.6	200	28.1	11.5	291
11-BA-33A	9	12	3.07	<0.02	8.7	124	14	1	2.9	1.1	300	12	112	55.5
11-BA-33B	9	9.8	3.93	<0.02	20.3	100	17	0.84	5.9	1.2	720	19.4	171	77.4
11-BA-34A	39	7.9	4.7	<0.02	2.6	49	71	0.6	0.8	1.5	60	3.5	28.4	367
11-BA-34B	20	10.6	5.03	<0.02	15.5	65	35	1.43	2.5	1.7	680	25	34	239
11-BA-35A	24	8.9	4.01	<0.02	3.6	54	23	1.26	1.2	1.9	90	10.5	20.7	222
11-BA-35B	25	3.2	5.84	<0.02	3.9	65	18	0.82	0.9	9.8	70	4.9	17.4	262
PMT06-1	15.8	7	8	<0.2	1.5	40	—	<2	<1	8	—	<5	12	916
PMT06-1A	14.8	<5	15	<0.2	1.3	50	—	<2	<1	11	—	<5	10.3	530
PMT06-2	11.8	8	12	<0.2	3.3	80	—	<2	<1	6	—	7	9	644
PMT06-3	6.1	8	12	<0.2	0.3	60	—	<2	<1	12	—	<5	3.7	204
07PM1	6	0.9	9.99	<0.02	0.7	18	69	0.6	0.2	0.5	60	0.9	3.4	396
07PM2	10	2.6	7.64	<0.02	16.9	82	67	0.38	1.6	1.8	140	5.7	90.3	159
07PM4	11	22.7	6.27	<0.02	13.4	11	29	0.43	2.8	<0.5	240	9.5	9.3	111
07PM6	13	5.3	7.33	<0.02	13.8	70	117	3.65	0.6	1	200	5.9	119	2,890
07PM8	10	1.3	7.07	<0.02	1.1	122	99	0.45	0.1	1.1	<50	1.4	7	101
07PM9	12	5.3	6.27	<0.02	5.4	81	98	0.82	1.7	1.3	90	3.4	9.3	120
07PM10	15	6.7	5.06	<0.02	11.4	162	76	0.82	1.8	1.4	380	4.7	19.9	109
07PM11	6	1.5	8.93	<0.02	0.6	18	186	1.22	<0.1	1.1	<50	1.2	4.3	198
07PM14	9	6.5	12.5	<0.02	22.7	106	54	0.92	6	3.2	340	38.9	14.6	399
07PM12	9	1.1	1.51	<0.02	2.1	96	124	1.85	6.6	0.8	<50	3.8	7.5	250
07-BA-20	18	4.9	6.02	<0.02	1.1	53	140	0.95	0.2	1.6	60	4.9	72.9	130
07-BA-20A	34	10.4	8.85	<0.02	5.4	83	48	0.19	0.7	3.7	80	5.2	192	81.8

**Table 1-9.** Minor element concentrations in rock samples from the Paramount-Bald Peak alteration zone.—Continued

[Hg, mercury; HgS, mercury sulfide; mm, millimeter; cb, cinnabar; py, pyrite; —, no data]

Sample number	Sc ppm	Sn ppm	Sr ppm	Te ppm	Th ppm	Tl ppm	U ppm	V ppm	W ppm	Y ppm	Zn ppm	Se ppm	C %
ATAS06-1	<5	<1	340	<0.5	3.3	1.8	0.79	11	19	1.5	6	<0.2	<0.01
06-BA-5	0.9	0.5	456	<0.1	5.7	0.8	0.7	18	125	1	3	—	—
06-BA-6	0.5	0.4	257	<0.1	4.1	1.6	0.5	11	20.9	0.7	5	—	—
06-BA-7	2.7	0.9	155	<0.1	6.9	2.1	8.7	47	123	4.5	9	—	—
06-BA-8	2.7	1.3	72.6	<0.1	9	0.3	4.9	28	69.7	3.5	6	—	—
11-BA-43	2.1	0.7	45.8	<0.1	14.2	0.3	5.4	83	147	6.3	13	0.3	—
11-BA-33A	1	0.4	194	0.1	6.1	3.4	3.1	6	5	2.8	2	—	—
11-BA-33B	1.8	0.5	491	<0.1	9.5	4.7	4.7	14	15.9	6.2	10	0.9	—
11-BA-34A	0.8	0.3	106	0.2	2.5	0.7	0.9	9	2.9	1	3	0.4	—
11-BA-34B	1.6	0.4	361	<0.1	4.9	0.9	3.1	23	21.6	4.1	9	0.7	—
11-BA-35A	1	0.3	209	<0.1	2.7	0.8	2.2	19	7.8	1.8	6	<0.2	—
11-BA-35B	1.5	0.3	102	<0.1	2.5	1.9	6.1	20	5.9	2.5	14	<0.2	—
PMT06-1	<5	2	80.4	<0.5	0.3	0.7	0.27	<5	16	0.9	<5	0.6	<0.01
PMT06-1A	<5	<1	49.6	<0.5	0.4	<0.5	0.35	<5	7	0.8	<5	0.3	<0.01
PMT06-2	<5	1	59.6	<0.5	0.6	<0.5	0.36	<5	10	1	6	0.3	0.01
PMT06-3	8	<1	25.8	<0.5	<0.1	<0.5	0.06	8	2	<0.5	9	<0.2	<0.01
07PM1	0.2	<0.1	20.2	0.1	<0.2	0.4	0.1	1	1.1	0.2	<1	—	—
07PM2	2.3	0.5	114	0.1	3.1	1.2	1.1	18	6.1	2.8	5	—	—
07PM4	1.7	0.5	181	<0.1	4.2	0.3	1.7	15	10.7	2.7	2	—	—
07PM6	2.3	0.5	135	<0.1	3.7	6	1.8	21	7.5	4.2	8	—	—
07PM8	0.3	<0.1	45.5	<0.1	0.4	0.3	0.1	1	0.6	0.4	3	—	—
07PM9	2.3	0.3	114	<0.1	2.2	0.5	0.8	10	8.5	2.9	3	—	—
07PM10	2.5	0.4	104	0.1	2.5	0.7	0.8	14	14.4	2	11	—	—
07PM11	0.2	<0.1	19.2	<0.1	<0.2	0.2	<0.1	1	0.7	0.2	<1	—	—
07PM14	3.4	1.2	285	<0.1	8.3	0.5	2.2	25	59.4	5.4	9	—	—
07PM12	2	0.8	45.6	<0.1	3.2	0.4	1.6	6	28.9	2.6	2	—	—
07-BA-20	0.5	0.2	129	0.1	0.4	1.8	0.2	5	0.7	0.3	6	0.6	—
07-BA-20A	1.2	0.4	116	<0.1	2	4.7	0.8	13	2.6	1.6	6	0.3	—

**Table 1-9.** Minor element concentrations in rock samples from the Paramount-Bald Peak alteration zone.—Continued

[Hg, mercury; HgS, mercury sulfide; mm, millimeter; cb, cinnabar; py, pyrite; —, no data]

Sample number	Latitude	Longitude	Description1	Location	Au ppm	Hg ppm	Al %	Ca %	Fe %
07-BA-21	38.2767	-119.0567	Altered tuff, Paramount Mine	Paramount Mine hill	0.015	0.12	3.21	0.1	0.38
07-BA-22	38.2767	-119.0567	Banded chalcedony vein with local bladed texture, Paramount Mine	Paramount Mine hill	0.741	5.03	1.18	0.05	0.45
07-BA-24	38.2778	-119.0577	Chalcedony vein in open cut, Paramount Mine	Paramount Mine hill	0.057	16.3	0.7	0.02	0.87
07-BA-25	38.2788	-119.0591	Leached, silicified pumiceous tuff, Paramount Mine dump	Paramount Mine hill	0.054	213	0.34	0.02	0.1
08-BA-13	38.27807	-119.05771	Leached pumice-rich tuff	Paramount Mine hill	0.017	0.24	4.21	0.06	0.46
08PT1	38.2675	-119.0642	Quartz-carbonate	SW Paramount hill	0.017	0.57	2.43	0.06	4
08PT2	38.2675	-119.0642	Argillically-altered, unwelded tuff	SW Paramount hill	<0.005	1.77	4.01	0.06	1.37
08PT3	38.2679	-119.0640	Breccia with silicified quartz vein	SW Paramount hill	0.089	1.42	0.92	0.05	0.38
08PT4	38.2682	-119.0634	Chalcedony-quartz veins	SW Paramount hill	1.99	4.16	1.66	0.06	0.96
08PT6	38.2688	-119.0615	Black silicified tuff	SW Paramount hill	0.033	1.37	4.78	0.05	1.54
08PT9	38.2686	-119.0593	Quartz vein adjacent to waste pile	SW Paramount hill	0.422	34.4	0.4	0.06	2.66
08PT11	38.2683	-119.0564	Porphyritic block of dacite breccia	SW Paramount hill	0.022	0.02	7.65	0.09	1.76
08PT13	38.2680	-119.0667	Banded chalcedony vein with sulfides in dacite breccia	SW Paramount hill	0.21	14.4	1.11	0.06	1.28
08PT14	38.2701	-119.0666	Chalcedonic banded vein cutting breccia	SW Paramount hill	0.2	0.26	1.87	0.06	0.35
08PT15	38.2713	-119.0686	Tuff with red-brown matrix	SW Paramount hill	0.03	2.63	4.81	0.23	1.31
09-BA-59	38.2682	-119.0606	Silicified tuff locally with cinnabar	SW Paramount hill	0.125	10.2	1.46	0.09	1.98
09-BA-60	38.2682	-119.0627	3-inch banded white quartz vein with carbonate pseudomorphs; local fine-grained pyrite	SW Paramount hill	1.68	2.85	0.9	0.04	0.53
09-BA-60A	38.2682	-119.0627	3-inch banded white quartz vein with carbonate pseudomorphs; local fine-grained pyrite	SW Paramount hill	2.05	0.75	0.58	0.02	0.23
08PT16	38.2699	-119.0515	Silicified tuff breccia with black matrix	South Paramount Mine hill	<0.005	0.01	0.62	0.04	0.2
08PT7C	38.2731	-119.0570	Quartz vein with carbonate pseudomorphs	South Paramount Mine hill	<0.005	0.24	5.74	0.17	1.37
09-BA-51	38.26194	-119.04214	Hydrothermally brecciated silicified tuff; possible vent for laminated sinter?	SW Paramount basin	0.016	0.12	1.06	0.15	0.28
09-BA-52	38.2651	-119.0449	Silicified conglomeratic breccia; locally hematite rich	SW Paramount basin	0.125	0.37	0.66	0.08	0.76
08-BA-17	38.27596	-119.03622	Silicified breccia	SW Paramount basin	<0.005	3.83	0.47	0.05	1.39
08-BA-18	38.27651	-119.03602	Prospect pit in silicified breccia with cinnabar + barite(?)	SW Paramount basin	<0.005	1,290	0.22	0.03	0.08
10-BA-32	38.26275	-119.03353	Silicified knob with strong E-W jointing	SW Paramount basin	<0.005	0.99	4.88	0.03	0.34
10-BA-33	38.26275	-119.03353	Pumice-rich tuff	SW Paramount basin	<0.005	0.26	4.37	0.34	0.68

**Table 1-9.** Minor element concentrations in rock samples from the Paramount-Bald Peak alteration zone.—Continued

[Hg, mercury; HgS, mercury sulfide; mm, millimeter; cb, cinnabar; py, pyrite; —, no data]

Sample number	K %	Mg %	Na %	S %	Ti %	Ag ppm	As ppm	Ba ppm	Be ppm	Bi ppm	Cd ppm	Ce ppm	Co ppm	Cr ppm
07-BA-21	4.2	0.02	0.04	0.02	0.07	<1	22	941	3.6	0.05	<0.1	42.8	0.3	2
07-BA-22	1	0.02	0.03	0.04	0.03	13	89	657	19.6	<0.04	0.2	7.72	0.4	5
07-BA-24	0.12	<0.01	0.03	0.03	0.03	<1	89	1,530	10.3	<0.04	<0.1	6.89	0.1	4
07-BA-25	0.08	<0.01	0.02	0.03	0.22	<1	7	1,030	4.6	<0.04	<0.1	7.38	0.2	4
08-BA-13	0.1	0.03	0.02	0.04	0.13	<1	63	413	2.7	0.16	0.2	43	1.4	2
08PT1	1.86	0.03	0.05	0.02	0.08	<1	324	436	5.3	0.06	0.2	28.5	3.8	19
08PT2	4.15	0.12	0.08	0.04	0.33	<1	387	907	2.6	0.07	<0.1	27.2	0.5	3
08PT3	0.27	0.05	0.02	0.05	0.03	<1	57	339	7.6	<0.04	<0.1	14.6	0.3	9
08PT4	1.6	0.02	0.03	0.06	0.05	7	116	714	6.2	<0.04	<0.1	11	0.6	22
08PT6	5.65	0.03	0.07	0.05	0.1	<1	270	1,830	2.8	0.08	<0.1	53.3	0.5	12
08PT9	0.15	0.01	0.01	0.14	<0.01	<1	896	1,460	12.6	0.09	<0.1	4.22	0.8	13
08PT11	5.58	0.09	0.46	0.01	0.19	<1	73	1,820	1.8	<0.04	<0.1	48	2.9	6
08PT13	0.91	0.02	0.03	0.65	0.04	1	133	291	2	<0.04	<0.1	6.6	0.3	12
08PT14	2.01	0.02	0.03	0.12	0.08	<1	128	373	3.4	<0.04	<0.1	16.3	0.5	7
08PT15	5.81	0.09	0.08	0.11	0.24	<1	13	1,460	3.1	0.06	0.1	54.5	4.3	5
09-BA-59	1.41	0.06	0.02	0.58	0.1	<1	4,000	2,540	4.2	<0.04	<0.1	17.6	0.8	2
09-BA-60	0.71	0.01	<0.01	0.3	0.04	5	696	605	3.3	<0.04	<0.1	8.2	0.4	2
09-BA-60A	0.38	<0.01	<0.01	<0.01	0.02	1	79	150	3.6	<0.04	<0.1	3.4	0.4	1
08PT16	0.17	0.01	0.12	0.09	0.7	<1	15	1,490	0.2	0.45	<0.1	9.03	0.4	11
08PT7C	3.75	0.45	0.04	0.03	0.31	<1	222	740	3.7	0.1	<0.1	80.5	1.6	3
09-BA-51	0.1	0.02	0.01	0.07	0.48	<1	23	367	0.7	0.24	0.2	14.2	1.5	6
09-BA-52	0.08	0.02	0.02	0.1	0.46	<1	151	957	0.8	0.16	<0.1	14.2	0.9	2
08-BA-17	0.04	0.01	<0.01	0.15	0.62	<1	219	4,440	0.5	0.51	0.1	5.97	0.7	6
08-BA-18	0.03	<0.01	<0.01	0.04	0.26	<1	14	1,180	0.5	0.22	<0.1	2.92	0.2	2
10-BA-32	0.06	<0.01	0.01	0.07	0.29	<1	66	758	0.7	0.06	<0.1	53.6	0.2	6
10-BA-33	0.08	0.01	<0.01	0.19	0.07	<1	133	223	0.6	0.38	<0.1	30.2	0.3	3

**Table 1-9.** Minor element concentrations in rock samples from the Paramount-Bald Peak alteration zone.—Continued

[Hg, mercury; HgS, mercury sulfide; mm, millimeter; cb, cinnabar; py, pyrite; —, no data]

Sample number	Cs ppm	Cu ppm	Ga ppm	In ppm	La ppm	Li ppm	Mn ppm	Mo ppm	Nb ppm	Ni ppm	P ppm	Pb ppm	Rb ppm	Sb ppm
07-BA-21	18	2	7.6	<0.02	22.5	83	72	0.2	2.5	0.6	150	14.3	264	49.6
07-BA-22	29	6	21.2	<0.02	4.2	79	41	0.36	0.8	2.4	70	4	85.3	151
07-BA-24	22	5.4	12.3	<0.02	4	39	27	0.21	0.1	1.7	<50	2.7	16.4	122
07-BA-25	11	4.6	2.27	<0.02	4.1	79	67	0.27	1.5	1.3	<50	6.8	10.2	231
08-BA-13	6	6.3	11.8	0.03	24.3	49	170	0.62	8.5	2.3	330	13.3	8.6	59.7
08PT1	7	18.4	4.44	<0.02	18.8	111	175	0.93	1.3	7.5	1,080	6.3	117	65
08PT2	21	11.9	11.7	0.03	15	90	31	0.35	7	0.5	140	9.2	312	69.2
08PT3	30	4.3	2.71	<0.02	6.7	121	22	1.57	0.3	1.2	130	2.4	31.5	363
08PT4	10	6.7	4.02	<0.02	6.1	101	59	0.88	0.6	2.5	380	4.1	98.1	104
08PT6	11	6.2	11	0.03	32.1	58	39	0.67	2.9	1.2	590	11.7	414	50.8
08PT9	<5	8.2	3.47	<0.02	1.5	48	28	2	<0.1	1.3	280	1.3	5.2	620
08PT11	11	13	18	0.03	26.9	16	96	0.48	3.5	2.7	920	15.8	351	18.5
08PT13	12	7.2	2.03	<0.02	4.2	139	33	0.4	0.6	<0.5	540	8.4	64	120
08PT14	15	4.3	6.48	<0.02	8.7	59	23	0.41	1.8	1.1	210	4.2	142	57
08PT15	15	13.3	11.4	0.03	32.3	90	97	0.41	6.2	3.8	470	12.1	457	54
09-BA-59	24	105	4.4	<0.02	8.8	90	35	0.93	2.4	0.5	490	5.4	110	197
09-BA-60	8	3.7	4.98	<0.02	3.7	81	28	2.34	0.3	<0.5	80	3.4	49	349
09-BA-60A	<5	3	4.77	<0.02	1.8	84	54	0.48	0.1	1.1	80	2.4	27.2	55.1
08PT16	32	5.2	1.02	<0.02	5.6	1	12	2.29	18.5	6.2	150	17.4	22.7	0.81
08PT7C	56	3.5	16.4	0.04	41	36	93	0.6	12	1.2	1,640	19.7	403	56.6
09-BA-51	6	18.4	3.1	<0.02	7.8	45	161	2.44	8.5	1.6	940	15.4	7	52.2
09-BA-52	<5	12.5	4.01	<0.02	7	33	98	4.38	9.7	1.1	250	15.7	4.9	64.7
08-BA-17	<5	11.2	0.98	<0.02	4.3	25	74	2.38	23.8	2.9	360	6.2	2.1	29.7
08-BA-18	<5	4.9	0.89	<0.02	2	17	36	0.61	9	0.8	<50	5	1.4	4.89
10-BA-32	6	5.4	10.8	<0.02	29.6	42	25	4.23	8	0.7	170	8.7	3.9	56.2
10-BA-33	6	7.7	11.4	<0.02	16.3	48	31	1.98	13.8	0.6	150	17.9	4.5	35.4

**Table 1-9.** Minor element concentrations in rock samples from the Paramount-Bald Peak alteration zone.—Continued

[Hg, mercury; HgS, mercury sulfide; mm, millimeter; cb, cinnabar; py, pyrite; —, no data]

Sample number	Sc ppm	Sn ppm	Sr ppm	Te ppm	Th ppm	Tl ppm	U ppm	V ppm	W ppm	Y ppm	Zn ppm	Se ppm	C %
07-BA-21	1.3	0.7	54.8	<0.1	6.3	1.9	2.1	25	2	4.1	9	<0.2	—
07-BA-22	1	0.3	121	<0.1	1.2	1.7	0.5	72	2.6	1.5	20	1.3	—
07-BA-24	0.9	0.2	74.4	<0.1	1.3	0.4	0.8	18	9.8	0.9	4	<0.2	—
07-BA-25	2.2	0.5	50.6	<0.1	4.1	0.2	1.8	5	2.3	2.5	2	0.4	—
08-BA-13	2.7	1.1	69.9	0.1	13.2	0.1	4.3	29	16.6	10.1	19	—	—
08PT1	3.2	0.3	114	<0.1	2.5	1.7	1.7	33	3.3	5.3	83	—	—
08PT2	7	1.3	62.2	<0.1	8	5.4	2.8	70	10.6	6.8	6	—	—
08PT3	1.3	0.3	92.7	<0.1	1.2	1.1	0.4	16	1.3	1.6	3	—	—
08PT4	1.5	0.3	102	<0.1	1.3	1.6	0.6	12	2.4	1.5	9	—	—
08PT6	3.2	0.9	195	<0.1	5.4	7.3	1.8	37	3.5	5.7	22	—	—
08PT9	0.9	<0.1	67.7	<0.1	0.2	13.7	0.5	8	16.7	2.2	14	—	—
08PT11	5.9	0.8	356	<0.1	8.1	10.8	2.6	55	13.3	5.1	21	—	—
08PT13	1.8	0.3	87.1	<0.1	0.9	3.7	1	17	2.5	0.9	2	—	—
08PT14	2.3	0.3	106	<0.1	2.1	2.1	0.9	25	4.8	2.2	5	—	—
08PT15	5.2	1.2	314	<0.1	8.4	8	3.1	49	7.4	14.7	53	—	—
09-BA-59	2.1	0.7	240	<0.1	3.2	6.8	1.7	17	4.3	3.4	3	1	—
09-BA-60	0.8	0.8	77.6	<0.1	1	3.8	0.4	6	1.1	1.6	1	0.5	—
09-BA-60A	0.5	0.3	41	<0.1	0.5	0.4	0.2	5	0.7	0.7	3	<0.2	—
08PT16	3.5	3.3	101	0.1	6	1.7	3.8	10	1.3	2.4	3	—	—
08PT7C	6.9	1.9	60.7	<0.1	14.2	5.5	4.9	30	13.7	11.9	22	—	—
09-BA-51	1.5	2	82.9	0.3	4.9	0.2	4.3	27	37.2	3.3	9	—	—
09-BA-52	1.4	1.4	70.3	<0.1	7.7	0.2	3.4	53	83.3	4.2	6	0.4	—
08-BA-17	5.7	2.5	123	0.2	5.4	<0.1	6.2	38	27.7	9.4	13	—	—
08-BA-18	2.2	0.8	44.5	0.2	4	<0.1	3.5	5	5.4	3	15	—	—
10-BA-32	4.4	1.1	79.5	0.1	14.2	5.5	4.1	62	21.9	7.4	3	—	—
10-BA-33	1.7	0.7	65.8	0.2	20.9	1.2	4	16	6.4	4.5	4	—	—

**Table 1-10.** Minor element concentrations in rocks samples from the Cinnabar Canyon-US 395 alteration zone.

[alt, alteration; DDH, diamond drill hole; Fe, iron; FeOx, iron oxide; HgS, mercury sulfide; K, potassium; RDH, rotary drill hole; S, sulfur]

Sample number	Description	Latitude	Longitude	Au ppm	Hg ppm	Al %	Ca %	Fe %	K %	Mg %	Na %
CCD7	Cinnabar Canyon S resource DDH	38.19268	-119.1597	0.084	28.9	0.07	0.02	1.62	0.01	0.01	<0.01
CCD8B	Cinnabar Canyon S resource DDH	38.19087	-119.1597	0.018	42.6	0.07	0.05	2.16	0.01	0.02	<0.01
CCD16	Cinnabar Canyon S resource DDH	38.19317	-119.16045	0.014	84.1	0.14	0.05	3.96	0.02	0.02	0.02
07-BA-10	S resource RDH cuttings, opal-montmorillonite-altered porphyritic dacite	38.18924	-119.15404	<0.005	0.24	0.44	0.03	0.58	0.03	<0.01	0.06
07-BA-11	Silicified volcanoclastic breccia	38.18967	-119.15578	<0.005	0.14	0.08	0.02	0.05	<0.01	0.01	<0.01
07CC1	Calmono Hg Mine; HgS in altered andesite	38.18625	-119.15728	0.037	92	8.62	0.22	0.97	1.89	0.05	0.58
07CC2	Calmono Hg Mine; HgS in altered andesite opal	38.18625	-119.15728	<0.005	337	8.18	0.16	2.14	1.32	0.03	0.36
07CC5	Calmono Hg Mine; calcines from Hg mine	38.18625	-119.15728	0.006	21.6	8.67	0.58	4.99	0.98	0.19	0.38
07CC6	Calmono Hg Mine; sulfide in white opal	38.18625	-119.15728	<0.005	0.71	0.26	0.06	0.54	0.11	<0.01	0.01
07-BA-8	Cinnabar Canyon, argillized/opal-altered porphyritic dacite	38.2765	-119.16040	0.03	0.11	9.12	0.13	0.42	0.23	0.05	0.04
07-BA-9	Silicified, Fe-oxide-rich breccia, Cinnabar Canyon	38.2736	-119.13960	0.009	66.5	0.36	0.04	6.14	0.07	<0.01	0.03
07-BA-14	Argillized andesite with opal pods, Cinnabar Canyon	38.2907	-119.1406	<0.005	181	7.81	0.12	3.63	1.44	0.03	0.31
07-BA-16	Quarry in acid-leached breccia, mouth of Cinnabar Canyon	38.2984	-119.1387	<0.005	0.55	0.44	0.05	0.23	0.13	0.01	0.06
08CC3	Argillic-leached lithic tuff	38.17418	-119.1523	<0.005	0.03	9.59	0.1	1.33	2.93	0.04	1.49
08CC4	Biotite rhyolite porphyry flow	38.17166	-119.15484	<0.005	0.01	7.42	1.35	1.23	3.47	0.31	2.63
08CC5	Plagioclase-K-feldspar dacite porphyry	38.17445	-119.15487	<0.005	<0.01	7.68	3.04	3.12	2.83	1.21	2.8
08CC6	Porphyritic andesite with fractures	38.17403	-119.15355	<0.005	0.03	0.51	0.06	2.16	0.14	<0.01	0.08
08CC7	Fault zone in dacite breccia	38.18449	-119.15257	<0.005	0.04	3.42	0.14	2.12	0.17	0.04	0.07
08CC8	Andesite porphyry with plagioclase phenocrysts	38.18832	-119.14996	<0.005	0.21	0.13	0.02	2.76	0.07	<0.01	0.06
08CC9	Knob of opalized porphyritic andesite	38.18931	-119.14887	<0.005	0.07	0.27	0.05	0.31	0.14	0.01	0.04
08CC10	Partially leached dacite porphyry	38.19052	-119.14950	<0.005	0.01	7.19	0.69	2.29	2.61	0.33	1.52
08CC11	Opalized andesite	38.18790	-119.14996	<0.005	0.15	0.18	0.03	0.63	0.11	<0.01	0.02
08CC12	South end of opalite hill	38.18754	-119.14703	<0.005	0.15	1.38	0.09	0.43	0.27	0.03	0.1
08CC13	White opal cutting opalized porphyritic andesite	38.18605	-119.15802	<0.005	0.05	6.02	0.1	1.02	2.48	0.01	0.12
08CC14	Hematite and goethite cemented breccia	38.19149	-119.15797	<0.005	10.2	1.26	0.06	23.6	0.07	<0.01	0.02
08CC15B	Altered	38.19207	-119.15808	<0.005	57.7	0.2	0.03	2.09	0.07	<0.01	0.05
08CC16	Massive chalcedony breccia	38.19147	-119.15773	<0.005	0.13	0.13	<0.01	0.06	<0.01	<0.01	<0.01
08CC17	Andesite with fractures filled by opal	38.19324	-119.15959	0.008	15.6	0.13	0.03	3.34	0.03	<0.01	0.01
08CC21	Andesite with plagioclase phenocrysts	38.19104	-119.15895	<0.005	106	0.06	<0.01	4.19	0.01	<0.01	<0.01
08CC22	Kaolinite north of road with some pyrite	38.19871	-119.17207	<0.005	0.08	6.34	0.39	1.01	2.14	0.11	0.61
08CC23	Tan opalite/porphyritic dacite	38.18489	-119.17728	<0.005	0.04	0.34	0.1	0.82	0.07	0.03	0.02
08CC24	Opalite-chalcedony	38.18813	-119.17698	<0.005	0.48	0.08	0.02	0.08	0.01	<0.01	0.01
08CC25	Opalite brecciated chalcedony with sulfides	38.18680	-119.17733	0.028	0.67	0.33	0.02	0.19	0.09	<0.01	0.02
39509-3	White-beige, quartz-clay-alunite-altered volcanoclastics, US 395 layback	38.20793	-119.22751	<0.005	1.28	2.11	0.08	0.84	0.44	<0.01	0.29
39509-6	Quartz-clay-alunite-altered porphyritic volcanic rock, Hot Springs Canyon	38.22064	-119.19188	<0.005	1.41	8.23	0.36	3.18	1.88	0.05	0.67
39509-8	Quartz-clay-altered porphyritic volcanic rock, Hot Springs Canyon	38.21008	-119.1871	<0.005	1.97	5.63	0.14	3.29	1.78	0.06	0.45
39509-9	Brown, coarse volcanoclastics, minor FeOx, upper Hot Springs Canyon	38.2056	-119.18252	<0.005	4.96	7.94	0.93	2.63	2.84	0.3	1.63

**Table 1-10.** Minor element concentrations in rocks samples from the Cinnabar Canyon-US 395 alteration zone.—Continued

[alt, alteration; DDH, diamond drill hole; Fe, iron; FeOx, iron oxide; HgS, mercury sulfide; K, potassium; RDH, rotary drill hole; S, sulfur]

Sample number	S %	Ti %	Ag ppm	As ppm	Ba ppm	Be ppm	Bi ppm	Cd ppm	Ce ppm	Co ppm	Cr ppm	Cs ppm	Cu ppm	Ga ppm
CCD7	1.87	0.39	17	50	428	<0.1	50.6	0.2	2.59	32.1	9	<5	53.3	0.57
CCD8B	2.42	0.71	2	32	164	<0.1	67.3	0.2	0.72	35.7	7	<5	31.7	0.5
CCD16	4.58	1.08	20	68	49	<0.1	125	0.6	2.47	25.3	16	<5	111	0.74
07-BA-10	0.75	0.76	<1	53	1,650	<0.1	1.62	0.4	5.49	4.4	4	<5	20.2	1.64
07-BA-11	0.02	0.41	<1	3	584	<0.1	12	<0.1	0.47	0.1	2	<5	4.1	0.39
07CC1	0.08	0.67	<1	16	1,630	2.3	0.11	<0.1	101	0.6	43	<5	5.7	23.6
07CC2	0.32	0.62	1	30	1,180	2.2	0.1	<0.1	92.3	1.1	39	<5	40.6	22.4
07CC5	0.13	0.57	<1	92	1,240	1.7	1.55	0.1	67.3	3.3	65	<5	43.4	23.9
07CC6	0.2	0.46	3	129	407	0.1	0.85	0.2	4.63	1.8	6	<5	4.2	1.5
07-BA-8	0.42	0.39	2	3	1,810	0.5	0.35	0.5	57.1	0.9	96	<5	48.2	25.2
07-BA-9	0.06	0.9	<1	33	995	0.5	87.7	0.2	5.68	9.4	23	<5	67.8	3.36
07-BA-14	1	0.55	<1	49	1,640	1.5	0.34	<0.1	71.1	1.1	54	<5	52.7	25.2
07-BA-16	0.13	0.47	<1	32	3,920	<0.1	0.21	<0.1	6.18	0.2	8	9	4.1	1.98
08CC3	7.14	0.28	<1	252	306	0.2	0.13	<0.1	43.4	0.2	23	14	7.6	20.7
08CC4	0.04	0.14	<1	6	1,970	2.3	0.16	<0.1	39.1	3	2	<5	9.6	18.6
08CC5	0.03	0.35	<1	2	1,300	2.7	0.06	<0.1	71	15.5	75	<5	17.3	19.8
08CC6	0.08	0.36	<1	396	504	<0.1	0.17	0.1	9.17	0.7	10	12	17.7	6.63
08CC7	0.1	0.53	<1	190	542	0.5	0.29	0.3	8.96	2.5	38	5	23.9	3.7
08CC8	1.79	0.62	<1	298	1,870	<0.1	44.7	1.3	1	24.2	24	<5	12.2	1.18
08CC9	0.31	0.48	<1	14	2,460	<0.1	10.8	0.1	3.88	11	7	<5	7.2	1.23
08CC10	0.14	0.46	<1	9	2,200	1.4	0.16	<0.1	86.7	3.3	100	5	15.8	24.7
08CC11	0.35	0.7	<1	124	3,490	<0.1	30	0.2	2.46	13	16	<5	11.5	1.12
08CC12	0.3	1.04	<1	28	1,630	0.3	52.3	<0.1	34.9	0.9	18	<5	5.4	15.5
08CC13	4.23	0.62	<1	84	1,510	0.5	0.12	<0.1	44.2	0.7	28	<5	69.5	16.2
08CC14	0.27	1.47	<1	38	1,810	1.7	14.7	0.3	22.5	3.1	77	<5	174	14.7
08CC15B	2.75	0.47	8	74	438	0.1	216	0.2	1.77	19.2	19	<5	14.2	0.98
08CC16	0.02	0.48	<1	<1	296	0.1	0.64	<0.1	2.17	0.2	12	<5	2.3	0.37
08CC17	3.78	1.26	10	31	273	0.3	32.8	0.1	3.86	15	10	<5	45.4	0.43
08CC21	4.47	0.91	7	37	242	0.1	101	0.3	2.38	44.4	17	<5	27.9	0.78
08CC22	0.19	0.39	<1	15	1,770	1.4	0.26	<0.1	61.6	0.7	21	<5	8.5	21
08CC23	0.18	1.01	<1	78	5,880	0.1	0.2	<0.1	1.75	0.5	13	<5	6.9	3.97
08CC24	0.06	0.15	<1	1	1,200	<0.1	0.06	<0.1	1.25	0.4	1	<5	1.8	0.28
08CC25	0.4	3.47	<1	3	8,120	<0.1	0.06	<0.1	1.72	0.1	44	<5	6.2	0.88
39509-3	1.85	0.26	<1	15	632	0.2	0.28	<0.1	20.9	0.2	10	<5	3.9	4.51
39509-6	0.74	0.4	<1	31	1,450	1.6	0.53	<0.1	85.2	0.6	12	7	15.2	17.5
39509-8	2.4	0.38	<1	28	346	0.7	0.79	<0.1	50.7	1.4	6	<5	16.7	20.6
39509-9	1	0.48	<1	14	1,260	2.2	0.45	<0.1	53.6	1.9	25	6	16.6	19



**Table 1-10.** Minor element concentrations in rocks samples from the Cinnabar Canyon-US 395 alteration zone.—Continued

[alt, alteration; DDH, diamond drill hole; Fe, iron; FeOx, iron oxide; HgS, mercury sulfide; K, potassium; RDH, rotary drill hole; S, sulfur]

Sample number	In ppm	La ppm	Li ppm	Mn ppm	Mo ppm	Nb ppm	Ni ppm	P ppm	Pb ppm	Rb ppm	Sb ppm	Se ppm
CCD7	0.03	1	5	23	2.42	11.3	43.6	<50	63.2	0.4	63.6	—
CCD8B	<0.02	<0.5	4	25	2.4	14.3	42.3	<50	88.8	0.5	72.5	—
CCD16	0.08	1.5	3	81	2.24	24.7	32.3	60	185	1.1	84.7	—
07-BA-10	0.03	2.9	2	9	2.03	17.3	15.5	120	266	1.8	22.2	—
07-BA-11	<0.02	<0.5	12	9	0.65	8.7	1	60	3.5	0.4	8.65	—
07CC1	<0.02	47.3	24	23	3.44	13.9	1.7	1,560	20.2	82.3	3.73	—
07CC2	0.04	44.2	17	38	3.19	11.3	2.4	1,520	21.3	30.4	3.39	—
07CC5	0.06	33.4	11	64	3.23	11.6	6.3	1,050	7,510	41.5	53.3	—
07CC6	0.02	3	<1	12	1.42	6.2	2.7	180	71.3	3.6	4.17	—
07-BA-8	0.06	31	11	17	1.44	9.4	5.1	1,790	82.6	3.3	19.2	—
07-BA-9	0.04	3.8	3	96	4.25	14.1	15.5	760	82.3	3.9	106	25.7
07-BA-14	0.07	38.9	22	25	2.52	10.2	3	1,050	29.5	33.6	4.39	<0.2
07-BA-16	<0.02	3.2	<1	15	3.21	9	1.6	150	16.1	10.6	0.83	—
08CC3	0.1	19.2	1	5	8.41	8.8	1.2	1,840	30.6	106	0.73	—
08CC4	<0.02	21.2	23	262	1.59	5.5	2.5	510	36.3	85.5	1.01	—
08CC5	0.03	36.4	16	416	0.91	9.9	71.5	1,540	20.2	102	0.56	—
08CC6	0.07	5.6	<1	6	4.55	10.7	5.4	330	45.9	12.7	0.76	—
08CC7	0.09	5.7	2	70	8.36	12.5	20.6	640	136	7.5	1.3	—
08CC8	0.1	0.8	<1	6	2.31	15.3	19.6	130	239	1.6	162	—
08CC9	<0.02	2.1	<1	7	1.82	8.7	15.7	230	25.6	2.5	14.1	—
08CC10	0.04	44.3	3	73	7.82	10.9	16.1	1,550	21	91.6	1.15	—
08CC11	<0.02	1.8	<1	6	31.4	7.1	30.3	950	107	1.8	67.8	—
08CC12	0.04	22.1	3	23	6.45	22.8	2.4	1,070	140	9.7	34.7	—
08CC13	0.15	30.9	2	19	2.47	10.4	2.4	1,320	81.1	8.7	0.83	—
08CC14	0.16	16.1	3	103	16	31	5.7	2,180	171	2	43.6	—
08CC15B	<0.02	1.2	3	9	2.1	9.9	34.9	80	174	3.1	231	—
08CC16	<0.02	1.4	4	6	0.7	10.5	0.6	160	3.4	0.4	3.71	—
08CC17	<0.02	2.2	3	22	1.74	24.1	17.3	<50	107	1.5	59.1	—
08CC21	<0.02	0.9	6	65	1.99	13.1	46.5	50	237	0.6	111	—
08CC22	0.03	36	4	28	1.74	13.1	1.5	1,020	25.4	78.2	0.83	—
08CC23	<0.02	1.3	<1	23	5.33	18.2	1.3	140	67.4	3.7	8.31	—
08CC24	<0.02	0.9	<1	18	0.82	2.7	0.9	<50	2.7	0.8	0.44	—
08CC25	<0.02	1.9	<1	6	15.3	64.7	0.7	110	11.9	1.1	1.02	—
39509-3	<0.02	9.7	<1	<5	1.24	4.3	0.8	430	6.1	5.3	1.93	—
39509-6	0.05	39.6	9	25	2.23	11.5	2.4	2,870	21.9	52	3.74	—
39509-8	0.05	29.1	5	24	1.79	10.9	2.7	1,340	23.1	22.8	2.19	—
39509-9	0.04	31	4	102	1.99	13.5	2.8	1,200	21.5	109	1.69	—

**Table 1-10.** Minor element concentrations in rocks samples from the Cinnabar Canyon-US 395 alteration zone.—Continued

[alt, alteration; DDH, diamond drill hole; Fe, iron; FeOx, iron oxide; HgS, mercury sulfide; K, potassium; RDH, rotary drill hole; S, sulfur]

Sample number	Sc ppm	Sn ppm	Sr ppm	Te ppm	Th ppm	Tl ppm	U ppm	V ppm	W ppm	Y ppm	Zn ppm
CCD7	1.4	4.8	29.7	4.3	0.9	2	2.2	4	2.5	1.2	9
CCD8B	0.7	9.3	16.8	1.8	1	3.4	1.4	5	2.9	0.6	3
CCD16	3.1	6.5	42.2	2.2	1.5	6.4	4.3	9	7.2	3.4	12
07-BA-10	4.2	2.8	64.4	1.9	3.3	5.9	5.9	16	7.2	7	6
07-BA-11	0.6	3.2	4.6	0.2	0.3	<0.1	1.3	4	1.1	0.2	1
07CC1	14	2.5	719	<0.1	12.4	0.6	4.7	153	3.6	18.8	7
07CC2	16.2	2.1	657	<0.1	16.4	0.8	4.7	153	2.5	21	8
07CC5	16.6	2	388	0.2	17.1	0.9	4.4	173	3.4	9.2	30
07CC6	1.9	2.1	112	2.8	1.4	2.7	2.9	10	2.7	0.4	1
07-BA-8	17.3	1.2	1,180	1	12.9	0.1	2.8	167	1.4	3.2	43
07-BA-9	4	13.9	51.4	7	3.7	0.1	5.1	15	1.3	3.4	17
07-BA-14	15.5	1.8	420	0.2	24.5	1.3	4.9	192	1.9	11.4	12
07-BA-16	1.2	1	71.8	0.1	3.1	1.1	1.8	14	1.7	0.7	4
08CC3	8.7	1.1	1,640	0.5	12	20.1	1.8	149	1.3	2.1	5
08CC4	3	0.8	869	<0.1	6	0.5	2.2	28	2.3	5.9	44
08CC5	12.1	1.2	829	<0.1	14.8	0.7	5.3	107	0.9	14.4	62
08CC6	2.1	2.2	144	0.3	3.3	3.7	3.6	14	1.7	0.6	3
08CC7	3.3	2	77.8	0.2	3.5	1.4	5.2	66	1.9	2.5	23
08CC8	3.1	8.1	17.8	6.1	0.7	9.8	3.4	7	2.5	0.1	4
08CC9	2	4	193	1.8	1.4	1.7	1.5	6	1.1	0.9	2
08CC10	18.7	1.2	945	<0.1	14.6	0.4	6.6	155	2.3	12.3	23
08CC11	8.9	18.7	57.6	5.6	0.8	3	6.1	5	12	0.2	7
08CC12	5.8	5	1,070	8.7	31.1	1.5	5.8	23	12.2	3	10
08CC13	9.5	1.8	794	<0.1	11.1	0.5	8	94	1.8	4.3	10
08CC14	4.9	27.2	1,330	0.7	5.7	<0.1	6	90	5	3.8	43
08CC15B	1.5	7.8	50.1	4.8	0.8	10.9	1.4	5	9.3	0.6	6
08CC16	1	6.2	12.2	<0.1	0.3	<0.1	0.8	4	0.8	0.3	1
08CC17	2	4.4	60	0.8	1.7	1.3	2.6	14	6.1	1.4	4
08CC21	0.8	8.4	37.4	3.4	0.7	5.6	1	5	2.3	0.6	8
08CC22	8.4	1.6	342	1.1	16.3	1.4	5.5	64	1.5	7.8	10
08CC23	3.1	2	58.9	3.7	2.3	1.3	8.3	33	2.2	2.5	3
08CC24	0.4	0.2	48.7	<0.1	<0.2	<0.1	0.1	3	0.4	0.3	<1
08CC25	1.9	2.5	89.9	<0.1	0.9	<0.1	0.9	16	3.8	0.3	2
39509-3	2.3	0.7	186	0.7	2.9	0.1	0.9	40	1.1	1.3	3
39509-6	7.7	1.6	1,380	0.4	13.6	0.3	4.4	101	1.8	7.3	24
39509-8	5.5	1.4	885	0.7	10.7	0.7	3.4	51	1.2	1.9	15
39509-9	12.6	1.4	730	1.3	15	0.8	5.3	118	1.7	9.2	23

**Table 1-11.** Minor element concentrations in rock samples from the Bodie Mining District.

[cm, centimeter; K, potassium; Kspar, potassium feldspar; —, no data]

Sample number	Description, Location	Latitude	Longitude	Au ppm	Hg ppm	Al %	Ca %	Fe %	K %	Mg %	Na %
Sinter											
BODB06-4A	Sinter, silicified volcaniclastics, Bodie Bluff	38.21883	-119.99921	0.011	0.44	0.36	0.04	0.07	0.07	<0.01	<0.01
BODB06-4B1	Sinter, silicified volcaniclastics, Bodie Bluff	38.21883	-119.99921	0.014	0.23	0.45	0.08	0.18	0.17	<0.01	<0.01
BODB06-4B2	Sinter, silicified volcaniclastics, Bodie Bluff	38.21883	-119.99921	0.01	0.42	0.44	0.07	0.17	0.2	<0.01	<0.01
07-BA-3A	Sinter block, Bodie Bluff	38.21923	-118.99823	0.007	0.15	0.35	0.04	0.15	0.24	<0.01	0.02
07-BA-3B	Sinter block, Bodie Bluff	38.21923	-118.99823	0.008	0.09	0.16	0.02	0.05	0.06	<0.01	0.03
BB13-SINA	Dismembered sinter, Bodie Bluff summit	38.21924	-118.99822	0.051	0.06	0.38	0.02	0.11	0.11	<0.01	0.03
BB13-SINB	Dismembered sinter, Bodie Bluff summit	38.21924	-118.99822	0.004	0.01	0.15	0.02	0.07	0.08	<0.01	0.03
BB13-CLD	Sinter clast in volcaniclastic deposits, Bodie Bluff summit	38.21883	-119.99921	0.008	0.01	0.1	0.01	0.07	0.03	<0.01	<0.01
BB13-CLH	Sinter clast in volcaniclastic deposits, Bodie Bluff summit	38.21881	-119.9992	0.051	<0.01	0.16	0.07	0.05	0.1	<0.01	0.02
BB13-CLI	Sinter clast in volcaniclastic deposits, Bodie Bluff summit	38.21841	-119.99921	0.018	<0.01	0.08	0.04	0.05	0.02	<0.01	<0.01
BB13-CLK	Sinter clast in volcaniclastic deposits, Bodie Bluff summit	38.21883	-119.99919	0.002	<0.01	0.11	0.05	0.05	0.02	<0.01	0.01
BB13-CLL	Sinter clast in volcaniclastic deposits, Bodie Bluff summit	38.21884	-119.99921	0.002	<0.01	0.12	0.03	0.11	0.03	<0.01	0.01
Incline series veins											
BB13-VEINA	Incline veins next to sinter, Bodie Bluff summit	38.21975	-118.99942	0.965	0.02	1.41	0.04	0.1	2.28	<0.01	0.05
BB13-VEINB	Incline veins next to sinter, Bodie Bluff summit	38.22047	-118.99931	>10	0.07	1.13	0.05	0.06	1.71	<0.01	0.03
BODB06-3	Banded quartz vein, dump, Bodie Bluff	38.21783	-119.99832	5	0.54	0.15	<0.01	0.02	0.03	<0.01	<0.01
11-BA-26A	Vein, Upper Hobart Tunnel dump, Bodie Bluff	38.21968	-119.00265	5.93	0.08	2.61	0.09	0.38	2.29	0.05	0.18
11-BA-26B	Vein, Upper Hobart Tunnel dump, Bodie Bluff	38.21968	-119.00265	146	2.97	1.91	0.04	0.04	2.28	<0.01	0.03
11-BA-26C	Vein, Upper Hobart Tunnel dump, Bodie Bluff	38.21968	-119.00265	107	0.1	3.55	0.06	0.79	4.6	0.1	0.07
BOD11-11D	Banded quartz-Kspar vein, minor sulfides	38.21497	-119.00273	1.84	1.39	0.81	0.07	0.17	0.48	0.04	0.02
BOD11-12	Banded quartz-Kspar vein, minor sulfides	38.21591	-119.003	0.061	0.39	4.08	0.03	0.12	4.58	0.02	0.05
BOD11-13	Banded quartz-Kspar vein, minor sulfides	38.21497	-119.00356	12.9	0.1	4.09	0.07	0.99	4.91	0.09	0.17
BOD11-14	Banded quartz-K-mica vein, minor fluorite	38.21725	-119.00039	10.1	0.55	1.99	0.04	0.18	2.39	<0.01	0.03
BOD11-18A	Quartz vein, minor sulfide	38.21434	-119.00523	21.2	0.06	1.63	0.03	0.34	1.78	0.02	0.04
BOD11-19	Banded quartz-Kspar vein, minor sulfides	38.21872	-119.00031	46	1.96	2.65	0.04	0.07	3.43	<0.01	0.04
BOD13-1A	SW summit Standard Hill	38.21482	-119.00456	4,860	0.12	1.36	0.04	0.14	1.44	<0.01	0.05
BOD13-2B	SW slope Standard Hill	38.21568	-119.00385	2,740	0.09	0.63	<0.01	0.09	0.97	<0.01	0.01
BOD13-5B	Upper Hobart Tunnel dump	38.21971	-119.00266	2,280	0.11	5.52	0.08	2.13	4.46	0.03	0.1
BOD13-5C	Upper Hobart Tunnel dump	38.21971	-119.00266	>10,000	2.81	5.34	0.02	0.49	2.51	0.01	0.08

**Table 1-11.** Minor element concentrations in rock samples from the Bodie Mining District.—Continued

[cm, centimeter; K, potassium; Kspar, potassium feldspar; —, no data]

Sample number	S %	Ti %	Ag ppm	As ppm	Ba ppm	Be ppm	Bi ppm	Cd ppm	Ce ppm	Co ppm	Cr ppm	Cs ppm	Cu ppm	Ga ppm
Sinter														
BODB06-4A	<0.01	0.01	1	<30	150	<5	<0.1	<0.2	1.6	0.5	<10	25.4	<5	10
BODB06-4B1	<0.01	0.02	<1	100	315	<5	<0.1	<0.2	2.7	<0.5	<10	34.8	<5	6
BODB06-4B2	<0.01	0.02	<1	90	211	<5	<0.1	<0.2	2.7	<0.5	<10	37.2	<5	4
07-BA-3A	0.02	0.02	<1	35	278	1.1	<0.04	<0.1	4.12	0.4	5	23	1.3	8.16
07-BA-3B	<0.01	<0.01	<1	20	33	0.6	0.04	0.5	2.19	0.2	3	20	2.6	12
BB13-SINA	0.02	<0.01	<1	22	39	1.6	<0.04	<0.1	3.03	0.6	4	25	82.2	20.6
BB13-SINB	<0.01	<0.01	<1	16	33	0.6	0.06	<0.1	0.81	0.1	5	21	9.5	14.3
BB13-CLD	<0.01	<0.01	<1	17	52	0.3	0.09	<0.1	0.33	<0.1	3	6	10.9	8.47
BB13-CLH	0.03	<0.01	<1	12	52	2.3	0.14	<0.1	0.73	0.1	4	16	12.6	61.6
BB13-CLI	0.02	<0.01	<1	15	67	0.4	0.19	<0.1	0.57	<0.1	4	<5	3.1	7.12
BB13-CLK	0.02	<0.01	<1	12	59	0.2	<0.04	<0.1	0.58	0.2	4	5	5.2	4.82
BB13-CLL	0.02	<0.01	<1	29	88	0.3	<0.04	<0.1	1.35	0.1	6	9	10.4	2.2
Incline series veins														
BB13-VEINA	<0.01	<0.01	37	4	28	0.7	0.05	<0.1	0.88	0.6	2	12	8.3	1.67
BB13-VEINB	<0.01	<0.01	135	5	27	1.6	0.06	<0.1	0.34	0.7	1	14	7.1	1.21
BODB06-3	<0.01	<0.01	<1	<30	31.9	<5	<0.1	<0.2	0.7	<0.5	<10	15.4	<5	17
11-BA-26A	0.07	0.09	41	104	1,290	4.4	0.31	<0.1	13.7	0.3	2	23	22.7	5.31
11-BA-26B	<0.01	<0.01	268	8	86	1.5	0.04	<0.1	0.36	1.2	1	8	5.6	2.06
11-BA-26C	<0.01	0.06	122	27	250	2.5	0.07	<0.1	7.41	22.6	8	15	34.4	5.91
BOD11-11D	0.11	<0.01	17	41	330	4.3	80.8	<0.1	2.74	0.3	1	13	9.1	4.28
BOD11-12	0.01	<0.01	4	11	497	2.7	8.52	<0.1	8.75	7.6	1	10	10	3.91
BOD11-13	0.1	0.1	53	71	479	3.1	1.08	<0.1	10.8	3.2	4	9	12.7	7.45
BOD11-14	0.01	<0.01	51	17	93	2.8	2.39	<0.1	2.3	0.4	1	11	3.6	2.5
BOD11-18A	0.23	0.05	800	286	269	1.2	0.39	<0.1	8.37	0.3	2	6	5.8	7.24
BOD11-19	<0.01	<0.01	153	11	44	5.5	1.93	<0.1	1.24	0.2	<1	11	11.7	3.71
BOD13-1A	0.02	<0.01	23	9	78	1.1	0.08	<0.1	3.34	23.1	2	6	12.6	1.11
BOD13-2B	<0.01	<0.01	11	8	42	0.9	0.07	<0.1	2.02	9.2	2	<5	11.2	0.8
BOD13-5B	1.93	0.1	71	949	578	1.5	0.12	<0.1	24.3	2.8	8	18	48.5	8.9
BOD13-5C	0.01	0.03	254	108	199	1.6	0.07	<0.1	4.53	0.4	3	15	34.7	5.52

**Table 1-11.** Minor element concentrations in rock samples from the Bodie Mining District.—Continued

[cm, centimeter; K, potassium; Kspar, potassium feldspar; —, no data]

Sample number	In ppm	La ppm	Li ppm	Mn ppm	Mo ppm	Nb ppm	Ni ppm	P ppm	Pb ppm	Rb ppm	Sb ppm	Sc ppm
Sinter												
BODB06-4A	<0.2	1.5	70	—	4	<1	6	—	<5	10.1	539	<5
BODB06-4B1	<0.2	2.2	100	—	7	<1	13	—	<5	19.1	279	<5
BODB06-4B2	<0.2	1.9	120	—	7	<1	8	—	8	20.5	245	<5
07-BA-3A	<0.02	3.1	57	127	2.64	0.3	0.9	<50	1.8	24.5	136	0.8
07-BA-3B	<0.02	5	45	24	3.21	<0.1	1.1	<50	56.5	7.7	333	0.4
BB13-SINA	<0.02	1.6	43	45	4.83	0.1	3.5	<50	1.1	7.5	863	0.3
BB13-SINB	<0.02	<0.5	37	42	4.3	<0.1	1.9	<50	<0.5	5.8	819	0.2
BB13-CLD	<0.02	<0.5	20	34	5.82	<0.1	1.8	<50	<0.5	1.4	425	0.1
BB13-CLH	<0.02	<0.5	36	19	2.55	<0.1	2	<50	1	6.8	522	0.1
BB13-CLI	<0.02	<0.5	9	15	3.11	<0.1	2	<50	<0.5	1.3	1,190	<0.1
BB13-CLK	<0.02	0.6	18	22	3.92	<0.1	2.4	<50	<0.5	1.4	369	0.1
BB13-CLL	<0.02	0.7	17	28	4.12	<0.1	5.8	<50	0.8	2.1	675	0.2
Incline series veins												
BB13-VEINA	<0.02	<0.5	88	42	3.47	<0.1	7.7	<50	1.4	116	18.7	0.1
BB13-VEINB	<0.02	<0.5	87	41	2.77	<0.1	1.9	<50	1.6	77.7	23.2	<0.1
BODB06-3	<0.2	1	30	—	5	<1	7	—	<5	5.3	>1,000	<5
11-BA-26A	<0.02	6.9	64	17	11.9	2.2	0.6	220	11.8	166	56.8	1.7
11-BA-26B	<0.02	<0.5	130	24	0.28	<0.1	<0.5	<50	3.5	133	11.7	<0.1
11-BA-26C	<0.02	3.2	128	564	6.07	1.6	14	120	5.8	317	25.5	1.2
BOD11-11D	<0.02	1.1	101	41	1.63	<0.1	3.1	120	18.6	34.7	58.3	1.6
BOD11-12	<0.02	1.9	123	471	1.27	0.2	15.2	<50	10.3	247	19.1	0.5
BOD11-13	<0.02	5.8	132	268	0.52	2.2	10	310	7.8	275	14.3	2.1
BOD11-14	<0.02	1.3	55	94	5.85	0.1	1.3	70	3.9	161	27.1	0.4
BOD11-18A	<0.02	5.1	153	24	3.82	1	1	140	13.7	108	48.5	1.2
BOD11-19	<0.02	0.8	56	30	0.53	<0.1	0.8	60	5.3	214	21.3	0.2
BOD13-1A	<0.02	0.9	206	875	1.43	<0.1	12.2	<50	1.9	71.7	20.2	0.2
BOD13-2B	<0.02	0.6	15	447	0.62	<0.1	8.2	<50	1.3	51.1	19.1	0.1
BOD13-5B	0.02	13.5	45	41	6.12	3.3	6.9	430	13.8	373	49	2.5
BOD13-5C	<0.02	3.4	71	24	2.15	0.7	2.2	120	4.5	373	38.3	0.7

**Table 1-11.** Minor element concentrations in rock samples from the Bodie Mining District.—Continued

[cm, centimeter; K, potassium; Kspar, potassium feldspar; —, no data]

Sample number	Se ppm	Sn ppm	Sr ppm	Te ppm	Th ppm	Tl ppm	U ppm	V ppm	W ppm	Y ppm	Zn ppm	C %
Sinter												
BODB06-4A	<0.2	<1	43.5	<0.5	0.2	<0.5	0.14	<5	5	0.5	<5	0.02
BODB06-4B1	0.5	<1	66.5	<0.5	0.2	0.9	0.16	10	16	0.9	7	0.03
BODB06-4B2	0.4	<1	70	<0.5	0.2	1.2	0.16	12	16	0.7	8	<0.01
07-BA-3A	<0.2	0.1	46.7	<0.1	0.7	0.4	0.2	6	4.5	0.7	<1	—
07-BA-3B	<0.2	<0.1	13.8	0.4	0.3	0.3	0.1	3	3.3	0.7	8	—
BB13-SINA	<0.2	0.5	20.6	<0.1	0.3	0.3	0.1	5	3.6	0.4	4	0.03
BB13-SINB	<0.2	0.2	10.8	<0.1	<0.2	0.1	<0.1	2	2.4	0.3	1	0.01
BB13-CLD	<0.2	0.2	6.9	<0.1	<0.2	<0.1	<0.1	3	0.5	0.1	2	0.01
BB13-CLH	<0.2	0.5	15.6	<0.1	<0.2	<0.1	<0.1	2	1.8	0.2	5	0.03
BB13-CLI	<0.2	0.3	6.6	<0.1	<0.2	<0.1	<0.1	2	0.7	0.2	2	0.02
BB13-CLK	<0.2	0.4	10.1	<0.1	<0.2	<0.1	<0.1	2	0.2	0.3	2	0.02
BB13-CLL	<0.2	0.3	11.7	<0.1	0.2	<0.1	0.1	5	0.8	0.3	2	0.03
Incline series veins												
BB13-VEINA	1.9	0.2	86	<0.1	<0.2	1.2	<0.1	2	0.4	0.2	19	0.02
BB13-VEINB	2.2	0.4	101	<0.1	<0.2	1	<0.1	1	0.3	<0.1	10	0.06
BODB06-3	0.2	<1	11.1	<0.5	<0.1	<0.5	<0.05	<5	10	<0.5	9	0.09
11-BA-26A	—	0.5	191	0.9	2.1	1.8	0.8	16	4.9	2.4	10	—
11-BA-26B	—	<0.1	101	<0.1	<0.2	1.8	<0.1	<1	<0.1	<0.1	4	—
11-BA-26C	—	0.6	104	<0.1	1.4	4.9	0.8	13	4.6	2	43	—
BOD11-11D	0.9	1.2	143	4.4	<0.2	0.5	5.9	5	1.6	8.8	12	—
BOD11-12	<0.2	0.5	120	0.7	0.3	4.4	0.3	4	4.6	2.3	11	—
BOD11-13	0.3	0.4	186	<0.1	2.2	4.2	1.9	23	2.5	4.1	37	—
BOD11-14	0.3	0.3	132	0.2	<0.2	1.9	0.5	2	1.7	3.7	2	—
BOD11-18A	8.9	0.4	78	<0.1	1.9	1.9	3.2	664	1.7	8.1	5	—
BOD11-19	1.6	0.2	145	0.2	<0.2	2.8	0.7	3	0.2	5.8	4	—
BOD13-1A	<0.2	0.2	70.7	<0.1	0.2	2.2	<0.1	2	0.8	0.7	21	0.01
BOD13-2B	<0.2	0.2	28.3	<0.1	<0.2	1.2	<0.1	2	0.7	0.7	9	0.01
BOD13-5B	1.5	1.1	131	<0.1	3.3	8.8	1.3	23	8.3	4.2	11	0.03
BOD13-5C	5.3	0.8	150	<0.1	0.8	6	0.4	6	1.9	1	11	0.01

**Table 1-11.** Minor element concentrations in rock samples from the Bodie Mining District.—Continued

[cm, centimeter; K, potassium; Kspar, potassium feldspar; —, no data]

Sample number	Description, Location	Latitude	Longitude	Au ppm	Hg ppm	Al %	Ca %	Fe %	K %	Mg %	Na %
Burgess series veins											
11-BA-22A	Bodie Mine dump, Standard Hill	38.21257	-119.00402	10.7	0.14	1.67	0.07	0.1	1.81	0.28	0.03
11-BA-22B	Bodie Mine dump, Standard Hill	38.21257	-119.00402	4.62	0.08	1.64	0.03	0.05	1.83	0.19	0.03
11-BA-22C	Bodie Mine dump, Standard Hill	38.21257	-119.00402	65	0.27	3.86	0.14	0.52	5.06	0.49	0.07
11-BA-22D	Bodie Mine dump, Standard Hill	38.21257	-119.00402	1.69	0.09	1.62	0.08	0.54	1.87	0.07	0.04
11-BA-22E	Bodie Mine dump, Standard Hill	38.21257	-119.00402	19.8	0.07	1.33	0.1	0.39	0.81	0.14	<0.01
07-BA-2	Quartz vein bladed texture south of Bodie Bluff	38.21595	-119.00299	1.34	7.72	4.1	0.15	1.88	4.98	0.02	0.69
99-DJ-71A	Banded quartz vein, Bulwer Mine dump, Standard Hill	38.21452	-119.00385	20	0.103	1.41	0.13	0.57	1.56	0.08	0.13
99-DJ-71B	Pyritic quartz vein, Bulwer Mine dump, Standard Hill	38.21452	-119.00385	1	<0.096	4.84	0.36	1.54	6.71	0.04	0.08
99-DJ-71C	Pyritic quartz vein, Bulwer Mine dump, Standard Hill	38.21452	-119.00385	1.55	<0.095	6.58	0.31	1.38	9.3	0.04	0.11
99-DJ-71D	Silicified wall rock(?) with pyrite, Bulwer Mine dump	38.21452	-119.00385	0.11	<0.091	5.52	0.26	2.11	7.89	0.35	0.11
Silver Hill series veins											
BODB07-8	Quartz-sulfide-K-mica breccia, Contention dump	38.20524	-119.0056	>10	1.43	2.12	0.21	0.66	0.82	0.05	<0.01
09-BA-28A	Red Cloud Mine dump	38.20151	-119.00363	3.85	1.6	2.16	0.34	0.39	0.87	0.03	0.03
09-BA-28B	Red Cloud Mine dump	38.20151	-119.00363	37.9	0.72	1.08	0.1	1.99	0.46	0.03	0.01
09-BA-28C	Red Cloud Mine dump	38.20151	-119.00363	23.3	2.05	1.38	0.31	0.3	0.57	0.02	0.01
09-BA-28H	Red Cloud Mine dump	38.20151	-119.00363	0.61	0.14	2.73	0.11	0.88	1.1	0.04	0.02
09-BA-28I	Red Cloud Mine dump	38.20151	-119.00363	2.05	0.1	3.14	0.15	3.72	3.31	0.04	0.06
07-BA-5A	Silver Hill dump samples, Bodie	38.20517	-119.00479	6.81	2.76	1.54	0.11	0.92	0.64	0.04	0.02
07-BA-5B	Silver Hill dump samples, Bodie	38.20517	-119.00479	13.3	0.77	1.43	0.22	0.48	0.59	0.04	0.02
99-DJ-70A	sulfide-rich vein, Silver Hill	38.20517	-119.00479	0.03	0.759	1.07	0.71	1.87	0.54	0.13	0.01
99-DJ-70B	1-cm-wide quartz vein, Silver Hill	38.20517	-119.00479	0.027	0.967	1.22	0.65	1.76	0.64	0.13	0.02
99-DJ-72A	Sulfide-rich quartz vein, Red Cloud Mine	38.20151	-119.00363	13	0.34	1.94	0.29	2.62	0.93	0.03	0.03
99-DJ-72B	Sulfide-rich quartz vein, Red Cloud Mine	38.20151	-119.00363	0.403	0.213	3.27	0.22	1.25	1.45	0.09	0.03
11-BA-6E	Red Cloud Mine dump	38.20130	-119.00460	42.8	0.12	2.31	0.04	0.17	1.05	0.07	<0.01
11-BA-7A	Oro Mine dump	38.20420	-119.00649	1.71	1.35	1.46	0.18	2.77	1.38	0.03	0.02
11-BA-7E	Oro Mine dump	38.20420	-119.00649	0.052	0.22	4.03	0.16	0.68	4.26	0.15	0.05
11-BA-7F	Oro Mine dump	38.20420	-119.00649	7.8	1.12	2.21	0.19	1.69	0.9	0.03	0.02
11-BA-9A	Contention Mine dump	38.20547	-119.00472	2.04	0.4	1.08	0.23	0.51	0.46	0.03	<0.01
11-BA-9B	Contention Mine dump	38.20547	-119.00472	16.9	0.44	2.77	0.15	0.99	1.15	0.06	0.01

**Table 1-11.** Minor element concentrations in rock samples from the Bodie Mining District.—Continued

[cm, centimeter; K, potassium; Kspar, potassium feldspar; —, no data]

Sample number	S %	Ti %	Ag ppm	As ppm	Ba ppm	Be ppm	Bi ppm	Cd ppm	Ce ppm	Co ppm	Cr ppm	Cs ppm	Cu ppm	Ga ppm
Burgess series veins														
11-BA-22A	0.04	<0.01	327	5	60	0.7	0.69	0.1	0.88	1.1	<1	<5	51.2	2.12
11-BA-22B	0.03	<0.01	212	<1	58	0.4	0.3	<0.1	0.54	0.6	<1	<5	24.1	1.37
11-BA-22C	0.41	0.05	243	129	424	0.6	0.29	0.3	11.8	1.9	2	7	74.5	4.18
11-BA-22D	0.33	0.08	164	51	309	0.9	0.32	0.1	15.1	1.9	3	5	185	3.28
11-BA-22E	0.24	0.04	171	7	52	0.8	1.46	3	8.22	0.9	2	5	24.6	6.45
07-BA-2	1.86	0.1	13	335	736	0.6	0.12	<0.1	12.5	1.4	4	6	8.2	6.14
99-DJ-71A	—	0.05	41.6	12.6	154	1	<0.244	<0.097	—	2	—	—	9.94	0.588
99-DJ-71B	—	0.39	20.8	45.1	164	1	0.743	<0.096	—	2	—	—	16.8	1.24
99-DJ-71C	—	0.36	23.2	45.5	240	1	0.665	<0.095	—	<2	—	—	6.77	1.33
99-DJ-71D	—	0.25	3.68	21.4	183	1	<0.229	<0.091	—	5	—	—	9.88	2.52
Silver Hill series veins														
BODB07-8	0.09	0.04	312	250	173	<5	72	29.6	15	1.8	<10	12.1	>10,000	11
09-BA-28A	0.48	0.01	430	573	464	0.4	9.57	1.2	4.94	0.7	2	7	8,790	17.9
09-BA-28B	2.46	0.05	3,090	196	119	0.2	309	57.4	9.51	3.8	3	<5	25,400	6.31
09-BA-28C	0.9	0.02	837	534	195	0.3	106	36.3	11.8	1.5	2	<5	11,800	12.7
09-BA-28H	1.01	0.08	26	33	307	0.4	3.63	0.1	13.2	1.7	3	8	517	17.3
09-BA-28I	4.8	0.24	115	84	75	0.5	21.1	1.9	14.2	11	8	<5	442	7.71
07-BA-5A	3.38	0.04	72	62	122	0.3	37.6	406	14.4	1.9	3	5	6,990	63.7
07-BA-5B	0.86	0.01	56	185	153	0.5	38.6	16.9	8.46	1.6	2	7	8,930	9.21
99-DJ-70A	—	0.27	4.75	56.5	296	1	0.797	<0.097	—	6	—	—	9.14	<0.484
99-DJ-70B	—	0.31	5.21	47.2	244	1	1.07	<0.094	—	6	—	—	10.3	<0.47
99-DJ-72A	—	0.09	298	127	182	<1	29.4	9.76	—	4	—	—	5,072	0.972
99-DJ-72B	—	0.13	18.1	27.5	252	1	2.96	0.261	—	3	—	—	500	<0.491
11-BA-6E	0.13	0.02	352	68	120	0.5	1.48	0.7	4.23	0.4	1	7	218	5.9
11-BA-7A	>5	0.08	171	49	225	0.3	82.1	258	28.3	7	3	<5	33,100	40.9
11-BA-7E	0.78	0.1	9	23	818	0.7	0.58	0.6	18.5	2	3	12	151	6.37
11-BA-7F	2.55	0.09	432	248	126	0.3	41.8	42.5	12.7	5.9	5	<5	14,600	9.63
11-BA-9A	0.85	0.03	249	124	114	0.3	28.7	7.5	14.7	1.2	2	<5	6,290	6.53
11-BA-9B	1.72	0.07	305	36	163	0.4	65.8	9.4	14.8	1.8	3	13	10,700	16.4



**Table 1-11.** Minor element concentrations in rock samples from the Bodie Mining District.—Continued

[cm, centimeter; K, potassium; Kspar, potassium feldspar; —, no data]

Sample number	In ppm	La ppm	Li ppm	Mn ppm	Mo ppm	Nb ppm	Ni ppm	P ppm	Pb ppm	Rb ppm	Sb ppm	Se ppm
Burgess series veins												
11-BA-22A	<0.02	<0.5	85	179	0.48	<0.1	2.5	<50	30.3	113	12.9	—
11-BA-22B	<0.02	<0.5	83	107	0.26	<0.1	1.8	<50	10.3	97.7	8.21	—
11-BA-22C	0.03	6.6	56	272	8.87	2.1	4.7	190	59.8	241	23.5	—
11-BA-22D	<0.02	8.3	84	67	13.7	2.8	2.1	180	36.1	85.1	26.3	—
11-BA-22E	0.06	4.9	51	99	1.34	1.3	0.8	120	239	42.5	6.06	—
07-BA-2	<0.02	8.6	38	20	7.23	2.4	3.1	260	27.8	254	56.8	1.5
99-DJ-71A	—	2	—	153	2.48	3	15	80	2.93	—	1.02	<1
99-DJ-71B	—	19	—	75	56.3	14	8	350	30.5	—	2.83	4
99-DJ-71C	—	17	—	61	54.1	9	5	280	29.5	—	2.61	5
99-DJ-71D	—	19	—	147	2.62	6	17	790	12.5	—	2.4	5
Sample number	In ppm	La ppm	Li ppm	Mn ppm	Mo ppm	Nb ppm	Ni ppm	P ppm	Pb ppm	Rb ppm	Sb ppm	Sc ppm
Silver Hill series veins												
BODB07-8	1.6	8.3	50	—	14	1	7	—	2,630	43.9	>1,000	<5
09-BA-28A	0.35	2.6	38	84	8.89	0.4	1.6	730	1,520	41.3	126	0.3
09-BA-28B	4.06	5.8	24	28	48.6	1.5	1.4	370	2,260	20.3	3,080	0.6
09-BA-28C	3.08	6.1	32	39	14	0.4	<0.5	1,470	2,870	27	6,380	0.4
09-BA-28H	0.1	7.8	40	35	6.12	2.5	2.7	500	549	56.5	37.3	0.9
09-BA-28I	0.4	8.5	23	48	16.7	4.8	15.1	460	1,880	148	22.5	3.8
07-BA-5A	10.7	6.6	43	55	8.15	1.1	2.3	450	<0.5	28.7	510	0.5
07-BA-5B	0.7	4.4	34	56	6.85	0.3	1.7	960	2,170	32.3	3,910	0.4
99-DJ-70A	—	19	—	76	119	8	13	730	26.7	—	4.64	3
99-DJ-70B	—	25	—	68	162	9	16	1,360	31.9	—	6.91	3
99-DJ-72A	—	10	—	51	13.7	3	17	860	1,112	—	1,457	<1
99-DJ-72B	—	9	—	77	7.76	5	8	250	145	—	33.2	—
11-BA-6E	0.05	2.3	52	54	1.46	0.9	1	140	96.4	65.5	149	0.3
11-BA-7A	13.2	15.1	23	57	37.3	3.3	7.7	530	19,000	53.6	394	1.4
11-BA-7E	0.06	10.3	52	61	7.85	4.8	2.9	340	62.6	231	23.1	1.5
11-BA-7F	3.31	6.7	52	37	78.5	2	5	570	1,280	45.1	4,830	1.1
11-BA-9A	0.37	7.1	33	21	5.9	1.1	1.4	680	1,190	27	758	0.5
11-BA-9B	0.78	8.3	34	35	13.7	2.5	2	380	778	58.2	880	1

**Table 1-11.** Minor element concentrations in rock samples from the Bodie Mining District.—Continued

[cm, centimeter; K, potassium; Kspar, potassium feldspar; —, no data]

Sample number	Sc ppm	Sn ppm	Sr ppm	Te ppm	Th ppm	Tl ppm	U ppm	V ppm	W ppm	Y ppm	Zn ppm	C %
Burgess series veins												
11-BA-22A	<0.1	0.4	39.1	3	<0.2	1.4	<0.1	4	0.5	0.2	34	—
11-BA-22B	<0.1	0.2	36.2	1.3	<0.2	1.2	<0.1	3	0.3	0.1	20	—
11-BA-22C	0.9	0.3	170	3	2.3	3.6	0.8	7	6.1	2	100	—
11-BA-22D	1.2	0.5	68.4	0.3	3.2	1.5	1.1	19	4.7	2.4	11	—
11-BA-22E	0.6	0.3	43.3	0.9	1.6	0.7	0.7	22	18.6	1.1	464	—
07-BA-2	0.7	0.4	147	0.2	2.9	7.7	0.8	13	2.1	1.4	6	—
99-DJ-71A	<0.975	<2	79	<0.487	—	<0.487	—	9	<4	<2	23	—
99-DJ-71B	1.36	2	154	<0.48	—	0.554	—	50	17	5	6.82	—
99-DJ-71C	2.05	<2	205	<0.477	—	<0.477	—	48	13	4	7.99	—
99-DJ-71D	<0.914	<2	331	<0.457	—	0.667	—	44	<4	5	24.4	—
Sample number	Se ppm	Sn ppm	Sr ppm	Te ppm	Th ppm	Tl ppm	U ppm	V ppm	W ppm	Y ppm	Zn ppm	C %
Silver Hill series veins												
BODB07-8	4.6	67	40.4	181	2	0.7	1	24	3	2.1	1,870	<0.01
09-BA-28A	—	67.1	35.4	19.8	0.6	0.9	0.1	17	1.1	0.3	31	—
09-BA-28B	—	183	12.2	>500	1.6	0.4	0.4	14	2.4	0.7	3,530	—
09-BA-28C	—	205	26.9	234	1.1	1.2	0.3	18	1.2	0.5	2,600	—
09-BA-28H	—	15.2	33.8	8.4	3.3	0.9	1.2	22	6.1	1.3	9	—
09-BA-28I	—	0.7	78	8.5	2.3	3.1	1.2	38	22	3.2	210	—
07-BA-5A	85.4	2.7	25	280	1.7	0.6	0.5	19	1.9	1.1	27,900	—
07-BA-5B	7.9	36.5	28.9	86.9	0.8	0.5	0.2	18	1	1.1	1,380	—
99-DJ-70A	<0.969	<2	24	<0.484	—	0.569	—	26	21	4	10.8	—
99-DJ-70B	<0.94	<2	19	<0.47	—	0.615	—	33	30	4	9.79	—
99-DJ-72A	13.5	54	64	110	—	<0.492	—	25	<4	<2	618	—
99-DJ-72B	1.64	12	34	4.94	—	<0.491	—	48	9	2	14.8	—
11-BA-6E	—	3.7	5.5	34.1	1	0.7	0.3	13	1.7	0.5	49	—
11-BA-7A	—	17.9	48	135	7.2	1.5	0.7	12	2.5	2	20,700	—
11-BA-7E	—	0.8	157	2.4	4	3.2	1.2	17	6.1	2.5	41	—
11-BA-7F	—	47.8	52.7	191	3.2	1	1	21	4	1.5	1,470	—
11-BA-9A	—	10.5	18	41.7	1.7	0.4	0.5	9	1.2	2.7	479	—
11-BA-9B	—	70.7	18.6	230	2.7	0.9	0.8	29	4.5	1.5	674	—

**Table 1-11.** Minor element concentrations in rock samples from the Bodie Mining District.—Continued

[cm, centimeter; K, potassium; Kspar, potassium feldspar; —, no data]

Sample number	Description, Location	Latitude	Longitude	Au ppm	Hg ppm	Pd ppb	Pt ppb	Al %	Ca %	Fe %	K %	Mg %	Na %
Silver Hill series veins													
11-BA-10A	Addenda Mine dump	38.20556	-119.00543	1,150	0.38	—	—	2.65	0.25	1.32	1.02	0.03	0.02
11-BA-10B	Addenda Mine dump	38.20556	-119.00543	579	0.91	—	—	2.66	0.25	1.11	1.11	0.03	0.02
BOD11-1ME	Quartz-sulfide, minor K-mica vein, Oro dump	38.20432	-119.00746	77	0.82	1	2.3	2.25	0.27	5.51	2.28	0.05	0.04
BOD11-2ME	Banded quartz-Kspar, minor sulfide vein, Noonday dump	38.20023	-119.00991	>10	0.22	<1	<0.5	5.83	<0.01	0.06	4.72	<0.01	0.08
BOD11-2AME	Quartz-sulfide-K-mica breccia, Contention dump	38.20524	-119.0056	29	3.24	3	2.4	1.42	0.21	1.18	0.54	0.02	0.01
BOD11-5ABCME	Quartz-sulfide breccia, Red Cloud dump	38.20133	-119.00588	>10	1.34	<1	<0.5	1.81	0.14	0.44	1.01	0.06	0.02
BOD11-22A	Quartz vein with chalcopyrite, pyrite	38.21209	-119.00122	6.75	1.46	—	—	1.13	0.02	0.42	0.67	0.02	0.01
BOD11-22B	Quartz vein with chalcopyrite, pyrite	38.21209	-119.00122	1.23	1.24	—	—	3.83	0.1	0.44	1.74	0.09	0.03
Sample number	Description, Location	Latitude	Longitude	Au ppm	Hg ppm	Al %	Ca %	Fe %	K %	Mg %	Na %	S %	Ti %
Uncorrelated veins													
11-BA-21A	Noonday Mine dump	38.20037	-119.00919	5.81	0.06	1.13	23.4	0.02	1.6	0.03	0.02	0.04	<0.01

**Table 1-11.** Minor element concentrations in rock samples from the Bodie Mining District.—Continued

[cm, centimeter; K, potassium; Kspar, potassium feldspar; —, no data]

Sample number	S %	Ti %	Ag ppm	As ppm	Ba ppm	Be ppm	Bi ppm	Cd ppm	Ce ppm	Co ppm	Cr ppm	Cs ppm	Cu ppm	Ga ppm
Silver Hill series veins														
11-BA-10A	2.11	0.08	335	507	163	0.3	552	46.4	12.7	3.1	5	7	24,400	21.4
11-BA-10B	2.58	0.07	250	858	163	0.3	478	70.5	11.1	2.6	4	6	30,600	19.8
BOD11-1ME	>5	0.09	1,080	206	160	0.3	61.5	181	21.8	5.9	4	<5	>50,000	12.9
BOD11-2ME	0.02	<0.01	180	11	92	1.1	0.33	0.2	1.81	1.1	<1	14	91.7	5.16
BOD11-2AME	3.27	0.06	497	1,210	91	0.2	156	101	11.4	5.3	5	<5	45,600	8.55
BOD11-5ABCME	0.59	0.04	1,030	416	311	0.3	34.5	15.8	11.8	0.8	3	7	4,060	7.76
BOD11-22A	0.64	0.03	2,900	236	27	0.4	169	22.6	14.1	17.3	2	<5	9,090	5.85
BOD11-22B	0.4	0.12	326	31	49	0.9	30.9	2.8	25.1	12.6	2	5	3,760	20.7
Sample number	Ag ppm	As ppm	Ba ppm	Be ppm	Bi ppm	Cd ppm	Ce ppm	Co ppm	Cr ppm	Cs ppm	Cu ppm	Ga ppm	In ppm	La ppm
Uncorrelated veins														
11-BA-21A	137	<1	22	20.2	1.36	0.2	0.35	0.4	<1	<5	68.2	1.04	<0.02	<0.5

**Table 1-11.** Minor element concentrations in rock samples from the Bodie Mining District.—Continued

[cm, centimeter; K, potassium; Kspar, potassium feldspar; —, no data]

Sample number	In ppm	La ppm	Li ppm	Mn ppm	Mo ppm	Nb ppm	Ni ppm	P ppm	Pb ppm	Rb ppm	Sb ppm	Se ppm	Sc ppm
Silver Hill series veins													
11-BA-10A	4.05	7.3	36	20	38	2.6	<0.5	1,160	2,180	52.8	6,780	1.1	—
11-BA-10B	5.14	6.8	28	24	44.1	1.8	<0.5	1,080	2,970	55.6	>10,000	1	—
BOD11-1ME	13.2	10.9	26	75	28.7	1.1	5.9	750	4,890	76.8	3,580	47.1	0.8
BOD11-2ME	<0.02	1.1	71	83	0.63	1.3	<0.5	<50	17.6	273	39.5	1.4	0.2
BOD11-2AME	5.01	6.7	33	38	28.8	1.1	<0.5	1,180	2,710	24.8	>10,000	36.6	0.6
BOD11-5ABCME	1.51	6.3	51	37	16.5	1.2	0.8	600	1,600	52.1	983	58.3	0.3
BOD11-22A	1.49	8.2	43	25	7.62	0.8	9	150	329	38.5	962	4.5	0.5
BOD11-22B	0.35	15.4	49	42	3.84	4	9.9	310	225	94.7	191	2.5	1.9
Sample number	Li ppm	Mn ppm	Mo ppm	Nb ppm	Ni ppm	P ppm	Pb ppm	Rb ppm	Sb ppm	Sc ppm	Se ppm	Sn ppm	Sr ppm
Uncorrelated veins													
11-BA-21A	51	311	0.18	<0.1	<0.5	<50	12.7	89.9	26.4	<0.1		0.8	811

**Table 1-11.** Minor element concentrations in rock samples from the Bodie Mining District.—Continued

[cm, centimeter; K, potassium; Kspar, potassium feldspar; —, no data]

Sample number	Sn ppm	Sr ppm	Te ppm	Th ppm	Tl ppm	U ppm	V ppm	W ppm	Y ppm	Zn ppm
Silver Hill series veins										
11-BA-10A	192	52.1	>500	3.4	0.8	1.2	31	10.7	1.6	3,780
11-BA-10B	258	32.4	>500	2.9	0.8	0.9	36	7	1.9	6,870
BOD11-1ME	37.6	68	340	3.3	2.6	0.7	12	2.6	1.3	11,800
BOD11-2ME	1.1	139	4	<0.2	6.8	<0.1	<1	3.9	0.3	12
BOD11-2AME	68.4	39.1	340	2	0.7	0.7	18	3.8	1	5,760
BOD11-5ABCME	132	27.7	128	1.6	0.9	0.4	17	1.9	1	1,410
BOD11-22A	26.9	42.4	53.9	1.4	0.7	3	15	2.6	9	2,260
BOD11-22B	7.1	57	11.9	4.6	1.2	2	39	15.1	7.6	246
Sample number	Te ppm	Th ppm	Tl ppm	U ppm	V ppm	W ppm	Y ppm	Zn ppm	C %	
Uncorrelated veins										
11-BA-21A	2.5	<0.2	1.1	<0.1	<1	2.1	0.2	16	—	

**Table 1-12.** Minor element concentrations in rock samples of Spring Peak sinter and subjacent rocks.

Sample number	Description	Latitude	Longitude	Au ppm	Hg ppm	Pd ppb	Pt ppb	A %	Ca %	Fe %	K %	Mg %
06-BA-2	Banded quartz vein beneath sinter	38.24908	-118.85782	0.026	0.19	—	—	0.66	0.09	0.08	0.2	0.01
SPK06-1	Sinter, north edge of terrace	38.24928	-118.85268	0.042	0.84	—	—	0.33	0.03	0.08	0.06	<0.01
SPK06-2	Sinter, prospect pit	38.24868	-118.85293	0.0066	0.1	—	—	0.18	0.04	0.04	0.02	<0.01
SPK06-3	Sinter, north edge of terrace	38.24932	-118.85239	0.053	1.02	—	—	0.2	0.03	0.04	0.04	<0.01
SPK11-10	Silicified, pyritic clastic sediments, sub-sinter	38.24770	-118.85113	0.007	3.63	—	—	5.38	0.37	1.8	3.63	0.16
SPK11-1ME	Silicified pyritic tuff beneath sinter	38.24853	-118.84904	0.004	1.28	3	<0.5	5.16	0.44	0.95	3.8	0.1
SPK11-4ME	White-beige, granitic rock altered to quartz, clay	38.24960	-118.86053	0.003	6.05	<1	<0.5	6.3	0.09	0.97	1.77	0.03
SPK11-2ME	Banded vein beneath sinter, in granitic rock	38.24876	-118.85513	0.126	26.5	<1	<0.5	0.66	0.14	0.19	0.34	0.01

**Table 1-12.** Minor element concentrations in rock samples of Spring Peak sinter and subjacent rocks.—Continued

Sample number	Na %	S %	Ti %	Ag ppm	As ppm	Ba ppm	Be ppm	Bi ppm	Cd ppm	Ce ppm	Co ppm	Cr ppm	Cs ppm	Cu ppm	Ga ppm	In ppm
06-BA-2	0.02	<0.01	<0.01	2	28	52	1.9	<0.04	<0.1	1.16	0.3	5	24	2	2.68	<0.02
SPK06-1	<0.01	0.01	<0.01	1	<30	85	11	0.5	<0.2	1.7	0.8	<10	61.1	40	11	<0.2
SPK06-2	<0.01	<0.01	<0.01	<1	<30	90	<5	<0.1	<0.2	0.4	<0.5	<10	12.2	7	18	<0.2
SPK06-3	<0.01	<0.01	<0.01	<1	—	—	—	—	—	—	—	—	—	—	—	<0.2
SPK11-10	0.54	1.45	0.22	<1	1,560	731	4.3	0.14	<0.1	29.3	9.7	4	44	117	18.8	0.03
SPK11-1ME	0.95	0.12	0.19	<1	252	815	2	0.62	<0.1	26.2	1.2	3	71	18.8	12.1	0.02
SPK11-4ME	0.08	0.26	0.15	<1	293	1,440	0.4	0.07	<0.1	46.6	0.3	2	115	19.9	15.4	<0.02
SPK11-2ME	0.03	0.03	<0.01	<1	62	178	1.2	<0.04	<0.1	4.13	0.1	2	110	6.5	5.81	<0.02

**Table 1-12.** Minor element concentrations in rock samples of Spring Peak sinter and subjacent rocks.—Continued

Sample number	La ppm	Li ppm	Mn ppm	Mo ppm	Nb ppm	Ni ppm	P ppm	Pb ppm	Rb ppm	Sb ppm	Sc ppm	Se ppm
06-BA-2	0.6	123	138	36.3	<0.1	1.1	70	1.5	22.1	272	0.2	<0.2
SPK06-1	0.9	20	—	<2	<1	<5	—	<5	13.2	664	<5	<0.2
SPK06-2	0.3	20	—	<2	<1	8	—	<5	5.4	835	<5	<0.2
SPK06-3	1	30	—	<2	<1	6	—	<5	7.6	>1,000	<5	0.4
SPK11-10	15.3	75	90	2.04	4.3	3.1	810	10.6	236	208	7.7	<0.2
SPK11-1ME	12.8	93	49	2.23	5.4	0.9	490	12.3	219	259	5.2	<0.2
SPK11-4ME	24.6	6	27	7.64	6.7	<0.5	320	11.9	75.7	242	1.6	<0.2
SPK11-2ME	2.5	36	21	2.79	0.4	<0.5	420	1.4	28.5	566	<0.1	<0.2

**Table 1-12.** Minor element concentrations in rock samples of Spring Peak sinter and subjacent rocks.—Continued

Sample number	Sn ppm	Sr ppm	Te ppm	Th ppm	Tl ppm	U ppm	V ppm	W ppm	Y ppm	Zn ppm	C %
06-BA-2	<0.1	97.9	<0.1	0.2	0.4	0.2	<1	0.5	1.4	<1	—
SPK06-1	<1	39.9	<0.5	0.4	1.1	0.23	6	3	<0.5	8	0.01
SPK06-2	<1	21.3	<0.5	<0.1	<0.5	0.1	<5	1	<0.5	—	0.02
SPK06-3	<1	22.5	<0.5	<0.1	<0.5	0.22	<5	5	0.5	<5	0.05
SPK11-10	1.5	166	<0.1	5.6	14	2.3	124	42.4	11.5	27	—
SPK11-1ME	0.9	271	<0.1	6.4	3.9	2.2	82	73.2	6.6	9	—
SPK11-4ME	0.9	531	<0.1	13.2	2.7	6.2	28	37	3	6	—
SPK11-2ME	0.2	122	<0.1	1.3	3.1	0.7	4	2.2	2.6	3	—

Menlo Park Publishing Service Center, California  
Manuscript approved for publication January 23, 2015  
Edited by Sarah Nagorsen  
Layout and design by Kay Naugle

